*Volume 17, No. 5*

*November, 1964*

# SOVIET ATOMIC ENERGY

АТОМНАЯ ЭНЕРГИЯ
(ATOMNAYA ÉNERGIYA)

TRANSLATED FROM RUSSIAN

CONSULTANTS BUREAU

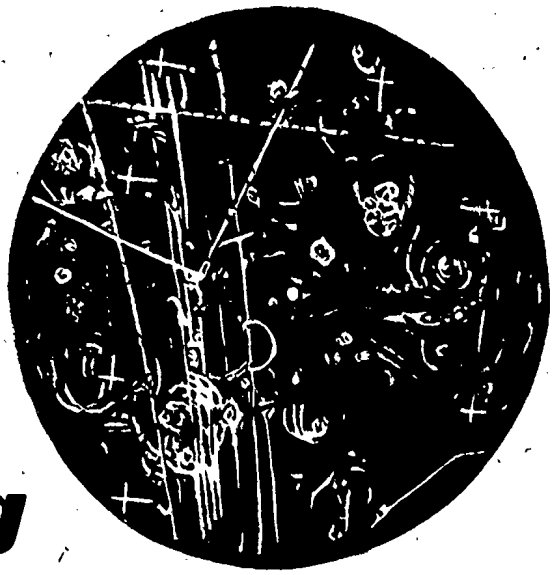

VOLUME 9

# Advances in Cryogenic Engineering

## Proceedings of the 1963 Cryogenic Engineering Conference August 19-21 at Boulder, Colorado

Edited by K.D. Timmerhaus

The 69 papers contained in this volume (the latest in a series recognized as the most authoritative compilation for low temperature engineering) examine such widespread areas as: insulation, heat transfer, mechanical properties, seals, fluid phenomena, engineering aspects of superconductivity, thermodynamics, phase equilibria, safety, instrumentation, cryopumping, and various developments in processes and equipment. Of particular importance are the chapters describing mechanical properties, which will be of interest to all those in materials research (especially for the new alloy 7039) the sections on superconducting materials and properties for all those working with solid-state devices, and papers concentrating on thermodynamic properties for designers of cryogenic systems.

The information on recent developments contained in this volume will be a valuable aid to all low temperature engineers in the resolution of such practical problems as heat transfer in cryogenic storage and in flight, space-simulation chamber design and operation, fluid transfer of large cryogenic flows, mechanical property selection, seal evaluation for cryogenic applications, and many others. The equipment and procedures used by various investigators in performing the work reported in this volume—varying from such complex and elaborate apparatus as a space rocket, to intricate and special testing equipment—indicate the breadth and scope of the topics covered. An author and a cumulative subject index (Volumes 1-9) are included. Every paper accepted for publication in ADVANCES IN CRYOGENIC ENGINEERING is being published for the first time.

**598 pages** **$17.50**

Complete contents of Volumes 1-8 will be sent on request.

PLENUM PRESS 227 W. 17th St., New York, N.Y. 10011

# SOVIET ATOMIC ENERGY

*A translation of* **ATOMNAYA ÉNERGIYA**
*A publication of the Academy of Sciences of the USSR*



Vol. 17, No. 5 November, 1964

## CONTENTS



**Annual Subscription: $95** **Single Issue: $30** **Single Article: $15**

# CONTENTS (continued)



*Two page insert facing page 336.

The Russian date "Podpisano k pechati" of this issue was 10/16/1964 . This is equivalent to "approved for printing." Publication did not occur prior to this date, but must be assumed to have taken place reasonably soon thereafter.

Publisher

# THE THIRD INTERNATIONAL GENEVA CONFERENCE

A. M. Petros'yants
Chairman

USSR State Committee for the Utilization of Atomic Energy
Translated from Atomnaya Énergiya, Vol. 17, No. 5,
pp. 323-328, November, 1964

In August and September of this year, the third UN international scientific and technical conference on the peaceful use of atomic energy, the largest meeting of the past decade, was held in Geneva.

This conference was the most representative of all those held. Where 35 countries participated in the first Geneva conference, about 2000 scientists from 71 countries participated in the third conference. The principal countries participating (38 countries) were represented by 750 reports including more than 100 from the USSR. About 350 reports were heard and discussed in 7 plenary and 35 sectional sessions.

Whereas mainly scientific work was reported at the first conference in 1955, the main significance lay in the lifting of secrecy from some research and in the reestablishment of ties between the scientists and specialists of the world, which were broken in the course of the Second World War. A great deal of experimental work was made public at the second conference in 1958 which was of value in commercial applications, and direct contacts between countries and scientists working in the fields of atomic energy and nuclear physics were expanded.

The third conference in 1964 summed up the experience with commercial application of atomic power installations accumulated in the intervening years, emphasized confidence in the economic efficiency of atomic power stations in the immediate future, and stressed the inevitability of the widespread use of atomic power stations in many regions and countries of the globe.

In some countries, they have come to the conclusion that it is now impossible to get along without the use of nuclear reactors for power purposes and that atomic energy will become one of the important factors in long-range economic development; in the immediate future, atomic energy will make it possible to satisfy the continually growing requirements for electric power in those regions and countries of the world where the reserves of fossile fuels are either exhausted or are close to exhaustion.

Among the participants in this great international forum of scientists and engineers, were not only representatives of the highly developed industrial countries where atomic energy finds application in various fields of science and engineering, but also representatives of the countries of Asia, Africa, and Latin America which are just taking the first steps in the utilization of atomic energy, and of nuclear power in particular, or which are preparing to proceed to its use.

The main task of the third conference was consideration and discussion of questions connected with the development of nuclear power. UN Secretary General U. Thant noted in his speech that "the problems of nuclear power are key problems in the future development of the greater part of the world."

The report of Prof. H. Bhabha (India) noted the need for the use of nuclear energy, especially in developing countries: "The principal part of the world population lives in the developing countries of the world, i.e., 2200 million people out of 3069 million or 71.8%, but the power requirement in these countries in only 20.6% of power produced and electric power production is only 14.8%. If one assumes that the yearly increase in electric power requirements is 5%, the total power requirements of the world in 1960, which amounted to 4200 million tons of coal (equivalent per year), will increase to almost 30,000 million tons in the year 2000." Assuming that the growth in power requirements will be approximately 5% per year, H. Bhabha concludes that the world reserves of coal will be used up in approximately 75 years. One need not agree with these figures, but one ought to recognize that the position with regard to power resources in the world is not bright at all.

In their report, the representatives of the Japanese Atomic Energy Commission said that "Japan has great interest in the peaceful use of atomic energy..." The Japanese program for the development of nuclear power states:

"For the introduction of new power production, the use of hydroelectric power in Japan is limited, and therefore the main efforts will be directed toward the construction of thermal (ordinary) stations. A large part of the fuel for thermal stations must be imported. The development of new power sources is required. This consideration has led the Japanese economic authorities to realize necessity for the production of atomic power."

The representatives of a number of other governments also emphasized in their reports that nuclear power is, for many countries, a realistic and completely dependable means for obtaining power.

The third Geneva conference took place under very favorable circumstances for international cooperation among scientists of all countries. The signing of the Moscow agreement on August 5, 1963 banning the testing of nuclear weapons in three media, the announcement by the three nuclear powers – the Soviet Union, the United States, and Great Britain – concerning the reduction in production of fissionable materials for military purposes, all these created broad possibilities for using the power of the atom for the good of mankind and facilitated a successful discussion at the conference concerning the problems of using intranuclear energy for peaceful purposes.

All the main trends in the peaceful use of atomic energy were considered and discussed at the conference, some in greater detail, others in summary. However, most attention was paid to atomic power stations.

Reports and papers on various problems were heard and discussed: atomic power stations and the economics of nuclear power, research reactors, the physics of nuclear reactors, the application of radioactive isotopes and radiations in science and industry. Also discussed were problems directly connected with nuclear power such as problems in the chemical processing of nuclear fuel, the problems of materials for atomic technology, the question of nuclear safety, and the medical and biological aspects of the use of atomic energy. New methods for utilizing atomic energy were discussed: various methods for the direct conversion of nuclear and thermal energy to electricity, the use of atomic reactors for desalinization of sea water, the problems in achieving controlled thermonuclear reactions, and many others.

In the six years which have gone by since the second international conference, nuclear power has made great strides forward. In 1955, at the time of the first Geneva conference, only the first atomic power station, also the first commercial type of station in the USSR (Obninsk), was operating at a power of 5 MW; by 1958, several atomic power stations with a capacity over 180 MW were operating throughout the world, and by the end of 1964, the total capacity of all the atomic power stations in the world will reach almost 5000 MW.

Sufficient practical experience in the operation of atomic power stations was accumulated by the time of the third conference. Now, more than 35 atomic power stations throughout the world are producing electric power, and there are about 30 atomic power stations in various stages of construction. It is well known that there are operating commercial atomic power stations in the USSR, the United States, Great Britain, France, and Italy. Atomic stations are operating, or are in the process of construction, in Canada, Japan, Czechoslovakia, East Germany, and other countries.

Thus, by the time of the Third International Conference of Atomic Scientists, nuclear power had been produced on a commercial scale, and a spirit of optimism prevailed with regard to the prospects for the development of commercial nuclear power as a decisive factor in the generation of electric power in a number of countries.

In accordance with their specialties and with local conditions, a number of countries have developed characteristic national methods and programs for the development of nuclear power. These plans and programs were reported at the conference. Some of them provide for an increase in the capacity of atomic power stations to tens of millions of kilowatts during the coming decade and for considerable decrease in the cost of electric power produced by atomic power stations.

Various countries are working on different types of reactors for atomic power stations depending on the particular conditions which obtain in a given country in the economic and industrial fields. For example, in the United States, where there are plants for the production of uranium highly enriched in the isotope $U^{235}$, a great deal of experience has been accumulated concerning reactor systems using pressurized water and boiling water. These are the fundamental types of reactors that have been developed in the United States; they are the foundation for the development of nuclear power in the United States in the coming years.

Great Britain is chiefly developing reactors with graphite moderation and gas cooling. France has also been working on gas-graphite reactors for a long time.

In Canada, the basic type has turned out to be the heavy water power reactor operating with natural uranium, which can be explained to a considerable degree by the lack of plants for the production of enriched uranium in Canada.

In the USSR, large reactors of the water-cooled, water-moderated (light water) type have been, and are being, constructed as well as reactors with graphite moderator and water coolant. In the Soviet Union, the I. V. Kurchatov atomic power station was built at Beloyarsk in the Urals, and a commercial power reactor operates there with nuclear superheating of steam directly in the 100-MW electrical output reactor, the first in use in the world. The construction of a second such reactor at the Beloyarsk atomic power station with an electrical output of 200 MW is going ahead at full speed – the assembly of the reactor proper will be completed this year.

Construction and assembly of the first section of the Novo-Voronezh atomic power station with a capacity of 210 MW has been completed; it supplies current to the Voronezh power system. Construction has begun on a second section of this station with an electrical output of 365 MW.

In the Ul'yanovsk region, at the Scientific Research Institute for Atomic Reactors in the Melekess area, construction of an atomic power station with an output of 50 MW has been complete. Its reactor, of the water-cooled, water-moderated "boiling" type, operates with ordinary water in a single-loop circuit and direct transmission of steam to the turbine.

As has been reported in the literature, a dual-purpose atomic power station with an electrical output of 100 MW is operating in Siberia, and the present total output of all the dual-purpose atomic reactors operating in Siberia is about 600 MW.

As reports and statements at the third Geneva conference have indicated, the present trend in the development of nuclear power reactors of various types is toward an increase in their individual outputs to powers of 500 MW (el) and higher. There exist planned power reactor developments in several countries, including the USSR, for outputs up to 1000 and even to 2000 MW (el). Such an increase in the individual output of a single unit of an atomic power station is explained by the attempt to reduce the cost of electric power production by reducing the cost per installed kilowatt. However, excessive increase in the output of an individual unit is not always advisable. The associated power systems must surely have to be of very high capacity in order to avoid system "breakdown" in the case of an emergency situation at such a large station. At the present time, one can consider as a most acceptable output that of an atomic power unit with a capacity of 500-800 MW (el).

In addition to the increase in the specific output of an atomic power station, the struggle for competitive position compels engineers and builders to look for means of reducing the cost of building and equipping an atomic power station. One of the steps in this direction is an increase in steam parameters. An improvement in the characteristics of the steam furnished the turbines makes it possible for an atomic power station to use mass-produced turbines of high output (200-300 MW and higher). This situation should play no small part in the improvement of the economic characteristics of atomic power stations.

A big problem for physicists and atomic power scientists is the increase in the amount of average burnup of nuclear fuel. This also has a direct effect, in a favorable way, on the economic characteristics of atomic power station operation. No less important a problem, as was made clear at the conference, is the reduction in the cost of nuclear fuel (fuel elements). In a number of cases, they are so expensive that they amount to as much as 30 or even 50% of the cost of the entire power unit.

All these problems, and many others, which determine the economics of atomic power station operation were well presented and discussed at the third Geneva conference.

As already pointed out, the various countries which are carrying out development and planning of power reactors have chosen for themselves more or less definite types of reactors with which they proposed to solve the problem of electric power production.

At the conference, the overwhelming majority of delegates was of the opinion that the future belonged to fast reactors since they, by their very nature, make it possible to produce more fissionable material than they themselves require, and in that way, increase the utilization of existing supplies of nuclear fuel by 10 or even 100 times because they bring $U^{238}$ and thorium into the cycle. However, a number of delegates, chiefly those from the United States, feel that the development of nuclear power must go through three stages. The first of these is the stage which was reached in recent years and which is based on slow reactors (gas coolant and graphite moderator; heavy water cool-

ant and moderator; light water coolant and moderator). The second stage is the use of improved reactors of the converter type. The third stage is the further development of reactor technology with the use of breeder reactors. A prolonged existence for the second stage is assumed by this group. The chairman of the American delegation, Prof. G. Seaborg, remarked in his report, "considering the number of shortcomings associated with the economic outlook for the development of breeder reactors, the construction of improved converter reactors would possibly seem extremely reasonable for many countries. . ." And, further, ". . . we shall never see the widespread use of breeder reactors if the technology for their production does not achieve an economically favorable stage."

As is well known, the Soviet consensus with regard to the development of nuclear power supposes a more rapid transition to the construction of breeder reactors as the general trend in nuclear power although it is clear to us, of course, that fast breeder reactors, being the most promising of the new reactor types (keeping commercial application in mind), still require a great deal of creative engineering work.

The Canadian atomic power scientists feel that breeder reactors will not be needed for many years. This is reflected in the long-range Canadian plans for the construction of atomic power stations. We, together with the representatives of Great Britain, France, Germany, and a number of other countries, cannot agree with this position.

It should be noted that extensive work on the production of economical fast reactors is already being carried on in many countries. The Soviet Union has performed a large amount of research work with the BR-1 and BR-5 reactors and with the experimental setup at the BFS which has made it possible to proceed to the construction of a large commercial fast reactor with an output of 300-350 MW (el) in the Caspian Sea region. Great Britain has accumulated a large deal of experience with the breeder reactor at Dounreay. The United States has recently proceeded to the power mode for the EBR-II reactor. The operation of the Enrico Fermi atomic power station using fast neutrons will facilitate the accumulation of experience. The French Atomic Energy Commission is completing the construction of a fast reactor. Several other countries have also joined in these efforts.

At the Geneva conference, the reports of this work were heard with a great deal of interest, and they evoked lively discussions.

Along with work on large atomic stations, the results of work on the production of atomic power stations of low and medium capacities were discussed at the conference. Interest was expressed in the reports of Soviet scientists about construction in the USSR of the modular atomic power station "Arbus" with an output of 750 kW containing an organic-cooled, organic-moderated reactor in which hydrostabilized diesel fuel acts as coolant. A distinguishing feature of this reactor is the special regenerative apparatus which maintains the coolant in a specified condition.

Great interest was aroused at the conference by reports concerning the operation of the first experimental model of the transportable caterpillar driven TES-3 atomic power station with an electrical output of 1500 kW. This mobile power station has already been operating for three years and more at the Physics and Power Engineering Institute of the USSR State Committee for the Utilization of Atomic Energy.

A report on the experience in the operation of the flagship of the USSR icebreaker fleet, the atomic ship "Lenin," was highly regarded by the specialists at the conference. As is well known, the first atomic icebreaker in the world, the "Lenin," has already successfully carried out five successive voyages, and has successfully coped with its difficult responsibilities in the rugged Arctic conditions of the icy northern seas; it has actively assisted our freighter fleet by guiding ships carrying lumber and other cargos. This unique ship has practically an unlimited sailing range without fuel loading, and sails in any Arctic region, breaking ice two to three meters thick. The atomic ship "Lenin" conclusively demonstrates all the advantages of using atomic energy in a commercial marine fleet.

The American atomic passenger-freighter "Savannah," having this year made its first trip across the Atlantic to the shores of Europe, has also demonstrated its excellent seagoing capabilities. At the time of the conference, the USAEC organized a trip to Sweden aboard the atomic ship "Savannah" for representatives from the delegations of several countries. An acquaintance with the "Savannah" reveals that it is a comfortable and cozy ship for ocean travel. At present, the "Savannah" is a demonstration ship propagandizing for the creation of an atomic freighter fleet. The "Savannah" only partly fulfills its function as a freight and passenger ship because of the lack of confidence in it by commercial firms and passengers. In comparison with the difficult, great, and honorable service rendered by our famed atomic icebreaker "Lenin," the "Savannah" is being used insufficiently.

The experience in operating the atomic ship "Lenin" and the discussions of the Soviet report at the Geneva conference indicated that the production of marine atomic installations in a commercial fleet, along with the development of nuclear power, is one of the promising trends for the use of atomic energy.

Several other countries are also working on the production of atomic ship installations. Thus, the atomic commercial cargo vessel "Otto Hahn," whose hull was launched recently, is being built in Germany. In Japan, which is a country of ship navigators and ship builders, they are proceeding to the development of a technology for manufacture of ship reactors. In 1963, a special Japanese agency was created for the development of atomic ships which, in particular, was given the responsibility for the construction of an atomic oceanographic ship. A pressurized water reactor with an output of 35 MW will be installed in the ship. Construction of the ship should be completed in 1968.

Thus, atomic steam-producing marine equipment is starting gradually to earn a place in the civilian commercial marine fleet.

In every new field and particularly in such a rapidly developing one as the use of atomic energy, nuclear power engineering follows not only previously laid out paths but also completely new ones whose scientific development is only just beginning.

For the first time in engineering history, there were reported at the third Geneva conference by Soviet scientists the practical results of research and experimental work on the direct conversion of nuclear energy to electricity. A high-temperature fast reactor with silicon-germanium converters which was built in the USSR at the I. V. Kurchatov Atomic Energy Institute was brought up to power on August 14, 1964, operated at a power of 500 W for about 2500 h, and continues to operate successfully. This apparatus bears the poetic name of "Rmashka" (Daisy). Incidentally, it reflects an actual situation since the highly enriched $U^{235}$ dicarbide is disposed in the form of flower petals.

The report of our scientists and a film on this new type of converter-reactor aroused great interest at the conference. Now, the Russian word "Romashka" appears in all specialized technical, and ordinary, publications, along with reports on the construction of a new form of power source without the use of any sort of auxiliary equipment in the form of turbines, pumps, etc.

The manufacture of similar equipment, with a small number of moving parts, to be sure (pump, coolant), is being completed in the United States (SNAP-10A). It is intended for installation in space vehicles (satellites). American scientists read a report on this equipment and showed films of its construction. Apparently, it will be operating under ground-level conditions in a short time.

There were also reports at the conference about low-power installations in which the heat source is a radioactive isotope. Ordinarily, they are very simple, their useful power is small (of the order of 5-100 W), and they operate with direct conversion of heat to electricity by means of semiconductors. Soviet scientists have reported on such equipment, in particular, on the "Beta-1" apparatus. The β-radioactive isotope $Ce^{144}$ is used in it, and it has now been in service for a year as the power supply for a standard automatic radiometeorological station providing power for a transmitter with an output of about 150 W by means of an accumulator.

Isotopic current sources for various purposes have been manufactured, and are being operated, in the the United States also. At the scientific and technical exhibition in Geneva, the Americans demonstrated a model of a barge-mounted meteorological station with a 60-W isotopic current source operating with $Sr^{90}$.

Nuclear power holds a more distant prospect — controlled thermonuclear fusion. The thorough and extremely complex scientific investigations have a completely clear and concrete purpose — the creation of thermonuclear power stations. The reports which were presented and discussed at the conference indicate that, during the six years since the second Geneva conference, definite successes have been achieved in this field. Although scientists have not yet arrived at a complete solution of this important power problem, there have been successes in the area of finding the field.

The Soviet section of the exhibits, which occupied 1000 $m^2$, occupied a central position both with respect to location and to the large number of excellently executed models, exhibits, and photographs. Visitors and conference participants were particularly interested in models of the icebreaker "Lenin" and the Beloyarsk atomic power station, and two working thermonuclear laboratory machines from the Novosibirsk Nuclear Physics Institute.

Quite good exhibits were arranged by other countries. The exhibits, on the whole, realized their purpose, and helped direct contact between scientists of various countries very successfully.

Some countries prepared interesting films on particular problems in the use of atomic energy. The Soviet Union presented 24 films which were shown continuously while the exhibit was open.

The Geneva conference showed that science is an excellent means for intercourse between all the peoples of the world, particularly when there is a desire for it. The spirit of international cooperation was clearly evident at this conference. All the work of the conference was carried on in an efficient and friendly atmosphere.

But, speaking of peace and friendship, of cooperation between scientists and specialists, between all the people of the world, we cannot forget that the military atom hinders the thorough development of the peaceful atom. This thought occupies the minds of many scientists and many progressive people in all countries. The peaceful use of nuclear fuel on a widespread scale is only possible when the path to thermonuclear war is completely closed to the military atom by the efforts of the people of the world.

# HIGH-TEMPERATURE REACTOR-CONVERTER "ROMASHKA"*

M. D. Millionshchikov, I. G. Gverdtsiteli, A. S. Abramov, L. V. Gorlov, Yu. D. Gubanov, A. A. Efremov, V. F. Zhukov, V. E. Ivanov, V. K. Kovyrzin, E. A. Koptelov, V. G. Kosovskii, N. E. Kukharkin, R. Ya. Kucherov, S. P. Lalykin, V. I. Merkin, Yu. A. Nechaev, B. S. Pozdnyakov, N. N. Ponamarev-Stepnoi, E. N. Samarin, V. Ya. Serov, V. A. Usov, V. G. Fedin, V. V. Yakovlev, M. V. Yakutovich, V. A. Khodakov, and G. V. Kompaniets

Translated from Atomnaya Énergiya, Vol. 17, No. 5, pp. 329-335, November, 1964

The effective use of atomic energy in various kinds of apparatus is bound up with the quest for new methods of transforming energy and their study. The development of converters with the direct transformation of thermal into electrical energy is of special interest.

One such system is the experimental power reactor "Romashka" in the I. V. Kurchatov Institute of Atomic Energy. This apparatus uses one of the most structurally-simple and operationally-reliable systems, based on a reactor and converter combined into a single unit, in which the heat generated in the active zone of the reactor is transferred to a thermoelectric converter situated at the outer surface of the reflector, by way of the thermal conduction of the materials.

The reactor uses fuel elements based on uranium carbide, which by virtue of its properties (high-working temperature and fairly high-thermal conductivity) is a promising material for this purpose. Good thermophysical and neutronophysical parameters are ensured for the reactor by using metallic beryllium as reflector material and graphite as structural material for the active zone. Use of these materials in the reactor makes is possible to employ a high-temperature converter based on semiconductors consisting of a silicon-germanium alloy.

## Description of the Reactor-Converter

The nuclear reactor (Fig. 1) constitutes a neutron-physical system operating with fast neutrons. This serves as a source of thermal energy, which is converted into electrical energy by means of the thermoelements.

The heat evolved as a result of the fission of $U^{235}$ in the active zone of the reactor is transferred in the radial direction by thermal conduction to the reflector, and then from the side surface of this to the semiconductor converter

* Report No. 873 presented by the USSR to the Third International Conference on the Peaceful Uses of Atomic Energy, Geneva, 1964.

The converter "Romashka," the first nuclear-power system in the world with direct energy conversion, began delivering power on August 14, 1964. Since then the system has operated under optimum load with a temperature of 1770°C in the center of the active zone and 1000°C at the surface of the reactor. The electric current taken from the converter with thermoelement groups connected in parallel reaches 88 A. According to the situation on November 18, more than 1000 kWh electrical power have been produced.

Tests have enabled us to draw one important conclusion regarding the characteristics of "Romashka," namely, the stability of its operation. Although automatic control is provided, it has not proved necessary to set this in motion, since the system requires little regulating. After setting in the nominal condition, the power and temperature are maintained to a high accuracy at the assigned level on account of the self-regulation of the reactor, which has a negative temperature coefficient of reactivity. The results of the tests confirm the high efficiency of the silicon-germanium-alloy semiconductor thermoelements in the radiation fields of a fast-neutron reactor. After 2500 h operation, changes were found in the main characteristics of the thermoelements. Neither the electrical power nor the emf of the converter had changed appreciably.

The results of the tests are being studied. These should lead to a series of important conclusions for use in future investigations and the development of new converters.

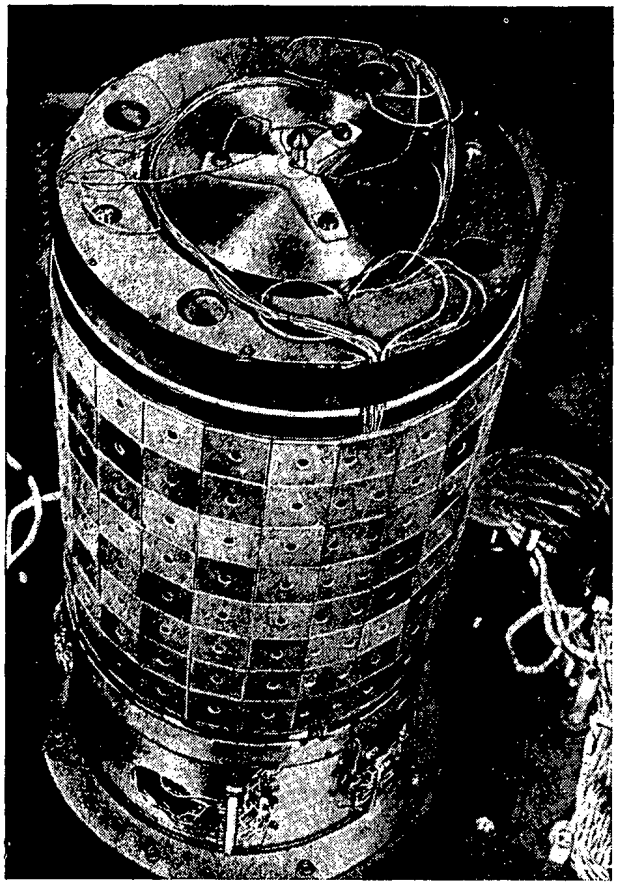

Fig. 1. General view of the reactor.

adjacent thereto. The reactor is of cylindrical form, comprising an active zone and a reflector; it is disposed vertically.

The active zone of the reactor is made up of fuel elements, each of which comprises a graphite body and uranium dicarbide plates with 90% enrichment with respect to $U^{235}$. The total weight of $U^{235}$ in the active zone is 49 kg. The radial reflector is composed of coaxially-disposed beryllium and graphite elements. The end reflectors are made of metallic beryllium. To reduce the leakage of heat through the ends of the reactor, thermal insulation is applied.

The control system of the reactor consists of four rods, set in the radial beryllium reflector, and the lower end reflector. An AC (automatic control) rod, consisting of beryllium and beryllium oxide in a stainless-steel shell, effects the automatic control of the reactor. Hand control is effected by the motion of HC (hand control) rods comprising a scattering section based on beryllium oxide and an absorbing section based on a boron-containing alloy. The temperature effect is compensated by motion of the lower end reflector. For emergency protection of the reactor, two scram rods (SR) are used; these are set in the radial reflector and the lower end reflector. In construction the SR are similar to the HC rods. All the control devices, apart from the automatic-control AC rod, are driven by a hydraulic system. The AC rod is moved by a servomechanism, electrically driven. The drive mechanism for the control and protection devices is disposed underneath the reactor body.

The thermoelectric converter used in the system comprises thermoelements based on a germanium-silicon alloy. The thermoelements comprise two thermopiles with n- and p-type conductivity connected on the hot side by a switching plate. On the cold side the individual couples of the thermopiles are switched into a single circuit. The whole thermoelectric converter is divided into four groups of thermoelements, each of which has independent power leads. Thus the construction of the converter part of the system enables us to study the characteristics of individual groups as well as the whole converter for either series or parallel connection of the groups. Inside each of the four groups of the converter, the thermoelements are switched in series into four parallel circuits. The general view of the converter appears in Fig. 2.

Below we present the main parameters of the reactor-converter:

Thermal-Energy Parameters of the System

| | |
|---|---|
| Electrical power, kW [1] | 0.50-0.80 |
| Total thermal power, kW [2] | 40 |
| Maximum temperature of beryllium reflector, °C | 1200 |
| Maximum temperature of outer surface of Be reflector, °C | 980 |
| Mean temperature of base of radiating fins, °C | 550 |
| Maximum temperature of $UC_2$ fuel elements, °C | 1900 |

Neutron-Physical Characteristics of the Reactor

| | |
|---|---|
| Charge of $U^{235}$, kg | 49 |

[1] Depending on the temperature conditions.
[2] Allowing for leakage.

| | |
|---|---|
| Efficiency, %: | |
| AC rods | 0.2 |
| HC rods | 0.4 |
| Scram rods | 0.4 |
| All control rods | 1.4 |
| Movable end reflector | 3.5 |
| Total neutron flux, neutrons/cm$^2$·sec: | |
| In center of active zone | $10^{13}$ |
| At active-zone boundary | $7 \cdot 10^{12}$ |
| Leakage of neutrons from reactor, neutrons/cm$^2$·sec | $3 \cdot 10^{11}$ |

## Choice of Parameters for the System

The power potentialities of a reactor-converter without a heat-carrier are determined by the limiting characteristics of the materials used, the dimensions of its main elements and their structural arrangement. The close interconnection between these parameters demanded the execution of a wide range of theoretical computations and experimental work on thermophysical and neutron-physical aspects and properties of matter, all directed towards finding the optimum characteristics of the apparatus and a basis for the efficiency of its components.

Thermal-Energy Calculations. The electrical power of the system is ultimately determined by the thermal conditions of the converter, its structural parameters, and the physical properties of the materials. An expression describing the electrical power may be written in the form

$$W = \frac{M}{(1+M)^2} \cdot \frac{1 - \frac{r_s s}{l(\varrho_1+\varrho_2)} - \frac{2\varkappa_3 s_3}{s(\varkappa_1+\varkappa_2)}}{1 + \frac{2Q_T l\alpha^2\left[\frac{1}{M+1}\cdot\frac{T_H}{T_H-T_C} - \frac{1}{2}\frac{1}{(M+1)^2}\right]}{nms(\varrho_1+\varrho_2)(\varkappa_1+\varkappa_2)}} \cdot \frac{\sum_{i=1}^{n_s}\sum_{k=1}^{n_s}\alpha_i\alpha_k Q_i Q_k}{(\varkappa_1+\varkappa_2)^2\frac{s}{m}\sum_i n_i(\varrho_{1i}+\varrho_{2i})},$$

where $Q_i$ is the thermal flux through the i-th zone, $Q_T$ the total thermal flux through the converter, $\varkappa$ the thermal conductivity, $\rho$ the specific electrical resistance, $\alpha$ the thermo-emf coefficient, $l$ the length of a thermopile, s the

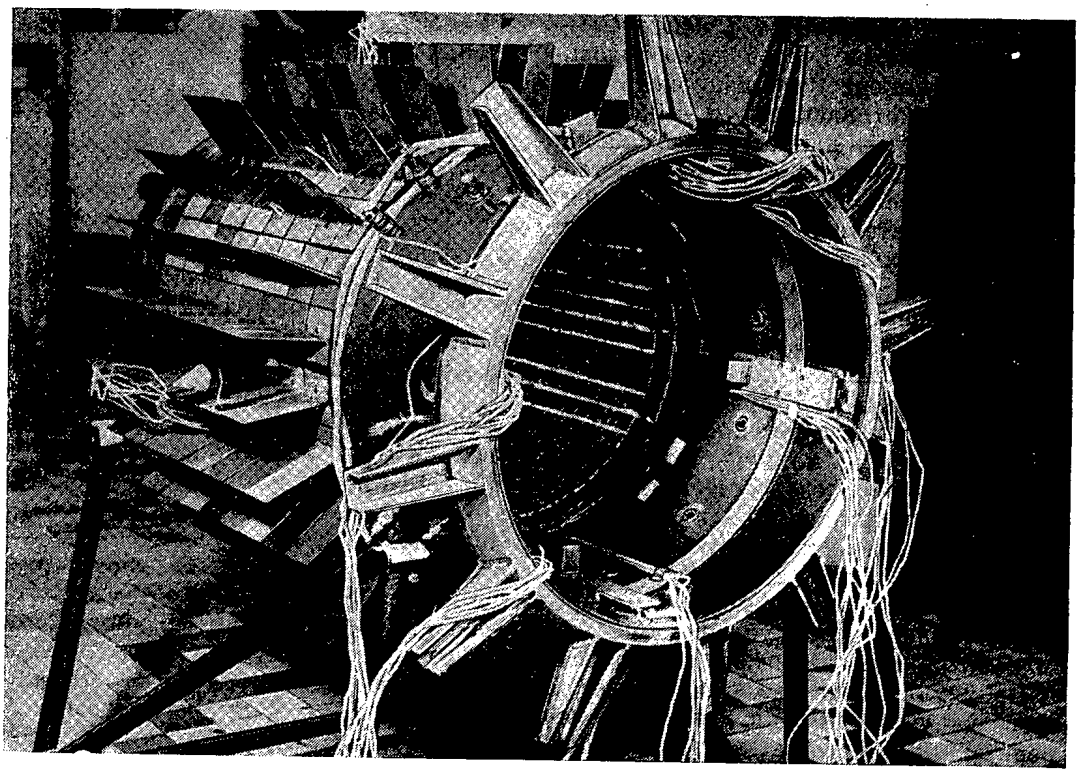

Fig. 2. General view of thermoelectric converter.

cross section of the thermopiles, $s_3$ the cross section of the thermal insulation between the piles, $n_s$ the number of zones, $n_z$ the number of series-connected couples, m the number of parallel-connected couples, $T_H$ and $T_C$ the temperatures of the hot and cold junctions of the semiconductors, $r_s$ the switching resistance of one thermocouple, and M the ratio of the external-load resistance to the internal resistance of the converter. (Indices 1 and 2 relate to semiconducting material of the n and p types; i or k gives the zone numbers.)

Nonuniformity in the distribution of temperatures and thermal flux over the outer surface of the radial reflector is taken into account in this formula in an approximate fashion by dividing the converter vertically into annular zones, the thermal conditions being considered constant over each. The influence of nonuniformity in the Joule and Peltier effects is neglected.

A characteristic of the system is the fact that the operating conditions of the converter, and hence also its electrical power output, are determined by the attainable level of temperature in the individual elements of the reactor and converter elements and the possibility of heat loss by radiation. In view of this, it was necessary, in order to determine the power parameters of the system, to make a thermal calculation of the reactor-converter system as a whole.

The problem of determining the temperature in the active zone, the reflector, and the converter, reduces to solving the heat-conduction equations in a multizone system with nonlinear boundary conditions, describing the transfer of heat by radiation. Numerical solution of these equations was effected on an electronic computer.

The distribution of temperature in the radial reflector for one operating condition is shown in Fig. 3.

The elements of the active zone of the reactor are in stressed conditions both with respect to temperature level and the temperature drops determining the thermal stresses. In this connection we solved the problem of the influence of possible breaks in the continuity of the fuel element on the temperature rise in the active zone. This was done by electrically simulating the temperature fields on conducting paper.

In the system considered, the heat which has passed through the converter is carried away by radiation. The maximum heat removal from the surface, for a given mean temperature of the cold layers of the converter, secures the greatest electrical power, other conditions being equal. In order to find the optimum form of the radiating surface (number of fins, size, shape), we solved a system of integrodifferential equations describing the distribution of temperature in the fins, allowing for the mutual irradiation of the elements and for thermal conduction. Figure 4 shows the heat removal as a function of the weight and number of fins.

Allowing for the results of the thermal calculations of the system, the electrical power was determined as a function of the thermal power passing through the converter on varying the quality factor of the thermoelement.

Neutron-Physical Calculations. The neutron-physical characteristics of the reactor were calculated on an electronic computer using the multigroup method of statistical tests (Monte-Carlo method). Use of this method in the present case enabled us reliably to allow for the geometric and physical features of the system associated with the heterogeneous structure of the active zone, the presence of channels and gaps of complex configuration, the sharply inhomogeneous physical properties of the materials of the active zone and the reflector, the specific system of reactor control, and so forth. In the calculations we used the multigroup (21 groups) system of constants which allows for the resonance structure of the $U^{238}$ cross section, the (n, 2n) reaction for beryllium, and inelastic transitions in the first nine groups. In the course of the calculation, some 50,000 neutron histories were traced.

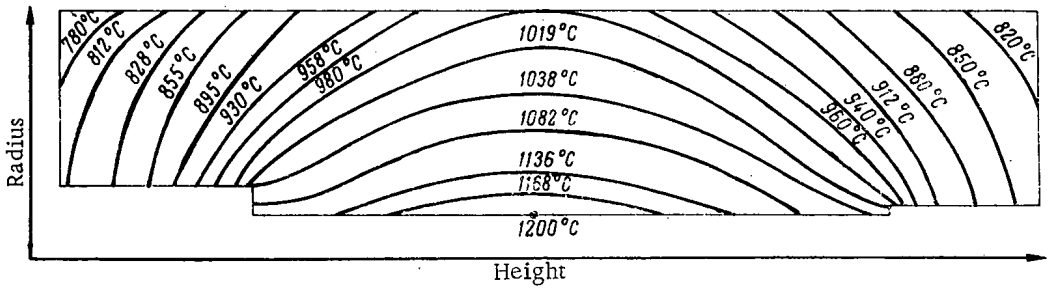


Fig. 3. Distribution of temperature over the cross section of the radial reflector.

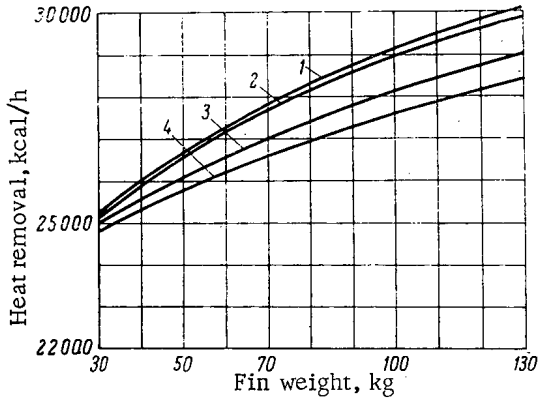


Fig. 4. Variation of heat removal with fin weight (temperature at the base of the fins 600°C): 1) 6 fins; 2) 9 fins; 3) 18 fins; 4) 36 fins.

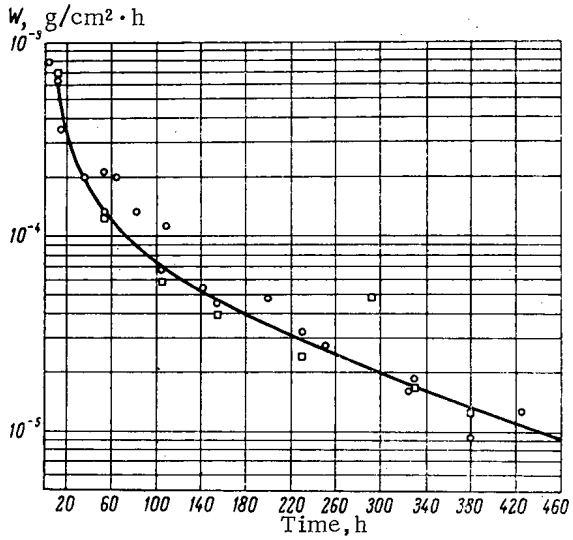


Fig. 5. Evaporation rate w of uranium dicarbide in an inert medium at t = 2000°C (different points, different samples). Data of L. K. Mizrakhi and Yu. M. Utkin.

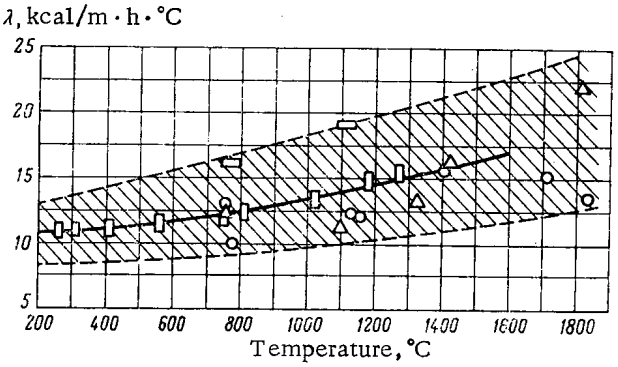


Fig. 6. Thermal conductivity of uranium carbide as a function of temperature (different points, different samples). Data of A. G. Kharlamov.

Experimental Study of the Characteristics of Elements of the System. In order to gain a basis for the projected parameters of the system, we made experimental thermophysical and metallophysical studies of its materials and components.

We studied the contact interaction of the uranium dicarbide with graphite and the volatility of uranium dicarbide in an inert medium and in vacuum at temperatures up to 2000°C (Fig. 5). We examined the temperature dependence of the thermal conductivity of uranium dicarbide (Fig. 6), the linear-expansion coefficient, and other characteristics, over a wide temperature range. Together with a study of the thermal-strength characteristics of uranium dicarbide, tests on mockup fuel elements, and loop tests of uranium-carbide samples, these demonstrated the efficiency of the fuel elements in working conditions.

The use of a beryllium reflector, working at large thermal fluxes in a temperature range close to the melting point, in the reactor demanded an experimental study of the interaction between metallic beryllium and various structural materials, the thermal conductivity of beryllium, and its deformability and thermal strength.

In order to reduce the heat leakage through the ends of the reactor and between the thermoelements of the converter, high-temperature thermal insulation was used in the system. In connection with this, we studied the thermal conductivity of the thermal insulation in various media at working temperature.

One of the important aspects of the investigation was the efficiency of the thermoelectric-converter elements in neutron and $\gamma$-radiation fluxes. Repeated many-hour tests of the thermoelements in the loops of the RFT (Physical and Technical Research) reactor at total neutron fluxes of $3 \cdot 10^{19}$ thermal neutrons/cm$^2$ led to the conclusion that the main properties of the thermoelements varied within permissible limits (Fig. 7).

## Test-Bed Studies of the Neutron-Physical and Thermal-Power Characteristics of the System

Study of Neutron-Physical Characteristics. Five different arrangements were set up, differing in the concentration of the fissile material. For each arrangement we made a series of investigations embracing a wide range of questions: the dependence of the critical loadings on the composition of the active zone, the efficiency of the reflectors

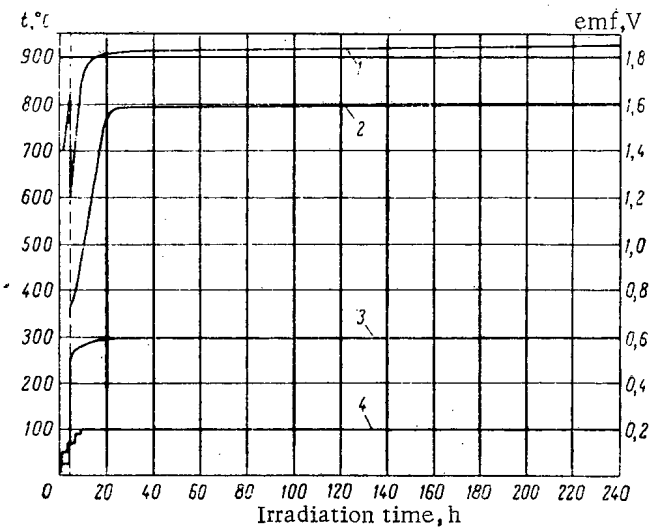


Fig. 7. Variation in the main parameters of the semiconductor thermoelements during reactor irradiation (maximum total neutron flux $\sim 3 \cdot 10^{19}$ neutron/cm$^2$). Data of G. M. Pavlov. 1) Temperature of hot junction; 2) thermo-emf of section; 3) temperature drop in thermoelements; 4) reactor power.

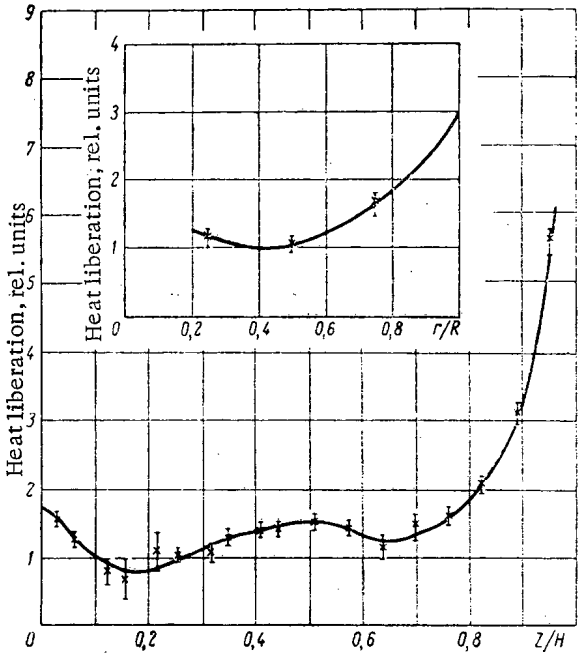


Fig. 8. Relative distribution of heat liberation over the radius and height of the active zone (R and H = radius of active zone; r and z are coordinates). Data of A. M. Krutov.

and control mechanisms, the distribution of heat evolution in the active zone, the effect of structural gaps on the reactivity, and so forth.

Great attention was paid to studying the effect of moving the lower end reflector and shaping the active zone on the neutron-physical characteristics of the reactor system, and also to examining the efficiency of the control rods and the heat liberation fields. Some of the results obtained appear in Fig. 8, which shows the distribution of heat liberation over the radius and height of the active zone. The reactivity in all these cases was measured by different methods: from the acceleration period, and pulse and integral methods.

Comparison between the results of measuring activity by different methods enabled us to estimate the effectiveness of delayed photoneutrons due to the presence of the beryllium reflector. It was established that in reactors of this type photoneutrons are practically absent, and that for analyzing the experimental results the characteristics of six groups of delayed neutrons may be used.

Study of the Thermal-Energy Characteristics. The final stage of testing the reactor-converter on a full-scale test-bed was preceded by complex tests of a full-scale thermal model of the reactor-converter on an electric-heating bed. The aim of these tests was to check the efficiency of the whole system and its individual components, and also to study the working parameters in the steady and nonsteady states.

During the tests, the temperature fields in various elements of the system were constantly measured. For this purpose, 53 tungsten-rhenium and 86 Chromel-Alumel thermocouples were set in the reactor and converter.

The electrical characteristics of the converter were measured by means of a special electric panel, which made it possible, first, for each of the four groups of thermocouples, to vary the load smoothly from 0.1 to 10 Ω and make measurements of emf, short-circuit current, working current, and voltage, and secondly, to make electrical measurements not only separately in the groups but also with the groups connected in series or parallel. The electrical power of the converter was determined in the maximum-power condition. In the nominal condition the apparatus was tested more than 1000 h.

Analysis of the results of testing the system led to the conclusion that all the main components of the reactor-converter were very efficient. The characteristics of the system were quite stable over the whole testing period. The thermo-emf of the converter remained practically constant over the whole test. Toward the end of the testing,

a certain rise in the internal resistance of the converter was noted, in association with which the electrical power taken from the converter (in the maximum-power condition) fell on average by 10%.

The tests made enabled us to study and demonstrate the efficiency of the active zone, the reflector, and the converter in operating conditions.

# DEVELOPMENT OF SUPERHEATING POWER REACTORS OF THE BELOYARSK NUCLEAR POWER STATION TYPE*

N. A. Dollezhal', I. Ya. Emel'yanov, P. I. Aleshchenkov, A. D. Zhirnov, G. A. Zvereva, N. G. Morgunov, Yu. I. Mityaev, G. D. Knyazeva, K. A. Kryukov, V. N. Smolin, L. I. Lunina, V. I. Kononov, and V. A. Petrov

Translated from Atomnaya Énergiya, Vol. 17, No. 5, pp. 335-344, November, 1964

## Introduction

Ever increasing needs for electrical power have promoted an increase in the rates of development of energy production. It was found to be most profitable to construct installations with a high unit out.

At present in the Soviet Union, turbounits, which operate on various steam parameters, are planned and manufactured (Table 1).

TABLE 1. Steam Parameters and Outputs of Turbogenerators, in Production and Planned, within the Soviet Union

| Steam parameters prior to turbine | | Electrical output, MW |
|---|---|---|
| pressure, atm. | temperature, °C | |
| 90 | 535 | 100 |
| 130 | 565/565 | 105, 200 |
| 240 | 580/565 | 300, 500, 800, 1000 |

As can be seen from Table 1 an increase in output of the turbounit is associated with an increase of temperature and pressure of the steam used.

Progress in nuclear power development, as well as in conventional power engineering, is based on construction of nuclear power stations with a high-unit output. It is therefore advantageous to install power reactors which will ensure the generation of steam with high parameters, thus enabling the high-output turbounits, which are being manufactured and developed, to be used and which will ensure a high efficiency for the nuclear power station.

Uranium-graphite channel-type uncased reactors meet the stated requirements completely. These reactors are similar to the superheating nuclear steam reactors of the Beloyarsk Nuclear Power Station. A channel-type reactor has been operated successfully in the First Nuclear Power Station in the USSR [1]. Of the two Beloyarsk reactors, the first is at the stage of startup with the planned parameters and the second is at the assembly stage. A description of the design of the first reactor was presented in a report at the Second International Conference on the Peaceful Uses of Atomic Energy [2], and a report is devoted to its startup and adjustment at the present Conference [3]. The steam parameters, generated by the Beloyarsk nuclear power station reactors, are 90 atm and 500°C.

Planning studies show that the most advantageous development for the reactors being considered is the transition from high-steam parameters directly to the use of supercritical parameters with a straight-through system of coolant utilization. On the contrary, as will be shown below, the use of turbounits at a pressure of 130 atm and with intermediate steam superheating is less advantageous.

## Technological Flowsheet Development

The choice of a proper flowsheet is of importance when constructing high-power plants. The principal criteria in choosing nuclear power station designs, just as in conventional thermal power installations, are reliability, simplicity, and efficiency. In addition, a particular demand is imposed by the leak-tightness of the loops in the nuclear power station water cycle.

The correct choice of the technological flowsheet, in conjunction with the constructive solution of problems associated with the temperature operating regime of the channels, allows its output to be increased considerably

* Paper No. 309, presented by the USSR at the Third International Conference on the Peaceful Uses of Atomic Energy, Geneva, 1964.

without increasing the over-all size of the reactor, just as was achieved in the second Beloyarsk nuclear power station reactor, whose output was increased by a factor of two compared with the first reactor.

Figure 1 shows several possible technological flowsheets for uranium-graphite reactors of the channel type.

Figure 1a represents the flowsheet of the first Beloyarsk NPS reactor with an electrical output of 100 MW. Figures 1b and 1c show the flowsheet of the second Beloyarsk NPS reactor with and without steam scrubbing. These designs, with certain structural changes in the channels, have enabled the electrical output of the reactor to be increased to 200 MW. Figures 1d-1g show possible designs for operating a reactor installation with supercritical steam parameters, thus allowing its power to be increased to 800-1000 MW. These designs are considered in detail below. Naturally, the straight-through design of reactor unit is considerably more simple and inexpensive than the multiloop design, which requires additional cumbersome and expensive heat exchangers, separators, circulating pumps with the framework for their conduits and fixtures, and also higher coolant parameters. By the use of a design with nuclear steam superheating and especially a straight-through design, radiation safety of the maintenance sections of the station and in particular the turbounits is ensured. From this point of view it is impossible not to notice the advantages of the Beloyarsk NPS reactors.

By using reactors of this type, the radiation environment in the technological flowsheet rooms is determined by the salt and oxygen activity of the coolant, since the tubular design of the fuel elements in the event of damage excludes the possibility of fission fragments getting into the coolant. Tests carried out on the First Nuclear Power Station have shown that from the point of view of activity the use of superheated steam in the reactor is entirely possible under conditions of good quality water in the separators and reliable separation of the steam produced [4]. These requirements are guaranteed relatively simply in the first Beloyarsk NPS reactor. In the second reactor, because of the repeated circulation of the water, a buildup of salt activity is possible in the steam separators and also its subsequent introduction by the steam into the steam superheating channels and into the turbine. Consequently, in the second reactor provision has been made for specially careful cleaning of the circuit to remove salt and corrosion products: Ionite filters are installed after the turbine condenser, the purging of water from the steam separators has been increased and increased demands are also imposed on the quality of the makeup water and the compactness of the tubular plates of the condenser.

The measures ennumerated are necessary to an even greater degree as a result of using straight-through systems.

The increase of output of the reactor above 200-300 MW with conservation of its dimensions and superheated steam pressures of 90 or 100 atm is not sufficiently economical, since in this case either the most efficient operating circuit of one reactor with a single turbine (or as a last resort, with two) must be rejected or the turbine must be used with intermediate steam heating. In addition to the complexity of the installation and maintenance of the power station, in this case the size of the conduits is increased, additional heat exchangers emerge, the separators are considerably increased in cost and the resistance of the multicirculation circuit is increased. The increase of the surface area of the intermediate superheaters leads not only to their increased cost but also to an increase in the content of corrosion products in the circuit, which causes deterioration of the water cycle of the installation. The reactor power may be significantly increased by transition to supercritical steam parameters. In this case, the technological layout of the installation is considerably simplified since the necessity for coolant and circulatory pumps in the multicirculation loop is removed and also separators are eliminated. By using a coolant of supercritical parameters the limitations associated with crises in heat transfer and with the appearance of hydrodynamic instabilities in the operating channels are removed.

Figure 1d shows one of the possible schematic layouts for a nuclear power station operating on supercritical steam parameters. Feed water from the de-aerator is fed to the channels of the first group, producing superheated steam, part of which is fed to the external intermediate superheater and the other part is led off via a throttling unit to the main steam pipe and is then directed into the turbine. From the intermediate superheater, steam at supercritical pressure is directed into the second group of reactor operating channels and is superheated in them to a specified temperature and also enters the turbine. In order to increase the reliability of operation of the equipment in the transition regimes, a temperature regulator has been provided after the intermediate steam superheater.

Figure 1e shows the layout of an energy generating installation similar to the one being considered but without high-pressure preheating, which can be excluded to reduce corrosion products in the circuit. As a result of giving up high-pressure regeneration the efficiency of the unit is reduced by approximately 1.5% in comparison with the efficiency of the unit operating on the scheme depicted in Fig. 1d, but in this case the water cycle of the station is considerably improved.

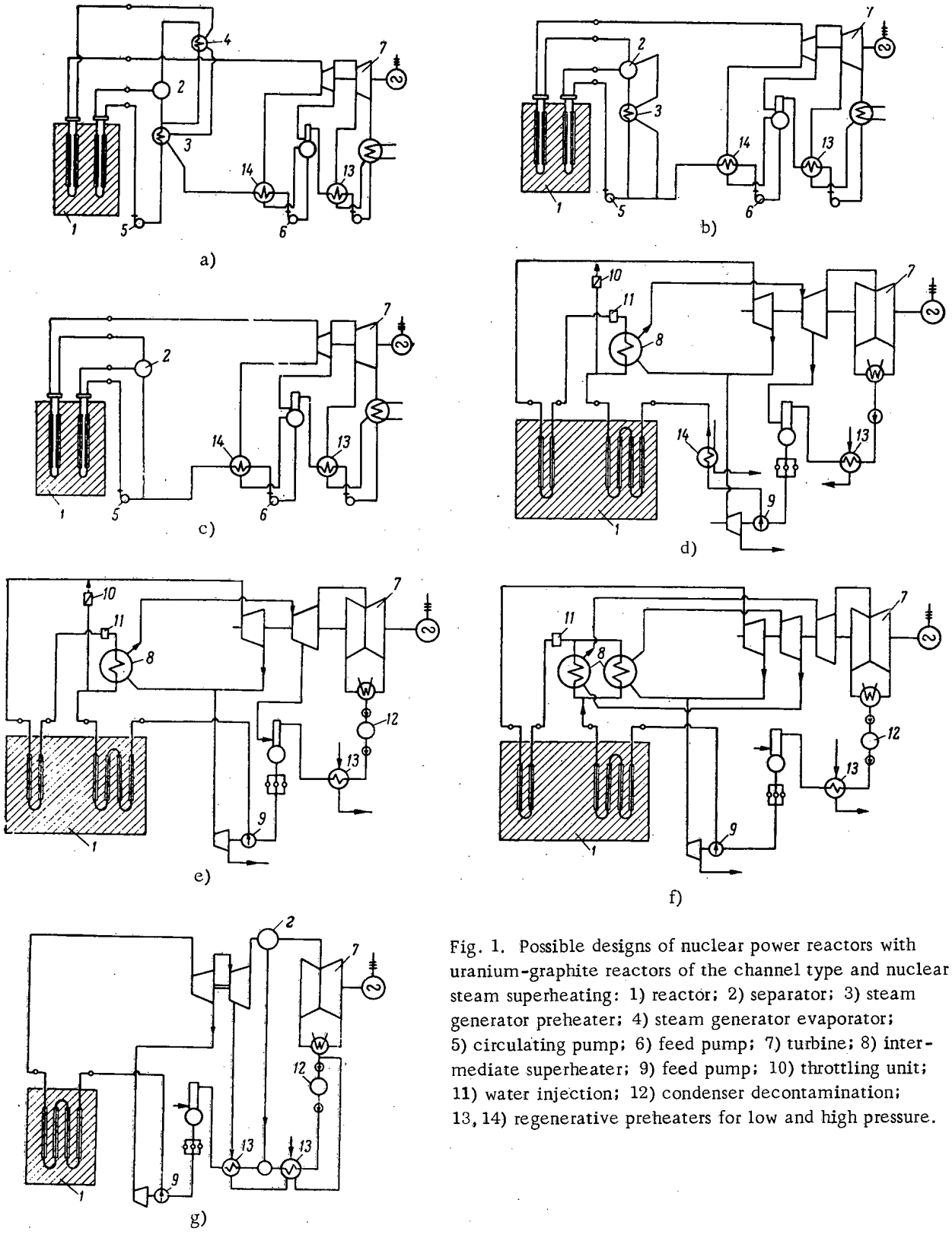


Fig. 1. Possible designs of nuclear power reactors with uranium-graphite reactors of the channel type and nuclear steam superheating: 1) reactor; 2) separator; 3) steam generator preheater; 4) steam generator evaporator; 5) circulating pump; 6) feed pump; 7) turbine; 8) intermediate superheater; 9) feed pump; 10) throttling unit; 11) water injection; 12) condenser decontamination; 13, 14) regenerative preheaters for low and high pressure.

Figure 1f shows an arrangement with a turbine which has two intermediate steam superheaters. In this arrangement, the requirement for steam superheating in the throttling section after the first group of operating channels is eliminated. All the steam passes from the intermediate superheaters to the second group of channels and then to the turbine.

The most promising arrangement for a nuclear power station with supercritical parameters is the once-through arrangement with a single group of operating channels and without intermediate steam superheating (see Fig. 1g). The turbounit used in this arrangement consists of three stages: The first stage uses steam with supercritical parameters and the two subsequent stages operate on saturated steam. A separator is necessary for removing moisture from the steam at the entrance to the low-pressure cylinder.

Of course, the arrangements which have been considered for uranium-graphite reactors of the channel type and with supercritical steam parameters do not exhaust all the possibilities for developing nuclear power stations in this direction. The increase in unit power and the correct choice of flowsheet of the power generation equipment have a considerable effect on the efficiency index of a nuclear power station, firstly on the cost per kilowatt. The reactor output is directly connected with the operating cycles of the evaporative and steam superheating channels which will be considered below.

## Operating Cycle of the Evaporative Channels

A safe operating cycle for the evaporative channels can be accomplished by ensuring reliable and trouble-free cooling of the fuel elements and the elimination of interchannel and intrachannel fluctuations in the coolant supply. In designing the first reactor for the Beloyarsk Nuclear Power Station, experiments were carried out to study water boiling regimes in small diameter tubes [2].

For the second reactor, because of the increase in power, the internal diameter of the fuel element tubes was increased from 8.2 to 10.8 mm, which necessitated additional tests to determine the possibility of crisis-free boiling of water in tubes of small diameter.

The experiments were carried out in an electrically heated arrangement of tubes of 10.4 mm diameter and 3.8 m length. The relationship between the steam content at the site of origination of a heat transfer crisis and the mass velocity for various thermal fluxes and a pressure of 150 atm are shown in Fig. 2. A heat transfer crisis for the experiments was organized by a stepwise increase of temperature of the tube wall.

Investigations, carried out at different pressures and identical thermal loadings, steam content, and coolant mass flow velocities, showed that the temperature increase of the wall as a result of a crisis is higher, the lower the pressure of the coolant. At the same time, it was established that by reducing the pressure of the coolant the critical steam content increases.

In addition, a test rig simulating the technological flowsheet of the second Beloyarsk nuclear power station reactor and electrically heated channels were used to investigate the hydrodynamic stability of coolant flow rate along parallel channel tubes in the boiling regime at pressures of 20-150 atm; the coolant flow rate through the channel was 500-5000 kg/h and the channel power was 50-800 kW.

Pulsations of the flow rate were observed in the experiments, in the region of low (up to 5 wt.%) and high (above 40 wt.%) steam content. In the latter case, the pulsations ceased with increase of flow rate of pressure. Thus, with a coolant feed of about 1500 kg/h, a pressure of 40 atm and a power of 400 kW the pulsations in the coolant feed began at a steam content of about 40 wt.%, and for a pressure of 60 atm and the same conditions the pulsations began at a steam content of 80 wt.%.

It followed from the experiments that the pulsations in the coolant supply in the region of high-steam content do not present a danger for reactors of the Beloyarsk nuclear power station type, since the nominal pressure in the evaporative loop is not less than 90 atm and the steam content at the channel output is not greater than 35 wt.%.

Figure 3 shows the experimental curves obtained on the test rig and which delimit the region of hydrodynamic stability of the interchannel coolant flowrates and the region of interchannel pulsations originating in the evaporative channels with low steam contents of the coolant. The curves are drawn as functions of the flow rate and pressure of the coolant for a different power of the evaporative channels. The curves shown in Fig. 4 also define the regions of stable and unstable interchannel coolant flow rates, but as a function of various flow rates and steam contents of the coolant at the channel output as a result of varying its power from 50 to 800 kW. In plotting the curves,

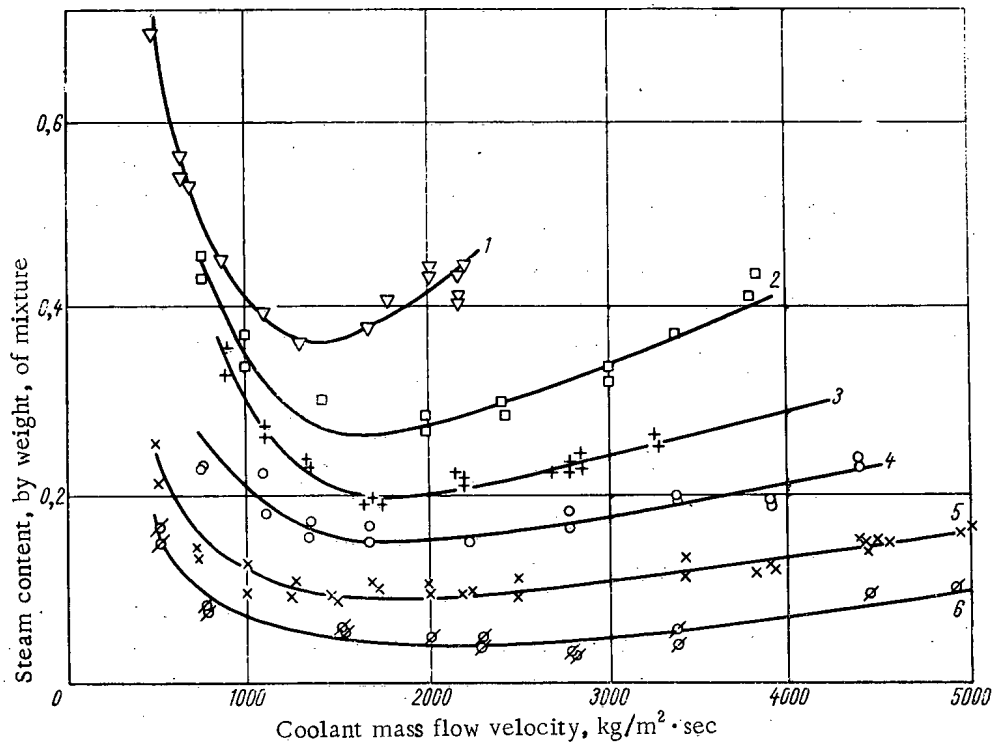


Fig. 2. Relationship between critical steam content by weight and the coolant mass flow rate at constant specific thermal loading for the following thermal flux values, kcal/m$^2$ · h: 1) 0.31 · 10$^6$; 2) 0.45 · 10$^6$; 3) 0.64 · 10$^6$; 4) 0.94 · 10$^6$; 5) 1.28 · 10$^6$; 6) 1.62 · 10$^6$.

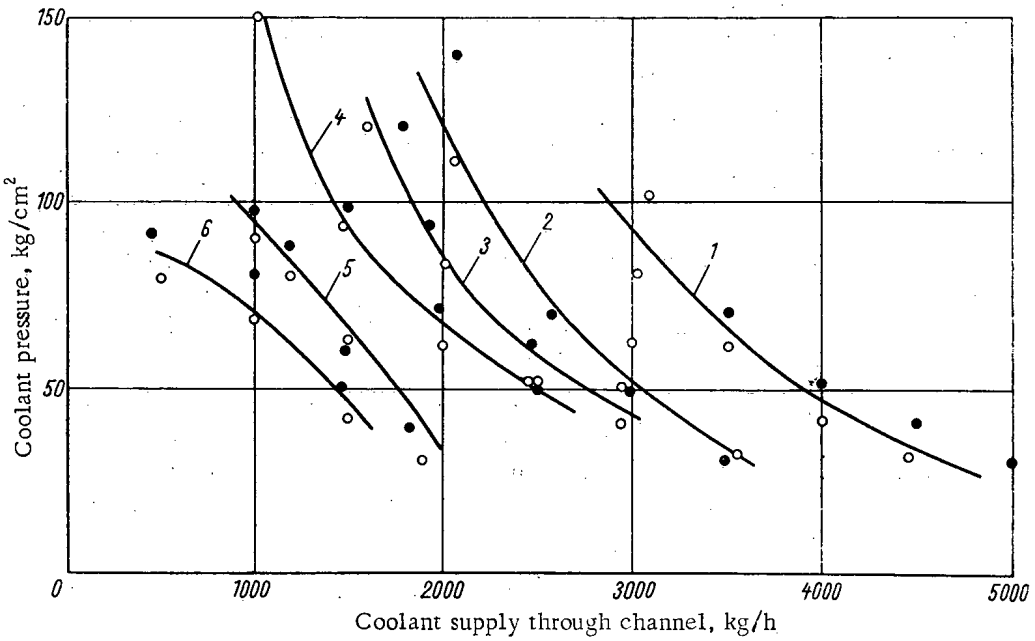


Fig. 3. Curves, delimiting regions of stable and unstable interchannel coolant flow rates as a function of the pressure and flow rate of coolant through the channel for different power outputs, kW: 1) 800; 2) 400; 3) 300; 4) 200; 5) 100; 6) 50. The black points correspond to regimes without pulsation.

it was observed that their position is almost independent of the coolant pressure. The regions of stable channel flow rates are found to be higher, in Fig. 3 as well as in Fig. 4, than the corresponding curves for the evaporating channel. It follows from Figs. 3 and 4 that with increase in the channel power the stable flow-rate region decreases.

TABLE 2. Evaporative Channel Characteristics

| Characteristic | Reactor of the First Nuclear Power Station | First reactor of the Beloyarsk Nuclear Power Station | Second reactor of the Beloyarsk Nuclear Power Station | | | | |
|---|---|---|---|---|---|---|---|
| | | | I zone | II zone | III zone | IV zone | V zone |
| Channel power, kW | 300 | 405 | 771 | 634 | 617 | 545 | 517 |
| Coolant supply through channel, kg/h | 2500 | 2400 | 5500 | 4700 | 4150 | 3550 | 3250 |
| Steam content at exit from reactor, % | — | 33.6 | 27.6 | 29.3 | 30.5 | 32.1 | 34.2 |
| Pressure at inlet to channel, atm | 100 | 155 | 155 | 155 | 155 | 155 | 155 |
| Pressure at exit from channel, atm | 98 | 150 | 145 | 145 | 145 | 145 | 145 |
| Coolant temperature at channel inlet, °C | 200 | 300 | 303 | 303 | 303 | 303 | 303 |
| Coolant temperature at exit from channel, °C | 290 | 335 | 338 | 338 | 338 | 338 | 338 |
| Maximum thermal loading, $kcal/m^2 \cdot h \cdot 10^{-6}$ | 1.8 | 0.5 | 0.8 | 0.7 | 0.6 | 0.5 | 0.5 |
| Circulation velocity, m/sec | 4 | 3.5 | 4.6 | 4.0 | 3.5 | 3.0 | 2.7 |
| Maximum temperature, °C: | | | | | | | |
| of tube inner wall | 324 | 355 | | | 365 | | |
| of nuclear fuel | 382 | 400 | | | 415 | | |
| Minimum reserve prior to critical thermal loading | — | 2 | 1.85 | 1.9 | 1.9 | 2.0 | 1.95 |

TABLE 3. Characteristics of the Steam Superheating Channels

| Characteristic | First reactor of Beloyarsk NPS | Second reactor of Beloyarsk NPS | |
|---|---|---|---|
| | | descending fuel elements | ascending fuel elements |
| Maximum channel power, kW | 368 | 767 | 767 |
| Minimum channel power, kW | 202 | 548 | 548 |
| Steam supply through channel with maximum power, kg/h | 1900 | 3600 | 3600 |
| Steam supply through channel with minimum power, kg/h | 1040 | 2570 | 2570 |
| Pressure at channel inlet, atm | 110 | 132 | 124 |
| Pressure at channel outlet, atm | 100 | 125 | 110 |
| Channel inlet temperature of steam, °C | 316 | 328 | 397 |
| Channel outlet temperature of steam, °C | 510 | 399 | 508 |
| Maximum thermal loading, $kcal/m^2 \cdot h \cdot 10^{-6}$ | 0.48 | 0.82 | 0.68 |
| Maximum steam velocity, m/sec | 57 | 76 | 112 |
| Maximum temperature, °C: | | | |
| of tube inner wall | 530 | 426 | 531 |
| of nuclear fuel | 550 | 482 | 565 |
| of graphite | 725 | — | 735 |

As a result of the origination of interchannel coolant flow rate pulsations, fluctuations of tube temperatures were observed, which coincided in frequency with the flow fluctuations. With increase of pressure, the amplitude of the temperature and coolant flow rate fluctuations was reduced. This same effect was observed by reducing the thermal loading or increasing the supply of coolant through the channels. Thus, at a coolant pressure of 50 atm and a channel power of 200 kW, the amplitude of the tube temperature fluctuations with a coolant feed of 1000 kg/h amounts to 65°C, and with a coolant feed of 1500 kg/h it is only 30°C.

The experiments carried out to determine the conditions of origination of heat exchange crises and coolant feed pulsations have enabled the operating regimes of the evaporative channels to be chosen correctly as far as their operating conditions and their possibilities are concerned. The distribution of coolant supplies in this reactor is not accomplished proportionately with the channel power, but such that identical reserves are ensured prior to a thermal

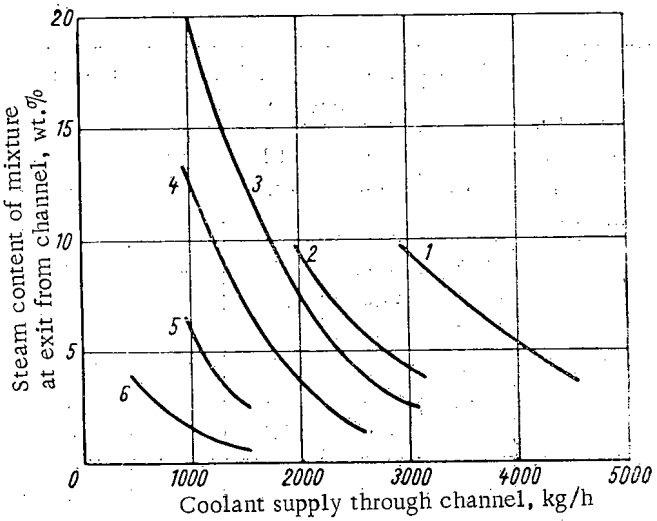


Fig. 4. Averaged curves, delimiting regions of stable and unstable interchannel flow rates as a function of steam content by weight and the flow of coolant through the channel at various power outputs, kW: 1) 800; 2) 400; 3) 300; 4) 200; 5) 100; 6) 50. (The curves are plotted according to the results of steam content determination corresponding to regimes without pulsation, for different pressures and flow rates of coolant.)

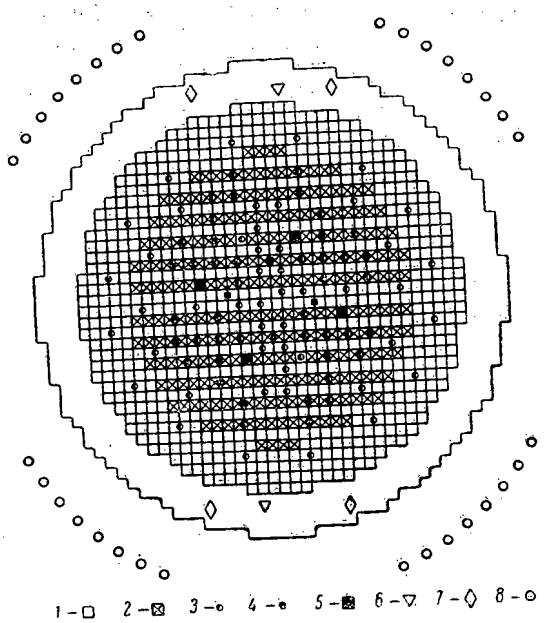


Fig. 6. Diagram of channel arrangement: 1) operating evaporative channels (732); 2) operating steam superheating channels (266); 3) compensating rod channels (80); 4) channels for shut-off rods (16); 5) automatic control rod channels (4); 6) channels for counting chambers (2); 7) channels for triggering chambers (4); 8) ionization chamber channels (30).

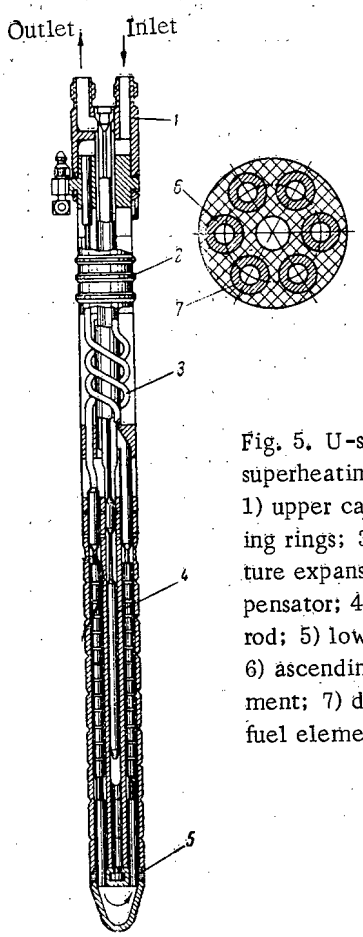


Fig. 5. U-shaped steam superheating channel: 1) upper cap; 2) sealing rings; 3) temperature expansion compensator; 4) absorbing rod; 5) lower cap; 6) ascending fuel element; 7) descending fuel element

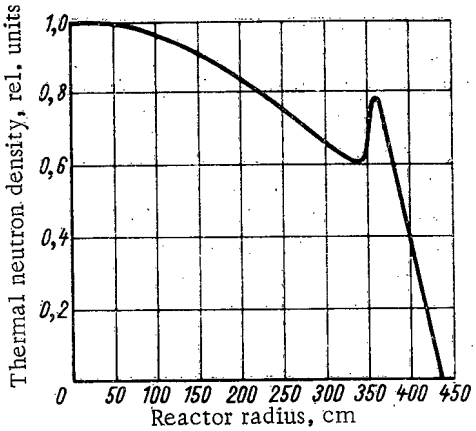


Fig. 7. Thermal neutron distribution along the reactor radius.

excursion in the most dangerous section of the channel, taking account of the change of the steam content and the thermal loading throughout the channel height. This coolant supply distribution permits the average steam content at the exit from the reactor to be somewhat increased. Thus, for a steam content by weight at the exit from the most heavily loaded central evaporative channels of 27%, the steam content at the exit from the

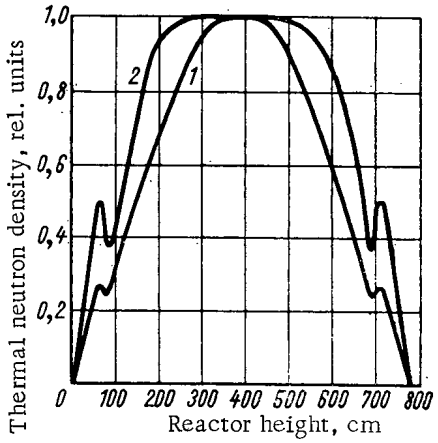


Fig. 8. Thermal neutron distribution throughout the height of the reactor. 1) At the start of the running period; 2) at the end of the running period.

peripheral channels can be increased to 35%, which permits an average steam content of 31% to be produced at the exit from the reactor.

In order to reduce the thermal loadings and to decrease the hydraulic resistance of the loop, fuel elements are used in the evaporative channels of the second Beloyarsk reactor which have internal tubes of larger diameter than the tubes of the evaporative elements of the first reactor. For an identical external diameter of 20 mm, the dimensions of the inner tubes of the evaporative fuel elements of the first reactor are 9.4×0.6 mm, and for the second reactor 12 × 0.6 mm. In the channels of the second reactor, the diameter of the central tube, through which the coolant supply is effected, has also been increased somewhat. In the remainder of the evaporative channel construction, the first and second Beloyarsk reactors are identical. Uranium-molybdenum alloy is used as nuclear fuel in the evaporative channels of both reactors, with a magnesium filler for obtaining thermal contact. The evaporative channel characteristics are shown in Table 2.

## Operating Regimes of the Steam Superheating Channels

The steam superheating channels are the most highly stressed elements of reactors with nuclear steam superheating, since they are operated at temperature conditions which are very high in comparison with the evaporative channels. The high operating temperatures of the steam superheating channels limit the choice of nuclear fuel and structural materials.

The design of the steam superheating channels in the Beloyarsk reactors differs somewhat from the design of the evaporative channels, although fuel elements of almost the same dimensions as in the evaporative channels are used here. The initial design of the steam superheating channels specified to the supply of steam through the central tube of the channel and it was heated by motion through six fuel elements. Subsequently, the so-called U-shaped design of the steam superheating channels was developed (Fig. 5). Its distinctive special feature consists in that it ensures sequential heating of the steam by its motion initially through three fuel elements downwards and then through the next three fuel elements upwards. The U-shaped design of the channels delimits the operating temperature conditions of the descending and ascending fuel elements and consequently permits the use of simpler down-leading elements and elements which are cheaper to manufacture than the evaporative channels. The use of channels of U-shaped design with sequential steam superheating also makes it possible to reduce the temperature of the graphite masonry of the reactor. Thus, as a result of transition from the initial design of the steam superheating channels to the U-shaped design, the temperature of the graphite block is reduced approximately by 100°C (with a channel power of 360 kW). Reduction of the temperature of the graphite is ensured by the fact that heat in the U-shaped channels, which is extracted from the graphite block is led off to the down-leading fuel elements which have a relatively low temperature. Reduction of the graphite temperature has a favorable effect on the operating conditions of the graphite as well as on the physical characteristics of the reactor which are improved somewhat as a result of reducing the temperature of the neutron gas. Finally, as a result of transition to the U-shaped steam superheating channels the central tube is eliminated which reduces the quantity in the active zone. In place of the central tube an absorbing rod with fine control, allowing the power of the operating channels to be trimmed within known limits is installed. The design of the ascending steam superheating elements and the fuel composition, based on uranium dioxide, guarantees heating of the steam to 500°C, which was confirmed by loop experiments in the reactor of the first nuclear power station [4].

Table 3 shows the characteristics of the steam superheating channels in the Beloyarsk Nuclear Power Station reactors.

The steam superheating channels of U-shaped design are a species of multipass channels, in which the coolant passes successively through a number of fuel elements. The sequential motion of the coolant ensures different operating temperature conditions for the fuel elements and permits these conditions to be varied within specified limits by the appropriate choice of the power of sequentially engaged elements. Thus, in the multipass channels the number of the most important and complex fuel elements, located only at the outlet section of the coolant flow is con-

siderably reduced. In the remaining sections of the coolant flow, simpler and more cheaply produced elements can be used. The most complete advantages of multipass channels are manifested as a result of transition to the once-through arrangement with supercritical steam parameters.

## Arrangement of the Operating Channels in the Reactor

Because operating channels of two types (evaporative and steam superheating) are used in the reactors of the Beloyarsk Nuclear Power Station, it is appropriate to discuss the question of their optimum disposition in the active zone. For the startup and cooling regimes of the reactor, the most favorable arrangement is the composite arrangement of channels of different type, since this ensures the return flow of heat from the steam superheating channels to the evaporative channels, which facilitates the operating conditions of these channels in these regimes. The arrangement of the steam superheating channels on the periphery of the active zone increases their number, but in return it reduces the loss of pressure in the steam circuit. The operating temperature conditions of the fuel elements and the graphite block depend weakly on the place of insertion of the channel. Thus, by installing the steam superheating channels of the first reactor of the Beloyarsk Nuclear Power Station in the center or at the periphery of the active zone, the maximum fuel element temperature should differ by only 20°C and the maximum temperature of the graphite block by 60°C.

In the second reactor of the Beloyarsk Nuclear Power Station a patterned central arrangement of the steam superheating channels has been adopted (Fig. 6), which with the use of fine control rods makes possible a balanced distribution of the energy release along the reactor radius. Nonuniformity of distribution of the energy release along the radius of the second reactor has been reduced to 1.3, while in the first reactor, it is 1.4. Figure 7 shows the thermal neutron distribution along the radius of the second reactor, which determines the energy release and which quite closely corresponds to the distribution established at the end of the running period because of nonuniformity of fuel burnup. Figure 8 shows the thermal neutron distribution throughout the height of the second Beloyarsk NPS reactor. The kink in the distribution curve at the end of the running period is due to nonuniformity of fuel burnup.

In reactors with supercritical coolant parameters and the once-through technological circuit, in which all the channels operate in identical regimes, the required distribution of energy release can be ensured by the appropriate spacing of the control rods and of the burnup absorber.

## Conclusions

Some possibilities have been discussed for developing uranium-graphite power reactors of the Beloyarsk Nuclear Power Station type with nuclear steam superheat. Thus, the transition from the double loop technological system of the first Beloyarsk reactor to a single loop system and some change in the design of the operating channels has enabled the power of the second reactor to be increased to 200 MW [5]. Even greater possibilities for reactors of this type are associated with the use of a coolant with supercritical parameters. In this case, the heat transfer and the hydrodynamics of the coolant flow are significantly improved which, combined with a straight-through technological system, will enable the net output of the reactor to be increased to 800-1000 MW with almost the same active zone dimensions as for the Beloyarsk NPS reactors. By using a straight-through technological system, the significantly greater advantages of multipass operating channels are revealed most completely from the point of view of the operating temperature conditions of the graphite masonry and the fuel elements as well as from the point of view of introducing a relatively small quantity of structural materials into the core. Calculations indicate that by using uranium of 5% enrichment, a fuel burnup can be guaranteed which is equivalent to an output of 40,000 to 45,000 MWD from a ton of uranium.

The increase in the unit power of the reactor, in the efficiency and uranium burnup will sharply improve the efficiency index of the nuclear power station with respect to cost per kW installed and also with respect to the cost of nuclear power sent out.

In uranium-graphite reactors of the channel type, a change in constitution of the active zone is easily accomplished, which is due to the interchangeability of the operating channels. This permits the use in subsequent reactor charges of more advanced operating channels and fuel elements, in particular it permits the use of low-absorption structural materials and fuel compositions with low nonproductive neutron absorption.

Since the active zone of the reactor is located in an airtight housing, it may affect the fragmentproof cladding of the fuel elements which, on the one hand makes it possible to remove gaseous fission products from the active zone and on the other hand leads to a significant reduction in the quantity of steel in the active zone (by ~30%).

It is obvious that this improves considerably the neutron balance and the other reactor characteristics which are associated with this.

Uranium-graphite reactors of the channel type are free from limitations associated with increase of power. Thus, as a result of increasing the diameter of the active zone by 35-40%, the output of a single reactor can be increased to 1500 MW.

## LITERATURE CITED

1. N. A. Dollezhal' et al., Proceedings of the Second International Conference on the Peaceful Uses of Atomic Energy; Report of the Soviet Scientists, 2, [in Russian], Moscow, Atomizdat (1959), p. 15.
2. N. A. Dollezhal' et al., ditto, p. 36.
3. A. N. Grigor'yants et al., Report No. 308, presented by the USSR at the Third International Conference on the Peaceful Uses of Atomic Energy, Geneva (1964).
4. G. N. Ushakov et al., Report No. 314, ditto.
5. N. A. Dollezhal' et al., Power Reactor Experiment, Vienna (1962), p. 41.

# NOVO-VORONEZH NUCLEAR POWER STATION – IN OPERATION

Dr. Mech. Sci. N. M. Sinev
Deputy Chairman

State Committee for the Utilization of Atomic Energy in the USSR
Translated from Atomnaya Énergiya, Vol. 17, No. 5, November, 1964
2 page insert following page 336

By the efforts of highly qualified teams of scientific, design and constructional organizations of many leading mechanical engineering concerns in the country, skilled builders and specialists in the construction of power generating complexes, the complicated many-year cycle of planning, acquisition, construction, and installation of the Novo-Noronezh Nuclear Power Station has been completed. Difficulties of construction and startup of the single-channel equipment, of the laborious scientific and engineering calculations, investigations and experiments have

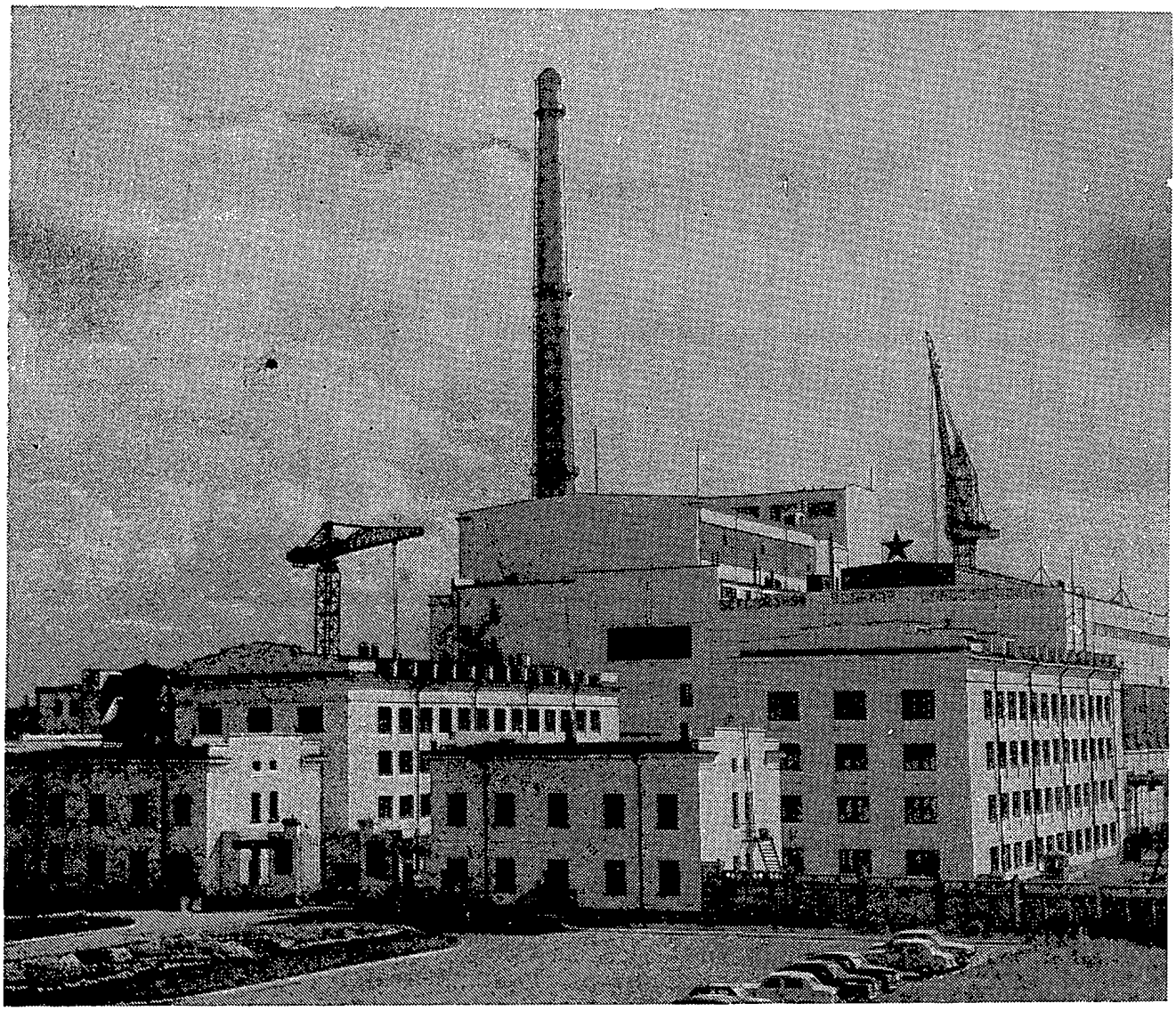

been overcome. Many days, weeks, and months of worry and anxiety of the startup and commissioning period, together with the intensive assembly and structural-finishing tasks, have been left behind.

At 1545 hours on September 30, 1964, the first turbogenerator of the Novo-Voronezh Nuclear Power Station took the load and fed electric current into the Voronezh Energy System and, by the morning of October 2, the first million kilowatt-hours were produced. Only about 200 g of $U^{235}$ were required for this instead of the 500-600 tons of coal for a conventional thermal power station. On the sixth day after startup, the turbogenerator load was raised to 65 MW; the thermal power of the reactor was 35% of the calculated power. During this period, two of the three installed turbines were tested in operation (alternately), various effects were checked which are important for evaluating the system that ensures the safety of operation of the reactor (for example, as a result of the sudden de-energizing of the station, actuation of the scram system, de-energizing of the load-breaker at the turbogenerator in the event of closure of the shutdown steam valve prior to the turbine), cut-out and switching-in of the steam generator loops was carried out, the reaction of the control mechanism was finalized, etc.

Investigations of the physical parameters of the active zone were undertaken in various ways and answers were provided to questions of interest, having verified the good agreement with the calculated data in the magnitude of the reactivity and distribution of the neutron fields as well as in the efficiency estimate and the action of the reactivity compensation controls, taking into account the effect of the temperature coefficient.

Construction and assembly of the first unit was achieved by organizations of the State Industrial Committee for Energy Generation and Electrification of the USSR, the ideological and scientific supervision in planning was carried out by the I. V. Kurchatov Institute of Atomic Energy, the general designer was the Moscow Division of the All-Union Design Institute "Teploénergoproekt" (MOTÉP). Development and supply of plant was undertaken by many well-known structural engineers, scientific research and machine construction enterprises.

The first unit of the Novo-Voronezh Nuclear Power Station, with an output of 210 MW is only the first "salvo" of this large-scale nuclear power station. At present, on the site of the Novo-Voronezh NPS and "flush" with the first unit, construction is taking place of a second unit with an electrical output of 365 MW. In the installation, structural and engineering decisions of the reactor portion of the second unit, accumulated experience as well as new advances in atomic science and technology have been taken into consideration.

The cost per kilowatt of installed power in the second unit will be only 60% of the cost in the first unit, i.e., 192 rubles/kW compared with 327 rubles/kW. We note that the estimated cost of a coal-fired station operating on Donets coal with a unit of 300 MW would be about 100 rubles/kW here without capital investments in the extraction and transportation of the coal, which for this locality – situated in the vicinity of Donbassa – would amount to about 70 rubles/kW. Thus, taking into account future development, large-scale units for nuclear power stations with water-cooled–water-moderated reactors enable the feasibility of earning capacity to be assessed, as a result of installing them in the European part of the country.

With the introduction into the system of the first units of the Beloyarsk and Novo-Voronezh Nuclear Power Stations, a new page in our country's energy generation has been opened. The time has come when the role and share of nuclear power stations in the fuel-energy generation balance of the European part of the USSR will steadily increase according to the extent of further accumulation of experience in the construction and operation of large-scale nuclear power stations, organization of mass production of special reactor plant and the development of pilot units of large power which are planned for construction in the immediate future.

In this process of development, a specially important role is played by the Beloyarsk and Novo-Voronezh Nuclear Power Stations, which have been transferred to the State Committee for the Utilization of Nuclear Energy in the USSR as experimental stations and as outposts of large-scale power generation in the USSR. It is planned to install at these stations several different units with high power reactors, which will enable all-round development of basic prototypes of economical nuclear power stations, to concentrate engineering experience and to create the basis of practical training of operating personnel for the future extensive program of nuclear power station construction.

"Let the atom be a worker and not a soldier" is inscribed on the pediment of the main building of the Novo-Voronezh Nuclear Power Station. And all involved in the construction of this station – scientists, engineers, and workers – have endowed this great goal with their labor, with their enormous many-year efforts, expended on the construction of the first-born of Soviet nuclear power generation, making its first spectacular contribution in the building of a material-technological basis for communism.

# SODIUM-COOLED FAST REACTORS*

A. I. Leipunskii, O. D. Kazachkovskii, I. I. Afrikantov, M. S. Pinkhasik, N. V. Krasnoyarov, and M. S. Poido

Translated from Atomnaya Énergiya, Vol. 17, No. 5, pp. 345-348, November, 1964

The fuel breeding capabilities of fast reactors open up new potentialities to the development of large-scale nuclear power. Fast neutron chain reactions yield large numbers of secondary neutrons per single fission event, reduce nonproductive neutron capture with no fission in the fuel, or nonproductive capture in structural materials, and make it possible to increase the contribution of fissions in the raw material. As a result, the fuel breeding ratio exceeds unity and fast reactors may be developed which use all the reserves of uranium and thorium, rather than just $U^{235}$, as the raw material.

Attainment of high parameters in the steam turbine cycle and high efficiency is important in the case of power facilities. The sodium used as coolant in fast reactors makes it possible to achieve such parameters in a radioactive reactor loop at relatively low pressures. Sodium retains the basic radioactive fission products in the event of rupture of fuel elements.

Fast reactors using liquid metal coolants are currently in operation in the USSR, in the USA, and in Britain, and experience is being accumulated in the operation of these facilities. The experimental sodium-cooled fast reactor BR-5 [1] has been operating successfully for the past half decade in the Soviet Union. Parameters such as up to 500 kW/liter power density, up to 6% fuel burnup, sodium temperatures to 500°C at the reactor exit, come close to the characteristics of large power reactors being developed which will provide appreciable savings.

The first stage in the development was reached in the designing of a full-scale industrial power facility, the BN-50, with 200 MW(th), 50 MW(e) output rating, sodium temperature of 315°C at the pile entrance and 450°C at the pile exit. The core was a cylinder 67 cm in diameter and standing 67 cm high. Suggested fuel materials were uranium-molybdenum alloy, uranium oxide in a nickel matrix and nickel cladding, or sintered uranium oxide in a stainless steel jacket. The breeding ratio of the reactor using uranium-molybdenum alloy fuel was 1.35.

Engineering designs for the BN-50 facility were frozen in 1960. The work on this project revealed not only the feasibility of building a reactor of this type, but also the possible design of power reactors of still greater output and improved performance. A decision was made in this connection to shelve the plans for the BN-50 project as an intermediary stage.

Work on the design of a new reactor project is currently entering the finishing stages; this is to be a prototype of high-output nuclear fueled electric power stations of 1000 MW thermal rating and 350 MW electrical rating (BN-350). The basic reactor components are housed in a variable-diameter sodium-filled tank (sodium volume of 165 $m^3$).

The sodium coolant runs down six tubes at 300°C through the tank bottom to collect in the discharge header. The sodium becomes heated to 500°C, on the average, as it courses through the reactor, and it is then pumped through the heat exchangers from the reactor tank. The discharge header plenum has grids for mounting the fuel element assemblies. The central 211 assemblies contain the core fuel elements in the middle and the fuel elements belonging to the upper and lower blankets on the face of the reactor in their top and bottom, respectively. The peripheral 500 assemblies form the lateral blanket. Cells beyond the side blanket are used as storage area for the cool-down of fuel element assemblies before they are removed entirely from the pile. Steel slugs positioned beyond the storage area constitute neutron shielding for the reactor tank. A general view of this reactor appears in an accompanying diagram.

The core volume (about 2000 liters) and the irradiation level (500 kW/liter) minimize the fuel quantity in a cycle. As the irradiation level is stepped up, the amount of fuel used increases because of the increased fuel used in chem-

*Report No. 311 presented by the USSR delegation to the Third International Conference on the Peaceful Uses of Atomic Energy, Geneva, 1964.

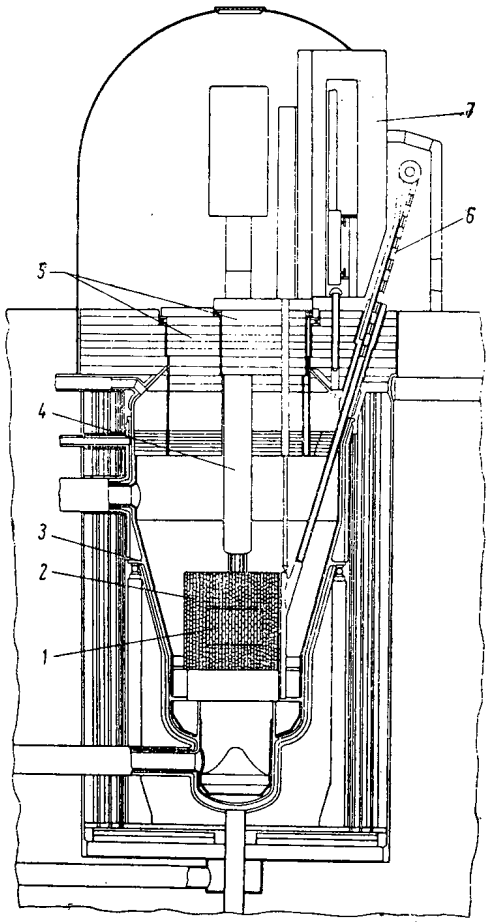


Fig. 1. General view of reactor. 1) Core; 2) blanket; 3) vessel; 4) central column with control rod drives; 5) rotating plugs; 6) discharge elevator; 7) discharge control box.

ical reprocessing or fabrication of fuel elements, and as the irradiation level is lowered the amount of fuel increases because of the increased critical load.

The core shape determines the fraction of coolant present in the breeding zone, the flowspeed of the sodium and the hydraulic resistance to the pumped flow, as well as the extent to which the sodium becomes heated. These factors improve measurably as the core diameter/height ratio (D/H) is increased. However, the ratio of the volumes of the face shield and side shield increases concomitantly, and at D/H > 1 the critical mass increases. A D/H ratio of 1.4 was decided upon in view of the heat transfer, hydraulic, and nuclear physics characteristics of the reactor. The core diameter was 1.5 m, core height 1.06 m, maximum sodium flowspeed 10 m/sec, average heating level of sodium in the core 230°C, volume fraction of sodium 39%. In order to effectively minimize neutron leakage from the reactor, the thickness of the side and face blankets was set at 60 cm. The reactor is so designed that the core dimensions can be either expanded or contracted by varying the power density, and to facilitate conversion to fuel element assemblies incorporating different fuel materials.

Ceramic fuel: a mixture of plutonium dioxide (19% plutonium) and $U^{238}$, is used as fuel material for the BN-350 reactor. A loading of enriched (23%) uranium dioxide is possible in the first stage. Criticality is attained at 780 kg plutonium (950 kg $U^{235}$). As in the case of the BR-5 fast reactor, BN-350 fuel elements constitute a stainless steel tube 5 mm in diameter and 0.4 mm thick filled with sintered dioxide pellets.

The pressure exerted by the gaseous fission products sets up stresses in the cladding even when they have been completely released from the oxide, but these stresses combined with thermal stresses fail to exceed tolerances. Higher burnup levels can be attained when the average dioxide density is brought below that in BR-5 fuel elements. The operating life of a fuel element must be 300 days to achieve 5% burnup. Fuel elements are assembled in hexahedral assemblies (of 217 fuel elements each) measuring 96 mm "across." Fins on the cladding aid in achieving an even distribution of the fuel elements. The fuel elements are spaced above and below with the aid of a grid into which the tailpieces of the fuel elements are fitted. The face reflectors are made up of 74 elements in the same assembly (37 above and 37 below, tube diameter 12 mm, tube thickness 0.4 mm) filled with depleted uranium dioxide pellets. The assemblies in the side reflector contain 37 elements each (14.2 mm in diameter, 0.5 mm thick), with depleted uranium dioxide. The fuel elements in the side and face shields are spaced to a density of 9.5 g/cm$^3$ on the average.

The described composition of the core and blankets provides for a fuel breeding ratio of ~1.5; the internal breeding ratio is 0.62. The reactivity change with reactor on-power was 0.6% over a month's time and was chiefly due to the lowered concentration of plutonium in the core. Reactivity losses were compensated by displacing six fuel element assemblies with elements positioned in the central part of the core and featuring 1.4% reactivity, thereby assuring operation free of shutdown for two months.

The reactivity change while the reactor is heating up and being brought up to full power is $2.4 \cdot 10^{-5}$/°C and $(0.5\text{-}0.7) \cdot 10^{-5}$/MW (a larger value is attained when burning fresh fuel, in which case the oxide pellets are not bonded to the cladding and the elongation of the oxide column takes place independently of the elongation of the cladding). The principal contribution to the power effect is that of the $U^{238}$ Doppler effect. The sodium ratio integrated over the core comes out negative.

The temperature and power effects are compensated by the withdrawal of fuel assemblies incorporating $B_4C$-loaded fuel elements from the core and shifting these to the top face reflector; $B^{10}$ enrichment here is as high as 60%. The total compensator efficiency is 1% when 0.7 kg $B^{10}$ is present.

During transients, one of the two automatic control rods will be operating in unisom with the temperature compensator. The control rods are made of enriched $B_4C$ compacted slugs enclosed in stainless steel tubes. The efficiency of each control rod is 0.2%. Since the control rods are constantly present in the core while the power level is being maintained, a special volume is provided in the rod design to collect the helium released in the rods.

Three assemblies of enriched $B_4C$ rods are employed for scramming the reactor. The total excess reactivity in these rods is 4.5%. Depending on the signals operating on the scramming system, boron rods may be dropped at various speeds. The shielding of fast reactors incorporates some special features due to the high fast-flux intensity coming out of the reactor. The neutron flux at the edge of the breeding blanket attains the quite considerable figure of $5 \cdot 10^{13}$ neutrons/cm$^2$ · sec. The side shield of the reactor is therefore designed as a primary shield to lower the flux impinging on the wall of the reactor tank, backed up by secondary shielding outside the tank to lower the radiation flux impinging on the concrete, and then the concrete shielding. Lowering the neutron flux striking the tank and a reduction by a factor of ten in the amount of heat released in the tank walls is achieved by means of steel slugs (120 mm thick) placed on the far side of the storage volume, by a layer of sodium (500 mm) and by the steel thermal shield of the tank (60 mm). The heat released in the tank wall is 0.1 W/cm$^3$. The secondary shield is made of a steel layer (150 mm) and an iron oxide layer (1000 mm) designed to lower the radiation flux to $5 \cdot 10^9$ MeV/cm$^2$ · sec. The ordinary concrete shielding is 2000 mm thick. The top shield incorporates a layer of sodium, a steel plate sunk in the sodium, and sandwiched iron and graphite layers.

A system of rotating shielded plugs carrying a reloading mechanism, and the refueling control box with transmission gearing, is provided for refueling the reactor with fresh fuel assemblies and for unloading spent fuel assemblies.

The first loop includes the reactor, a sodium-sodium heat exchanger, the pump, cleanup system, and a system for monitoring oxides in the coolant. Stop valves are installed on the exit and entrance piping (630 and 529 mm in diameter, 15 and 13 mm thick, respectively). Ahead of these stop valves, the piping is enclosed in a protective carbon steel jacketing 5 mm thick. Immersion-type vertical-shaft centrifugal pumps working in parallel build up a sodium flowrate of 14,100 tons/h through the reactor at a head of 12 kg/cm$^2$. The U-leg heat exchanger presents a heat transfer surface area of 850 m$^2$. The secondary loop includes a sodium-sodium heat exchanger, a sodium-water-steam steam generator, a pump, a cleanup system, and a system for monitoring sodium oxide in the flow.

The steam generator was designed for natural circulation with a single baffle. Wall rupture experiments and experiments involving interaction between sodium and water or steam were set up in steam generator models to test out the single-baffle design of the steam generator unit. The experiments demonstrated the feasibility of this design. Steam generated at 430°C temperature and 50 atm pressure is supplied to the turbogenerators.

The primary loop equipment is so fabricated and so arranged as to permit operation and replacement of the equipment under high-level radioactive contamination conditions. Acylindrical shielding cover of stainless steel, 9.5 m in diameter and 10.4 m high, is placed above the reactor to localize possible leaks of radioactive products. A removable access hole 2.5 m in diameter is situated above the cylindrical cover.

Emergency cool-down of the reactor is achieved by natural circulation and by utilizing the energy of inertia of the turbogenerators. For example, in the event of an outage of the electric power supplies, the greatest hazard to be faced of likely emergency situations, flow of sodium through the reactor during the first 60 to 100 sec will be brought about by circulation pumps powered directly by the inertia of the turbogenerators. The heat will be removed subsequently by natural circulation of the coolant through the primary and secondary loops.

The BN-350 is the USSR's first high-flux fast power reactor. This accounts for the decision to rely on already achieved and experimentally amply justified system parameters ensuring adequate reactor reliability in performance. The installation and operation of the BN-350 reactor, in addition to the development of research and experimental work with the reactor, provides sure grounds for assessing the possibility and feasibility of various new ideas holding promise of further progress in the field of fast power reactors.

Some new obvious pathways for improving this type of reactor are:

1. Improving fuel burnup, which entails reduction of the amount of fuel per cycle, reducing the number of fuel elements spent and reprocessed.

2. Reduction in the amount of steel in the core, and increasing the content of the fuel. At the present time, the choice of 0.4 mm thickness for cladding in BN-350 fuel elements rests primarily on the fabrication technology conditions and on the need to withstand stresses imposed by gaseous fission products. The use of fuel elements designed to release fission products in gaseous form into the coolant will make it possible to reduce the cladding thickness, and this will mean a substantial improvement in the breeding ratio.

3. The use of other fuel materials. Carbide and metal fuel makes it possible to achieve a breeding ratio higher than that associated with oxide fuel. To date, however, there is no record of any experiment on high burnup of compositions of that type. Uranium monocarbide fuel elements are now being tried out in the BR-5 reactor, and almost the entire core of BR-5 is scheduled to be converted to monocarbide fuel by the end of 1964.

4. The use of promising short-cut techniques in fuel reprocessing, combined with enhanced power density in the core to bring about a substantial reduction in the amount of fuel per cycle.

5. Increasing plant thermal efficiency. An increase in coolant temperature at the reactor exit makes it possible to raise the steam parameters.

Projects are now underway to develop a power facility with a rating of one million kW(e) (the BN-1000 project). The use of a mixture of uranium monocarbide and plutonium monocarbide will produce a breeding ratio of 1.75 in the BN-1000. In-core breeding will completely compensate for the fuel burnt up, and this will greatly simplify requirements for reactivity compensation, while facilitating long-term continuous reactor service life. The reactor core will be shaped flatter than the BN-350 core [2]. Steam parameters of 580°C and 240 atm are the goals of this project.

A decision has been made to proceed ahead on the development of the fast experimental reactor BOR, with an eye to providing the groundwork for the basic technological and design decisions relating to this type of high-temperature high-stress reactors, as well as other promising fast reactor types. The BOR sodium-cooled reactor is designed to achieve 40-60 MW(th) with up to 1500 kW/liter power density per unit core volume; the temperature of the sodium coolant leaving the facility will be 630-650°C. Plans call for studying the possibility of achieving higher than 10% burnup and employing thin-clad fuel elements capable of releasing gaseous fission products. The operation of the BOR reactor will provide extensive experience on the stability of fuel elements of different design and of different compositions of fissile materials at high-burnup levels, as well as experience in operation of the reactor, ancillary equipment and process instrumentation, experience in the technology of radioactive sodium at elevated operating temperatures. The experience accumulated will pave the way for the building of low-cost fast reactors providing cheaper electric power than that available from fossil-fuel power stations.

## LITERATURE CITED

1. A. I. Leipunskii et al., Report No. 312 presented by the USSR delegation to the Third International Conference on the Peaceful Uses of Atomic Energy, Geneva (1964).
2. A. I. Leipunskii et al., Report No. 369, ibid.

# OPERATING EXPERIENCE WITH THE NUCLEAR PROPULSION PLANT ON THE ICEBREAKER "LENIN"*

I. I. Afrikantov, N. M. Mordvinov, P. D. Novikov,
B. G. Pologikh, A. K. Sledzyuk, N. S. Khlopkin,
and N. M. Tsarev

Translated from Atomnaya Énergiya, Vol. 17, No. 5,
pp. 349-359, November, 1964

The nuclear-powered icebreaker "LENIN" undertook its shakedown cruise as part of the Arctic Sea Fleet of the USSR on December 3, 1959. Since that time, it has participated every year in Arctic navigational practice. By the end of 1963, the ship had traversed about 60,000 miles, including about 40,000 miles through the ice.

Together with its sister icebreakers, the nuclear-powered icebreaker opened a path for over 300 vessels on the Northern Sea Route. In October, 1961, the ship made a delivery of equipment and servicing personnel to the drifting patrol station "North Pole-10."

The use of a nuclear power plant made it possible to design an icebreaker capable of enormous power output and navigational independence, featuring excellent maneuverability and iceworthiness. The combination of these positive qualities on an icebreaker powered by a propulsion plant burning chemical fuels is unattainable in practice. The, by no means negligible, operational advantages to be had in using a nuclear propulsion plant are the possibility of keeping the water displacement of the icebreaker practically constant, and the possibility of operating at full power over a protracted time span combined with more reliable use of the icebreaker under severe ice conditions. The use of the powerful nuclear icebreaker on the Northern Sea Route contributes to a greatly increased speed through the ice of vessels negotiating icy and icebound seas, and to appreciable lengthening of cruise times. Cases of forced wintering of icebound ships are virtually eliminated, the number of accidents is reduced, and the possibility of loss of ships nipped by ice packs is minimized. This is exemplified by the successful trip by vessels on the Arctic run during 1960, when the icebreaker "LENIN" forestalled a threat of the loss of several ships in the Vil'kitskii Strait.

The long-term operation of the "LENIN" on the open seas under the most hazardous conditions in navigation showed that the nuclear propulsion plant operates in a stable manner, is easily controlled under any and all sudden changes in load, and fulfills all the power requirements of the vessel. The vibration- and shockproof equipment of the nuclear propulsion plant operates reliably in the face of collisions with ice formations and heaving and rolling of the ship.

The reactors on board the "LENIN" are now operating on their second fuel loading. The reactors were refueled in the spring of 1963. Each of the reactors operated for over 11,000 h on the first fuel loading, developing from 430,000 to 490,000 MWh of thermal power. The average burnup over the reactor cores was 11,000-13,000 MW·days/ton U, and the maximum burnup was about 30,000 MW days/ton U. The fuel elements were immersed for about 30,000 h in the water of the primary loop.

The reactors operated stably at all power levels, including the maximum level of 90 MW. The total power developed by the icebreaker was 44,000 hp, when all three reactors were developing 65 MW each.

## Performance Characteristics of the Nuclear Power Plant

The total weight of the nuclear propulsion plant, shielding included, is about 3100 tons. The plant is designed to handle 360 tons of steam per hour at a pressure of 28 kg/cm$^2$ and a temperature of 300-310°C.

Figure 1 shows a general view of the nuclear power plant, and Fig. 2 shows the basic layout of the plant. The primary loop is made up of three autonomous sections, each of which includes the following equipment: a reactor,

* Paper No. 313 presented by the USSR delegation at the Third International Conference on the Peaceful Uses of Atomic Energy, Geneva, 1964.

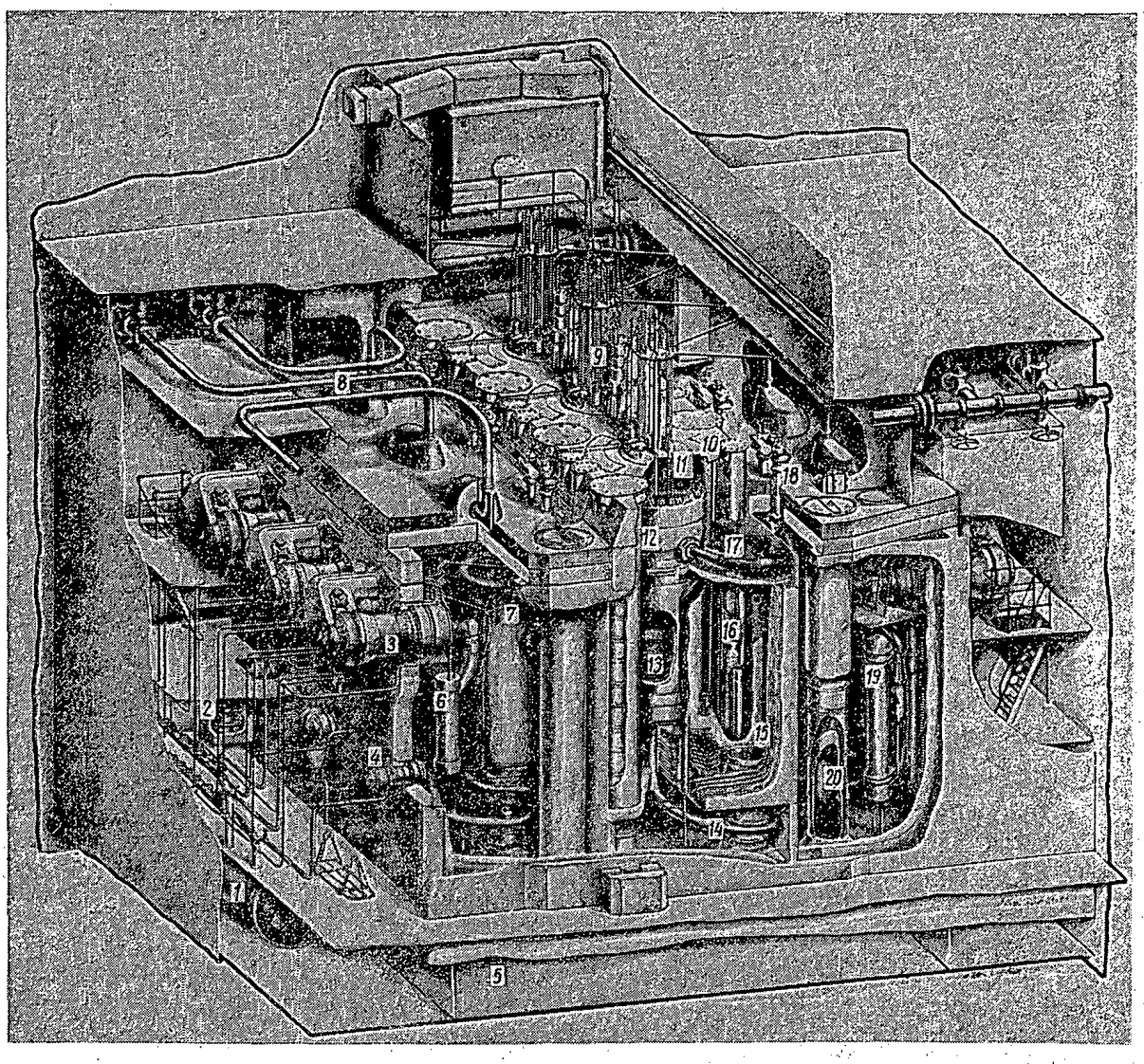

Fig. 1. General view of steam power plant. 1) Heat exchanger for third and fourth loops; 2) pump for internal cooling loop; 3) primary-loop principal circulation pump; 4) primary-loop emergency circulating pump; 5) temperature monitors display room; 6) cooler for primary-loop filter; 7) steam generator; 8) steam lines; 9) control and protection system actuators; 10) ionization chamber; 11) carborite; 12) reactor; 13) core; 14) primary-loop piping; 15) iron-water shielding block; 16) primary-loop filter; 17) concrete; 18) gate valve for primary-loop main line; 19) heat exchanger serving internal cooling loop; 20) pressurizer.

two steam generator units, four principal pumps and two emergency circulation pumps, four pressurizers, and two ion exchange filters. Each section has two loops: a fore loop and an aft loop; this is convenient both for regular operation and for maintenance of the fittings and equipment.

The principal operating mode is operation of both loops. One principal circulation pump is in operation in each loop in this mode, the other pump being on hot standby.

The reactor is capable of operating at up to 50 MW power output in the single-loop mode with the principal and emergency circulation pumps working.

The throughput of the pumps on the primary loop turned out to be slightly greater than the ratings, so that the water was not heated as high as originally planned in the reactor in compensation. This becomes particularly clear in Fig. 3, where we have the theoretically predicted (curve 1) and experimentally derived (curve 2) dependences of the temperatures at the reactor exit and entrance on the reactor power.

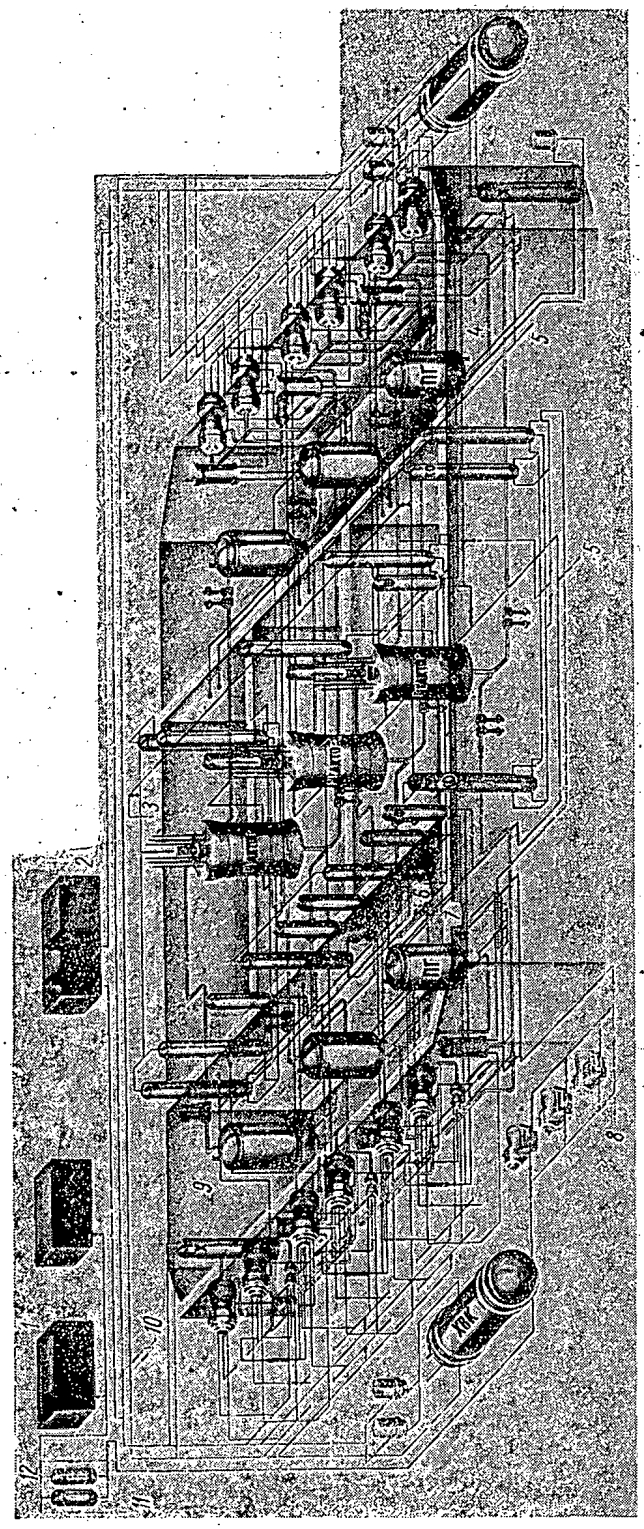

Fig. 2. Diagramatic flowsheet of power sheet: —— coolant loop; SG—steam generator; KO—pressurizer; MCP—main circulating pump; ECP—emergency circulating pump; IF—ion exchange filter; FC—filter cooler unit; X—cooler for internal coolant loop; FP—coolant make-up pump; 1) reserve coolant tanks; 2) surge tank; 3, 5, 10) to drainage system; 4) feedwater line; 6) from drainage tank; 7) to mixing tank; 8) feedwater line; 9) steam bleed line; 11) discard line in case of embrittlement; 12) filter.

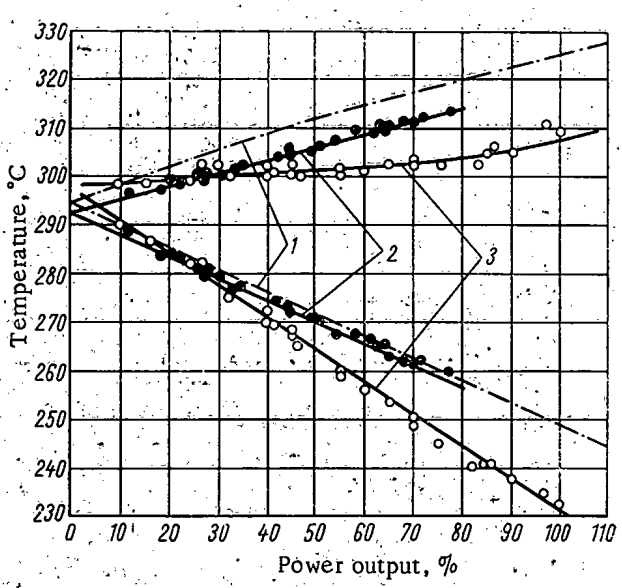


Fig. 3. Power dependence of reactor entrance and exit temperatures.

In 1961, an alteration was made in the temperature conditions of the reactors in order to bring them closer to self-regulating conditions where the temperature effect is practically entirely compensated by the Doppler effect. As we see in Fig. 3, the water temperature at the reactor exit remains practically constant (curve 3) at all power levels in the self-regulating mode.

The characteristics corresponding to the self-regulating mode changed slightly during the reactor operating period because of changes in the temperature effect and in the Doppler effect, but this did not occasion any need to readjust the control system.

The design of the mechanical side of the plant provides for the possible supplying of all on-board steam consuming units from an overall main line serving all parts of the ship: the main turbines, the electric power plants, evaporators, and so forth.

Sections including groups of steam generator units from one or two reactors furnishing steam to the fore or aft echelons of on-board equipment may be delineated in the common main steam line by means of valves and fittings. Experience has shown that operating all the steam generator units into a single common main steam line offers significant advantages not found in the echelon setup

When one of the reactors is scrammed with steam generators being operated on the echelon pattern, the supply of steam to consumer units from the steam generators of that reactor may be cut off.

When the steam generators are working into a single common main steam line, it seems possible to

TABLE 1. Design and Operational Performance Characteristics of the Icebreaker "LENIN" at Full Power

| Performance parameters | Design values for 65 MW | Performance data for reactors | | |
|---|---|---|---|---|
| | | 1 | 2 | 3 |
| Water flowrate in primary-loop lines, tons/h | 415 | 435/430 | 458/467 | 435/453 |
| Temperature at reactor exit (flowing through loops), °C | 317 | 311/311 | 312/313 | 311/313 |
| Temperature at reactor entrance, °C | 261 | 260 | 261 | 260 |
| Steam throughput on loops, tons/h | 43.3/43.3 | 42/42 | 47/42 | 43/46 |
| Steam pressure, kg/cm$^2$ | 29 | 32/31 | 31.5/30.5 | 31/31 |
| Steam temperature, °C | 307 | 310/309 | 308/308 | 308/308 |
| Power output computed for primary-loop parameters, % | 72.3 | 69.6 | 75.4 | 73.1 |
| Power output computed for secondary-loop parameters, % | 68 | 67.3 | 71.1 | 71.3 |

Remarks. Figures in numerators of fractions refer to fore loop, those in denominators to aft loop.

maintain the steam pressure in that main line by increasing the power output of the other reactors, so that there will be no need to completely shut off the steam consuming units on board. As a result, the number of valve operations in the transient and emergency modes of operation is reduced, and this diminishes the probability of erroneous judgments on the part of operators at the most crucial instants in the operation of the plant.

The operating experience showed that the measures provided for on the icebreaker are adequate to ensure outage-free electric power supplies for the nuclear propulsion plants, by relying on two electric power plants each generating an output of 3000 kW. In the event that the voltage should disappear at one of these electric power plants, there are two emergency diesel generators of 2100 kW total rating which would be switched on automatically, and a standby diesel generator unit of 1000 kW rating can be switched on manually if required.

On the suggestion of the servicing personnel, the originally planned two-way relay contactor circuitry for electric powering of the control and protection system for the reactors was replaced by a semiconductor switching system for enhanced reliability in operating the plant.

It is important to emphasize the fact that not a single instance of malfunction in the emergency protection equipment was encountered during the entire period the reactors were on-power. Studies showed that in some cases, when one of the circulation pumps in the primary loop was shut down for instance, there was no need to cut the power to zero; on the contrary it was quite sufficient to rely on an automatic rapid power drop to the 30% level, a procedure known as second-order emergency operation.

Some of the signals previously used to dump the power to zero level were converted to trigger second-order scramming signals. This meant an increase in the ship's service life and diminished the number of abrupt thermal surges experienced by the equipment. Automatic dumping of the power to zero level is known as first-order scramming in this context. The number of scrams during the sailing of the icebreaker over the Northern Sea Route was limited: six to eight such events for each of the reactors. The primary-loop equipment of the power plant on board the icebreaker underwent about 15,000 h of service under regular operating conditions (180 kg/cm$^2$ pressure and temperatures of 250-310°C), including service in 1963.

The main circulation pumps operated over 8000-9000 h without overhaul. Some of them were withdrawn from service because of a loss of resistance on the part of the insulation on the stator windings. The emergency circulation pumps operated reliably. The steam compensation system maintained the high stability of the pressure in the primary loops at constant levels and permitted pressure deviations no greater than ±5 atm during transients. Radioactive corrosion products were precipitated in components of the bottom parts of the pressurizers, and this added difficulties to the dismantling and replacement of the electric heater units. At this writing, that phase of the work had not been completed.

The ion exchange filters made it possible to maintain the required high quality of the water used in the primary and secondary loops of the propulsion plant: a resistivity of 1-2 MΩ·cm; chlorine ion content no greater than 0.02 mg/liter, and pH = 6-8. The ion exchange resins KU-2 and AV-17 have been used successfully in these filters in the recent period. Hydrazine was tried out in the water of the secondary loop. A short-term increase in the content of salts in the feedwater of the secondary loop was observed when the mechanical power of the icebreaker was first set into operation.

As a result of the heightened quality of individual units of equipment, and improvements in the inspection system, these phenomena occurred only very rarely subsequently, and were rapidly localized in their effects. The reader should take note of the effective use of double tubesheets for the condensers and coolers treating the on-board water, thereby practically eliminating any taking in of sea water.

The steam generators of the nuclear power plants operated stably under both steady-state and transient conditions. Cases of leaks in their piping systems did occur during operation. The detection of leaks and corrective action in cutting out the steam generator involved from the line were carried out with rapidity and in well organized steps. As a result, only a short-term increase in activity was observed in the secondary loop, with the background values exceeded only by several times.

Cases of dropwise leaks through the stuffing boxes of the principal slide valves due to the gland packing drying out were observed in the primary-loop lines. The packing was replaced by higher-quality material, but the stuffing boxes still had to be tightened up once every 1500 or 2000 h. Bellows valves in the drainage system of the primary loops proved to be insufficiently reliable components. These valves had to be checked out once a year.

There are no outstanding remarks to be made on the control and protection system actuators, all of which operated reliably.

The biological shielding around the reactors, around the equipment and the main steam lines of the primary loops, proved quite sufficient, and no damage of any kind was observed in this shielding as a result of impact loadings produced by the motion of the icebreaker ramming ice formations, or by heaving and rolling of the ship when sailing on stormy weather. Some highly active slurries did get into a few of the pulse tubes leading from the bottom of the pipes. The $\gamma$-emission levels were higher at the points where these tubes protruded beyond the biological shielding to the monitoring and measuring instruments, so that additional local shielding was provided for at those points.

Nuclear power plant overhaul needs dictated an expansion of the health physics room at the entrance to the rigorous exposure control zone and an increase in the volumes occupied by the storage areas for liquid and solid wastes. The health physics rooms and the storage racks were reequipped to handle the situation.

Health physics instrumentation was adequate to monitor the radiation environment on the icebreaker and to keep track of activities in the process loops of the nuclear plant. During operation some of the dosimetric instruments were replaced by new and improved counterparts. The system for monitoring high-level gases was also improved.

The results of personnel monitoring showed that the integrated radiation dose received by most of the personnel checked did not exceed one third or one half the maximum permissible dose (5 rem/yr). Only several persons who were engaged in radiation-hazardous work involving deactivation of rooms where water from the primary loop had penetrated actually received doses anywhere close to the maximum permissible dose [1, 2].

## Neutron Physics Parameters of the Core

The design of the reactor may be found in [3]. The core forms a total of 219 operating channels set at the nodes of a regular triangular grid of 64 mm pitch (Fig. 4). The core stands 1.6 m high and has an equivalent diameter of 1 m.

Eighty kilograms of $U^{235}$ were delivered to each of the three reactors in the first fueling. The core is designed to operate for 200 days at 90 MW peak output. During that time one third of the original supply of fuel will be burnt up. The initial excess multiplication factor corresponding to such high burnup ($\rho$ = 14%) was cut to half by the introduction of 92 g $B^{10}$ into the jacketed channel tubes in each reactor (for the first loading). The boron was arranged in a nonuniform pattern through the core: the concentration diminished from the reactor axis out to the periphery; boron was absent in the outer row of channels.

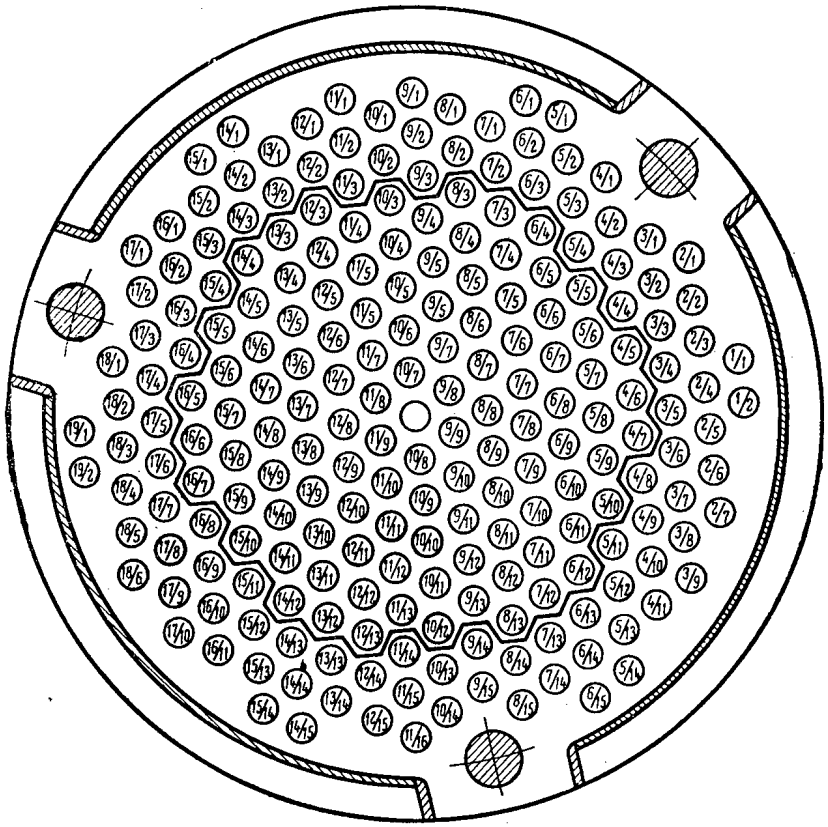

Fig. 4. Cross section through the core.

The operating channel (Fig. 5) contains a bundle of 36 cylindrical fuel elements in a framework designed to space them as required. The external diameter of the fuel elements is 6.1 mm, the rated clearance between fuel elements in the assembled bundle is 1.5 mm. The cladding thickness is 0.75 mm. The jacketed tubes of the operating channels, the cladding of the fuel elements, and the spacing framework were made of zirconium alloy in the first loading. The fuel employed consisted of sintered uranium dioxide pellets of 5% average enrichment.

The results of the loop tests run could not yield experimental information of the processes involved in fuel burnup when the reactivity compensators were in their actual positions and the neutron fields were distorted. These data could be secured only as a result of in-core burning of the fuel as a unit.

The reactor core was designed on the basis of computed data obtained from a high-speed electronic computer working on two standard one-dimensional programs (radial and height standard programs).

An approximation procedure based on the introduction of empirical corrections derived from processing a large number of critical experiments into the conventional classical model for thermal reactors served as the groundwork for calculating the multiplication parameters in the lattice of operating channels.

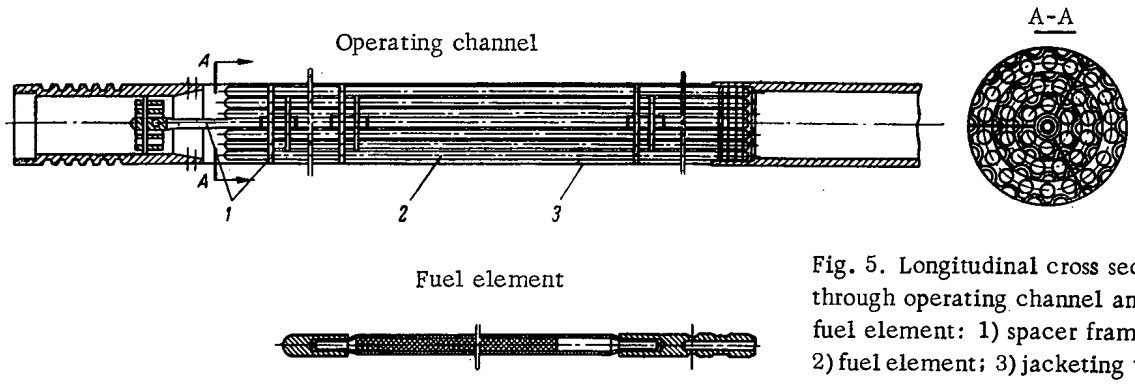


Fig. 5. Longitudinal cross section through operating channel and through fuel element: 1) spacer framework; 2) fuel element; 3) jacketing tube.

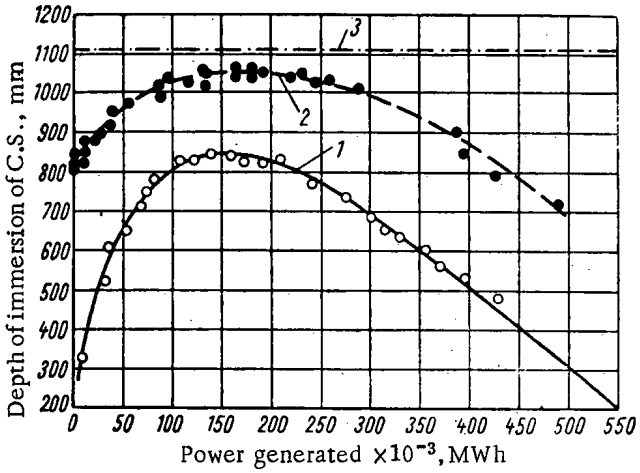


Fig. 6. Extent of immersion of compensating system in core as a function of reactor output.

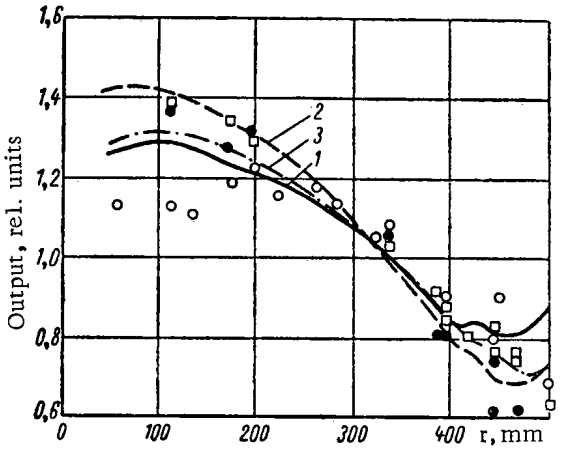


Fig. 7. Distribution of power output over core radius r

Prior to starting up the icebreaker reactors, investigations of the core on a test loop were undertaken. Final touches were made in this stage on the design of the core, control systems, and reactivity compensation.

Figure 6 shows the extent to which the compensating system becomes immersed in the core as a function of the reactor output (curve 1) when the reactor is operated over a long period under 40-60 MW loads. The theoretically predicted curve 1 was plotted on the basis of the one-dimensional axial computer program. This program provides excellent agreement with experimentally derived data points giving the positions of reactivity compensation system when the reactor has been operating over a long period at constant power levels. Despite the approximate nature of the design model, the theoretical description therefore yields entirely satisfactory results.

The rapid immersion of the compensation system at the beginning of the reactor period is accounted by the predominant role of the boron burned up: the reactivity release as a result of boron burnup is not compensated by boron losses through $U^{235}$ burnup. Equilibrium sets in only in 70 days of peak-power operation of the reactor.

The right branch of curve 1 (see Fig. 6) has a lesser curvature, which is explained by the release of slightly burned-up portions of the fuel channels as the compensation system is withdrawn from the core. The same diagram shows individual points plotted corresponding to positions of the compensating system of the reactors in depoisoned states, at temperatures of 40-80°C and at peak reactivity (curve 2). The minimum subcriticality of the reactor is 1-1.5% when the position of the compensating system is on the lower limit switches (curve 3) and when control and scram rods are completely withdrawn from the core during the reactor operating period; this makes for reliable shutdown of the reactor.

The radial distribution of the output with respect to the activity of the fuel channels irradiated in the core at about 20°C and the minimum power level was measured before the reactor was brought up to operating conditions. The radial variation factor for the energy released for this case is 1.2 (Fig. 7). The theoretically plotted curve 1 refers to the unevenness with respect to fuel channels in a hot poisoned reactor, and does not take into account the presence of thick-walled steel jackets in which the control rods and scram rods grouped near the reactor axis move. This accounts for the discrepancy between the theoretical design data and the experimental data for the central fuel channels.

During reactor operation, changes in the configuration of the energy field were monitored by taking measurements of the temperature drops across the fuel channels by means of resistance thermometers. Because of the boron burnup at the center of the reactor, the radial unevenness in energy released became maximized by the time maximum reactivity was attained (at power generated in the neighborhood of 160,000 MWd) at roughly 1.42 (see Fig. 7, curve 2). In the case of 160,000-420,000 MWd power generated, the radial unevenness in energy released was improved somewhat by more intense burnup of $U^{235}$ at the center of the core, and reached the figure of 1.28 (curve 3). The divergence between theoretical calculations and experiment is explained in this case by an error in the temperature measurements and by the approximate treatment of the axial component in the calculations.

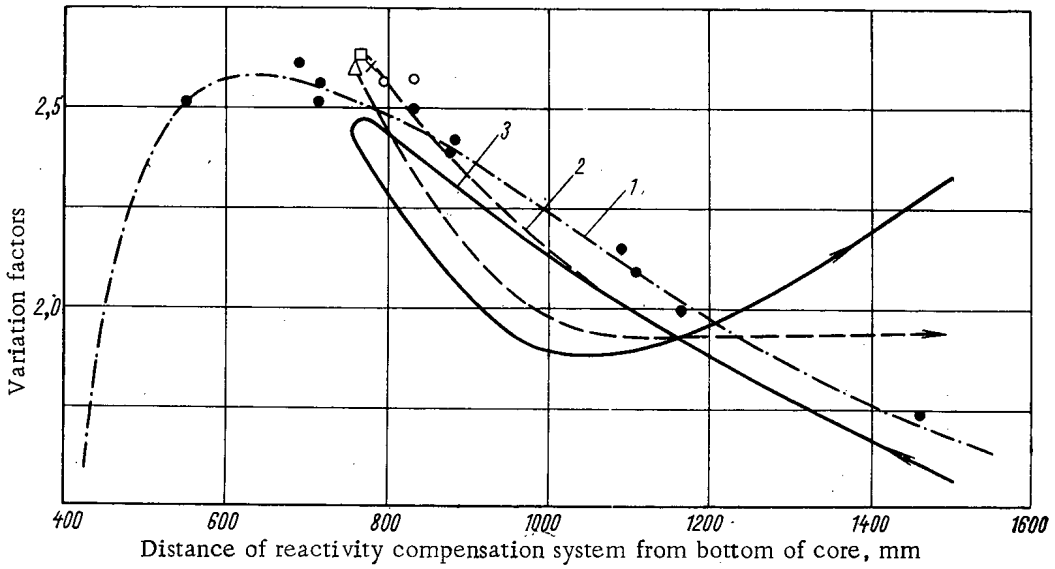


Fig. 8. Axial variation factors for field of thermal neutrons and energy released at various positions of reactivity compensation system. Experimental values plotted at respective power and power output: ○ – 18 MW and 60,000 MWh; □ – 55 MW and 70,000 MWh; × – 54 MW and 110,000 MWh; △ – 55 MW and 160,000 MWh; ● – minimum power monitored at start of run.

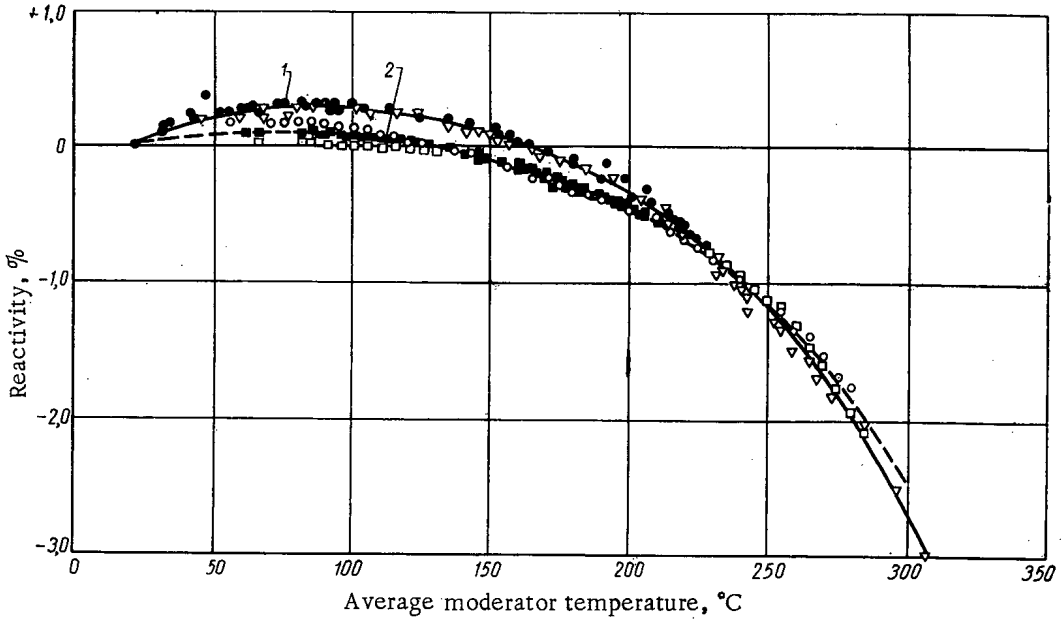


Fig. 9. Temperature effect of reactivity. Experimental values on heating: ●, □ – from external heat source; ▽, □ – from intrinsic heat; ○ – as reactor cools down.

Figure 8 shows the values of the axial variation factors for the field of thermal neutrons and energy released at different depths of immersion of the reactivity compensation system and at different reactor operating conditions. The theoretical curve 1 for the variation factor of the neutron field, corresponding to a cold unpoisoned reactor at the beginning of the reactor period, provides a good fit to the experimental data. Measurements were performed with the aid of miniature fission counters displaced within the steel jackets of the automatic controllers. The change in the axial variation of the thermal neutron field over the reactor period while the reactor is operated at 50 MW is presented by curve 2. Experimental data points on this curve were obtained by activating a copper wire at power levels from 18 to 55 MW. Curve 3 indicates the dependence of the axial variation in energy released on the depth of immersion of the reactivity compensation system.

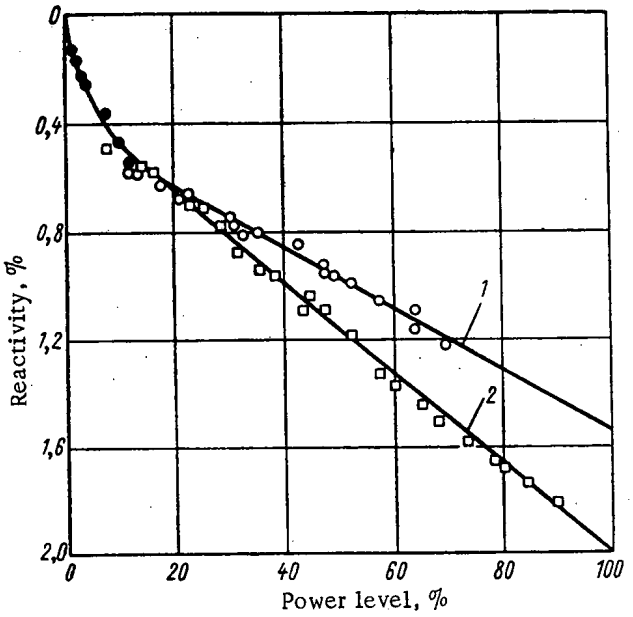


Fig. 10. Reactivity variation due to Doppler effect: ● – experimental data points corresponding to reactivity variation in response to power rise from 0 to 10%.

It should be emphasized that the fuel burns up more evenly along the axis of the fuel channels than would be inferred from the variation factors for energy release plotted in Fig. 8. By displacing the regions of peak neutron flux values along the reactor axis, the fuel burnup curve is brought to display a plateau in the central region (extending about 80 cm) with a burnup fraction amounting to as much as 47% of the amount of $U^{235}$ originally present.

Figure 9 presents curves of the variation in the temperature effect of reactivity. These curves refer to the beginning of the reactor period (1) and to the time when a total power in the neighborhood of 430,000 MWh is achieved (2). The effect of the geometry factor of the core is eliminated; in either case the depth to which the reactivity compensating system is immersed is practically the same. The core was heated up using both an external source of heat (by supply steam to the steam generators on the secondary-loop side and circulating coolant through the primary loop) and by the intrisic pile heat at power levels from 1 to 10 MW.

Figure 10 shows the reactivity change at the initiation of a reactor period (curve 1) and at total generated power of about 430,000 MWd (curve 2) as a function of power level. Up to the 10% power level, the data obtained by stepwise introduction of positive reactivities of different values and by determination of the power levels to which the reactor was brought. The values of the Doppler effect at power levels upwards of 10% were determined with constant circulation of coolant and with rapid power rise and fall, as well as at constant moderator temperature and variable water circulation through the reactor. Appropriate corrections to eliminate the effect introduced by heating up of the moderator were introduced into the results. An enhanced Doppler effect which appears to be related to some change in the structure and thermal conductivity of the fuel core material is observed at the end of the reactor period.

During the span of operation of the "LENIN" icebreaker reactors, the effectiveness of the automatic controllers was measured periodically. At the beginning of the reactor period, the effectiveness of one bank of automatic control rods (three rods) was 0.36%. At peak reactivity, when the power generated amounted to about 160,000 MWh, the effectiveness of the bank of control rods rose to 0.7% and remained practically constant at that level until the end of the reactor period. This increased control rod worth is primarily due to the increased neutron field in the region where the rods were situated, and to the increased diffusion length of thermal neutrons in the core as the burnup of fuel and boron burnout proceeded.

## Reactor Refuelings and Base Servicing

The first refueling of the icebreaker reactors was carried out in 1963. An auxiliary steamship, the "LEPSE," was employed for this purpose, the "LEPSE" being fitted with a storage room for spent-fuel channels and reloading gear, including a portable crane with load carrying capacity of 12 tons, shielded casks for unloading hot channels and control rods, a guide mechanism for setting the refueling cask into the proper site in the core, etc. The onboard crane of the icebreaker "LENIN" also figured in the reactor refueling operations.

The gist of the reactor fueling operations is as follows. The refueling cask 1 (Fig. 11) is set on the shielded plate of the guide mechanism 2 above the fuel channel 3 being prepared for discharge of spent fuel. The hand-operated winch 4 lowers a gripping device 5 inside the shielded fuel cask to engage the fuel channel at the channel head. A periscope 6 serves for monitoring the progress of the gripping device. The fuel channel is then hoisted by the winch into the shielded cask. A shielded gate closes beneath the cask, and the cask with channel inside is transferred by the "LENIN's" crane to the "LEPSE" for unloading into the fuel storage racks.

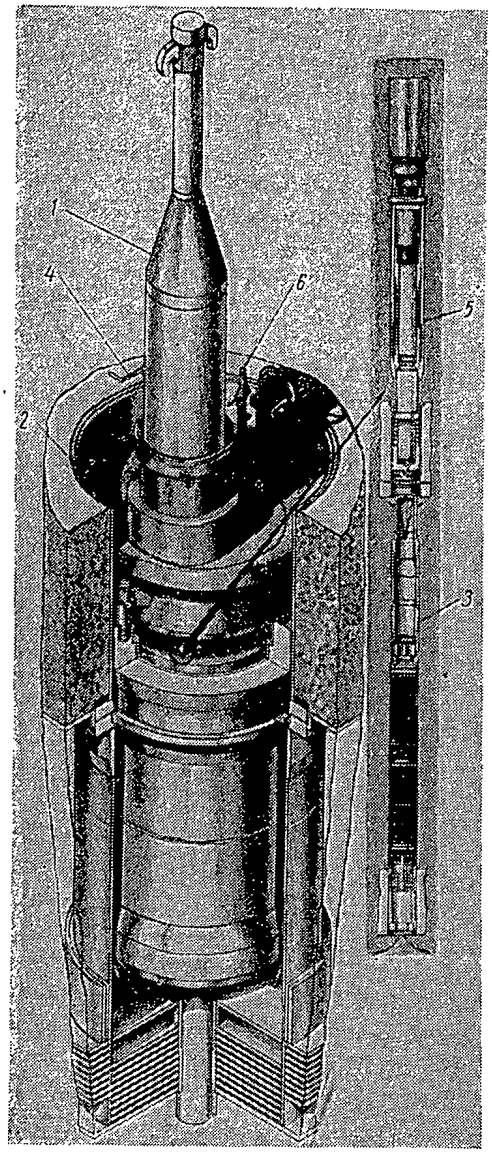


Fig. 11. Reactor and refueling mechanism.

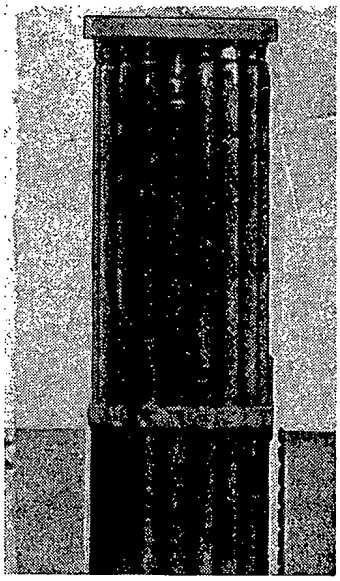

Fig. 12. Fuel channel with fuel elements after decladding removal of exterior jacket.

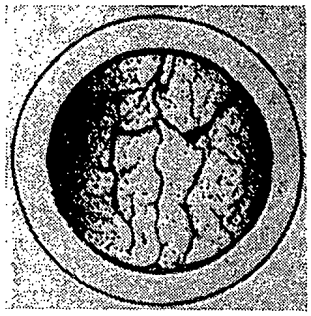

Fig. 13. Polished cross section through fuel element after total power generated ~ 15,000 MWd per ton U (x 25).

In the event that a fuel channel wedges mechanically in the reactor lattice, a jack can be used to pry it loose. Few such jammings occurred during reactor unloading operations. The average discharge time for a single channel is 15-20 min. The entire reactor unloading procedure took about three days.

Investigations of the fuel elements extracted from the icebreaker reactors revealed that they were still in an excellent state (Fig. 12). The fuel elements showed no swellings, bending, bowing, or signs of abrasion. No perceptible changes in rod diameter were observed either. The cladding surfaces were coated with a thin layer of scale, of dark coloration, several microns thick.

Figure 13 shows a section through a fuel element after production of about 15,000 MWd/ton of uranium. The fuel element core shows some cracks, but despite this the clearance between fuel core and cladding is unimpaired. The temperatures at the center of the core were lower than the melting point of uranium dioxide, as evidenced by the absence of abnormal grain growth and the absence of any central hole in the pellet.

After all the fuel channels had been withdrawn from the reactors, the reactors were blown down along with the primary loops. During the loading operations, the fuel channels were let down into the core with all absorber rods inserted to full depth and redundant monitoring in progress to detect any variation in neutron density. It took from 6 to 10 h to complete the reloading of a single reactor core with fresh fuel channels.

After the new and improved fuel channels had been loaded into the reactors, a controlled physical startup was undertaken with subsequent check-out of the physical weights of the control components and of the reactor shielding. The new fuel channels featured the same geometrical dimensions as their precursors, but an advanced technology was employed in their fabrication. Steel-clad fuel elements were loaded in one of the reactors.

The refueling of the icebreaker reactors took place in the vicinity of Murmansk, where a mooring facility was on hand and at least the minimum prerequisite equipment for servicing the icebreaker "LENIN" was available.

## Training of O-Board Personnel

The engineering personnel servicing the nuclear power plant on board the "LENIN" underwent a special training course at the Makarov Maritime Engineering School at Leningrad. They were then assigned to follow-up courses at nuclear power stations. Training and follow-up courses on reactor control culminated in examinations given by the State Commission. Daily examinations and rebriefings took place subsequently at the work assignment sites. The routine operating personnel serving the nuclear facility on board the "LENIN" acquired the necessary operating experience at nuclear industry enterprises.

The first two years of operation were years spent in mastering the intricacies of the nuclear plant. The relevant advantages and shortcomings were uncovered and systematized during that time, and ways of improving controls and smoothing transients were worked on. The servicing personnel of the nuclear and mechanical facilities evinced a high degree of creative initiative in this work and made interesting suggestions on the redesign of control circuitry and on particular components and systems. Some of these suggestions have been carried out in practice.

## Summary

Long-term operation of a nuclear-fueled steam-generating plant on board the icebreaker has provided a basis for a comprehensive assessment of the plant performance under a variety of sailing and weather conditions.

The basic layout and makeup of the nuclear power plant has proven highly successful, and the standby equipment provided for has been completely satisfactory.

No overexposures of service personnel occurred while the icebreaker was in operation. The nuclear plant proved so reliable that the nuclear plant compartment required only one visit a day to inspect the equipment installed there.

The first experiment in building and operating a nuclear maritime power plant, on the icebreaker "LENIN," has been crowned with complete success. The technical feasibility of building high-power nuclear icebreakers for service on the Northern Sea Route has been confirmed.

The experimental neutron-physics characteristics of the reactor cores on the icebreaker were reported by staff members N. A. Lazukov and A. K. Sledzyuk. Control panel logbooks and cruise reports kept by the operating staff of the icebreaker "LENIN" were utilized in preparing this paper.

## LITERATURE CITED

1. V. K. Kovalenko et al., Atomnaya énergiya, 15, 152 (1963).
2. Public-health rules and regulations governing the handling of radioactive materials and sources of ionizing radiations [in Russian], Moscow, State Atom Press (1960).
3. A. P. Aleksandrov et al., Second International Conference on the Peaceful Uses of Atomic Energy, Geneva (1958), P/2140.

# EXPERIENCE IN OPERATING THE FIRST NUCLEAR POWER STATION AS AN EXPERIMENTAL FACILITY*

G. N, Ushakov, L. A. Kochetkov, V. G. Konochkin,
V. S. Sever'yanov, V. Ya. Kozlov, O. A. Sudnitsyn,
N. T. Belinskaya, P. N. Slyusarev, and V. A. Ivanov

Translated from Atomnaya Énergiya, Vol. 17, No. 5,
pp. 359-366, November, 1964

The design of new nuclear power plants, and primarily the design of the I. V. Kurchatov nuclear power station, required a large number of special experiments whose purpose was to gain knowledge on the boiling of water and superheating of steam in fuel elements of tubular design. Other topics studied in these experiments were the conditions prevailing in the formation, buildup, and release of detonating gas, and other experiments were conducted on the study of water treatment, deposits of radioactive impurities from the superheated steam, the behavior of graphite and of steels inside the reactor. The most important problem, a decisive one in the building of new nuclear power generating stations, is however, as generally agreed upon, the problem of experimentally controlled exhaustion of fuel elements. Several experimental test loops had to be constructed as auxiliaries to the First Nuclear Power Station in order to carry out this research.

## Experimental Test Loops

Tests are being carried out at this writing on the following experimental test loops: 1) a two-circuit steam superheat test loop; 2) a natural-circulation water loop; 3) a water loop of water chemistry research; 4) a pressurized water loop; 5) test loops for research on organic fluids (with both high and low boiling points). A brief description of these loops follows.

Two-Circuit Steam Superheat Loop. Experiments are in progress on this loop, the object being to study and elaborate transient modes of operation, to study the water management of radioactive coolant loops (including the study of the formation, buildup, and removal of detonating gas, and scale formation fuel elements and on turbine vanes). The behavior of steels contacted by coolant at loop operating parameters is under investigation. But the chief problems to be resolved in this loop are problems in the testing of fuel elements and of individual components in the operating channels for use in the I. V. Kurchatov nuclear power station. The loop has two radioactive circuits; its design is similar to that of the I. V. Kurchatov power station.

The pump head drives the water into a distributor header, after which the water flows through the passages of individual evaporating channels. The water flowrate is controlled by valves installed in the intake piping of the channels. Downstream of the evaporation channels, the water or steam-water mixture flowing through the individual passages is once again collected into a common header and flows thence to the evaporator down a single pipe. Should the need arise, the water may be partially or entirely routed through a precooler unit.

In the evaporator, the heat in the primary loop is partially or completely transformed to the water in the secondary loop. The secondary loop is made up of an open circulation system and makes it possible to run tests on three steam superheat channels simultaneously. The water in the secondary loop is advanced by a piston feed pump to a combined heater – regenerative heat exchanger unit, where it is heated by cooling the superheated steam. Water heated to the saturation point is directed to the evaporator. Here it is completely evaporated by the heat extracted from the primary loop. Moist steam undergoes further dehumidification in a linear separator unit, after which it is distributed in the header through the individual passages of the steam superheat channels. Control valves and additional individual separators for removing the moisture formed in the supplying passages as a result of the pressure drop and heat losses through the piping walls are installed on each passage of the steam superheat channels.

* Report No. 314 presented by the USSR delegation to the Third International Conference on the Peaceful Uses of Atomic Energy, Geneva, 1964.

The superheated steam is directed, on emerging from the steam superheat channels, to the feedwater heater, and may also be partially bled to feed experimental devices (e.g., in static tests of turbine blading). The steam is finally condensed and cooled down in a condenser and in an additional cooler, after which it is dumped into a water tank after being passed through a flow throttling device.

Departures from the operating conditions which may prove dangerous in plant operation (raising or lowering of the primary-loop pressure, increase in the fuel-element temperature, rise or drop in water and steam flowrates, outage of the circulating pump) bring about an automatic scramming of the reactor.

Water Test Loop with Naturally Circulated Coolant. We should give attention to some features of a test loop with natural circulation of the coolant, features which render this type of loop quite appealing for capsule tests of new fuel-element compositions. First we note the simplicity in maintenance and servicing and the attendant reliability, and next we note the small volume, making it possible to cope with ease with the consequences of an accident due to fuel-element rupture.

The loop is set up in a two-circuit system. The first circuit is closed; it includes entrance and exit headers, a heat exchanger, experimental channels, a cooler designed to facilitate sampling, and a volume compensator.

Water Test Loop for Water Chemistry Research. The test loop described here is designed for the study of water chemistry, of the diffusion of nitrogen from the volume compensators, of corrosive attack on low-alloy steels, and for the study of how to protect these steels and slow down the corrosion rate, for tests on filters for removing corrosion products from the loop, etc. A regenerative heat exchanger and an experimental channel are employed to heat the coolant. Heat extraction takes place in the heat exchanger, where the heat is transferred to the secondary-loop water. A tank instrumented for preparing the necessary solutions and slurries, and provided with ion exchange filters and sampling devices, is placed in the loop for chemical research operations.

The heat transfer and heat control equipment makes it possible to carry out experiments over the temperature range 50-300°C. The principal design feature of this loop is the structure consisting of two parallel loops: one of these is of stainless steel, the other of low-carbon steel. This system was set up to facilitate a more objective comparative assessment of the corrosion rates of different steels subjected to identical environments.

Pressurized Water Test Loop. This loop was designed to test a variety of fuel element designs, and also for research on the percent burnup of fuel compositions, and for miscellaneous materials research and testing. Heat is removed from the experimental channels by the primary-loop water, which is circulated by a packless electrically driven pump. The primary-loop water is cooled in the heat exchanger by the secondary-loop water, and heat is extracted from the latter by the circulation water flowing through the over-all system.

The water temperature at the entrance to the experimental channels can be varied over a wide range (100 to 200°C) during the experiments. This measure of control is provided by a bypass line around the main heat exchanger valving the flow through the primary loop. Experimental research conducted in this loop concerned the probability that fission-fragment activity will gain access to the loop. As a consequence, all the basic primary-loop equipment has been enclosed in a special shielded box. Counters have been placed on the exit pipes of the channels to monitor the $\gamma$-ray dose rate of the coolant emerging from the reactor channel.

Organic Fluids Testing Loops. The building of these test loops is dictated by the need for studies on the radiation stability of organic coolants, studies of activation of organic coolants, of the deposition of polymerizates on the heating surfaces, etc. It is moreover mandatory that experience be acquired in the operation of organic-cooled plants, that the corrosion stability of structural materials in an organic medium under neutron irradiation conditions be studied, and that a study be made of the change in the heat transfer properties of organic coolant while the loop is in operation.

Test Loops for Research on High-Melting-Point Organic Fluids. The facility consists of a basic circulation loop and several auxiliary systems. The primary-loop coolant arrives, after passing through the operating channel where it is heated and irradiated, at a heat exchanger where it is cooled by process water. The coolant passes from the heat exchanger to a surge tank, and is pumped from the tank back into the channel. A loading tank is designed into the system, for meltdown of the solid organic and subsequent extrusion of the organic melt into the surge tank. Tonnage nitrogen is employed to set up an insert atmosphere in the surge tank and in the auxiliary devices of the loop.

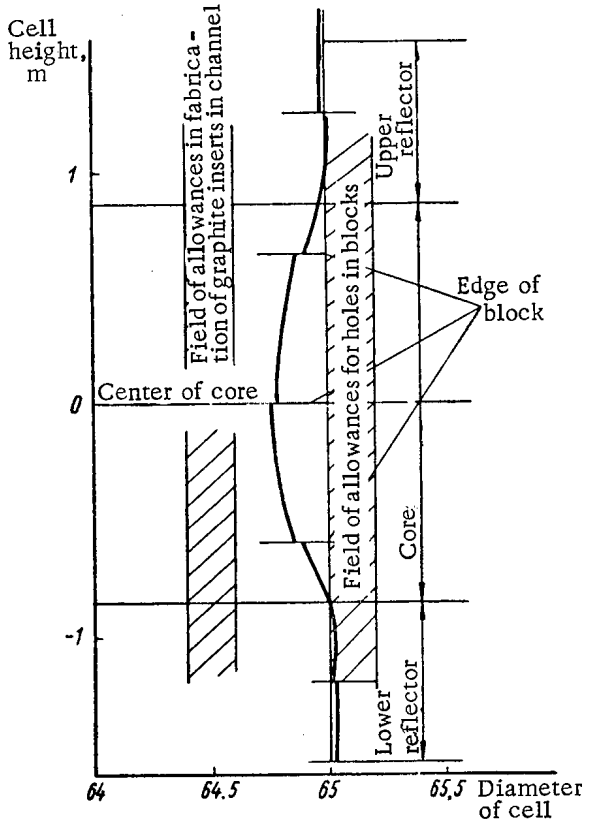


Fig. 1. Graphs showing variation in hole diameter in one of the stacking cells plotted versus reactor stack height.

Since the loop is designed for handling organic materials whose melting points are above room temperature, an electric heating system is included for heating the piping. The primary-loop heat exchangers and the sampling coolers are heated with hot water.

Test Loop for Studying Low-Melting-Point Organic Fluids. Included in the principal circulation loop are: an operating channel with fuel elements, circulation pumps, the basic heat exchanger, a combined surge tank and deaerator, a filter for mechanical cleanup of the coolant, piping, and fittings. A bypass line with control valve situated at the basic heat exchanger is included in the loop for altering temperature conditions.

The loop operating pressure is established by supplying an inert gas (nitrogen) to fill the gas volume of the surge tank. The gas volume of the surge tank consists of a receiver and simultaneously a storage tank for gases released from the coolant. The bulk of the coolant is found in the surge tank. The coolant level required in the tank is maintained by fresh coolant makeup or by pouring the coolant off into a drainage tank. In the event that the main circulation pumps should malfunction, there is an emergency shutdown pump which goes into action automatically. This same pump is used otherwise for feed and fresh coolant makeup, the makeup coolant being provided for beforehand in a special refill tank.

## Graphite Stacking of the Reactor

The high temperature of the coolant and the appreciable volume release of heat in the fuel element bring about a high temperature in the graphite stacking of the reactor. In order to prevent damage to the graphite at elevated temperatures, nitrogen with up to 0.2 vol.% oxygen content is employed to fill up the stack in the power station reactor.

The ten-year period of operation of the reactor graphite stacking at temperatures reaching 800°C and at high-neutron flux levels has demonstrated that very little of the graphite is affected in a nitrogen environment. It is imperative to stress that the content of oxygen, hydrogen, and carbon dioxide gas is kept constantly at a level of 1 vol.% under the operating conditions of the nitrogen filling the reactor stack. Visual inspection of the surface of the graphite blocks in the reactor and measurements taken of the diameters of holes in the blocks at various points up the stack support the conclusion that the graphite in the reactor stack is in an entirely satisfactory state after ten years of operation of the power station reactor.

Figure 1 shows a graph of the variation in hole diameter in one cell of the stack with respect to reactor height over the ten-year on-power period under high-neutron flux levels and high-nitrogen environment temperatures. Clearly, the graph shows maximum reduction in the diameter of holes in the graphite blocks at the center of the core, with holes narrowed from a rated diameter 65.0-64.8 mm, i.e., a narrowing of 0.1 mm radially. These volume deformations of the graphite blocks still do not affect the clearance anticipated in the design between the graphite block and the react channel, so that no hindrance results to installation or removal of reactor channels.

The integrated fast flux and integrated thermal flux over the center of the core in the given cell is $0.5 \cdot 10^{22}$ neutrons/cm$^2$, while the temperature of the graphite reaches 650°C on the inner surface of the block under operating conditions. Measurements of the hole diameters were taken with the aid of a specially designed device backed up by an automatic recorder. The precision of the measurement procedure enables us to assume that the volume changes in the graphite blocks over a protracted operating period do not exceed 0.15% under the operating conditions of the power station reactor.

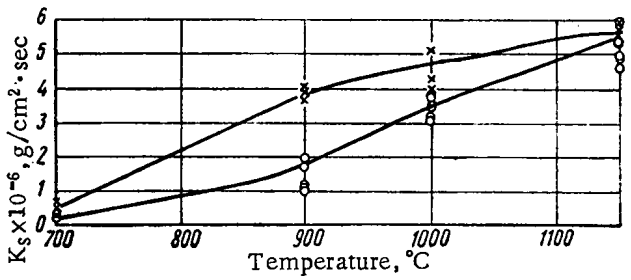


Fig. 2. Specific oxidation rate $K_S$ vs temperature: ×, ○ – unirradiated and irradiated nitrogen, respectively.

In order to clarify the possibility of further rises in the operating temperatures of the graphite, some studies were made to determine the stability of graphite in a nitrogen environment over the 700-1150°C temperature range. In order to determine the rate of oxidation of graphite, a method of continuous weighing of the specimen to be tested in a stream of gas was decided upon. These investigations were carried out in what is known as the kinetic mode of operating conditions, when the reaction rate of the oxidation process is independent of the flowspeed of the gas (at gas flowrates upwards of 200 liters/h), in order to eliminate the effect of the velocity of the gas stream.

To provide a quantitative evaluation of the process, we took the specific oxidation rate

$$K_s = \frac{\Delta x}{S \Delta t} \ \text{g/cm}^2 \cdot \text{sec},$$

where $\Delta x$ is the weight change of the sample in g, $\Delta t$ the experiment time in sec, and S the surface area of the sample studied in $cm^2$.

The investigations were carried out on graphite specimens irradiated under reactor operating conditions at an integrated dose of $(0.4\text{-}0.8) \cdot 10^{21}$ neutrons/$cm^2$ (fast neutrons and thermal neutrons) in an environment of nitrogen irradiated in the reactor and of unirradiated nitrogen. On the basis of the experiments, a graph was constructed of the specific oxidation rate as a function of temperature (Fig. 2). The graph clearly shows that as the temperature is raised from 700 to 1150°C, the rate of the oxidative reaction in a nitrogen medium increases by roughly a factor of ten. A certain difference discerned in the oxidation rate in irradiated nitrogen and in unirradiated nitrogen over the 700-1000°C range may be accounted for by the difference in the integrated exposure doses received by the specimens studied (as may be ascertained from the literature, high oxidation rates correspond to large integrated doses). It should be stressed that starting at 1000°C this difference in oxidation rate evens out and completely vanishes by 1150°C. The phenomenon alluded to may be accounted for by annealing of radiation damage in the graphite such as occurs at elevated temperatures.

The original nitrogen employed in the experiments contained the following impurities (in vol.%): oxygen (0.001-0.002); carbon dioxide gas (0.04-0.4); carbon monoxide (0.04); hydrogen (0.16-0.4). Oxidation of the graphite, which took place in a nitrogen medium, may be explained by the presence of these impurities in the nitrogen.

The preliminary data which we obtained do not yet substantiate any inference on the possibility or feasibility of using graphite stacks in a nitrogen environment at temperatures above 800°C.

Since steam may get into the nitrogen medium under certain conditions affecting the operation of graphite-water reactors, studies were also made to determine the behavior of graphite in an environment of nitrogen and steam at elevated temperatures.

Experiments to determine the oxidation rate of irradiated graphite were carried out at steam-gas medium flowrates of 900 liters/h. As a result of these experiments, it was established that the rate of the oxidation reaction over the 700-1000°C temperature range increases by approximately 50% as the steam concentration is raised from 5 to 20 vol.%, and then remains more or less constant as the steam concentration is raised still higher. For practical purposes, it is safe to assume that at steam concentrations above 20% the oxidation reaction rate will undergo only an insubstantial increase.

## Channels and Fuel Elements of Tubular Design

The design of reactor channels and fuel elements for the reactor serving the First Nuclear Power Station under high neutron irradiation conditions and high-thermal loads has gone through extremely protracted tests and come out with flying colors. The design of a channel with tubular fuel element is a design for universal application and makes it possible to utilize such a channel under boiling, and even under steam superheat, conditions. No far-reaching changes in channel design are required to achieve such operating conditions. All changes reduce to the introduction

of additional resistance, such as spacers on the intruding ends of fuel elements. As far back as September, 1956, boiling water operation was achieved in one of the operating channels of the reactor, and by mid-1957 over one half the channels were operating under boiling water conditions; by the beginning of 1960, in fact, boiling water conditions had been achieved in all the operating channels. Following on the heels of this accomplishment, the possibility of operating channels with tubular fuel elements and under steam superheat conditions was confirmed. The most complicated problems encountered in resolving this task involved the startup conditions. In order to achieve reliable cooling of the steam superheat channels during the reactor startup period in the face of a constant rise in reactor power, an experimental try-out was made of a procedure for effecting a continuous transition from water cooling to steam cooling with a smooth rise in steam content in the channels right up to the point where dry saturated steam was achieved first, to be followed by achievement of steam superheat conditions.

A channel of conventional design successfully underwent tests over 1000 h of steam superheat conditions; the reactor was brought up to steam superheat conditions some 50 odd times, each time involving a transition from water cooling to steam cooling. In addition to the universal applicability of the channel mentioned earlier, successful use was made of the channel in natural circulation of pressurized water and in boiling water operation. It was ascertained experimentally that a thermal power of 110 kW can be reliably extracted from the channel in natural circulation under both boiling and nonboiling conditions, even with the natural circulation loop falling far short of optimum performance.

Below, we list the basic engineering data for the channels and fuel elements in the First Nuclear Power Station, while their operating conditions in the various operating modes are entered in Table 1.

| | |
|---|---|
| Height of fuel element, mm | 1700 |
| Fuel element O.D., mm | 14 |
| Thickness of fuel element cladding, mm | 0.2 |
| Fuel element I.D., mm | 8.2 |
| Thickness of fuel element inner lining, mm | 0.4 |
| $U^{235}$ enrichment, % | 5-7 |
| Total amount of uranium in channel, kg | 4 |
| Total heat transfer surface of channel, $m^2$ | 0.175 |
| Water flowspeed in channel, m/sec | 3.5-4.5 |
| Structural material | Stainless steel |

The design of the tubular fuel element excludes any possibility, even in the event of rupture, of the fission products and fissile material getting into the circulation loop, since the pressure in the loop is consistently far in excess of the gas pressure in the reactor stack. The many years of experience in operating the reactor confirmed this point and at the same time demonstrated the optimistic outlook for the use of tubular fuel elements in direct flow single-loop systems. The operating practice of process channels has resulted in a substantial lengthening of the planned service life in-pile of the channels.

An imposing number of fuel elements (about 70% of the total) in the reactor outlived their planned service life. There was also a small number of fuel elements (about 3% of the total) which lasted 400-500 effective days of in-pile service.

Moreover, one group of fuel elements (0.5% of the total) was subjected to long-term tests (lasting 600 effective days) in order to determine the maximum allowable operating time for structural members of the channel and for fuel elements.

$U^{235}$ burnup of 30-32 kg/ton of uranium was achieved, and the scheduled operating life of the channels was about 44,000 h. The indicated burnup levels were achieved by resorting to the method of partial refuelings loading individual channels with enhanced enrichment (to 7%) into the reactor.

Some instances of loss of pressure tightness in individual operating channels without a concomitant rupture of fuel elements were observed while the reactor was on-power. The number of leaked channels constituted no more than 0.3% of the total number of channels in use over a protracted period of reactor operation (from 1955 through 1964). Practice showed that even in the presence of leaks involving 100-1000 g/h, the channels and the reactor itself remained operative and capable of answering to the need to keep the power station on the line at the present power leve. Channels and fuel elements of similar design are also used in the I. V. Kurchatov power station reactor.

TABLE 1. Operating Conditions of Channels and of Fuel Elements in the First Nuclear Power Station under Different Operating Conditions

| Process parameters | Operating conditions | | | | |
|---|---|---|---|---|---|
| | water | boiling | superheat | natural circulation | |
| | | | | nonboiling | boiling |
| Maximum temperature of fuel element wall, °C | 340—450 | 340—450 | 470—500 | 360 | 340 |
| Maximum coolant flowrate, kg/h | 1000—2000 | 700—1000 | 600 | 550 | 460 |
| Operating pressure, kg/cm² | 100 | 100 | 90 | 100 | 100 |
| Coolant temperature, °C: | | | | | |
| at channel entrance | 180—190 | 190 | $t_s$ | — | — |
| at channel exit | 270—310 | $t_s$ | 370 | 309,5 | $t_s$ |
| Heat load, kcal/m²·h | 0,8—1,8·10⁶ | — | — | — | — |
| Thermal rating of channel, kW | — | — | — | 110 | 117 |
| Maximum steam content by wt. at channel exit, % | — | 2—25 | — | — | 27 |
| Composition of water, mg/kg | | | | | |
| dry residue in water | 2—3 | 1,5—3 | 0,6—1,1 | 2,0—3 | 1,5—3 |
| pH | 5,6—6,8 | 5,6—6,2 | 5,5 | 5,4—5,8 | 5,4—5,8 |
| $O_2$ | 4,5—7,0 | 4,5—7,0 | 4,6 | 3—7 | 3—7 |
| $CO_2$ | 0,5—1,0 | 0,5—1,0 | 0,9 | 0,5—1,0 | 0,5—1,0 |
| $NO_3^-$ | 0,1—0,8 | 0,1—0,7 | 0,1—0,15 | 0,1—0,7 | 0,1—0,7 |
| $Cl^-$ | 0,02 | 0,02 | 0,02 | 0,02 | 0,02 |
| $CrO_4''$ | 0,05—0,20 | 0,05—0,20 | 0,015 | 0,05—0,09 | 0,05—0,09 |
| $Cr^{+++}$ | 0,002—0,05 | 0,005—0,05 | 0,015 | 0,005—0,05 | 0,005—0,05 |
| Fe | 0,05—0,1 | 0,05—0,1 | 0,05 | 0,05—0,1 | 0,05—0,1 |
| Ni | 0,005—0,02 | 0,005—0,02 | 0,005 | 0,005—0,04 | 0,005—0,04 |
| $H_2$ | 0,4—0,7 | 0,4—0,8 | 0,3—0,5 | — | — |
| $N_2$ | 5—12 | 5—12 | 5—12 | — | — |

TABLE 2. Data on I. V. Kurchatov Power Station Fuel Element Tests

| Percentage tested of total fuel elements | Burnup MWd/ton | Heat flux, kcal/m²·h | Fuel element wall temperature, °C |
|---|---|---|---|
| 10 | 10000—15000 | 1,3—1,6·10⁶ | 400—430 |
| 30 | 6100—6500 | 0,75—0,85·10⁶ | 400—440 |
| 30 | 5500—6000 | 0,75—0,85·10⁶ | 400—440 |
| 10 | 5000—5400 | 0,75—0,85·10⁶ | 400—440 |
| 20 | 1000—5000 | 0,5—0,8·10⁶ | 430—550 |

Various tests were run on these fule elements at the experimental water test loops of the reactor in the First Nuclear Power Station. Table 2 cites some data on tests of fuel elements used in the I. V. Kurchatov power station.

## Investigation of Radiolysis of Water and of Superheated Steam

In loop tests, the burden of the investigators' attention is focused on the study of the radiolysis of steam in the superheat mode, since this is the basic operating mode in the I. V. Kurchatov power station reactor.

An equilibrium concentration of water radiolysis products is established in the operation of the reactor in the primary loop (pressure 135 kg/cm², temperature 250°C at channel entrance, 330°C at channel exit). At a specific loop power of 1.1 kW/kg, the hydrogen concentration will not exceed 2.5 ncm³/kg, that of oxygen 1.2 ncm³/kg. In the secondary loop (pressure 40-80 kg/cm, steam temperature at exit 410°C), the yield of water radiolysis products will depend to a marked extent on the operating conditions in the system and on the concentration of free (dissolved) oxygen in the water (Table 3). Hydrogen leaks in the system were detected when the experimental studies were carried out, and these leaks may be accounted for by sorption and diffusion through the walls of the operating channels, since other causes are excluded. Hydrogen leaks are aggravated when the temperature of the walls rises.

At water and steam temperatures up to 300°C under heating conditions and transients, leaks account for up to 50% of the hydrogen released in radiolysis, while under superheat conditions up to 400°C leaks account for 75-80% of the hydrogen. The most probable leak sites for hydrogen are in the channel, since the thickness of its walls ranges 0.6-0.7 mm; weld seams provide equally likely leak sites.

TABLE 3. Yield of Radiolytic Gases (Hydrogen and Oxygen) Compared to Operating Conditions and Concentration of Dissolved Oxygen

| Operating conditions | Concentration of free (dissolved) oxygen, mg/kg | Yield of radiolytic gases in $ncm^3/100$ kWh | |
|---|---|---|---|
| | | hydrogen | oxygen |
| Heating. . . . . | 1,0—1,5 | 500—600 | 250—300 |
| Transient. . . . . | 1,0—2,5 | 1660 | 830 |
| Superheat. . . . . | 0,3—1,1 | 330—410 | 160—200 |
| Superheat. . . . . | 0,01 | 2400 | Oxygen chemically bound |

## Investigation of Deposits of Radioactive Impurities from Superheated Steam on Turbine Blade Models

A turbine blading test stand has fixed blades simulating the blading of the VK-100 turbine in that region where formation of the largest amount of deposits is observed (from conventional power practice). The operating experience of industrial turbines demonstrates that the chemical composition of the deposits found on rotor and stator turbine blades is more or less the same in either case. The test stand featured three stages of models of the VK-100 turbine blading operating at a variety of steam parameters: first stage at steam pressure 30 $kg/cm^2$ and steam temperature 350°C; second stage at steam pressure 10 $kg/cm^2$, and temperature 250°C; third state at steam pressure 2 $kg/cm^2$, and temperature 140°C.

The basic purpose envisaged in these tests is to determine which long-lived isotopes settle out on the models of the turbine vanes as steam superheated directly in the reactor channels is passed over them. It was established experimentally that radioactive deposits actually occur.

At an average activity of $5 \cdot 10^{-9}$ Ci/kg on the part of the superheated stem, the $\gamma$ activity and the $\beta$ activity of the deposits averages out the same on models of turbine blades in one month of operation: $2.7 \cdot 10^{-7}$ on the first stage, $2.0 \cdot 10^{-7}$ on the second stage, and $4.0 \cdot 10^{-8}$ on the third stage (figures refer to $Ci/cm^2$). In two days after the test stand is shut down, 70% of the total radioactivity in the deposits will have decayed. The residual activity of the first two stages was 10% of the initial radioactivity after a month had elapsed.

The long-lived radioactivity of the deposits on the turbine vane models under the operating conditions of the experimental test stand is due to $Fe^{59}$, $Cr^{51}$, and $Co^{60}$.

The investigations revealed the highest activity of the deposits to be on the first two stages of the turbine models at steam pressures of 30 and 12 $kg/cm^2$. The depositions occurred primarily on the convex faces of the blade models, and were virtually nonexistent on the other faces.

As a result of a spectrochemical analysis, it was found that the principal components of all the deposits studied consisted of iron, chromium, nickel, and calcium; cobalt was detected only by radiometric means.

The radioactive deposits are chemically stable compounds unaffected by the water or steam.

# CONTAINMENT OF PLASMA IN A TRAP WITH COMBINED MAGNETIC FIELD

(UDC 533.9)

M. S. Ioffe and R. I. Sobolev

Translated from Atomnaya Énergiya, Vol. 17, No. 5,
pp. 366-375, November, 1964
Original article submitted September 10, 1964

The containing properties of an adiabatic trap with a magnetic field increasing in the longitudinal and radial directions are investigated. This field is obtained from a combination of the ordinary mirror field configuration (main field $H_{0\parallel}$) and the field of a system of current-carrying conductors laid parallel to the axis of the trap (stabilizing field $H_\perp$). The conductors are placed uniformly in azimuth around the side walls. The trap is filled with plasma of density $n \approx 10^9$-$10^{10}$ cm$^{-3}$ and proton energy $T_i \approx 5$ keV ($T_e \approx 20$ eV). The plasma lifetime is measured as a function of $H_\perp$ and the neutral gas pressure. From the results obtained, it is concluded that such combined fields ensure stable containment of the plasma, unbroken by magnetohydrodynamic instabilities [at any rate for $\beta = nI/(H^2/8\pi) \approx 10^{-4}$]. The stabilization of the instability is confirmed by analysis of the plasma oscillations for various values of $H_\perp$. The disintegration of the plasma is determined by the charge exchange of fast ions in the residual gas; the maximum containment time which can be achieved is 0.06 sec for $p = 7 \cdot 10^{-9}$ mm Hg. A qualitative picture of the plasma density over the radius of the trap is obtained.

## Introduction

Investigations on the containment of plasma in traps with magnetic mirrors carried out on a number of experiment systems ("Ogra" [1], "Ion Magnetron" [2] in the Soviet Union, "Table Top III" [3] in the United States, "Phoenix" in England [4], etc.) show that the primary reason for the lack of success in achieving prolonged containment is instability of the flute type, which engenders transport of the plasma across the magnetic field. We know from magnetohydrodynamical considerations [5-7] that the cause of this instability is the fall in the magnetic field intensity away from the axis of the trap in a radial direction.

Recently a kinetic theory of flute instability has been developed [8-10], and a stabilizing effect associated with the finiteness of the ionic Larmor radius has been observed. It is shown in [8] that, if the Larmor radius $\rho_i$ is not too small compared with the dimensions of the trap, in other words, when $(\rho_i/a)^2 \gtrsim a/R$ (a is the characteristic transverse dimension of the plasma, R the effective radius of curvature of the magnetic lines of force), a plasma of fairly high density should be stable with respect to perturbations $m > 1$. For low densities, when the ionic Debye radius $[(kT_i/4\pi ne^2)^{1/2}]$ becomes comparable with $\rho_i$, the stabilizing effect vanishes [10].

The conclusions drawn from this theory have not yet received reliable experimental confirmation.

The adiabatic trap with combined field described in the present paper differs from the ordinary trap with mirrors in that its magnetic field does not fall off in the radial direction, but in fact rises. Hence, the conditions for the development of flute instability should not arise.

This field distribution is achieved by the introduction of an additional so-called stabilizing winding. Schematically, this winding constitutes a system of rectilinear current-carrying conductors disposed uniformly around the trap parallel to its axis; the currents through neighboring conductors travel in mutually opposite directions. The field created by the stabilizing winding is in structure analogous to the field of a trap with hyperbolic geometry.

Preliminary studies on the stability of plasma in this kind of combined system were set out in a report to the Conference on Plasma Physics in Salzburg (1961) [11]. Later the experimental PR-5 system was set up, specially designed for the study of combined field properties. The main parameters of this system and the results of the first experiments carried out on it are described in [12].

The present paper presents results of more detailed investigations into the behavior of the plasma, and also a more detailed description of the contruction of the system.

## Description of the System

A general view of the PR-5 system is shown in Fig. 1. The main (longitudinal) field, constant in time, is created by eight coils. The distribution of the longitudinal field along the axis of the system is shown in Fig. 2. The region G forms the actual trap. To the left of this, is placed the injection part of the system, containing the plasma source and an arrangement for the differential evacuation of neutral hydrogen coming out of the source.

The maximum field intensity in the center of the trap is $H_{0\parallel} = 5$ kG, and in the mirrors $H_{0\,max} = 8.5$ kG; accordingly the longitudinal mirror ratio is $\alpha_{\parallel} = 1.7$. The distance between the mirrors is 120 cm.

The stabilizing winding is placed in the gap between the main field coils in the vacuum chamber. The winding is made in the form of three single layer plane frameworks of rectangular shape, uniformly disposed around the vacuum chamber along its generatrix. Each frame consists of ten turns of thick walled copper tubing of rectangular cross section 12 x 15 mm. The frames are connected in series. The length of the frames is 250 cm. The winding is firmly fixed to the inner surface of a massive textolite cylinder of diameter 50 cm. This cylinder takes up the

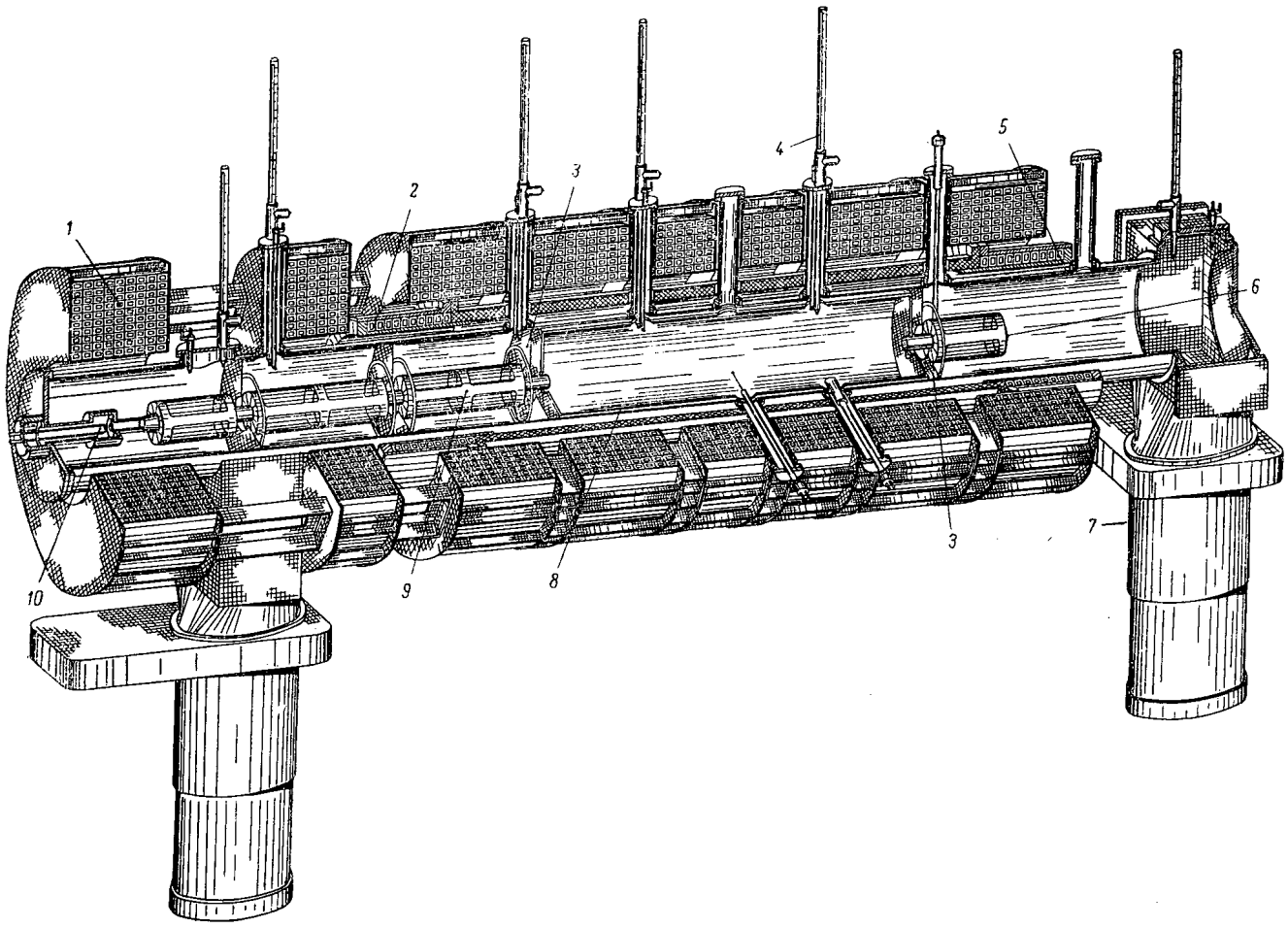


Fig. 1. General view of the PR-5 apparatus. 1) Main (longitudinal) field coils; 2) stabilizing winding; 3) diaphragms; 4) titanium evaporators; 5) vacuum chamber; 6) receiver electrode; 7) oil vapor pumps; 8) azotite 9) perforated screens; 10) plasma source.

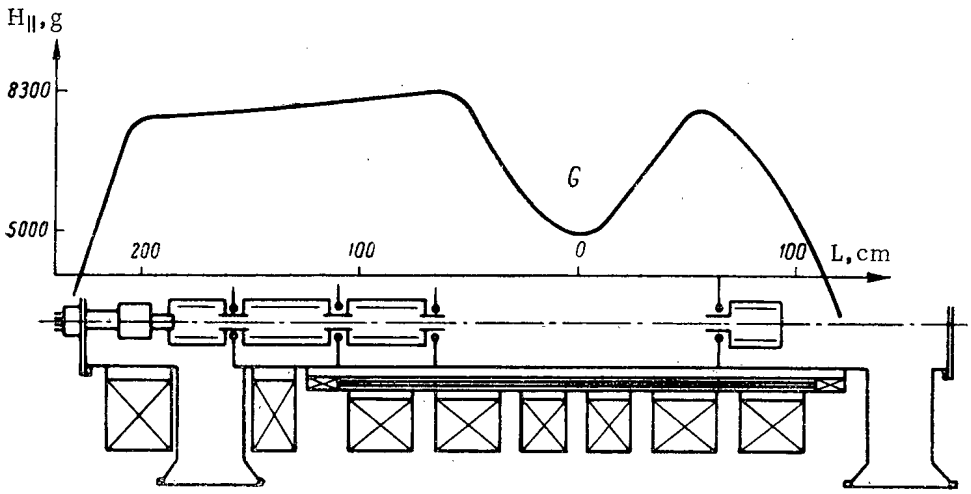


Fig. 2. Main magnetic field distribution along the axis of the system.

mechanical stresses acting during the passage of current through the windings, and simultaneously serves as a structural element ensuring the proper adjustment and reliable positioning of the winding. A calculation for the stabilizing winding is given, together with the adiabatic parameter of the combined field, in [13]. The field created by this coil will hereinafter be called the stabilizing field. The maximum value of this field at the vacuum chamber walls ($H_\perp$) is 4.5 kOe. The radial ("wall") mirror ratio in the central section of the trap $\alpha_\perp = [1 + (H_\perp / H_{0\parallel})^2]^{1/2}$ is 1.4 for the maximum value of $H_{0\parallel}$.

The winding is fed from a battery of condensers of the IM-5/150 type with total capacity 0.15 F. The switching of the battery on to the winding is effected by ignitrons IVS-100/15. The electrical arrangements provide for unipolar current pulses of sinusoidal form with duration up to 75 msec every 10-20 sec.

The vacuum chamber, 4 m long and 40 cm in diameter, is made of stainless steel. The chamber is preliminarily pumped out to a pressure of $10^{-6}$ mm Hg by two oil vapor pumps furnished with nitrogen traps. In order to obtain high vacuum, sorption pumping with sputtered titanium is employed. The chamber is divided into five compartments by diaphragms, and a titanium evaporator is placed in each. Inside the central compartment, comprising the working space of the trap, is placed an "azotite" [14]. The azotite is made in the form of a double walled cylinder of stainless steel; in the space between the walls is placed liquid nitrogen. Titanium is sputtered on to the inner surface of the azotite. The diameter of the working space of the trap equals 38 cm.

Three sections in the injection part of the apparatus form a differential sorption pumping system for the hydrogen coming out from the plasma source.

The hydrogen is admitted to the source by way of a palladium leak in individual pulses 0.1 sec long to the extent of $10^{-2}$ cm$^3$ at atmospheric pressure.

The differential pumping system used in conjunction with the azotite ensures a pressure drop of 500-1000 times between the source compartment and the working space of the trap. The minimum pressure in the trap under working conditions is $(0.7\text{-}1.0) \cdot 10^{-8}$ mm Hg. The pressure is measured by the ionization manometer MI-12; the sensitive element is set in a special tube 50 cm long and 6 cm in diameter and is protected by a magnetic screen.

The plasma source operates under pulse conditions: A rectangular voltage pulse 300 μsec long and with amplitude up to 1000 V is applied between the incandescent cathode and anode of the source; the discharge current is 10-20 A.

The cold plasma formed in the source is propagated in the form of a beam along the magnetic field and neutralized at the receiver electrode.

In order to fill the trap with plasma containing fast ions, pulsed magnetron injection from the cold plasma beam is used, as described in [2]. To the plasma source and its related beam, is applied a positive potential in the form of a rectangular pulse of amplitude 30 kV and duration 20-30 μsec (accelerating voltage pulse). The radial electric field so created accelerates the ions out of the beam.

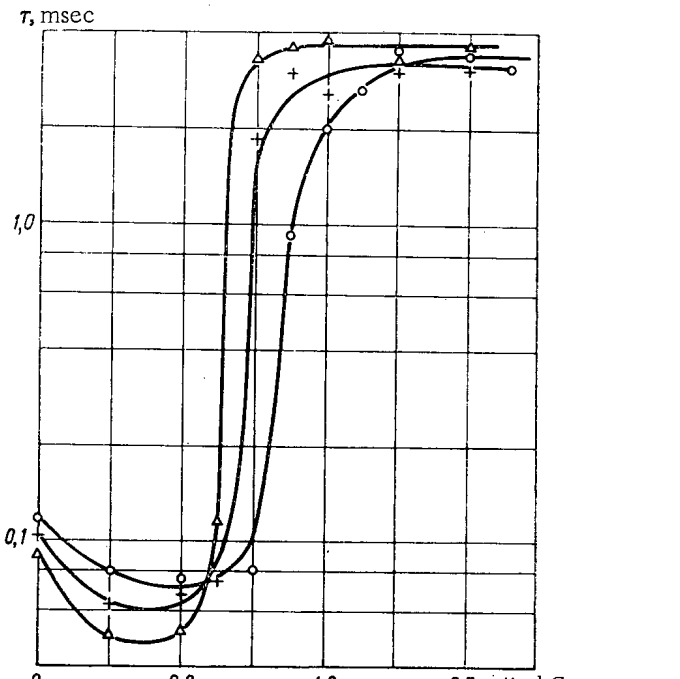


Fig. 3. Plasma lifetime as a function of stabilizing field intensity.

In order to prevent the cold plasma beam from breaking up in the electric field on the way from the source to the entrance into the trap and on leaving the latter (which could lead to a considerable loss of vacuum), the parts of the beam lying outside the trap are surrounded by cylindrical perforated screens, which are insulated from the diaphragms and held at source potential.

The accelerating voltage pulse is synchronized with the discharge pulse in the source in such a way that both come to an end simultaneously. The discharge pulse in its turn is synchronized with the current pulse in the stabilizing winding, and can be displaced relative to the start of the latter within wide limits.

The plasma filling the trap at the moment when injection ends has the following parameters in the presence of a stabilizing field: $n \sim 10^9$-$10^{10}$ cm$^{-3}$, $T_i \approx 5$ keV, $T_e \approx 20$ eV.

## Experimental Results

The behavior of plasma obtained by magnetic injection in an ordinary trap with mirrors was discussed in detail earlier [2, 15]. The chief data on plasma instability so obtained is based on measurements of plasma lifetime and the radial distribution of plasma density, as well as observations on local density oscillations within the trap.

In this paper we carry out an analogous cycle of measurements for the combined field trap and compare the results from the two systems.

1. Measurements of Plasma Lifetime. Plasma lifetime was measured from the fall in the flux of fast neutral charge exchange particles after the end of injection. For a constant neutral gas pressure, the rate of fall of this flux characterizes the mean time of existence of the fast ions in the trap.

The detection of the fast particles was effected by means of secondary electrons, using the method of [2].

Plasma Lifetime as a Function of the Stabilizing Field. The effect of the stabilizing field on the containing properties of the trap may be most clearly followed by measuring the plasma lifetime $\tau$ as a function of $H_\perp$ for constant main field $H_{0\parallel}$. Figure 3 shows the results of such measurements made for trap pressure $1.5 \cdot 10^{-7}$ mm Hg and several values of $H_{0\parallel}$. The horizontal axis shows $H_\perp$ and also the radial mirror ratio $\alpha_\perp$ for each of the $H_{0\parallel}$ values.

The curves presented show that the application of field $H_\perp$ produces a very considerable increase in $\tau$. The characteristic feature of this increase lies in that it takes place almost in one jump, when $H_\perp$ reaches a certain value. This value grows with increasing $H_{0\parallel}$; it further appears that at the jump point $\alpha_\perp$ remains the same for different $H_{0\parallel}$ values, being approximately 1.1.

The "jumpy" behavior of the $\tau(H_\perp)$ curves enables us to distinguish two different plasma containment conditions: the stabilized state with large $\tau(\alpha_\perp > 1.1)$, and the unstabilized state with small $\tau(\alpha_\perp < 1.1)$.

In the series of measurements shown in Fig. 3, the unstabilized $\tau$ lies within the limits 0.05-0.1 msec, in agreement with data obtained in [2] for the ordinary trap. As shown in [2], the lifetime is determined by plasma losses due to convective instability. Under stabilized conditions $\tau$ is around 3.5 μsec. An estimate shows that for the conditions of the present experiment this time is close to the charge exchange time of the ions (more will be said below of the ion energy determination).

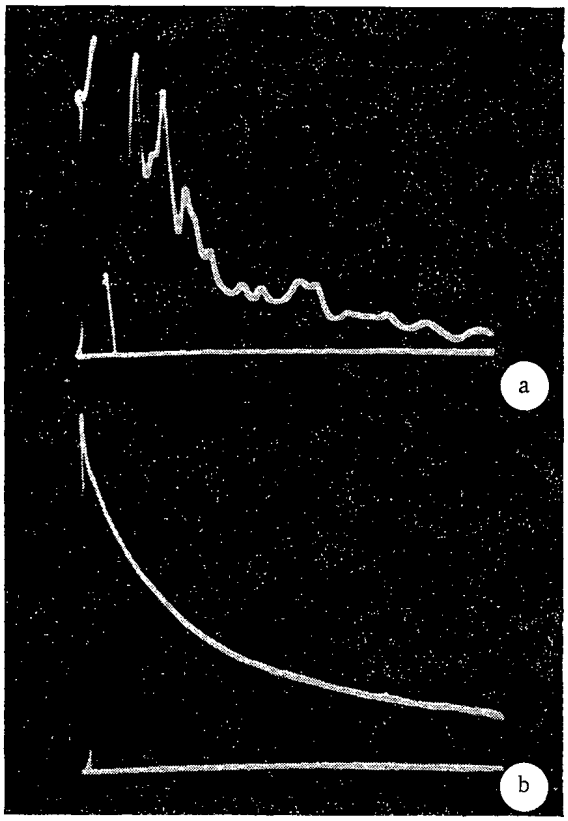


Fig. 4. Oscillograms of charge exchange neutral particle flux ($H_{0\|}$ = 3.3 kG, p = $10^{-7}$ mm Hg): a) $\alpha_\perp$ = 1.0, time base 500 μsec; b) $\alpha_\perp$ = 1.22, time base 10 μsec.

Together with the rapid increase in $\tau$ near $\alpha_\perp$ = 1.1, the oscillograms for the charge exchange neutral particle flux also change their shape. Figure 4 shows two oscillograms, one relating to the unstabilized state ($\alpha_\perp$ = 1.0) and the other to the stabilized state ($\alpha_\perp$ = 1.22). The first of these contains severe, disordered oscillations, reflecting plasma density pulsations caused by instability, whereas the second is conspicuous not only because of the increased steady fall in the signal but also because of the absence of noticeable oscillations.

The sharp transition between the two states of containment is strictly bound up with a change in the characterof the radial distribution of the total magnetic field on increasing $\alpha_\perp$. The graphs of Fig. 5 show the over-all field intensity as a function of radius in three cross sections of the trap for various $\alpha_\perp$. These graphs are constructed for the particular radial directions in which the field growth occurs most slowly.[1] As seen from the figure, for $\alpha_\perp < 1.1$ the fall in the main field $H_{0\|}$ over the radius is still not completely compensated by the stabilizing field $H_\perp$ for the whole length of the trap. Only for values of $\alpha_\perp \approx 1.1$ and upwards do we find a region with positive radial field gradient everywhere at the walls. As $\alpha_\perp$ rises above 1.1, the boundaries of this region shift towards the axis of the trap.

Thus, the transition from the unstabilized to the stabilized state takes place at the very moment in which a field increasing in the outward direction is established around the plasma all along the length of the trap, i.e., the conditions needed for the suppression of convective instability are created.

Plasma Lifetime as a Function of Pressure. In order to ascertain how completely the plasma instability is suppressed under stabilized conditions, the value of $\tau$ was measured as a function of hydrogen pressure p in the trap.

If there is no instability, then practically the only source of fast ion loss is charge exchange (for the energies and ion densities considered, passage out through the mirrors as a result of Coulomb scattering may be neglected in comparison with charge exchange). In this case $\tau = 1/(n_0 \langle \sigma_n v_i \rangle)$ ($n_0$ is the density of neutral hydrogen, $\sigma_n$ the charge exchange cross section, and $v_i$ the velocity of ions), and hence the graph of $1/\tau = f(p)$ must be a straight line passing through the origin of coordinates. If there are still losses connected with plasma instability over and above those due to charge exchange, then the straight line $1/\tau = f(p)$ will intersect the axis of ordinates above zero at the point $1/\tau_0$, where $\tau_0$ is the characteristic time for instability losses.

Figure 6 shows the experimental variation of $1/\tau$ with p for $\alpha_\perp$ = 1.15 and a pressure range p = $6 \cdot 10^{-8}$ to $1 \cdot 10^{-5}$ mm Hg (curve 1). For comparison we show the variation of $1/\tau$ with p for the same conditions but in the absence of the stabilizing field (curve 2). We see from the figure that in the stabilized state the experimental points lie on a straight line which, on extrapolation to zero pressure, passes close to the origin of coordinates. The precision of the measurements and the corresponding precision of extrapolation enable us to assert that the characteristic time of losses not associated with charge exchange, if it exists at all, is not less than 25-30 msec. The maximum value of $\tau$ obtained in this series of measurements is 6 msec for p = $6 \cdot 10^{-8}$ mm Hg. Separate measurements carried out at lower pressures give considerably larger values of $\tau$. Figure 7 shows an oscillogram of the charge exchange neutral particle flux for p = $7 \cdot 10^{-9}$ mm Hg, the lowest pressure which could be obtained in the system. In this case, the

[1] These directions correspond to the middle of the gaps between the stabilizing winding conductors in which the field $H_\perp$ is directed oppositely to the radial component of the main field.

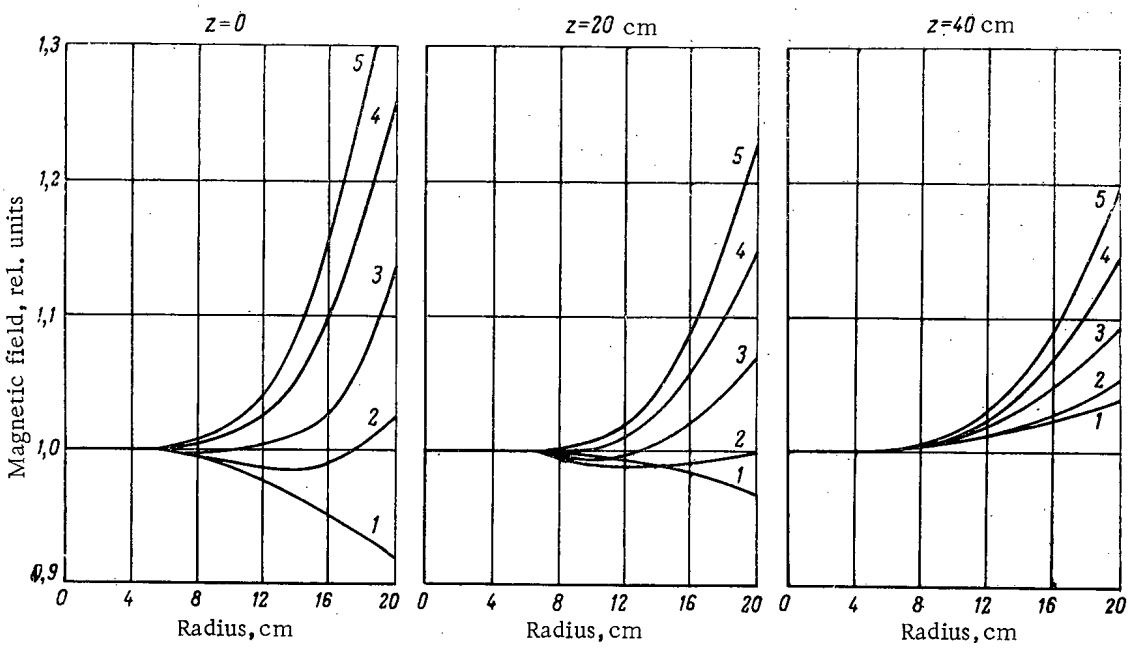


Figure 5. Radial distribution of total field in three cross sections of the PR-5 apparatus for various values of $\alpha_\perp$ (z = 0 is for the central section of the trap): 1) $\alpha_\perp$ = 1.0; 2) $\alpha_\perp$ = 1.07; 3) $\alpha_\perp$ = 1.14; 4) $\alpha_\perp$ = 1.22; 5) $\alpha_\perp$ = 1.3.

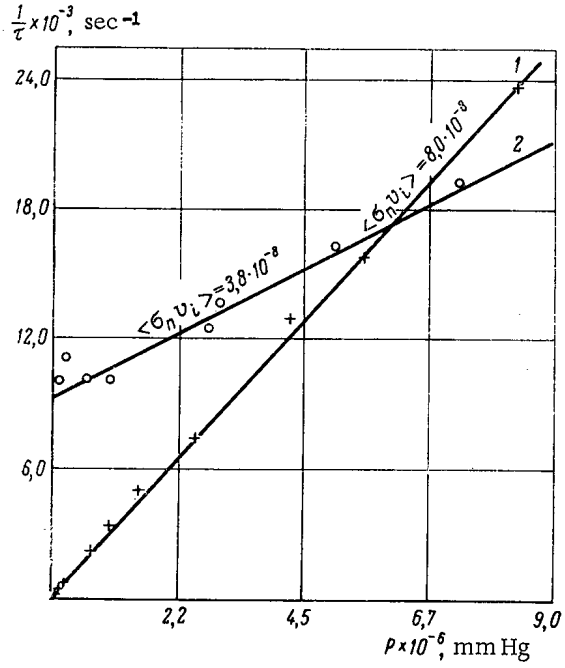


Fig. 6. Inverse lifetime of fast ions as a function of pressure ($H_{0\|}$ = 3.9 kG): 1) $H_\perp$ = 2.3 kG, $\alpha_\perp$ = 1.15 (stabilized state); 2) $H_\perp$ = 0.

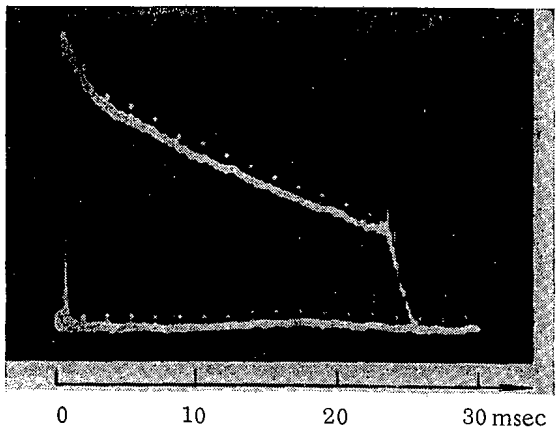


Fig. 7. Oscillogram of charge exchange neutral particle flux for p = $7 \cdot 10^{-9}$ mm Hg. ($H_{0\|}$ = 3.3 kG, $H_\perp$ = 1.8 kG, $\alpha_\perp$ = 1.15.)

value of $\tau$ was ~60 msec, which is also in good agreement with the charge exchange time. The break in the signal just before the end of the time base is caused when the stabilizing field has fallen to a value insufficient for the stabilization of the plasma in the trap ($H_\perp < 1.8$ kG, $\alpha_\perp \leq 1.1$). It should be mentioned that attempts to make an exact comparison between the observed lifetimes and the charge exchange times at the rather low pressures are to a certain extent lacking in meaning: with strongly sorbing walls such as those of the azotite, we cannot imagine a uniform neutral gas density in the trap space if there are local sources of gas evolution, and still less can we trust the indications of the vacuum gage when the ionization detector is not situated immediately inside the vacuum chamber. Hence conclusions regarding the presence or absence of losses not connected with charge exchange

can only be made to a precision determined by the lifetimes actually measured. The fact that these times continue to increase as the pressure falls, reaching values of 0.06 sec, gives grounds for concluding that there is practically no instability under the stabilized conditions.

Bearing in mind the fact that the slope of the straight line $1/\tau = f(p)$ is proportional to $\langle \sigma_n v_i \rangle$, and using the relations given in [2], we may determine the mean energy and evaluate the density of fast ions in the trap. In the experiments described in the present paper, the mean energy of the protons was 5 keV for $\alpha_\perp > 1.1$. The mean density in the central section of the trap depends on the working conditions of the source, and varies between the limits $10^9$ and $10^{10}$ $cm^{-3}$.

2. Effect of the Stabilizing Field on the Plasma Density Oscillations. Together with plasma stability characteristics such as the lifetime $\tau$, it is also interesting to consider data on local plasma density oscillations and the effect of the stabilizing field in this respect. Such data should enable us to form a more detailed concept of the mechanism whereby instability is suppressed by a field increasing with radius.

The density oscillations were indicated by variations in the current in a Langmuir probe placed in the plasma. The probe was made in the form of a sphere 3 mm in diameter fixed to a thin conducting wire. The wire was enclosed in a quartz tube wrapped in copper foil; the latter was grounded, and served as a screen eliminating the capacitive coupling between wire and plasma. In order to measure the saturation ion current, a potential of −80 V relative to ground was applied to the sphere. The probe was placed in the central cross section of the trap in an azimuth corresponding to the middle of the gap between the stabilizing winding conductors, and could be arranged to be at different distances from the axis. The probe current was oscillographed during the decomposition of the plasma for various values of stabilizing field.

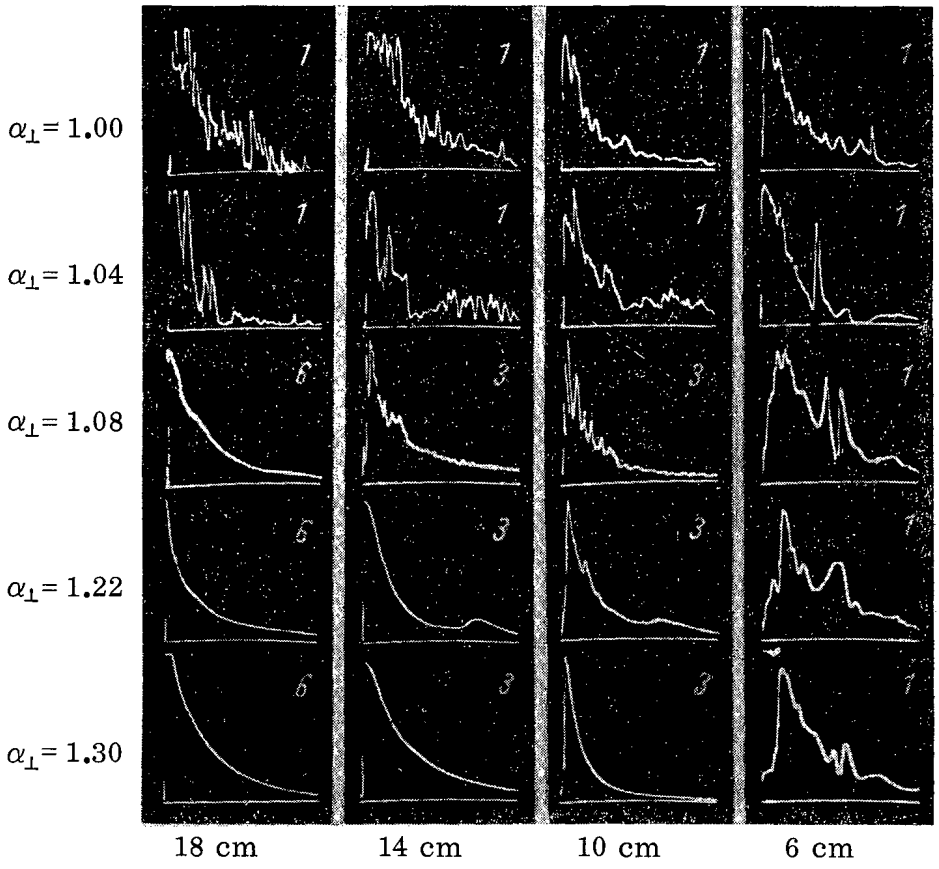


Fig. 8. Oscillograms of the ion current at the Langmuir probe at varisou distance from the trap axis. (In the right hand upper corner of each oscillogram is shown the length of the time base in msec.)

Figure 8 shows four series of oscillograms corresponding to distances 18, 14, 10, and 6 cm of the probe from the axis (the amplitudes of the signals on the various oscillograms are given on an arbitrary scale).

For $\alpha_\perp < 1.1$, we see severe oscillations, typical of an unstable plasma [13], at all distances from the axis.

For $\alpha_\perp > 1.1$, the oscillations in the peripheral regions (18, 14, and 10 cm) begin to fall rapidly, vanishing completely as the stabilizing field is increased. It is important here to note that the oscillations vanish at the walls first, and then at successively deeper layers in the plasma; near the axis there are even some strong oscillations at $\alpha_\perp = 1.3$.

If we compare the oscillograms of Fig. 8 with the curves relating the total magnetic field in radius (see Fig. 5), we realize that, for a given value of $\alpha_\perp$, the oscillations (and hence instability) are found at those distances from the axis at which the field either falls off with increasing radius, or, if it grows at all, does so very slowly. In regions in which the field rises fairly rapidly there are no oscillations.

In view of this, it is an interesting fact that, corresponding to the sharp rise in $\tau$ near $\alpha_\perp \approx 1.1$ and the transition into the stabilized state, the instability is only suppressed in the very outermost layer near the plasma surface. This nevertheless seems to be sufficient to stop the outflow of plasma from the trap almost completely. The increase of $\alpha_\perp$ above 1.1 only leads to a broadening of the stable region at the periphery.

Thus, according to experiment, instability in the inner regions of the trap does not hinder the possibility of prolonged plasma containment. The circumstance that for $\alpha_\perp > 1.1$ the signal decay rate increases on taking the probe away from the walls does not mean that the plasma decomposes more rapidly in the inner regions than at the periphery. Simultaneous measurements of the charge exchange neutral particle flux indicate that, on pushing the Langmuir probe into the trap, the lifetime of the whole plasma rapidly shortens, and this is associated with losses of charged particles at the probe and the conducting tube. These losses appear all the more strongly, the deeper the probe penetrates into the plasma.

## 3. Plasma Density Distribution over the Trap Radius

In order to measure the density distrbution over the radius, we used the Langmuir probe described above. The measurements weremade in the central section of the trap, on the radius passing through the middle of the gap between the conductors of the stabilizing winding. As a quantity characterizing the plasma density, we took the value of the ion current in the probe after the end of the accelerating voltage pulse (the probe was at a potential of −80 V with respect to ground).

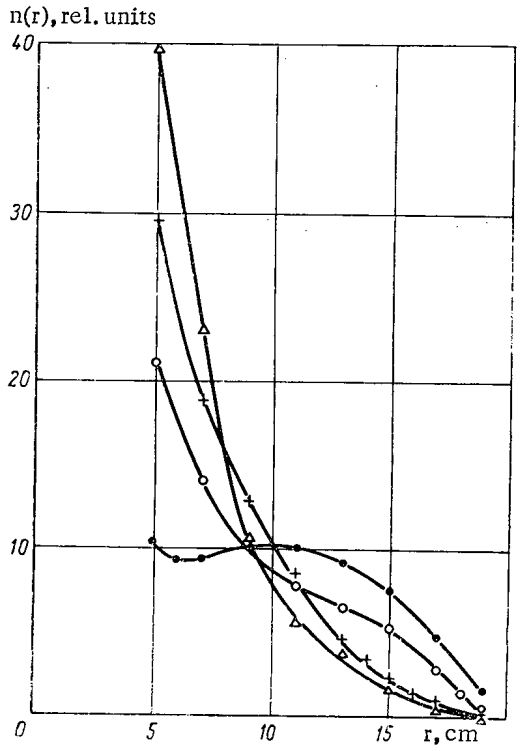


Fig. 9. Radial distribution of plasma density in the trap ($H_{0\parallel} = 3.3$ kG; $p = 1.5 \cdot 10^{-7}$ mm Hg): $\Delta - H_\perp = 2.07$ kG; $\alpha_\perp = 1.3$; + − $H_\perp = 1.8$ kG, $\alpha_\perp = 1.15$; O − $H_\perp = 0.9$ kG, $\alpha_\perp = 1.08$; ● − $H_\perp = 0$, $\alpha_\perp = 1$.

Figure 9 shows the radial distribution of plasma density for three values of stabilizing field $\alpha_\perp$ = 1.08, 1.15, and 1.3) at off-axial distances exceeding 5 cm. Measurements could not be made at distances less than 5 cm owing to breakdown taking place to the probe when the accelerating voltage was applied.

The curve taken in the absence of the stabilizing field closely reproduced the results of analogous measurements made earlier [15].

As explained earlier [15], the "defocused" plasma distribution in the ordinary trap with mirrors is caused by the intense convective transfer to plasma across the magnetic field.

On switching on the stabilizing winding, the radial density distribution is considerably deformed: The plasma is "squeezed" away from the walls and concentrates in the paraxial region of the trap; it does this the more strongly, the greater the value of $H_\perp$. Clearly this redistribution of density is the result of a change in the radial distribution of the magnetic field.

At the periphery, in the regions in which the field grows with radius, convective transfer ceases. Hence the plasma density here falls rapidly, whereas in the paraxial region it correspondingly rises. The approach of the regions with radially increasing field to the axis as the value of $\alpha_\perp$ rises results in a contraction of the radial density distribution.

It should be emphasized that the curves of Fig. 9 can only serve as an extremely rough, qualitative characteristic of the true density distribution over the trap cross section. This is because, first, as already noted, under conditions of prolonged plasma containment, even a probe of comparatively small dimensions introduces a severe perturbation owing to its absorption of charged particles, and, secondly, the radial distribution in a trap with combined fields should not have cylindrical symmetry. In view of the structure of the lines of force in the combined field, we should expect that, at azimuths corresponding to the middles of the gaps between the conductors of the stabilizing winding, where the lines of force intersect the wall and the containment of the plasma is effected by the radial mirrors, the distribution will be more diffuse than at other azimuths in which the lines of force do not intersect the walls. Unfortunately, the carrying out of measurements at different azimuths is greatly complicated by the existing construction of the stabilizing winding.

In conclusion, the authors consider it their duty to express gratitude to L. A. Artsimovich for constant interest in the present work, great help in carrying it out, and valuable comment, and to Yu. V. Gott, V. G. Tel'kovskii, E. E. Yushmanov, and M. V. Nezlin for many useful discussions.

The authors also express their gratitude to V. M. Petrov, who constructed the apparatus, Yu. T. Baiborodov, who developed the whole radio-electrotechnical system, and took part in the measurement, and also V. I. Abalikhin, B. I. Kanaev, and N. M. Kozlov for help in preparing and conducting the experiments.

## LITERATURE CITED

1. G. F. Bogdanov et al., Nucl. Fusion, Suppl., Part I, 215 (1962).
2. M. S. Ioffe et al., ZhÉTF, 39, 1602 (1960); 40, 40 (1961).
3. W. Perkins and R. Post, Phys. of Fluids, 6, 1537 (1963).
4. D. Sweetman, Symposium on Magnetic Traps [Russian translation], France, Fontaine-aux-Roses (1963).
5. M. Rosenbluth and C. Longmire, Ann. Phys., 1, 120 (1957).
6. B. B. Kadomtsev, ZhÉTF, 40, 328 (1961).
7. E. E. Lovetskii and A. A. Rukhadze, ZhTF, 33, 652 (1963); Radiofizika, 6, 716 (1963).
8. M. Rosenbluth, N. Krall, and N. Rostoker, Nucl. Fusion, Suppl., Part I, 143 (1962).
9. V. F. Kuleshov and A. A. Rukhadze, Yadernyi Sintez, 4, No. 3 (1964).
10. A. V. Mikhailovskii, ZhÉTF, 43, 509 (1962).
11. Yu. V. Gott, M. S. Ioffe, and V. G. Tel'kovskii, Nucl. Fusion, Suppl., Part III, 1045 (1962).
12. Yu. T. Baiborodov et al., Atomnaya énergiya, 14, 443 (1963).
13. Yu. V. Martynenko and R. I. Sobolev, Atomnaya énergiya, 17, 211 (1964).
14. V. A. Simonov et al., Nucl. Fusion, Suppl., Part I, 325 (1962).
15. M. S. Ioffe and E. E. Yushmanov, Nucl. Fusion, Suppl., Part I, 177 (1962).

# CALCULATION OF WATER-MODERATED WATER-COOLED REACTORS

(UDC 621.039.51)

E. A. Garusov and Yu. V. Petrov

Translated from Atomnaya Énergiya, Vol. 17, No. 5,
pp. 375-379, November, 1964
Original article submitted September 23, 1963

An expression is obtained for the probability of avoiding leakage in reactors with uniform energy evolution. From an analysis of this probability, together with the Fourier components of the experimental slowing-down function and the slowing-down functions of various diffusion models for ordinary water, it is concluded that the single group model is fairly accurate for the calculation of active zones containing not less than 10 liters of water. Increasing the number of energy groups without going over to nondiffusion theory lowers the precision.

The calculation of a nuclear reactor of given composition and dimensions should primarily give the correct value of the effective neutron breeding coefficient ($K_{eff}$). If the reactor operates mainly with thermal neutrons, the value of $K_{eff}$ will depend substantially on the probability of avoiding neutron leakage from the active zone during the slowing-down process. This probability depends on the distribution of fast neutron sources in the active zone and the geometry of the reactor, and also on the slowing-down function, i.e., the probability that a neutron generated at a point $\mathbf{r}_0$ will becomes thermal at the point $\mathbf{r} - G(\mathbf{r}, \mathbf{r}_0)$. Since the exact calculation of the slowing-down function is a complex problem, it is customary to use various computing models (age, theory, multigroup, approximations, etc.). In the particular case of an infinite moderating medium, the slowing-down function is usually known from experiment.

In using one or other of the moderating models, we need to be sure that it gives the correct value of neutron leakage, especially for smallish reactors, in which the leakage is considerable. It is most difficult to select moderating models for reactors with hydrogen containing moderators. In view of the sharp variation of the scattering cross section of hydrogen with energy and the small number of collisions needed for slowing down, it is not a priori clear whether it will be possible to use the diffusion approximation. It is thus interesting for reactors with ordinary water to compare the probability of avoiding neutron leakage calculated from the experimental slowing-down function with that calculated from the diffusion model of the process.

1. The function $G(\mathbf{r}, \mathbf{r}_0)$ was determined experimentally in [1], where the distribution of neutrons with indium resonance energy from a point source of $U^{235}$ fission slowed in ordinary water was measured at distances up to 92 cm. This distribution led to the neutron age $\tau = 30.7\,cm^2$. It was later shown, however, that there were some systematic errors in [1], mainly caused by the great thickness of the $U^{235}$ target, which gave rise to "corrosion" of the resonance neutrons near the source [2]. A new value given in [2, 3] was $\tau = 27.3 \pm 1.0\,cm^2$. The value of $G(\mathbf{r}, \mathbf{r}_0)$ was obtained for a very thin $U^{235}$ target up to distances of 40 cm in [3]. This distribution, however, contains a large error at great distances owing to the small dimensions of the water tank and the small number of counts. In order to obtain values of the function $G(\mathbf{r}, \mathbf{r}_0)$ correct for both small and great distances from the source, the curves of [1] and [3] were "sewn together" in the range 11.5-23.5 cm, in which one would expect the two curves coincide. The so-obtained slowing-down function $G_{exp}(\mathbf{r}, \mathbf{r}_0)$ was used in subsequent calculations. The values of the moments of the slowing-down function

$$\langle r^n \rangle = \frac{\int_0^\infty G_{exp}(r)\, r^{n+2}\, dr}{\int_0^\infty G_{exp}(r)\, r^2\, dr} \qquad (1)$$

TABLE 1. Experimental and Calculated Values of the Moments of Slowing-Down Functions

| Means of determination | $\tau=\frac{1}{6}\langle r^2\rangle$, $cm^2$ | $\langle r\rangle$, cm | $\langle r^3\rangle$, $cm^3$ | $\langle r^4\rangle$, $cm^4$ | $\langle r^6\rangle$, $cm^6$ |
|---|---|---|---|---|---|
| Experiment | 27,3±1,0 | 10,6 | $3,6\cdot10^3$ | $1,07\cdot10^5$ | $1,95\cdot10^8$ |
| Single group approximation | 27,3 | 10,5 | $3,4\cdot10^3$ | $0,89\cdot10^5$ | $1,03\cdot10^8$ |
| Two-group approximation ($\alpha=0.216$) | 27,3 | 10,9 | $3,2\cdot10^3$ | $0,74\cdot10^5$ | $0,68\cdot10^8$ |
| Age approximation | 27,3 | 11,8 | $2,6\cdot10^3$ | $0,45\cdot10^5$ | $0,17\cdot10^8$ |
| Flight-age approximation | 27,3 | 10,4 | $3,7\cdot10^3$ | $1,12\cdot10^5$ | $1,98\cdot10^8$ |

are given in Table 1. For comparison the table also shows the moments for several frequently used diffusion slowing-down functions as well as for the flight-age function. In calculating the moments of the slowing-down functions, the constants in them were chosen in such a way that the second moment should coincide with the experimental value.

2. A. Weinbert and E. Wigner [4] formulated the second basic theorem in reactor theory, according to which the probability of avoiding the leakage of neutron s out of a reactor without reflector (P) during the slowing-down process equals the Fourier component of the slowing-down function of neutrons from a point source in an infinite medium

$$P=\tilde{G}(B)\equiv\int G(\mathbf{r})\,e^{i\mathbf{B}\mathbf{r}}\,d\mathbf{r}. \tag{2}$$

Figure 1 shows the Fourier components for the experimental slowing-down function and for various theoretical functions in the diffusion approximation. We see from Fig. 1 that the one-group theory of decelerating neutrons agrees best with $\tilde{G}_{exp}$ (B). For values of $B < 0.23$ $cm^{-1}$, which corresponds to a spherical reactor with an active zone volume of around 10 liters, the difference between $\tilde{G}_{exp}$ (B) and $\tilde{G}_I$ (B) lies within the limits of experimental error. The $\tilde{G}_{II}$ (B) curve passes below the $\tilde{G}_I$ (B), and the difference between $\tilde{G}_{exp}$ (B) and $\tilde{G}_{II}$ (B) for spherical active zones less than 50 liters in volume lies outside experimental error.

From the general form of the Fourier component for the N-group approximation,

$$G(\tilde{B})=\prod_{i=1}^{N}\frac{1}{(1+\alpha_i\tau B^2)}\,,\quad\sum_{i=1}^{N}\alpha_i=1 \tag{3}$$

it follows that the breaking up of any energy group of neutrons into several groups can only reduce $\tilde{G}$ (B), i.e., we always have $\tilde{G}_{N+K}$ (B) < $\tilde{G}_N$ (B). For small B, all the functions $\tilde{G}_N$ (B) are close to each other; with increasing B, the difference between them rises. Hence, increasing the number of groups can only lead to an increase in the leakage of neutrons out of the reactor, especially for smallish active zones. The maximum error occurs for $N\to\infty$, i.e., on using the age theory (see Fig. 1).

The second fundamental theorem assumes that $G(\mathbf{r},\mathbf{r}_0)=G(|\mathbf{r}-\mathbf{r}_0|)$. This assumption is approximately valid for fairly large reactors. It is shown in [5, 6] that, for a direct-flight function with $P\sim0.5$, the difference between P and $\tilde{G}$ (B) in the case of a plane reactor is approximately 20%, increasing with increasing anisotropy of scattering. It is thus desirable to obtain the probability of avoiding neutron leakage from small active zones without using the second fundamental theorem.

3. The probability of avoiding neutron leakage during the slowing-down process for a reactor with an infinite reflector may be calculated quite simply if the slowing-down properties of the reflector and the active zone are the same. In this case $G(\mathbf{r},\mathbf{r}_0)=G(|\mathbf{r},\mathbf{r}_0|)$. Let the fuel in the reactor be so disposed that the number of fissions at each point of the reactor is the same. Then for a spherical active zone of diameter D the formula is given in the Appendix [see (A-3)]. Figure 2 shows P(G, D) for light water as a function of the inverse diameter, both for the experimental function $G_{exp}$ and for various theoretical functions in the diffusion approximation. As in the previous case, right up to volumes of the order of 10 liters ($D\approx27$ cm), the deviation between $P(G_{exp}, D)$ and $P(G_I, D)$ clearly lies within the limits of experimental error. The two-group and age theories give increased values of neutron leakage out of the active zone. The same result follows by substituting the values of $\langle r\rangle$ and $\langle r^3\rangle$ from the table given into

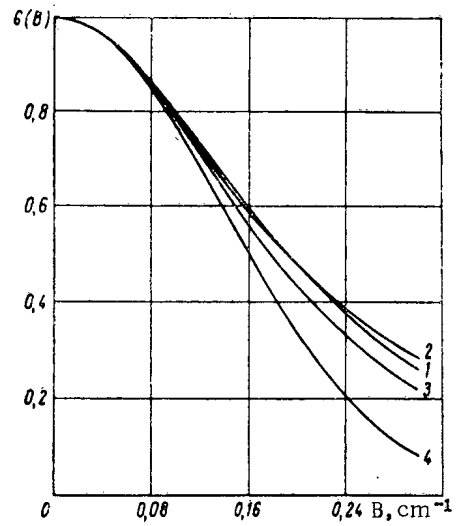


Fig. 1. Fourier component of slowing down functions in ordinary water: 1) $\tilde{G}_{exp}(B)$, the result of analyzing experimental data; 2) $\tilde{G}_I(B)$, one-group approximation; 3) $\tilde{G}_{II}(B)$, two-group approximation ($\alpha = 0.216$); 4) $\tilde{G}_B(B)$, age approximation.

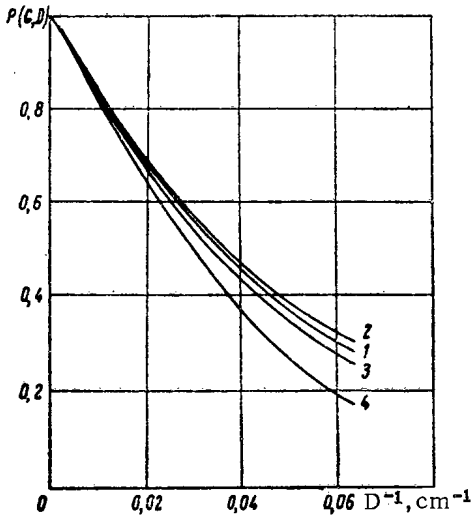


Fig. 2. Probability of avoiding neutron leakage from a spherical active zone: 1) $P(G_{exp}, D)$, the result of analyzing experimental data; 2) $P(G_I, D)$, one-group approximation; 3) $P(G_{II}, D)$, two-group approximation ($\alpha = 0.216$); 4) $P(G_B, D)$, age approximation.

the asymptotic formula [see (A-4)]:

$$P_{as}(G, D) = 1 - \frac{3}{2} \cdot \frac{\langle r \rangle}{D} + \frac{1}{2} \cdot \frac{\langle r^3 \rangle}{D^3} \qquad (4)$$

We see from formulas (A-6) and (A-8) of the Appendix that, for an active zone in the form of a cylinder of a parallelepiped, the sign in front of the main term $\langle r \rangle$ remains unchanged, and it is thus reasonable to suppose that the foregoing conclusions are not dependent on the specific form of the active zone.

4. It follows from the results given that the theory of one group of decelerating neutrons describes the leakage of neutrons out of the reactor with acceptable accuracy right up to volumes of water of the order of 10 liters in the active zone. Any attempt to improve on the energy spectrum, still remaining within the framework of the $P_1$ approximation will give worse agreement between theory and experiment. In particular, the splitting up of the decelerating neutrons into two groups, as proposed in [7], will cease to be valid for active zones containing less than 50 liters of water (see Figs. 1 and 2). The large error arising in calculations of uranium-water systems made in the $P_1$ approximation by the multigroup method, using 21 energy groups of neutrons, is noted in the monograph of G. I. Marchuk [8].

On increasing the number of points in the energy scale, the theory must be of the nondiffusion type. The physical reason for this is that the neutron picks up the main part of the migration area in water as a result of primary collisions. Inside the upper energy group there remain only those neutrons which were scattered at small angles, i.e., the neutron distribution is extended substantially forward, and full diffusion action fails to take place.

As seen from Figs. 1 and 2, nondiffusion corrections are especially important for active zones with volumes considerably below 10 liters, since the free path of the fast neutrons becomes comparable with the dimensions of the active zone. Furthermore, in this case the reactor operates mainly with intermediate neutrons, and the energy spectrum must be known more accurately.

It should be noted that the one group theory does not agree with experimental values in respect of the ratio of the thermal neutron flux to the power of the point source [9]. The reason for this is the divergence of the one group slowing-down function $G_I(\mathbf{r}, \mathbf{r}_0)$ at the point $\mathbf{r} = \mathbf{r}_0$. In order to remove the divergence, the following model may be proposed: The neutrons travel without energy loss, but after the first collision pass into the lower energy range, where, for example, the diffusion-age approximation may be used. The two parameters of the model (the effective free path of the fast neutrons, $\lambda$, and the effective age, $\tau_1$) may be obtained from experiment, if we postulate the conservation of the total migration area during the slowing-down process, $2\lambda^2 + 6\tau_1 = \langle r^2 \rangle$ and the value of the slowing-down function $G(0, 0)$. For neutrons decelerating to the indium resonance, $\lambda = 7.88$ cm and $\tau_1 = 6.56$ cm$^2$.

We see from the table that this flight-age model brings the theoretical and experimental moments into satisfactory agreement. Of course this is not the only model, and may well be far from the best.

We note in conclusion that we have considered either reactors with no reflector or those with a reflector as bad as water. The use of better reflectors lightens the requirements regarding the nondiffusion character of the theory.

The authors thank L. N. Yurova and A. A. Polyakov for permitting detailed study of their own results, and also G. A. Bat', A. N. Erykalov, and V. V. Orlov for discussing the results and for valuable comment.

## APPENDIX

The probability of avoiding neutron leakage from the reactor during the slowing-down process, when the retarding properties of the active zone and infinite reflector are identical, and when there are the same number of fissions at each point of the active zone, may be written in the following form:

$$P=\frac{\int d\mathbf{r}\int d\mathbf{r}_0 G(|\mathbf{r}-\mathbf{r}_0|)\,\vartheta(\mathbf{r}_s-\mathbf{r})\,\vartheta(\mathbf{r}_{s_0}-\mathbf{r}_0)}{\int d\mathbf{r}\int d\mathbf{r}_0 G(|\mathbf{r}-\mathbf{r}_0|)\,\vartheta(\mathbf{r}_{s_0}-\mathbf{r}_0)}, \tag{A-1}$$

where G(r) is the derivative of the slowing-down function, $\mathbf{r}_S$ the radius vector of a point on the surface, $\vartheta(\mathbf{r}_S-\mathbf{r}) = \begin{cases}0 \text{ for } \mathbf{r}>\mathbf{r}_S\\ 1 \text{ for } \mathbf{r}\le\mathbf{r}_S\end{cases}$ a three-dimensional $\vartheta$-function cutting out the corresponding integration range.

Introducing new variables $\rho = {}^1/_2(\mathbf{r}-\mathbf{r}_0)$, $\rho_0 = {}^1/_2(\mathbf{r}+\mathbf{r}_0)$, and noting that $d\mathbf{r}\,d\mathbf{r}_0 = 2^3\,d\rho\,d\rho_0$, we obtain

$$P=\frac{\int d\varrho\, G(|2\varrho|)\int d\varrho_0\vartheta(\mathbf{r}_s-\varrho_0-\varrho)\,\vartheta(\mathbf{r}_{s_0}-\varrho_0+\varrho)}{V\int d\varrho G(|2\varrho|)}, \tag{A-2}$$

where V is the volume of the reactor active zone.

Let us calculate P for several particular cases. For a spherical active zone of radius R, the integral with respect to $d\rho_0$ in (A-2) is taken over a range determined (Fig. 3) by the inequalities:

$$-1<\cos\psi<+\varphi(\varrho_0),\quad -\varphi(\varrho_0)<\cos\psi<+1,$$

where

$$\varphi(\varrho_0)=\frac{R^2-\varrho^2-\varrho_0^2}{2\varrho\varrho_0}.$$

Carrying out the integration, we obtain (D = 2R)

$$P=\frac{\int_0^D G(\varrho)\,\varrho^2\,d\varrho\left(1-\frac{3}{2}\cdot\frac{\varrho}{D}+\frac{1}{2}\cdot\frac{\varrho^3}{D^3}\right)}{\int_0^\infty G(\varrho)\,\varrho^2\,d\varrho}. \tag{A-3}$$

At large distances $G(\rho)$ falls off at least exponentially. Thus for large D the asymptotic expression

$$P_{as}=1-\frac{3}{2}\cdot\frac{\langle r\rangle}{D}+\frac{1}{2}\cdot\frac{\langle r^3\rangle}{D^3}, \tag{A-4}$$

is valid to exponential precision, $\langle r^n\rangle$ being the moments of the slowing-down function [see formula (1)].

For an active zone in the form of a rectangular parallelepiped, the three-dimensional integral in $d\rho_0$ decomposes into the product of three one-dimensional integrals over a region determined by the following inequalities (Fig. 4): $a_i+\xi_i\ge\xi_{i_0}\ge\xi_i$; $a_i-\xi_i\ge\xi_{i_0}\ge-\xi_i$, where $a_i$ is the length of the i-th edge of the parallelepiped, and $\xi_{i_0}$ and $\xi_i$ are current Cartesian coordinates.

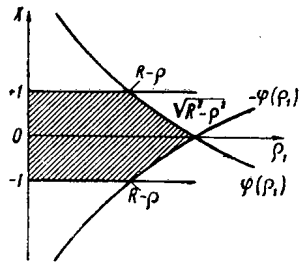


Fig. 3. Region of integration for circular section of the active zone.

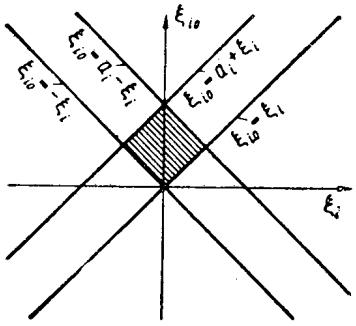


Fig. 4. Region of integration for a rectangular section of the active zone.

Integrating over $d\rho_0$, we obtain

$$P=\frac{2^3\int d\varrho G(\varrho)\prod_{i=1}^{i=3}\left(1-\frac{\xi_i}{a_i}\right)\vartheta(a_i-\xi_i)\,\vartheta(\xi_i)}{\int d\varrho G(\varrho)}. \qquad (A-5)$$

If the mean path of a neutron in the zone $\bar{l}=4V/s$ is much larger than the slowing-down length, then the following asymptotic expression holds to exponential exactness:

$$P_{as}=1-\frac{a_1a_2+a_2a_3+a_3a_1}{2a_1a_2a_3}\langle r\rangle+\frac{2}{3\pi}\cdot\frac{a_1+a_2+a_3}{a_1a_2a_3}\langle r^2\rangle-\frac{\langle r^3\rangle}{4\pi a_1a_2a_3}. \qquad (A-6)$$

For a cylindrical active zone of radius R and height H, the three-dimensional integral with respect to $d\rho_0$ splits into the product of a one-dimensional integral over the range indicated in Fig. 4 and a two-dimensional integral over the region shown in Fig. 3. By integrating over $d\rho_0$, we obtain

$$P=\frac{2\int d\varrho G(\varrho)\left(1-\frac{Z}{H}\right)\vartheta(H-Z)\,\vartheta(Z)\left[1-\frac{\varrho}{\pi R}\sqrt{1-\left(\frac{\varrho}{2R}\right)^2}-\frac{2}{\pi}\arcsin\frac{\varrho}{2R}\right]}{\int d\varrho G(\varrho)} \qquad (A-7)$$

If the dimensions of the active zone are large, then with an accuracy up to terms $\sim\langle r^4\rangle/D^4$ we obtain (D = 2R):

$$P_{as}=1-\frac{1}{2}\left(\frac{1}{H}+\frac{2}{D}\right)\langle r\rangle+\frac{4}{3\pi}\cdot\frac{D}{H}\cdot\frac{\langle r^2\rangle}{D^2}+\frac{1}{8}\cdot\frac{\langle r^3\rangle}{D^3}. \qquad (A-8)$$

## LITERATURE CITED


1. J. Hill, L. Roberts, and T. Fitch, Appl. Phys., 26, 1013 (1955).
2. D. Lombard and C. Blanchard, Nucl. Sci. and Engng, 7, 448 (1960).
3. L. N. Yurova, A. A. Polyakov, and A. A. Ignator, Atomnaya énergiya, 12, 151 (1962).
4. A. Weinberg and E. Wigner, Physical Theory of Nuclear Reactors [Russian translation], Moscow, IL (1961).
5. K. Inönü, Nucl. Sci. and Engng, 5, 248 (1959).
6. L. Dresner, Nucl. Sci. and Engng, 7, 419 (1960)
7. R. Dentsch, Nucleonics, 15, 47 (1957).
8. G. I. Marchuk, Methods of Calculating Nuclear Reactors [in Russian], Moscow, Gosatomizdat (1961).
9. E. A. Garusov and Yu. V. Petrov, Atomnaya énergiya, 15, 71 (1963).

# THE BURN-UP OF NATURAL URANIUM WHEN IT IS MOVED AXIALLY IN A REACTOR

(UDC 621.039.5 6.22)

V. Bartosek and V. Lelek

Nuclear Research Institute of the Czechoslovak Academy of Sciences, Prague—Rez

Translated from Atomnaya Énergiya, Vol. 17, No. 5,
pp. 380-384, November, 1964
Original article submitted December 13, 1963

We investigate the effect produced in the distribution of the neutron flux and the burn-up of the natural uranium in a heavy-water reactor when the fuel is moved continuously in an axial direction. Using a simplified model and taking into consideration the variations of the neutron multiplication factor as a function of uranium burn-up, we show that when the uranium is moved in one direction, the burn-up is about 20% higher than when the fuel elements are continuously recharged [1] and that the heat-transfer conditions of fuel-element operation are improved. When the fuel is moved simultaneously in two opposite directions, the uranium burn-up is increased by 40%, and the conditions of heat removal from the fuel elements remain almost unchanged.

## Introduction

The variation of the neutron multiplication factor k(s) as a function of irradiation in a volume element of a homogenized system can be represented with sufficient accuracy for our purposes by the formula

$$k(s) = k_0(1 + \alpha s + \beta s^2), \tag{1}$$

where the coefficients $\alpha$ and $\beta$ can be obtained, for example, by drawing a parabola through points calculated according to the method of long-term kinetics. A physically analogous problem for a linear variation of k as a function of s was considered in [2]. The irradiation is defined in the usual manner:

$$s = \int_0^t \Phi(\mathbf{r}, t')\, dt', \tag{2}$$

i.e., it is the integrated neutron flux measured in units of $10^{21}$ neutrons/cm$^2$.

## Flux Equation

The equation for the stationary distribution of the flux $\Phi(r, z)$ in a cylindrical reactor for the equilibrium state of fuel motion $\partial\Phi/\partial t = 0$ is of the form

$$\Delta\Phi(r, z) + \frac{k(s)-1}{M^2}\Phi(r, z) = 0, \tag{3}$$

where it is assumed that the variation of the migration length M as a function of fuel irradiation has a negligibly small effect on the change in the Laplacian of the reactor in comparison with the effect of the variation in the multiplication factor. If we impose the condition that the burn-up of the entire discharged fuel was uniform, i.e., was independent of the radius, then, as we shall see later, in the case of uniform fuel motion in the direction of the reactor axis the irradiation will depend only on the coordinate z: s = s(z). This makes it possible to solve Eq. (3) by separation of variables: $\Phi(r, z) = u(z)\,w(r)$. As a result, we obtain the following equations for the flux components in the radial and axial directions:

$$\frac{d^2w(r)}{dr^2}+\frac{1}{r}\cdot\frac{dw(r)}{dr}+B_r^2w(r)=0; \tag{4}$$

$$\frac{d^2u(z)}{dz^2}+\left\{\frac{k[s(z)]-1}{M^2}-B_r^2\right\}=0. \tag{5}$$

If the fuel is moved in the direction of the z axis at a velocity v(r), then z = v(r)t and dz = v(r)dt. Then, by a change of variables in formula (2), we obtain

$$s(z)=\frac{w(r)}{v(r)}\int_0^z u(z')\,dz', \tag{2'}$$

from which, by virtue of the condition that the irradiation is independent of the radius, we obtain the condition that the velocity of fuel motion must be proportional to the radial component of the flux. The latter is known, except for a constant; consequently, we may directly take v(r) = w(r).

If formula (2') is substituted into (5), then for the axial component of flux, we obtain the integro-differential equation

$$\frac{d^2u(z)}{dz^2}+\left\{\frac{k_0-1}{M^2}-B_r^2+\frac{\alpha k_0}{M^2}\int_0^z u(z')\,dz'+\frac{\beta k_0}{M^2}\left[\int_0^z u(z)\,dz'\right]^2\right\}(z)=0. \tag{5'}$$

The solution of Eq. (4) depends on the boundary conditions, determined by the presence or absence of a reflector. However, their form is manifested in the solution of Eq. (5) only through the constant $B_r^2$.

To solve Eq. (5'), we use substitution into formula (2'), which then becomes

$$\frac{d^3s}{dz^3}+\left(\frac{k_0-1}{M^2}-B_r^2+\frac{\alpha k_0}{M^2}s+\frac{\beta k_0}{M^2}s^2\right)\frac{ds}{dz}=0.$$

Its first integral will be

$$\frac{d^2s}{dz^2}+\left(\frac{k_0-1}{M^2}+B_r^2\right)s+\frac{\alpha k_0}{2M^2}s^2+\frac{\beta k_0}{3M^2}s^3=C_1. \tag{6}$$

In Eq. (6), the independent variable z appears in implicit form. Consequently, we can use the substitution

$$\frac{ds}{dz}=f(s),\quad \frac{d^2s}{dz^2}=f(s)\frac{df(s)}{ds}. \tag{7}$$

If formula (7) is substituted into (6), we obtain the formula

$$f\frac{df}{ds}+\left(\frac{k_0-1}{M^2}-B_r^2\right)s+\frac{\alpha k_0}{2M^2}s^2+\frac{\beta k_0}{3M^2}s^3=C_1,$$

the solution of which can be represented in the form

$$f^2(s)=2\left[C_2+C_1s-\frac{1}{2}\left(\frac{k_0-1}{M^2}-B_r^2\right)s^2-\frac{\alpha k_0}{6M^2}s^3-\frac{\beta k_0}{12M^2}s^4\right]. \tag{8}$$

The physical significance of the function $f$ follows from the definition (7); here we have

$$f(s)=\frac{ds}{dz}=\frac{d}{dz}\cdot\frac{1}{v}\int_0^z\Phi\,dz'=u(z),$$

i.e., the function $f$ is identical with the axial component of the neutron flux, the only difference being that it depends exclusively on the irradiation. It must satisfy the same boundary conditions as the function u(z):

$$u(0) = f(0) = 0 \quad [\text{since} \quad s(0) = 0]. \tag{9}$$

If the burn-up of the fuel discharged from the second zone is denoted by

$$s(H) \equiv S = \int_0^H u(z)\, dz,$$

then the second boundary condition becomes

$$u(H) = f(S) = 0. \tag{10}$$

From the boundary conditions (9) and (10), we obtain the following values for the constants $C_1$ and $C_2$:

$$C_1 = \frac{1}{2}\left(\frac{k_0 - 1}{M^2} - B_r^2\right) S + \frac{\alpha k_0}{6M^2} S^2 + \frac{\beta k_0}{12M^2} S^3,$$
$$C_2 = 0.$$

If we substitute the values of $C_1$ and $C_2$ into formula (8), we obtain

$$f(s) = \sqrt{s(S-s)\, F(S,\ s)}, \tag{11}$$

where

$$F(S,\ s) = \frac{k_0 - 1}{M^2} - B_r^2 + \frac{\alpha k_0}{3M^2} S + \frac{\beta k_0}{6M^2} S^2 + \left(\frac{\alpha k_0}{3M^2} + \frac{\beta k_0}{6M^2} S\right) s + \frac{\beta k_0}{6M^2} s^2.$$

From (8) it follows that

$$z = \int_0^s \frac{ds'}{\sqrt{s'(S-s')\, F(S,\ s')}}, \tag{12}$$

$$\frac{ds}{dz} \equiv u(z) = \sqrt{s(S-s)\, F(S,\ s)}. \tag{13}$$

Equation (12) characterizes the relationship between the coordinate z and the burn-up s for all the points of the interval (0, H), so that for z = H, we have

$$H = \int_0^S \frac{ds'}{\sqrt{s'(S-s')\, F(S,\ s')}}, \tag{14}$$

which characterizes the irradiation of the fuel S discharged from the reactor. If we are given the geometric and material parameters of the reactor, then the burn-up of the fuel S is completely determined by the solution of (14). But since Eq. (14) does not contain v(r), it is evident that the degree of fuel burn-up attained is independent of the velocity of fuel motion. If $H \to \infty$, then $S \to S_\infty$, and F(S, s) has a root $s_1 \to S_\infty$. From the physical viewpoint the value $S_\infty$ is important because it defines the maximum attainable burn-up.

The solution of Eq. (5') can be obtained as follows: 1) in Eq. (14) the value of S is calculated numerically; 2) for a known value of S, formula (12) determines the irradiation s at the point z; 3) the function (13), for a known value of irradiation s(z), determines the axial flux component u(z), which is the solution of Eq. (5').

## The Flattening Coefficient and the Velocity of Fuel Motion

Let us calculate the axial coefficient of flattening of the neutron flux, defined by the equation

$$u_z = \frac{\int_0^H u(z)\,dz}{Hu_{\max}}.$$

The equation

$$\int_0^H u(z)\,dz = \int_0^S ds = S.$$

follows from formulas (12) and (13). Let us use the notation $u_{max} = u(\zeta)$ and $s(\zeta) = \Sigma$. Then $\Sigma$ is the burn-up at the maximum point of the flux. From Eq. (13), it follows that

$$\frac{d}{ds}\left[s(S-s)F(S,\ s)\right]|_{s=\Sigma} = 0, \tag{15}$$

since $ds/dz \neq 0$ everywhere in the reactor. Then the axial coefficient is determined from the equation

$$\mu_z = \frac{S}{H\sqrt{\Sigma(S-\Sigma)F(S,\ \Sigma)}}. \tag{16}$$

The radial coefficient remains the same as in a reactor without any fuel motion.

From Eq. (2'), it follows that $v(r) = \text{const}\,J_0(B_r r)$. The constant is determined from the value at the maximum point. The $w_{max} = w(0) = \text{const} = \Phi_{max}/u_{max}$. The velocity of the motion, v(r), and the total residence time of the fuel, T(r), are determined by the formulas

$$v(r) = \frac{\Phi_{\max}}{\sqrt{\Sigma(S-\Sigma)F(S,\Sigma)}}J_0(B_r r); \tag{17}$$

$$T(r) = \frac{H}{v(r)} = \frac{H\sqrt{\Sigma(S-\Sigma)F(S,\ \Sigma)}}{\Phi_{\max}J_0(B_r r)}. \tag{18}$$

For ordinary flux values and reactor heights ($\Phi_{max} = 10^{14}$ neutrons/cm$^2$·sec, H = 700 cm), the total fuel residence time at the center, T(0), is 15 days, and the velocity of the motion, v(0), is 47 cm/day.

## Counter-Motion of the Fuel

The fuel in the reactor may also be moved in a different manner. Let us consider a case in which half of the fuel is moved in one direction while the other half is moved in the other direction. If, as before, the irradiation of the fuel moving in the axial direction is denoted by $s = \int_0^H u(z')\,dz'$ and its maximum irradiation is denoted by $\bar{S} = \int_0^H u(z)\,dz$, then it is evident that the irradiation of the fuel moving in the opposite direction will have the form

$$s_c = \int_z^H u(z')\,dz' = \bar{S} - s. \tag{19}$$

In order to obtain the exact variation of the multiplication factor in a plane perpendicular to the z axis, we would have to solve the balance equation of the fuel for a mixture of fuel components with different degrees of irradiation. However, to characterize the first-order effects, it is adequate to average the multiplication factors:

$$\bar{k}(s) = \frac{1}{2}\left[k(s) + k(s_c\right] = \bar{k}_0(1 + \bar{\alpha}s + \bar{\beta}s^2), \tag{20}$$

where

$$\bar{k}_0 = k_0\left(1+\frac{\alpha}{2}\bar{S}+\frac{\beta}{2}\bar{S}^2\right), \tag{21}$$

$$\bar{\alpha} = \frac{-\beta\bar{S}}{1+\frac{\alpha}{2}\bar{S}+\frac{\beta}{2}\bar{S}^2}, \quad \bar{\beta} = \frac{\beta}{1+\frac{\alpha}{2}\bar{S}+\frac{\beta}{2}\bar{S}^2} \tag{22}$$

By using this method, we reduce the case of counter-motion of the fuel to the problem of fuel motion in one direction, requiring only the following substitutions: $k_0 \to \bar{k}_0$, $\alpha \to \bar{\alpha}$, $\beta \to \bar{\beta}$, and $S \to \bar{S}$.

Comparison of Several Operating Regimes

In order to compare the advantages and disadvantages of the axial-motion regimes under consideration, it is convenient to estimate the average fuel burn-up in a reactor with the same characteristics but with different recharging regimes. The simplest method, of course, is the simultaneous recharging of all the fuel after its reactivity has been burned up. We assume that there is a slab of height H (geometric parameter $B_H$). The variation of the multiplication factor as a function of the burn-up $s_0$ of the central plane is expressed, according to the theory of perturbations, by

$$k^*(s_0) = \frac{\int_0^{\pi/2} k_0(1+\alpha s_0 \sin\xi+\beta s_0^2\sin^2\xi)\sin^2\xi\, d\xi}{\int_0^{\pi/2}\sin^2\xi\, d\xi},$$

i.e., as a function of the average fuel-element burn-up $\bar{s} = (2/\pi)s_0$,

$$k^*(\bar{s}) = k_0\left(1+\frac{4}{3}\alpha\bar{s}+\frac{3\pi^2}{16}\beta\bar{s}^2\right).$$

The criticality condition of such a system becomes

$$k^*(\bar{s}) = 1 + M^2B_H^2.$$

From this, we find

$$\bar{s} = \frac{\alpha+\sqrt{\alpha^2-\frac{27\pi^2}{64}\beta\left(\varrho_0-\frac{B_H^2M^2}{k_0}\right)}}{-\frac{9}{32}\pi^2\beta} \tag{23}$$

for the average fuel-element burn-up when we use up a reactivity excess $\rho_0 = (k_0-1)/k_0$.

If the fuel in such a system is continuously recharged in the manner proposed by B. O. Ioffe and L. B. Okun' [1], i.e., if the burned-out fuel elements are gradually removed from the reactor and fresh elements are inserted, so that elements of all "ages" will be contained in a fairly small volume, then the variation of the multiplication factor as a function of the average burn-up s* of the discharged fuel element will be of the form

$$k^{**}(s^*) = \frac{1}{s^*}\int_0^{s^*} k^*(\bar{s})\, d\bar{s} = k_0\left(1+\frac{2}{3}\alpha s^*+\frac{\pi^2}{16}\beta s^{*2}\right)$$

and the formula

$$s^* = \frac{\alpha+\sqrt{\alpha^2-\frac{9\pi^2}{16}\beta\left(\varrho_0-\frac{B_H^2M^2}{k_0}\right)}}{-\frac{3}{16}\pi^2\beta} \tag{24}$$

TABLE 1. Results of Calculations for Different Reactor Variants

| Parameter | Design variants | | | | | | | | | |
|---|---|---|---|---|---|---|---|---|---|---|
| | 1 | 2 | 3 | 4 | 5 | 6 | 7 | 8 | 9 | 10 |
| $H$, cm | 650,5 | 779,6 | 867,3 | 636,0 | 737,4 | 624,6 | 554,3 | 635,6 | 556,2 | 532,3 |
| $R$, cm | 325,3 | 389,8 | 308,7 | 318,0 | 262,5 | 312,3 | 277,2 | 317,8 | 278,1 | 266,1 |
| $M^2$, cm$^2$ | 377,7 | 344,7 | 370,8 | 344,4 | 387,4 | 340,7 | 377,2 | 337,6 | 369,4 | 402,4 |
| $k_0$ | 1,062 | 1,050 | 1,059 | 1,061 | 1,076 | 1,060 | 1,075 | 1,058 | 1,072 | 1,082 |
| $\alpha$ | 0,0235 | 0,0201 | 0,0279 | 0,0235 | 0,0235 | 0,0234 | 0,0235 | 0,0286 | 0,0235 | 0,0235 |
| $-\beta$ | 0,0764 | 0,0836 | 0,1011 | 0,0764 | 0,0764 | 0,0965 | 0,0764 | 0,0918 | 0,0764 | 0,0764 |
| $\mu_z$ | 0,3912 | 0,3401 | 0,3108 | 0,3866 | 0,3443 | 0,3997 | 0,4324 | 0,3898 | 0,4379 | 0,4537 |
| $\bar{\mu}_z$ | 0,5316 | 0,5007 | 0,4712 | 0,5250 | 0,5011 | 0,5389 | 0,5541 | 0,5286 | 0,5561 | 0,5636 |
| $s^*$, $10^{21}$ neutrons/sec$^2$ | 0,989 | 0,901 | 0,857 | 0,994 | 1,030 | 0,846 | 1,008 | 0,901 | 0,986 | 1,012 |
| $S$, $10^{21}$ neutrons/sec$^2$ | 1,235 | 1,085 | 1,029 | 1,224 | 1,255 | 1,054 | 1,277 | 1,116 | 1,246 | 1,287 |
| $\bar{S}$, $10^{21}$ neutrons/sec$^2$ | 1,408 | 1,262 | 1,206 | 1,400 | 1,456 | 1,199 | 1,432 | 1,272 | 1,394 | 1,430 |
| $Wt^*$, MW · day/ton | 4096 | 3730 | 3548 | 4115 | 4264 | 3501 | 4173 | 3728 | 4082 | 4190 |
| $Wt$, MW · day/ton | 5113 | 4492 | 4260 | 5067 | 5196 | 4364 | 5287 | 4620 | 5158 | 5328 |
| $\bar{W}t$, MW · day/ton | 5829 | 5225 | 4993 | 5796 | 6028 | 4963 | 5928 | 5266 | 5771 | 5920 |

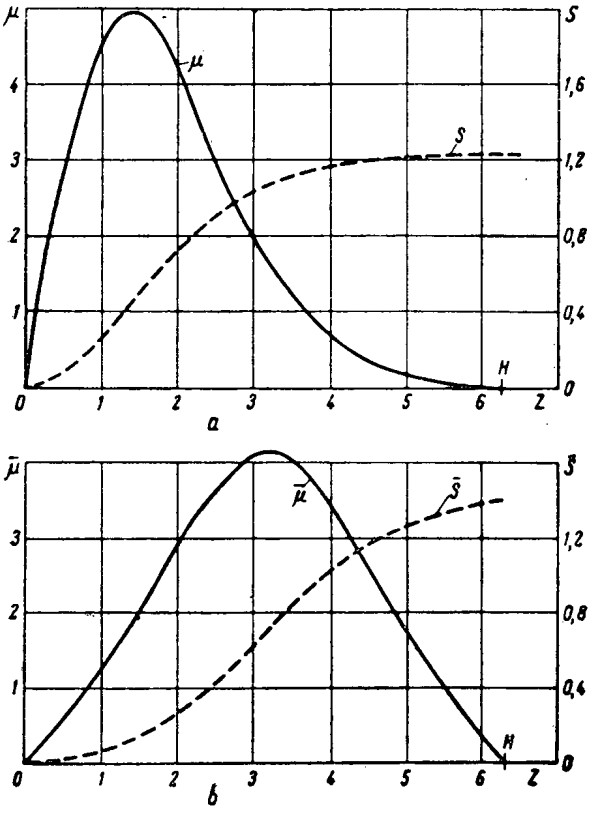


Fig. 1. Axial variation of neutron flux and fuel burn-up as functions of the coordinate z for fuel motion in one direction (a) and in opposite directions (b).

will determine the average fuel-element burn-up in the reactor for the case of continuous recharging.

Let us compare the burn-up for the above two element-recharging methods with the burn-up of the fuel in a cylindrical semiinfinite reactor whose radial geometric parameter has the value $B_r$. For the case when the fuel is moved in one direction, the burn-up as $H\to\infty$ takes on the value $S_\infty$, which is determined by the formula

$$S_\infty = \frac{\alpha + \sqrt{\alpha^2 \frac{9}{2}\beta\left(\varrho_0 - \frac{B_r^2 M^2}{k_0}\right)}}{-\frac{3}{2}\beta}. \qquad (25)$$

In the same reactor but with counter-motion of the fuel, the burn-up is given by the formula

$$\bar{S}_\infty = \frac{\alpha + \sqrt{\alpha^2 - \frac{16}{3}\beta\left(\varrho_0 - \frac{B_r^2 M^2}{k_0}\right)}}{-\frac{4}{3}\beta}. \qquad (26)$$

In order to obtain a rough qualitative idea of the relationship between the burn-up levels attained in the different types of operation, we substitute the values $\alpha = 0$, $B_r = B_H = 0$ into formulas (23)-(26). We then obtain

$$\bar{s} : s^* : S_\infty : \bar{S}_\infty = 1 : 1.73 : 1.93 : 2.36.$$

## Numerical Data and Conclusions

Table 1 shows the results of calculations for different variants of the reactors in regimes with fuel motion in one direction or opposite directions, for ten variants of the constants H, R, $M^2$, $k_0$, $\alpha$, and $\beta$, corresponding to a heavy-water reactor using natural uranium.

Figure 1 shows the axial variation of the neutron flux and the burn-up as functions of the coordinate z for motion in one direction (a) and for motion in two opposite directions (b) for the fourth variant of the table. The axial variation of the flux and the burn-up in the range we used for the constants changes relatively little, so that the relationships shown in the figure are typical for regimes with fuel motion.

When the fuel is moved in one direction, the flux maximum is displaced toward the location where fresh fuel is put in, and the burn-up is about 20% greater than the value in a regime using continuous recharging of fuel elements, apparently as a result of the significant leakage of neutrons at the point where the fuel is put in.

When the fuel is moved in two opposite directions, a burn-up value 40% greater than the value for continuous recharging can be obtained. The neutron flux distribution is symmetrical, although the flattening coefficient is less than for a uniform fuel distribution:

$$\bar{\mu}_z < \mu = \frac{2}{\pi} = 0.64.$$

## LITERATURE CITED

1. B. L. Ioffe and L. B. Okun', Atomnaya énergiya, 1, 80 (1956).
2. K. Meyer and E. Griepentrog, Kernenergie, 3, 11 (1960).

# COLUMN PACKINGS USED IN ISOTOPE SEPARATION

(UDC 621.039.31)

Yu. R. Akopov, I. G. Gverdtsiteli, V. A. Kaminskii, and G. L. Partsakhashvili

Translated from Atomnaya Énergiya, Vol. 17, No. 5, pp. 384-393, November, 1964
Original article submitted October 17, 1963; revision submitted February 13, 1964

The requirements for packings used in the separation of isotopes in columns are formulated. The properties of various wire packings are investigated, and their range of applicability is determined.

Distillation and chemical exchange processes carried out in packed columns have recently come into widespread use in the production of stable isotopes of light elements; however, the requirements to be imposed on the packings used in these processes have not yet been clearly formulated. Furthermore, the literature does not contain complete data on the properties of a number of efficient packings in common use, and without such data, it is impossible to determine the range of applicability of these packings and make the most expedient choice of a packing for a specific separation process. In the present study, we have made a detailed investigation of a number of efficient packings. We have formulated the basic requirements to be imposed on packings used in isotope separation and determined the range of applicability of the various packings.

## Requirements Imposed on Packings Used in Isotope Separation

The rate of mass exchange in a packed column is proportional to the phase contact surface between the liquid and the gas, which is measured by the height of a transfer unit (HTU), a quantity which characterizes the efficiency of the column. As is known,

$$\mathrm{HTU}=\frac{G}{aK},$$

where G is the gas flow density, expressed in moles, a the phase contact surface per unit volume, and K the mass transfer coefficient.

The HTU value and the number of stages S required in order to obtain a product of a given concentration determine the height of the column:

$$Z=\mathrm{HTU}\cdot S.$$

Since there is little difference between the physicochemical properties of isotopic compounds, the separation of isotopes is an extremely difficult problem, and in order to obtain an enriched product, it is necessary to have installations with hundreds or thousands of stages. It becomes a principal objective to obtain a small height for a separation stage by using packings which provide a large phase contact surface. The first basic requirement for packings used in isotope separation is that they must provide the maximum possible phase contact surface per unit volume of the column.

The magnitude of the phase contact surface depends on a number of different factors. A decisive role is played by the geometrical unit surface of the packing, which increases as the dimensions of the elements decrease. When isotopes are separated in amounts appropriate to laboratory equipment or small industrial installations, packings with elements measuring between 4 and 1.5 mm are used. The effect of the capillary forces, which hold the liquid at the points where it is in contact with the packing elements, comes into prominence when such element dimensions are used. In the case of packings with internal cavities — such as segments of closely wound-wire coil or cylindrical rings — when the elements are of small dimensions, the liquid is held by the capillary forces inside

the elements themselves. Consequently, the actual phase contact surface may be very different from the shape of the geometric surface formed by the elements of the dry packing. In addition, the true phase contact surface is affected by the distribution of the liquid along the cross section of the column and the wettability of the packing by the working liquid.

In order to increase the wetted surface, the use of most of the known packings requires flooding, a process which consists in filling the packing part of the column with liquid and then gradually removing this liquid, great care being taken to maintain the operating regime of the column. If the liquid is poorly retained by the packing, then after each interruption of the operating regime the packing must be artificially wetted again, so that a considerable amount of time is consumed in returning the system to the stationary state. The time required for establishing this state may be expressed approximately by the formula

$$t = \frac{H}{\varepsilon^2} f(X_p),$$

from which it is clear that the time consumed for reestablishing the stationary state is especially long for isotope separation processes, since the enrichment factor $\varepsilon$ is small. The flooding process considerably complicates the technology of bringing low-temperature columns into operation. In a number of processes used for isotope separation (chemical exchange and the distillation of thermally unstable compounds) the flooding is impossible in principle. These include processes of considerable interest, for example, chemical exchange between NO and $HNO_3$ and exchange distillation of the $(CH_3)_2O \cdot BF_3$ complex. Therefore, a second basic requirement for packings used in isotope separation is that they must be suitable for efficient operation without flooding or any other type of preliminary wetting.

This quality of the packing may be attained by improving its capillary properties, so that the liquid will satisfactorily wet the packing and will be held satisfactorily on its surface. However, improvement of the capillary properties leads to an increase in the amount of liquid held by the packing and concomitant increase in the time required for reaching the stationary state. Efforts must be made to develop packings which, in addition to their good capillary properties, will hold a small quantity of liquid, especially in cases with low values of the elementary coefficient of separation or of the amount of material to be separated.

Packings used for isotope separation are, as a rule, not subject to rigorous requirements with respect to their hydrodynamic resistance to the flow of vapor or gas and the maximum packing transmissivity which is related to this. Packings allowing a reflux density of 5 to 6 m liter/$cm^2 \cdot$ min at atmospheric pressure are regarded as satisfactory, those allowing 8 to 10 m liter/$cm^2 \cdot$ min as good. The considerable bulk of the apparatus and the necessity of using packing materials of small sizes sets increased demands on the simplicity of manufacturing the packing elements and the cost of unit volume.

In order to characterize a packing, we must know the geometrical shape of an element and its basic dimensions, the number of elements per unit of volume, the percentage of unoccupied space available for the passage of vapor or gas, and the packing density. The efficiency of the packing is measured by the value of the HTU or HETS [1] (for most isotope-separation processes these quantities are numerically equal), determined for the entire range of reflux density allowable for the given type of packing, as well as by the values of the pressure drop $\Delta P$ and the hold-up H.

Since it is difficult to make a detailed study of the properties of efficient packings by means of isotope mixtures because of the long times required for establishing the stationary state and the complications involved in analyzing a large number of samples, the efficiency of a packing is usually estimated by means of standard organic mixtures, the most widely used of which are benzene and carbon tetrachloride, n-heptane and methylcyclohexane, etc. For a comparison of different packings, one must compare the curves showing the variation of the HTU, $\Delta P$, and H which are obtained for identical mixtures in columns with identical diameter and height, as functions of the reflux density L. The reason for this is that when the column diameter is increased, the height of a stage generally increases and the pressure drop decreases as a result of the nonuniform distribution of liquid and gas flow along the cross section of the column. When different mixtures are used, the efficiency of the packings may be compared by using the criterion $\Phi = W\gamma/HTU$, where W and $\gamma$ are the velocity and specific gravity of the vapor. The greater the value of $\Phi$ the more efficient is the packing.

For a given packing, the height of a stage may vary considerably when changes are made in the substances to be separated; this is due both to the change in their molecular weight and to the change in the physical properties

[1] HETS – height equivalent to a theoretical stage.

TABLE 1. Efficiency of Triangular Packing, Determined by Means of Standard Organic Mixture and Isotope Mixtures

| Process | Column diameter, mm | Packing and its dimensions, mm | Reflux density, ml/cm² · min | HTU, cm |
|---|---|---|---|---|
| Distillation of a standard mixture of $C_6H_6$ and $CCl_4$ | 15,0 | Triangular, 2,2×2 | 1,8<br>2,5<br>4,0 | 1,3<br>1,75<br>2,0 |
| Chemical exchange $HN^{14}O_3+N^{15}O \rightleftarrows HN^{15}O_3+N^{14}O$ | 11,0 | The same | 0,9<br>1,3<br>2,6 | 2,7<br>3,1<br>5,0 |
| Distillation of $C_6H_6$—$CCl_4$ | 15,0 | Wire rings; $D_{in}$ = 1.2 | 1,1<br>1,7<br>2,8 | 1,4<br>1,8<br>2,0 |
| Distillation of $BF_3$ | 11,0 | The same | 0,9<br>1,6<br>2,7 | 1,9<br>2,1<br>2,3 |

TABLE 2. Efficiency of Various Packings, Determined in the Separation of Nitrogen Isotopes by the Method of Chemical Exchange between NO and $HNO_3$

| Packing, element, size, mm | Column diameter, mm | Height of packing layer, m | Reflux density, ml/cm²·min | HTU, cm | Literature |
|---|---|---|---|---|---|
| Single turns of circular coil, diameter 1.7 | 9,0<br>26,0 | 5,75<br>8,1 | 1,55<br>2,8 | 4,4<br>12,1 | [2] |
| Segments of triangular coil, 2 × 2 | 11,0<br>11,0<br>11,0 | 1,0<br>1,0<br>1,0 | 0,9<br>1,3<br>2,6 | 2,7<br>3,1<br>5,0 | Authors' own data |
| Fenske coils, 1.6 × 1.6 | 10,0<br>10,0<br>23,0 | 1,5<br>1,5<br>2,0 | 1,6<br>3,2<br>1,4 | 8,4<br>12,5<br>8,7 | [6] |
| Heli-Pak, 1.3 × 2.5 × 2.5 | 25,0<br>25,0<br>25,0 | 0,95<br>0,95<br>1,6 | 1,6<br>3,0<br>5,0<br>1,6 | 2,8<br>4,0<br>5,8<br>3,4 | [6] |

of the liquid and the gas, which determine the phase contact surface and the mass transfer coefficient. The greatest difference is found between the stage height values determined with the same packing for the processes of distillation and chemical exchange. As can be seen from Table 1, the latter process yields higher values of the HTU.

## Packings Used in Isotope Separation

In a number of original studies on isotope separation, the packing used consisted of single turns or segments of a circular spiral. Single turns with an internal diameter of 1.2 mm, in spite of their low transmissivity, were used in the concentration of the isotope $B^{10}$ by the low-temperature distillation of $BF_3$ [1]. This packing was used in obtaining the isotope $N^{15}$ in a high concentration by the method of chemical exchange between NO and $HNO_3$ [2]. Segments

of circular wire coil (Fenske coil) were used in concentrating $N^{15}$ by the method of chemical exchange between ammonia and a solution ammonium nitrate [3, 4]. In the distillation of liquid NO using this packing, fairly low values of stage height were achieved (1.72 and 1.85 cm), although the authors give no indications of the flow values in the column [5].

Reference [6] showed the advantages of Heli-Pak packing over Fenske coils for chemical exchange processes between NO and $HNO_3$ (Table 2). Heli-Pak consists of segments of a rectangular wire coil in which the spacing between adjacent turns is carefully kept constant. The usual dimensions of a packing element are $1.3 \times 2.5 \times 2.5$ mm or $0.9 \times 1.8 \times 1.8$ mm. Heli-Pak has been used chiefly for the industrial production of $N^{15}$ by the method of exchange between NO and $HNO_3$ [7], as well as for the separation of nitrogen isotopes using exchange between NO and $N_2O_3$ [8].

Dixon rings, which are small cylinders made of thin wire gauze and containing a partition, are no less efficient than Heli-Pak. Although Dixon rings are very difficult to manufacture and require special conditions for flooding [9], they have nevertheless been used for the industrial concentration of the isotope $B^{10}$ by the method of $BF_3$ distillation [10] and in the exchange distillation of the $(C_2H_5)_2O \cdot BF_3$ complex [11]. The Dixon packing has been used in concentrating the isotopes $C^{13}$ and $O^{18}$ by low-temperature distillation of carbon monoxide [12], as well as in the distillation of water [13]. This packing has a very low pressure drop, and consequently, it is convenient to use in processes carried out at low pressure.

One type of packing that has come into wide use in the Soviet Union is a packing consisting of fragments of triangular wire coils, in which the adjacent turns are displaced by 10-20° [14]. Triangular packing has been used in studies on the separation of the isotope $C^{13}$ by the distillation of CO [15], of $O^{18}$ by the distillation of $H_2O$ [16], and of $N^{15}$ by chemical exchange between NO and $HNO_3$ [18].

All of these packings must be flooded in order to increase their efficiency. Descriptions have been given of attempts to produce packings which eliminate the need for flooding. A packing consisting of perforated half-cylinders of metal foil has been developed in the United States [19]. The openings in the foil are not cleanly cut but are protuberant and have projections on one side which facilitate the retention of liquid on the surface. This type of packing, known as protruded packing, is used in columns with diameters of more than 40 mm. It has been used in concentrating $B^{10}$ by the exchange distillation of the complexes $(C_2H_5)_2O \cdot BF_3$ [20] and $(CH_3)_2O \cdot BF_3$ [21].

The Dixon, Heli-Pak, and protruded packings have been studied in detail by means of standard mixtures. However, up to the present time no complete study has been made of the properties of such widely used packings as triangular-coil and circular-coil segments.

Figure 1 illustrates several of the most efficient types of packing.

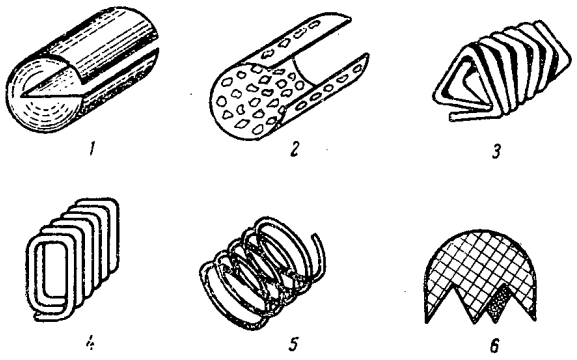


Fig. 1. High-efficiency packings for distillation and exchange columns: 1) Dixon rings; 2) Cannon's protruded packing; 3) triangular-coil segments; 4) Heli-Pak; 5) Fenske coil; 6) wire gauze cap.

## Study of the Properties of Triangular Packing and Improvement of Its Efficiency in Operation without Any Preliminary Wetting

We have studied the properties of triangular packing by means of a standard mixture of benzene and carbon tetrachloride. Table 3 shows the characteristics of packings of various dimensions investigaged in the present study. The effect of the element dimensions on the efficiency of the packing was determined in columns with diameters of 26 and 50 mm. We tested elements with dimensions of $1.3 \times 1.2$, $2.2 \times 2$, and $3 \times 2.4$ mm, made of wire 0.25 mm in diameter. The test results are shown in Fig. 2. They indicate that the thick packing has a much higher efficiency than the thin packing; this is due to the retention of liquid in the internal cavities of the elements by capillary forces and to the inaccessibility of part of the internal surface of the packing to exchange between liquid and gas. This is confirmed by the increase in the holdup when a change is made from the thick to the thin packing. Thus, it is not possible to obtain an efficiency comparable to that of the Dixon and Heli-Pak packings by reducing the dimensions of triangular packing elements.

TABLE 3. Characteristics of Various Wire Packings

| Packing | Packing size, mm | Number elements per $cm^3$ | Fraction of voids | Maximum packing density, $g/cm^3$ |
|---|---|---|---|---|
| Triangular-coil segments | 3×2,4 | 35 | 0,88 | 1,49 |
| | 2,4×3 | 45 | 0,84 | 1,57 |
| | 2,2×2 | 100 | 0,79 | 1,94 |
| | 1,5×2 | 230 | 0,73 | 2,07 |
| | 1,3×1,2 | 343 | 0,64 | 2,44 |
| Individual turns of circular coils | $D_{in}$ = =1,2 | 1000 | 0,68 | — |
| Wire gauze caps | 2,5×1,7 | 250 | 0,88 | — |
| Caps of two-ply gauze | 4,5×2,8 | 36 | 0,89 | 0,96 |
| | 3,0×1,8 | 150 | 0,85 | 0,84 |

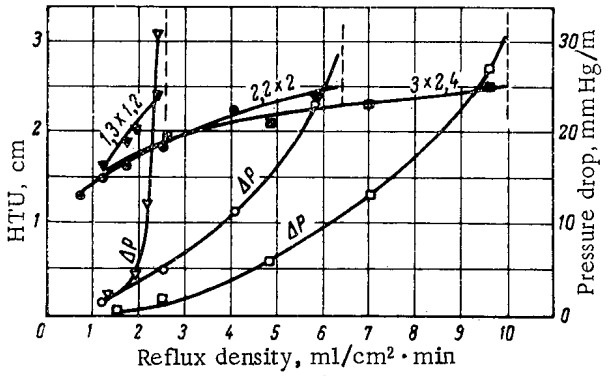


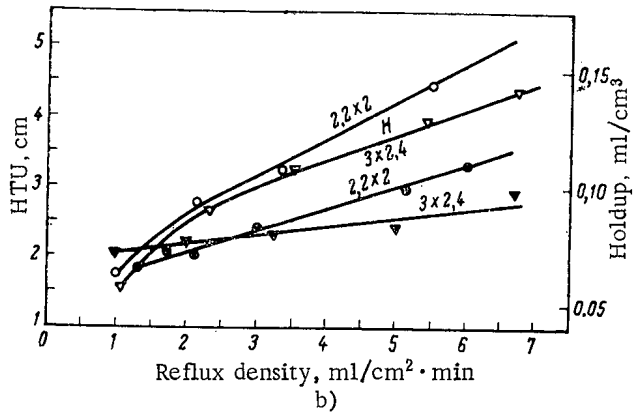


Fig. 2. Variation of separation efficiency as a function of element dimensions for triangular packing in columns with diameters of 26 and 50 mm (Figs. 2a and 2b, respectively; the dashed lines show the limiting transmissivity values for the packing).

We found that changing the length of the coil segment from 1 to 3 mm made practically no difference in the efficiency and transmissivity of the packing. The transmissivity is completely determined by the diameter of the circumscribed circle of the triangle.

Figure 3 shows the results of investigations made in a 26-mm diameter column with 2.4 × 3 and 3 × 2.4 mm packings (the first number refers to the diameter of the coil, and the second to the length of the segment). While the HTU values of these packings are approximately the same, the transmissivity is considerably higher for the larger-diameter elements. Consequently, it is expedient to use triangular packing elements in which the length of the coil segment is somewhat less than the diameter of the circumscribed circle. On the other hand, reduction of the coil segment to two or three turns is undesirable, since in this case the capillary properties of the packing become poorer. The effect of the column diameter on the efficiency of the packing was studied in columns with diameters of 15, 26, and 50 mm, and with a packing whose elements measured 2.2 × 2 mm. In all the tests the liquid was poured from the condenser onto the packing at the center of the column cross section. The test results, shown in Fig. 4, indicate that the efficiency is reduced as the column diameter is increased.

As can be seen from Table 4, when there is no preliminary wetting, the efficiency of the triangular packing is considerably reduced. In order to eliminate this defect, we may use a packing system consisting of layers of triangular packing and special capillary layers made of wire gauze [22]. Such capillary layers are completely wetted by the working liquid when the column is in operation, and in turn they supply the adjacent triangular packing layers with liquid and wet them.

In order to prepare the capillary layers, a wire gauze made of 0.1-mm diameter wire and having

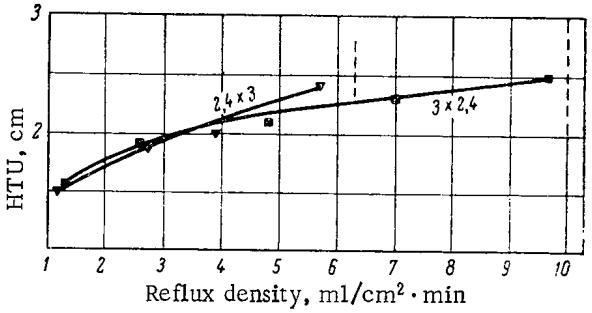


Fig. 3. Effect of coil diameter on the transmissivity of triangular packing (the dashed lines indicate the limiting transmissivity values of the packing).

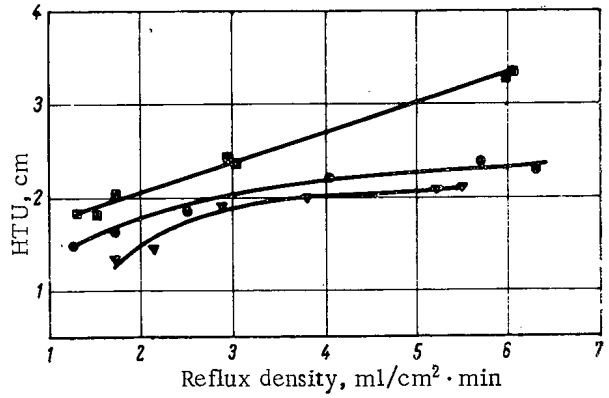


Fig. 4. Variation of the efficiency of triangular packing as a function of column diameter: ▼ – 15 mm; ● – 26 mm; ■ – 50 mm.

TABLE 4. Effective of Preliminary Wetting on the Efficiency of Triangular Packing (Column Diameter 50 mm, Packing-Element Dimension 2.2 × 2 mm)

| Reflux density, ml/cm² · min | HTU, cm | |
|---|---|---|
| | for flooded packing | for unflooded packing |
| 1,4 | 1,90 | 4,24 |
| 2,2 | 2,15 | 5,30 |
| 4,3 | 2,75 | 5,40 |
| 6,0 | 3,30 | 6,25 |

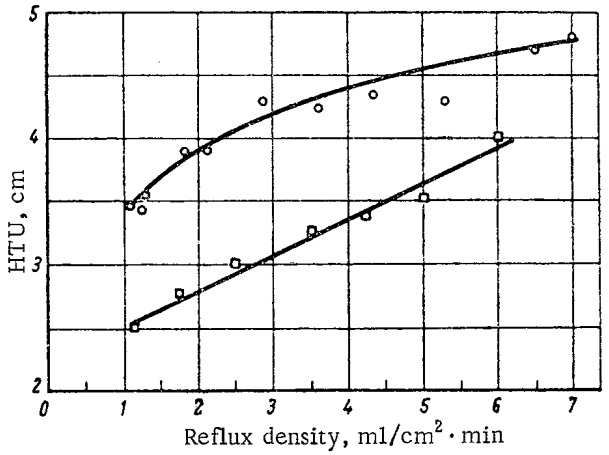


Fig. 5. Efficiency of a packing system consisting of triangular packing and capillary layers, operating without preliminary wetting: □ – column diameter 50 mm, packing-element dimension 2.2 × 2 mm; ○ – column diameter 94 mm, packing-element dimensions 3 × 2.4 mm.

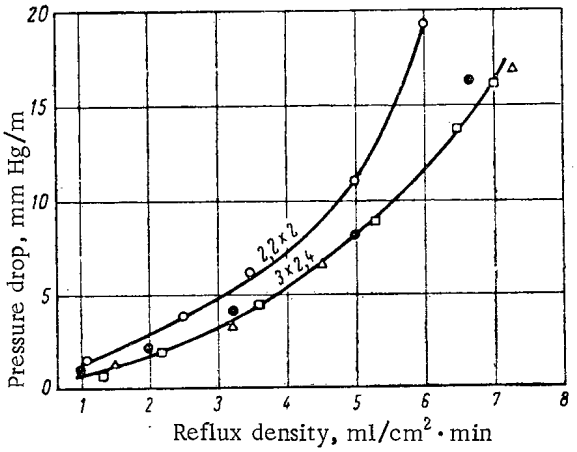


Fig. 6. Hydrodynamic resistance of triangular packing with capillary layers: ● – flooded packing without capillary layers, $D_{col}$ = 50 mm; ○, △ – unflooded packing with capillary layers, $D_{col}$ = 50 mm; □ – the same, $D_{col}$ = 94 mm.

cells which measure 0.18 mm along an inner side is cut into pieces 8-mm wide and with a length 5-10 mm less than the column diameter. The pieces so obtained are folded in half and smoothed out. Six to ten of these 4-mm wide strips of two-ply gauze are placed between adjacent layers of triangular packing 1 cm deep.

As was shown by the test results, the packing system consisting of triangular packing layers and capillary layers worked efficiently without any preliminary wetting (Fig. 5). The efficiency of such a system is higher than that of protruded packings specially prepared for processes in which flooding is not possible. The capillary layers of two-ply wire gauze not only wet the adjacent layers of packing but also make possible a more uniform distribution of the liquid along the cross section of the column; this is particularly conspicuous when the column has a large diameter and the packing layer is shallow. It should be noted that the capillary layers are not arranged precisely in the plane of the column cross section, and therefore their use does not produce any increase in the pressure drop (Fig. 6) and does not limit the throughput of the column.

An investigation of triangular packing with a displacement angle of 40-50° between the turns showed that it is completely unsuitable for processes in which preliminary wetting is not possible. The reason for this is that this arrangement breaks the capillary channels which are formed by adjacent turns in elements with small displacement angles.

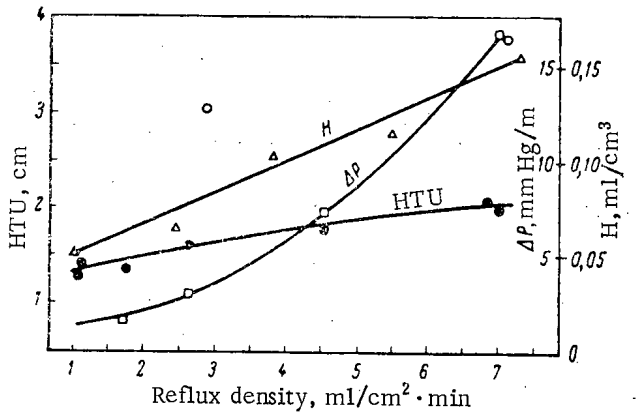


Fig. 7. Efficiency of circular-coil segments with packing-element dimensions of 2 × 0.7 mm (○ – HTU values obtained for operation without flooding).

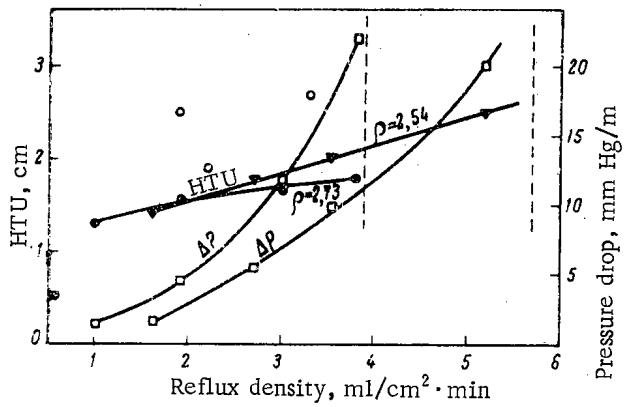


Fig. 8. Variation of the efficiency and transmissivity of single turns of a circular coil as functions of packing density; coil dimensions 1.2 × 0.25 mm, column diameter 26 mm (○ – HTU values obtained in operation without flooding).

TABLE 5. Efficiency of Single Turns of Circular Coil

| Inner diameter of ring and diameter of wire, mm | Diameter of column mm | Reflux density L, ml/cm² × min | HETS value, cm | Literature |
|---|---|---|---|---|
| 1,2×0,25 | 7,0 | 1,5<br>2,8 | 1,4<br>1,8 | Authors' own data |
| 2,38×0,25 | 25,4 | 1,7<br>3,3<br>10,0 | 1,9<br>2,1<br>3,0 | [23] |
| 1,59×0,16 | 25,4 | 1,61<br>3,30<br>10,0 | 1,6<br>1,7<br>2,5 | [23] |
| 1,2×0,25 | 26,0 | 1,0<br>1,9<br>3,8 | 1,3<br>1,55<br>1,8 | Authors' own data |
| 2,38×0,25 | 50,8 | 1,1<br>2,2<br>6,6 | 3,9<br>4,2<br>5,2 | [23] |
| 1,2×0,25 | 50,0 | 1,2<br>2,0<br>2,6 | 2,7<br>3,0<br>3,2 | Authors' own data |

## Properties of Packing Consisting of Circular-Coil Segments

The properties of a packing made of segments of a circular wire coil differ little from those of the triangular packing described above. Circular-coil segments containing six to eight turns have internal cavities in which the liquid can be "sealed" when the diameter is small. When the number of turns is reduced to 1-3 turns, this effect disappears, but at the same time the capillary properties of the coil become considerably poorer, since the depressions between adjacent turns constitute the capillary channels. Such packing does not work well without preliminary wetting (Fig. 7). However, short segments and single turns may be used in columns of small diameter (less than 10 mm), since in this case long coil segments and other types of packing do not give a sufficiently high-packing density. In small-diameter columns, it is also possible to use short segments and single turns of triangular coils; however, single turns of circular coils have come into wide use.

As can be seen from Fig. 8, the packing density $\rho$ has a strong influence on the HTU value, and especially on the transmissivity of single turns. Even though loose packing increases the transmissivity, it is undesirable because it may lead in the course of time to the formation of voids in the packed part of the column.

## Wire-Gauze Cap Packing

In columns designed for isotopes separation, we may use a new, highly efficient type of packing whose elements have the shape of hemispheres with four sharp teeth and are made of thin wire gauze (cell dimensions 0.18 mm, wire diameter 0.1 mm) [24]. These packing elements are manufactured by pressing square pieces of wire gauze through round holes.

TABLE 6. Comparison of the Efficiencies of Wire-Gauze Caps and Other Types of Packing

| Packing and dimensions, mm | Column diameter, mm | Maximum transmissivity, ml/cm²·min | HTU value (cm) when the liquid rate is 3 ml/cm² × min | HTU value (cm) when the liquid rate is 5 ml/cm² × min | Literature |
|---|---|---|---|---|---|
| Wire gauze caps 2,5×1,7 | 10,0 | 7,6 | 0,88 | 1,06 | [24] |
| Heli-Pak | 13,7 | 5,0 | 0,88 | 1,0 | [25] |
| Dixon rings 1,6×1,6 | 12,7 | 8,3 | 0,75 | 1,06 | [9] |

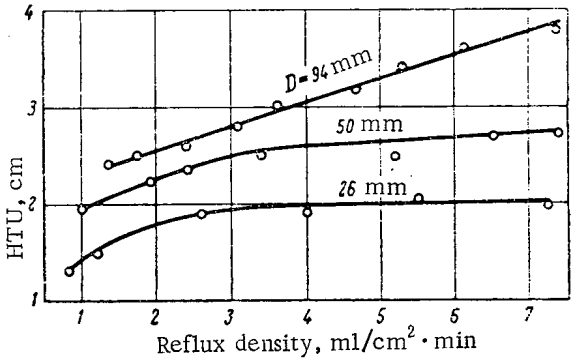


Fig. 9. Variation of the separation efficiency as a function of column diameter for cap packing made of two-ply wire gauze.

A packing with element diameters of 2.5 x 1.7 mm has an efficiency comparable to that of minimum-dimension Dixon or Heli-Pak packing (see Table 6), and has the advantage of being simpler to manufacture. Just as in the case of the Dixon packing, this type of packing requires artificial flooding at the working velocity of the vapor.

In order to increase the efficiency of the cap packing for operation without preliminary wetting, this packing may be made from two-ply pieces of wire gauze (pieces that have been folded in half). Figures 9 and 10 show the results of tests made on caps of two-ply wire gauze with element dimensions of 4.5 x 2.8 mm, used without preliminary wetting. In addition to its high efficiency, this packing has an extremely low pressure drop, but its retention value is somewhat higher than that of triangular packing. Cap packing made of two-ply wire gauze produces a good distribution of the liquid along the cross section of the column.

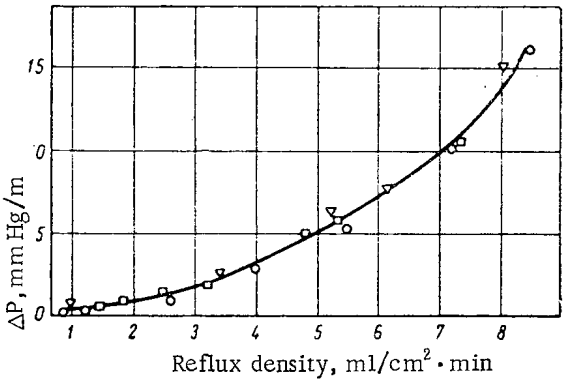


Fig. 10. Hydrodynamic resistance of cap packing for the following column diameters: ○ – 26 mm; ▽ – 50 mm; □ – 94 mm.

## Conclusions

1. The fundamental conditions which must be satisfied by packing used for isotope separation are: a) it must provide the maximum possible phase contact surface per unit of volume in the column; b) it must be capable of efficient operation without any preliminary wetting.

In addition, the amount of liquid retained by the packing when the column is in operation must be small, and the packing must offer little hydrodynamic resistance to the flow of vapor or gas.

2. The range of applicability of single turns of circular coils is limited to columns with diameters less than 10 mm and low reflux densities.

3. The Dixon and Heli-Pak packings are more efficient but require flooding. In addition, these packings are difficult to manufacture and are expensive.

4. Packings made of segments of triangular wire coils are easy to manufacture but also function poorly without preliminary wetting. This trouble may be eliminated by using a packing system consisting of triangular packing and capillary layers made of two-ply wire gauze. Such a packing system is more efficient than protruded packing, which was especially developed for processes in which flooding is impossible.

5. Segments of circular wire coils are as efficient as triangular packing but have poorer capillary properties.

6. Cap packing is about as efficient as Dixon rings and Heli-Pak and is superior to these in its simplicity of manufacture. This packing has a low pressure-drop value. Since it is made of two-ply wire gauze, it does not require preliminary wetting.

## LITERATURE CITED


1. J. K. Mühlenpfordt, G. G. Siewert, and T. A. Gagua, Proceedings of the International Scientific and Technical Conference on the Use of Radioactive and Stable Isotopes in the National Economy [in Russian], Moscow, Izd-vo AN SSSR (1958), p. 127.
2. I. G. Gverdtsiteli et al., Soobshchenyia AN SSSR, 24, 153 (1960).
3. H. Thode and H. Urey, J. Chem. Phys., 7, 34 (1939).
4. V. V. Ottesen and M. É. Aerov, Zh. fiz. khim., 30, 1356 (1956).
5. K. Klusius, K. Schleich, and M. Vecchi, Helv. chim. acta, 44, 343 (1961).
6. T. Taylor and W. Spindel, Proceedings of the Symposium on Isotope Separation, Amsterdam (1957), p. 158.
7. G. Begun, J. Drury, and E. Joseph, Industr. and Engng. Chem., 51, 1035 (1959).
8. E. Monse et al., J. Chem. Phys., 32, 1557 (1960).
9. O. Dixon, J. Soc. Chem. Ind. Lond., 68, 88 (1949).
10. P. Nettly, D. Gartwright, and H. Kronberger, Proceedings of the Symposium on Isotope Separation, Amsterdam (1957), p. 385.
11. R. McIlroy and F. Pummery, Ibid., p. 178.
12. H. London, Ibid., p. 319.
13. I. Dostrovsky and A. Raviv, Ibid., p. 336.
14. A. I. Levin, Neft. kh-vo, No. 10, 40 (1949).
15. M. V. Tikhomirov and N. N. Tunitskii, Zh. prikl. khim., 32, 531 (1959).
16. O. V. Uvarov, V. A. Sokol'skii, and N. M. Zhavoronkov, Khim. prom-st', No. 7, 404 (1956).
17. S. I. Babkov and N. M. Zhavoronkov, Khim. prom-st', No. 7, 388 (1955).
18. I. G. Gverdtsiteli et al., Atomnaya énergiya, 10, 487 (1961).
19. M. Cannon, Industr. and Engng. Chem., 41, 1953 (1949).
20. A. Edmunds and F. Loveless, In "Proceedings of the Second International Conference on the Peaceful Uses of Atomic Energy" [in Russian], Reports of Non-Soviet Scientists, 10, Moscow, Atomizdat (1959), p. 150.
21. G. Miller, R. Kralik, E. Belmore, and J. Drury, Report No. 1836, presented by the United States at the Second International Conference on the Peaceful Uses of Atomic Energy (Geneva, 1958).
22. V. A. Kaminskii and G. L. Partsakhashvili, Zh. prikl. khim., 36, 2007 (1963).
23. M. Fenske, C. Tongberg, and D. Quiggle, Industr. and Engng. Chem., 26, 1169 (1934).
24. V. A. Kaminskii, Zavodsk. laboratoriya, 28, 1382 (1962).
25. Distillation [Russian translation], edited by A. Weisberger, Moscow Izd-vo inostr. lit. (1954), p. 179.

# SOME CHARACTERISTICS OF RADIOLYSIS UNDER THE INFLUENCE OF A PULSED BEAM OF FAST ELECTRONS

(UDC 541.15 : 621.384.60)

V. L. Tal'roze and V. E. Skurat

Translated from Atomnaya Énergiya, Vol. 17, No. 5,
pp. 393-400, November, 1964
Original article submitted May 17, 1963

The purpose of this paper is to study the main characteristics of radiolysis associated with the use of electron pulse accelerators. On the basis of a typical mechanism of the chemical reactions of free radicals formed under the influence of a pulsed fast electron beam, the mean stationary concentration of free radicals $[R]_{st}$ is calculated as a function of the duty factor q of the electron current pulses. The calculation is carried out for various powers, corresponding to various rates of formation of the free radicals, various current pulse widths, and various free radical loss constants for reactions of the first and second orders. Graphs of $[R]_{st}$ as a function of q are presented.

Recently, charged-particle accelerators have found considerable application as sources of ionizing radiation, among them electron pulse accelerators. The use of electron pulse accelerators generating free radicals in liquids, together with spectroscopic methods of recording the radicals, enables us to measure their loss rates and determine their reaction rate constants [1]. In this case, the method constitutes a radiochemical variant of the well-known method of pulse photolysis. On the other hand, we may reasonably expect that, for certain relations between the intensity of the fast electron beam, the pulse duty factor, and the reaction rate constants of the free radicals formed by the radiation, it should be possible to measure the monomolecular and bimolecular loss rate constants, as is also done by the rotating sector method in photochemistry [2]. Aside from this, the possibilities of using ionizing radiations for chemical synthesis in industry, for example, in fixing atmospheric nitrogen [3], vulcanizing rubber [4], etc., are being studied. Thus, the question of the specific characteristics of radiolysis under the influence of an interrupted high intensity fast electron beam is of extremely great importance.

The present paper is aimed at discovering to what extent a change in the duty factor of the electron beam pulses (their mean power being kept constant) may affect the radiation yield of stable products formed in reactions of free radicals with molecules of the medium or with molecules of specially introduced additions, i.e., in the long run, at finding the effect of the "pulseness" of the irradiation on the yield and the direction of radiochemical reactions. Let us suppose, for example, that, in the first act of radiolysis of the molecule AB, free radicals A are formed

$$AB \sim\sim\sim\rightarrow A + B, \quad (1)$$

which under conditions of "nonpulsed" radiolysis form molecules AC by a substitution reaction with molecules of CD:

$$A + CD \rightarrow AC + D. \quad (2)$$

Under conditions of pulsed radiolysis characterized by an extremely high rate of A formation under the influence of the electron current pulse, reaction (2) is accompanied to a large extent by a reaction in which a dimer of A is formed:

$$A + A \rightarrow A_2, \quad (3)$$

and indeed this may predominate over reaction (2). Clearly, in this case, the radiation yield of AC will diminish, the diminution depending not only on the reaction rate constants for (2) and (3) but also on the characteristics of the electron beam (duty factor, pulse width, etc.).

For the calculations we started from the following scheme of reactions taking place in the radiolysis of K molecules:

$$K \sim\sim\sim\rightarrow mR + P \quad \text{formation of free radicals;}$$

$$\left.\begin{array}{l} 2R \rightarrow P_{b1} \quad k_{b1} \\ \cdots\cdots\cdots \\ 2R \rightarrow P_{bi} \quad k_{bi} \end{array}\right\} \text{transformation of R, second order;}$$

$$\left.\begin{array}{l} R + A_1 \rightarrow P_{f1} \quad k_{f1} \\ \cdots\cdots\cdots\cdots \\ R + A_i \rightarrow P_{fi} \quad k_{fi} \end{array}\right\} \text{transformation of R, first order;}$$

$$R + B_i \rightarrow P_{ci} + R \quad k_{ci} \quad \text{development of chain reaction.}$$

Here K is the molecule being radiolyzed, m a whole number, R the free radical, P, $P_{b1}$-$P_{bi}$, $P_{f1}$-$P_{fi}$, and $P_{ci}$ the stable or radical products (which may be disregarded), and $k_{bi}$ and $k_{fi}$ the rate constants of the reactions bi and $f$i. We calculated the mean stationary concentration $[R]_{st}$ of radicals R which could later enter into a subsequent reaction with molecules of the medium or added molecules, forming the product in which we were interested. In this case, the radiation yield G of the product will be proportional to the product of the stationary concentration of R, the concentration of the other reagent, and the corresponding rate constant. For example, for product $P_{f1}$

$$G(P_{f1}) \sim k_{f1}[R]_{st}$$

Thus, in order to solve the problem posed, we must find the variation of $[R]_{st}$ with the factors characterizing the electron pulsed beam and the factors determining the formation and loss of free radicals in the system.

It must be noted that the reaction mechanism postulated has a quite general character. An analogous array of reactions may also be written down formally for other unstable intermediate products (for example, charged particles) which from the mathematical point of view may play the part of R in the scheme under consideration.

In the present investigation, we calculated the relation between $[R]_{st}$ and the duty factor q of the electron current pulses for constant mean electron beam power, i.e., for a constant mean rate $\Phi$ of generating R. In the calculations, we assumed that the mean rate of generating radicals could vary between $10^{15}$ and $10^{21}$ radical/cm$^3$ · sec, the duty factor q between 10 and $2 \cdot 10^4$, the electron current pulse width $t_1$ between $10^{-6}$ and $10^{-4}$ sec. These values correspond to typical characteristics of modern pulse accelerators.

Let us take the following accelerator parameters: electron energy 5 MeV, q = 100, maximum pulse beam power 500 kW, maximum mean beam power 5 kW, electron beam diameter at exit around 1 cm. Thus, the maximum mean beam power is $5 \cdot 10^3 \cdot 6.3 \cdot 10^{18} = 3.15 \cdot 10^{22}$ eV/sec.

Since the stopping power of water and organic compounds for electrons of 5 MeV energy is 1.85-2.0 MeV/g · cm$^2$ [5], 1 cm$^3$ of liquid or solid matter with density $\sim 1$ g/cm$^3$ will absorb around $(1.2-1.3) \cdot 10^{22}$ eV energy in 1 sec. If we suppose that the radiation yield G of the transformation is 5-10 molecule/100 eV, then this dose will correspond to the formation of $(0.6-1.3) \cdot 10^{21}$ radical/cm$^3$ · sec. The maximum value of $\Phi = 10^{21}$ radical/cm$^3$ · sec. It is clearly impossible to act on static systems with such powerful electron beams owing to excessive heating. Simple calculation shows, however, that in a circulating system, or on agitating the substance in the reaction zone, irradiation by such beams may be used, without the substance being too rapidly moved across the irradiated zone (linear dimensions of zone $\sim 1$ cm). For example, a beam of mean power t kW will heat water or an aqueous solution not more than 100°C in $10^{-1}$ sec.

Thus, the thermal heating of water flowing at a rate of 20 cm/sec will not exceed 50°C. For a number of substances (paraffins), the permissible heating may turn out to be even higher. In such cases, the rate of flow may thus be reduced. For gases at atmospheric pressure, the density of which lies some $10^3$ times lower than that of the liquids, the maximum value of $\Phi = 10^{18}$ radical/cm$^3$ · sec. The minimum value of $\Phi$, taken in the calculation, was $10^{15}$ radical/cm$^3$ · sec.

Let us now estimate the parameters of the chemical reaction under consideration:

$$K_f = \sum k_{fi}, \quad K_b = \sum k_{bi}.$$

In the calculation we took values for $K_b$: $10^{-10}$ and $10^{-12}$ $cm^3/sec$. The first corresponds to the bimolecular reaction of the recombination of the radical, not having any activation energy. Of such an order, for example, is the $K_b$ in the recombination of $CH_3$ radicals in the gas phase [6]. The second value corresponds to recombination the rate of which may be determined by the rate of some other process, e.g., diffusion. Thus, $K_b \sim 10^{-12}$ $cm^3/sec$ for the bimolecular loss of radical $CH_3CHOH$ in aqueous solution at room temperature [7].

It was supposed that $K_f$ could vary from $10^2$ to $10^7$ $sec^{-1}$. As we shall see, the calculation becomes much simpler for $K_f \geq 10^8$ $sec^{-1}$. In such a case, the bimolecular loss of free radicals may be neglected. The lower limit of $K_f = 10^2$ $sec^{-1}$ in the case of the reaction of R with A, added to the medium to the extent of some 10% (R + A → product + R'), corresponds to the rate constant $K = 3.3 \cdot 10^{-20}$ $cm^3/sec$ (activation energy $E \sim 14$ kcal/mole)[1] of this reaction for liquid and $K = 3.7 \cdot 10^{-17}$ $cm^3/sec$ ($E \sim 10$ kcal/mole)[1] for gas. For the given limitations to the values of $\Phi$, q, $t_1$, and $K_b$, the effect of first order free radical loss reactions for $K_f < 10^2$ $sec^{-1}$ may be neglected.

The calculation was carried out by the method developed for analyzing results obtained in photochemistry by means of the rotating sector [8]. The formula derived by Shepp takes the following form:

$$[R]_{st} = \frac{M_e}{q}\left[1 + \frac{1}{\beta}\ln\frac{\left(\frac{M_2}{M_e}+\alpha+1\right)\left(\frac{M_1}{M_e}+\alpha\right)}{\left(\frac{M_1}{M_e}+\alpha+1\right)\left(\frac{M_2}{M_e}+\alpha\right)}\right],$$

where $M_e$ is the stationary concentration of radicals which would be established on neglecting the effects of the electron beam with the given pulse power,

$$\alpha = \frac{K_f}{2K_bM_e},\quad \beta = 2K_bM_et_1,$$

where $M_1$ and $M_2$ are the stationary concentrations of the radicals established at the moment when the action of the pulse ceases and at the moment of switching on, respectively. The scheme shown in Fig. 1 explains the significance of these quantities. For the case in which m = 2 in the kinetic scheme, $M_e$ is calculated from the formula

$$M_e = \frac{K_f}{4K_b}\left(\sqrt{1+\frac{16K_bF}{K_f^2}}-1\right).$$

In this formula F is the rate of generating free radicals during the action of the pulse. Since the variation of $[R]_{st}$ with q was calculated for constant mean generation rate R, i.e., for constant mean electron beam power, it was assumed that $F = \Phi q$. The formulas for calculating $M_1$ and $M_2$ have the form

$$\frac{M_1}{M_e} = -\frac{B}{2A} + [(B^2 - 4AC)/4A^2]^{1/2},$$

$$\frac{M_2}{M_e} = \left(c + b\frac{M_e}{M_1}\right)^{-1},$$

where

$$a = \exp(2+\alpha)\beta,\quad b = \exp[(q-1)\alpha\beta],$$

$$c = \frac{(b-1)}{\alpha},$$

$$A = (a-1) + c[a(1+\alpha)+1],$$

$$B = b[a(1+\alpha)+1] - c(1+\alpha)(a-1) - (a+1+\alpha),$$

$$C = -b(1+\alpha)(a-1).$$

[1] For steric factor equal to unity.

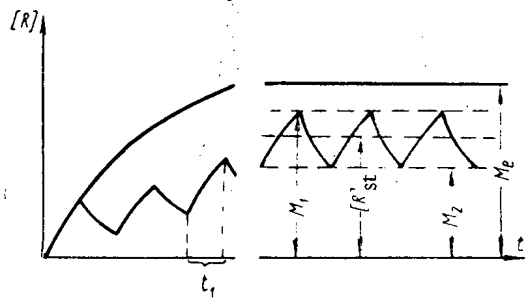


Fig. 1. Graph showing the significance of the quantities $[R]_{st}$, $M_e$, $M_1$, and $M_2$.

The various formulas given here are only valid for stationary conditions, i.e., for the case in which $[R]_{st}$, $M_1$, and $M_2$ are independent of time. The calculation relates only to fairly large times $t_1$ after switching on the electron beam (see Fig. 1).

We note that in this calculation the expediture of K and $A_1$ molecules is not taken into account.

The quantities $[R]_{st}$ were calculated from the above formulas on an electronic computer for the following values of the parameters characterizing the electron beams and free radical reactions:

$$q = 10;\ 10^2;\ 3\cdot10^2;\ 7\cdot10^2;\ 10^3;\ 3\cdot10^3;\ 7\cdot10^3;\ 10^4;\ 2\cdot10^4;$$
$$t_1 = 10^{-6};\ 10^{-5};\ 10^{-4}\ \text{sec};$$
$$K_b = 10^{-12};\ 10^{-10}\ \text{cm}^3/\text{sec};$$
$$K_f = 10^2;\ 10^3;\ 10^4;\ 10^5;\ 10^6;\ 10^7\ \text{sec}^{-1}$$
$$\Phi = 10^{21};\ 10^{19};\ 10^{17};\ 10^{15}\ \text{radical/cm}^3\cdot\text{sec}.$$

The results of the calculation are shown in Fig. 2 in the form of curves connecting $\log[R]_{st}$ with $\log q$. The various graphs relate to various values of $K_f$ the quantity $[R]_{st}$ practically ceases to depend on q. Let us find the values of $K_f$ for which this occurs. For this purpose we evaluate the term

$$1+\frac{1}{\beta}\ln\frac{(M_2/M_e+\alpha+1)(M_1/M_e+\alpha)}{(M_1/M_e+\alpha+1)(M_2/M_e+\alpha)},$$

which comes into the equation for $[R]_{st}$. The second term in this expression is

$$\frac{1}{\beta}\ln\frac{1+\dfrac{1}{M_2/M_e+\alpha}}{1+\dfrac{1}{M_1/M_e+\alpha}}=\frac{1}{\beta}\ln\frac{1+x}{1+y},$$

where

$$x=\frac{1}{M_2/M_e+\alpha},\quad y=\frac{1}{M_1/M_e+\alpha}.$$
$$\frac{1}{\beta}\ln\frac{1+x}{1+y}=\frac{1}{\beta}\ln\left(1+\frac{x-y}{1+y}\right)<\frac{1}{\beta}\cdot\frac{x-y}{1+y},$$

since we always have $\ln(1+n) < n$. Further

$$\frac{1}{\beta}\cdot\frac{x-y}{1+y}=\frac{1}{\beta}\,\frac{M_1-M_2}{M_e\left(\alpha+\dfrac{M_2}{M_e}\right)\left(\alpha+\dfrac{M_1}{M_e}\right)\left(1+\dfrac{1}{\alpha+M_1/M_e}\right)}$$

$$<\frac{M_1}{\beta M_e\alpha^2}=\frac{2K_bM_1}{K_b^2t_1}<\frac{2K_bM_e}{K_f^2t_1}=\frac{1}{2K_ft_1}\left(\sqrt{1+\frac{16K_b\Phi q}{K_f^2}}-1\right).$$

This correction may be neglected if its value is less, for example, than 0.05. Then the expression for $[R]_{st}$ reduces to the formula

$$[R]_{st}=\frac{M_e}{q}.$$

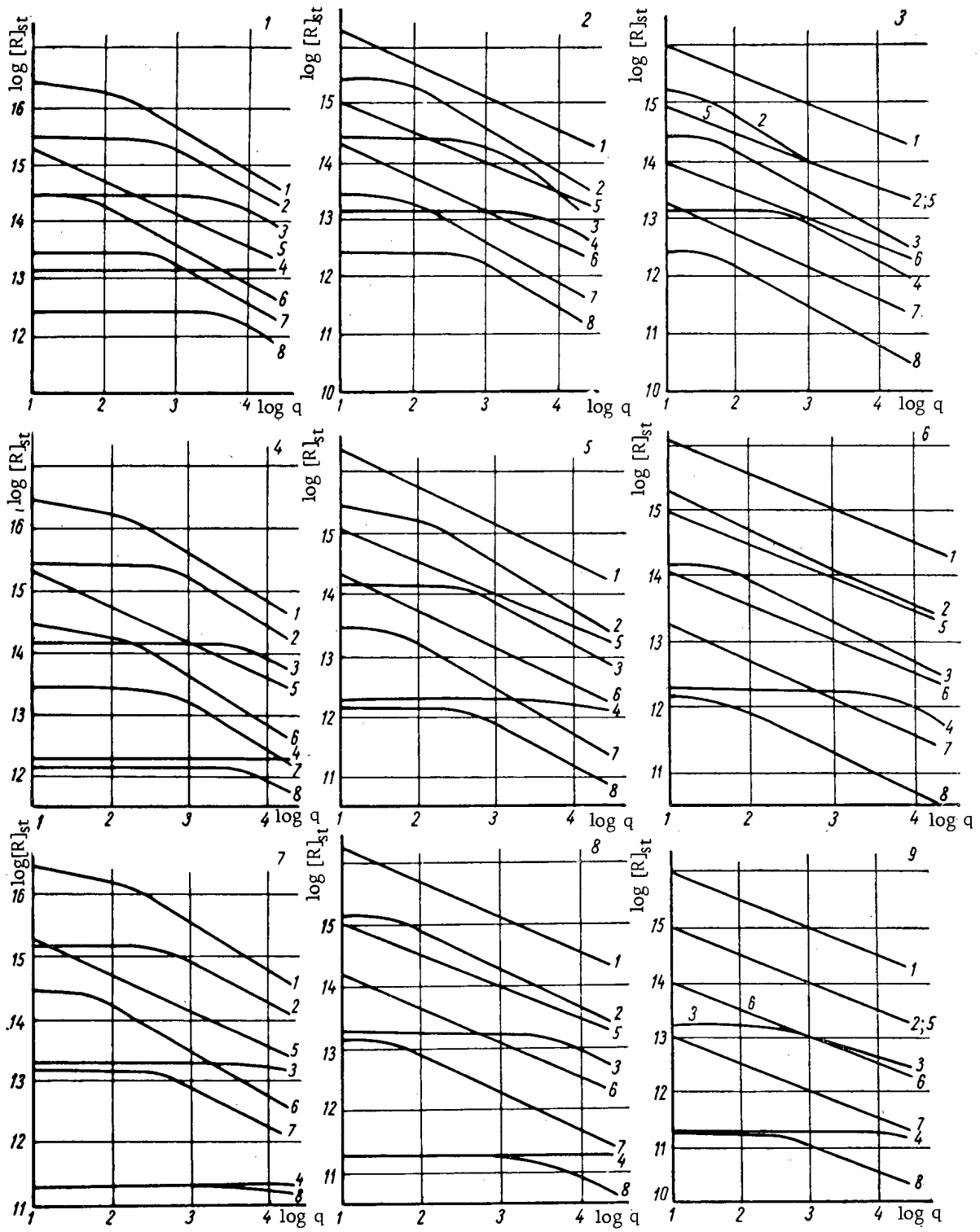


Fig. 2. Relation between $\log [R]_{st}$ and $\log q$. The various graphs correspond to various $K_f$: 1-3) $10^2$ sec$^{-1}$; 4-6) $10^3$ sec$^{-1}$; 7-9) $10^4$ sec$^{-1}$; 10-12) $10^5$ sec$^{-1}$; 13-15) $10^6$ sec$^{-1}$; 16-18) $10^7$ sec$^{-1}$. Graphs 1, 4, 7, 10, 13, 16 correspond to $t_1 = 10^{-6}$ sec; 2, 5, 8, 11, 14, 17 to $t_1 = 10^{-5}$ sec; 3, 6, 9, 12, 18 to $t_1 = 10^{-4}$ sec. In each figure, curves 1-8 correspond to the following values of $\Phi$ (radical/cm$^3$ · sec) and $K_b$ (cm$^3$/sec): 1) $\Phi = 10^{21}$, $K_b = 10^{-12}$; 2) $\Phi = 10^{19}$, $K_b = 10^{-12}$; 3) $\Phi = 10^{17}$, $K_b = 10^{-12}$; 4) $\Phi = 10^{15}$, $K_b = 10^{-12}$; 5) $\Phi = 10^{21}$, $K_b = 10^{-10}$; 6) $\Phi = 10^{19}$, $K_b = 10^{-10}$; 7) $\Phi = 10^{17}$, $K_b = 10^{-10}$; 8) $\Phi = 10^{15}$, $K_b = 10^{-10}$.

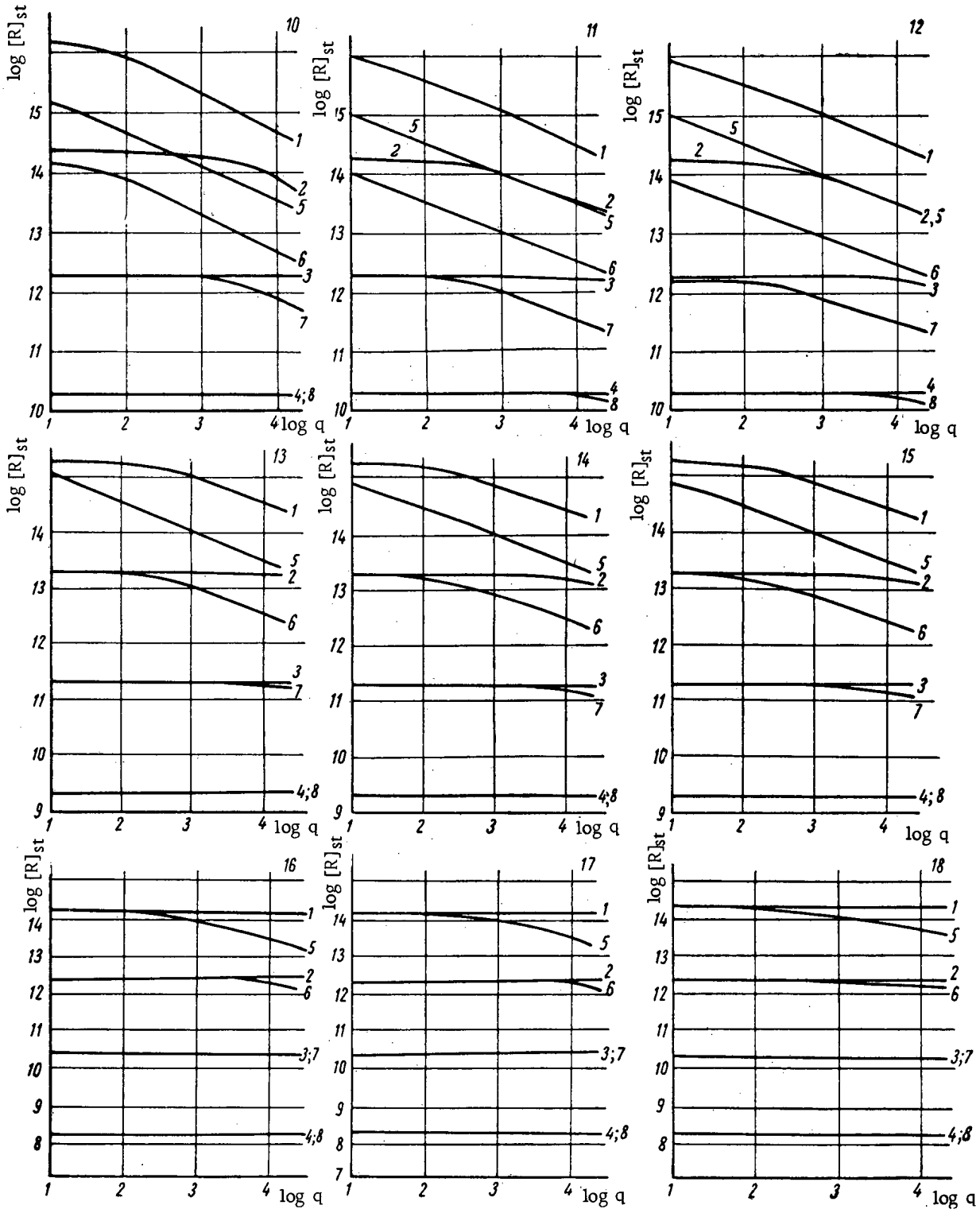


Fig. 2 (continued)

Let us substitute into the expression to be evaluated the maximum values of $K_b$, $\Phi$, and q, and the minimum value of $t_1$:

$$K_b = 10^{-10} \text{ cm}^3/\text{sec};$$
$$\Phi = 10^{21} \text{ radical/cm}^3 \cdot \text{sec};$$
$$q = 2 \cdot 10^4;$$
$$t_1 = 10^{-6} \text{ sec}.$$

Then we obtain

$$\frac{1}{2K_f \cdot 10^{-6}} \left( \sqrt{1 + \frac{16 \cdot 10^{-10} \cdot 10^{21} \cdot 2 \cdot 10^4}{K_f^2}} - 1 \right) < 0.05,$$

whence $K_f^3 (2 \cdot 10^{-7} + 10^{-14} K_f) > 32 \cdot 10^{15}$.

We can see that this condition is fulfilled for $K_f \geq 10^8 \text{sec}^{-1}$.

For fairly large $K_f$, for which the formula

$$[R]_{st} = \frac{M_e}{q},$$

is valid, we may write for $M_e$:

$$M_e = \frac{2\Phi q}{K_f},$$

or

$$[R]_{st} = \frac{2\Phi}{K_f}.$$

We shall now show that for $K_f < 10^2 \text{sec}^{-1}$, the part played by the first order R loss reactions in determining the value of $[R]_{st}$, may be neglected for the limits assigned to the $\Phi$, q, $t_1$, and $K_b$. Actually, the quantity $\alpha = K_f/2K_bM_e$ constitutes a lower limit for the ratio of the first and second order R loss rates (in precise calculations we should substitute some effective quantity $[R] < M_e$ for $M_e$). We shall assume that the contribution of monomolecular reactions to $[R]_{st}$ for $\alpha < 1$ may be neglected:

$$\alpha = \frac{2}{\sqrt{1 + \frac{16 K_b \Phi q}{K_f^2}} - 1} < 1,$$

i.e.,

$$K_f < \sqrt{2 K_b \Phi q}.$$

For the smallest values: $K_b = 10^{-12}$ cm$^3$/sec, $\Phi = 10^{15}$ radical/cm$^3 \cdot$ sec. q = 10, and

$$K_f < \sqrt{2 \cdot 10^{-12} \cdot 10^{15} \cdot 10} = 141 \text{ sec}^{-1}$$

Thus for $K_f < 140 \text{ sec}^{-1}$ and the above mentioned limits of $\Phi$, q, $t_1$, and $K_b$, the contribution of the first order free radical loss reactions may be neglected.

It follows from the data obtained that, for typical accelerators with maximum mean power 5 kW and duty factor q = 100, when the radiation yield of free radicals for material in the condensed phase is G = 5-10 molecules per 100 eV absorbed energy ($\Phi \approx 10^{21}$ radical/cm$^3 \cdot$ sec$^1$), the quantity $[R]_{st}$ differs little from the stationary concentration of radicals during continuous radiolysis for $K_f \geq 10^5 \text{sec}^{-1}$ and $K_b = 10^{-10}$-$10^{-12}$ cm$^3$/sec if $t_1 = 10^{-6}$-$10^{-4}$ sec. For $K_f < 10^5 \text{sec}^{-1}$, the difference becomes perceptible. A reduction in the mean generation rate of radicals reduces

this difference. In the gas phase (for given parameters $\Phi = 10^{18}$ radical/cm$^3$·sec), the difference between the stationary radical concentrations for $t_1 = 10^{-6}$ sec in the cases of continuous and pulsed irradiation is small over the whole range of $K_b$ and $K_f$ variation. For $t_1 = 10^{-5}$ or $10^{-4}$ sec, however, this difference is appreciable. For large q (over 100), pulse radiolysis may exert a considerable influence on the direction and yield of the radiochemical reactions in the gas as well as the condensed phase. If, on passing from continuous to pulse irradiation, the changes taking place in the product yield are undesirable (in obtaining a product of a radical reaction described by the first order kinetic law), an accelerator with a lower q value should be used. If, on the other hand, it is required to obtain a product of a recombination reaction or the disproportionization of free radicals (reaction between the radicals described by the second order kinetic law), then it is more appropriate to work with an accelerator of high q, while maintaining its mean power.

The graphs presented may also be of value from the point of view of an experimental determination of free radical reaction rate constants. For example, by varying $\Phi$, q, and $t_1$, and measuring $[R]_{st}$ by some method (for example, from the sum of the yields of products formed in a first order reaction of the free radical), we may determine $K_f$ if $K_b$ is known, or the ratio of these constants if neither is known, just as one does in photochemistry using a rotating sector.

The calculation presented is based on the assumption that the radicals formed by the radiation are uniformly distributed over the volume. In this, we neglect the fact that under the influence of radiation the radicals form groups or concentrations; for a rigorous consideration, the diffusion-kinetic equations should be solved. This approximation is justified for all cases of radiolysis in the gas phase and for radiolysis in the condensed phase for radicals having a fairly large diffusion coefficient (possibly also for hydrogen atoms in aqueous solutions at room temperature). In other cases, supplementary investigations are required in order to elucidate the validity of the above mentioned approximation.

## Conclusions

1. On the basis of a typical mechanism of the chemical reactions of free radicals formed by the action of a high energy pulsed electron beam, the mean stationary concentration $[R]_{st}$ of the free radicals has been calculated as a function of the duty factor q of the electron current pulses for various powers, corresponding to various free radical formation rates $\Phi$, various current pulse widths $t_1$, and various free radical loss constants for the first ($K_f$) and second ($K_b$) orders.

2. It has been established that the value of $[R]_{st}$ is highly dependent on q, especially at large q. This fact should be taken into consideration when constructing electron accelerators destined for the creation of radiochemical reactions. Graphs relating $[R]_{st}$ to q have been presented.

3. It has been shown that for specified limiting values of $\Phi$, q, $t_1$, and $K_b$, the first order free radical loss may be neglected for $K_f < 10^2$ sec$^{-1}$.

4. It has been found that for $K_f \geq 10^8$ sec$^{-1}$ the value of $[R]_{st}$ is independent of q.

The authors express their gratitude to A. M. Kogan and colleagues in the Mathematical Branch of the Institute of Chemical Physics, Academy of Sciences of the USSR for help given during this investigation.

## LITERATURE CITED

1. R. Mc Carthy and A. Mc Lachlan, Trans. Faraday Soc., 56, 1187 (1960).
2. The Photochemistry of Gases, Ed. W. A. Noyes, Jr. and P. A. Leighton, Reinhold Publ. Corp., New York (1941), p. 202.
3. P. Harteck and S. Dondes, J. Phys. Chem., 63, 956 (1959).
4. A. Charlesby, Nuclear Radiations and Polymers [Russian translation], Moscow, IL (1962), p. 252.
5. A. Charlesby, ibid, p. 41.
6. G. Kistiakowsky and E. Roberts, J. Chem. Phys., 21, 1637 (1953).
7. I. Taub and L. Dorfman, J. Amer. Chem. Soc., 84, 4053 (1962).
8. A. Shepp, J. Chem. Phys., 24, 939 (1956).

# PRODUCING HIGH-PURITY TANTALUM

(UDC 669.294)

O. P. Kolchin and I. K. Berlin

Translated from Atomnaya Énergiya, Vol. 17, No. 5,
pp. 400-405, November, 1964
Original article submitted December 2, 1963

Results of a study of the conditions for refining tantalum during production by the carbothermal method are presented. The behavior of a large number of impurities during the reduction is examined. Investigations showed that the carbothermal method of reducing tantalum with subsequent sintering is one of the most efficient means of producing high-purity tantalum, both in the form of compact metal, suitable for pressure treatment, and in the form of powder.

In recent years, considerable attention has been focused on the carbothermal method of reducing tantalum from the pentoxide by the reaction $n\,Ta_2O_5 + 5\,TaC_n = (5+2n)\,Ta + 5n\,CO$ with subsequent sintering of the metal. This method is used in particular by the "Wa Chang" organization, the largest supplier of tantalum in the United States [1].

One of the important advantages of the process in question is the possibility of producing high-purity tantalum by simultaneous vacuum refining. The efficient refining of tantalum is facilitated by its high melting point, low vapor pressure, the considerable and indeed open porosity of the carbothermal metal, and the presence of oxygen in the original charge.

A most important condition for good purification from foreign matter on high-temperature heating in vacuo is the large difference in vapor pressure between the tantalum and the impurities. It follows from Table 1 that all metals except columbium have considerably higher vapor pressures than tantalum, and that their evaporation rate should thus be considerably higher. Cadmium, lead, and antimony should volatilize rapidly, manganese and copper more slowly, and iron and titanium slower still.

The partial vapor pressure of an impurity element falls and the conditions for purifying the tantalum become more complex when the impurity forms a solid solution with the tantalum. The majority of impurities present in small quantities are apparently in solid solution, besides certain impurities present in large quantities (for example, columbium and β titanium, which form a continuous series of solid solutions with tantalum). Hence, although the vapor pressure of columbium, for example, is two orders lower than that of tantalum, when columbium occurs in solid solution to less than 1%, its vapor pressure will be roughly the same as that of the tantalum and refining will not take place.

Some impurity elements form intermetallic compounds with tantalum. For example, tin forms the intermetallic compounds $Ta_3Sn$ at 1200-1550°C (there is no published information on the degree of stability of this at high temperatures), while silicon forms $TaSi_2$, $Ta_5Si_3$, and $Ta_4Si$. When oxygen is present in the system, as usually happens in the first stages of production by the carbothermal method, purification from a number of impurities is improved. Since the vapor pressure of many oxides is greater than that of the metals, some of the impurities pass off in the form of oxides. Thus, the reduction of silicon dioxide, which contaminates tantalum pentoxide, takes place by way of the formation of silicon monoxide, which has a high-vapor pressure at the reduction and sintering temperatures of tantalum. The same applies to tin, since the vapor pressure of the monoxide even at 100°C equal 1 atm. A certain amount of the iron and titanium present also passes off in the form of lower oxides.

When there is a light excess of oxygen in the original charge, the oxygen taking part in the reaction passes off by way of the evaporation (or possibly dissociation) of tantalum oxide; this favorably contrasts tantalum with

TABLE 1. Vapor Pressure of Pure Substances [2] in mm Hg

| °K | Cd | Pb | Sb | Mn | Cu | Sn | Si | Fe | Ti | Nb | Ta |
|---|---|---|---|---|---|---|---|---|---|---|---|
| 800 | 22,0 | $4,07 \cdot 10^{-5}$ | $4,31 \cdot 10^{-8}$ | $3,59 \cdot 10^{-9}$ | — | — | — | — | — | — | — |
| 1000 | 466 | $1,11 \cdot 10^{-2}$ | $8,02 \cdot 10^{-5}$ | $1,53 \cdot 10^{-5}$ | $1,63 \cdot 10^{-8}$ | $5,10 \cdot 10^{-8}$ | $4,22 \cdot 10^{-10}$ | — | — | — | — |
| 1200 | — | $4,47 \cdot 10^{-1}$ | $9,30 \cdot 10^{-3}$ | $3,61 \cdot 10^{-3}$ | $8,15 \cdot 10^{-6}$ | $1,95 \cdot 10^{-5}$ | $8,59 \cdot 10^{-7}$ | $1,11 \cdot 10^{-7}$ | — | — | — |
| 1400 | — | 6,18 | $2,68 \cdot 10^{-1}$ | $1,69 \cdot 10^{-1}$ | $9,11 \cdot 10^{-4}$ | $1,33 \cdot 10^{-3}$ | $1,95 \cdot 10^{-4}$ | $2,95 \cdot 10^{-5}$ | $5,90 \cdot 10^{-8}$ | — | — |
| 1600 | — | 43,5 | 3,38 | 2,45 | $2,73 \cdot 10^{-2}$ | $3,11 \cdot 10^{-2}$ | $9,16 \cdot 10^{-3}$ | $1,87 \cdot 10^{-3}$ | $8,23 \cdot 10^{-6}$ | — | — |
| 1800 | — | 196 | 22,6 | 18,4 | $3,77 \cdot 10^{-1}$ | $3,65 \cdot 10^{-1}$ | $2,08 \cdot 10^{-1}$ | $4,60 \cdot 10^{-2}$ | $3,74 \cdot 10^{-4}$ | — | — |
| 2000 | — | 648 | — | 88,6 | 3,10 | 2,59 | 1,87 | $5,28 \cdot 10^{-1}$ | $7,68 \cdot 10^{-3}$ | $8,34 \cdot 10^{-9}$ | $7,02 \cdot 10^{-11}$ |
| 2200 | — | — | — | 307 | 16,9 | 13,0 | 11,1 | 3,39 | $8,41 \cdot 10^{-2}$ | $4,25 \cdot 10^{-7}$ | $5,00 \cdot 10^{-9}$ |
| 2400 | — | — | — | 771 | 68,6 | 49,5 | 48,8 | 19,0 | $5,63 \cdot 10^{-1}$ | $1,10 \cdot 10^{-5}$ | $1,76 \cdot 10^{-7}$ |
| 2600 | — | — | — | — | 224 | 153 | 171 | 73,7 | 3,06 | $1,74 \cdot 10^{-4}$ | $3,60 \cdot 10^{-6}$ |
| 2800 | — | — | — | — | 614 | 402 | 496 | 241 | 12,9 | $1,80 \cdot 10^{-3}$ | $4,80 \cdot 10^{-5}$ |
| 3000 | — | — | — | — | — | — | — | 523 | 47,3 | $1,30 \cdot 10^{-2}$ | $4,53 \cdot 10^{-4}$ |

such metals as titanium and zirconium, the oxides of which hardly evaporate at all, not only at the temperature of producing these metals but also on arc remelting, i.e., no purification from small quantities of oxygen takes place in vacuo.

Tantalum nitride (TaN) dissociates comparatively easily: the dissociation pressure reaches $10^{-2}$ mm Hg at 1600°C and 1 mm Hg at 1921°C. Hence, difficulties can only arise in removing nitrogen dissolved in the metal.

Considerable difficulties may be expected in purifying tantalum from carbon, since the carbides TaC and $Ta_2C$ are still more refractory than the metal itself; they are not at all volatile and dissociate poorly. The most efficient way of producing the metal with low carbon content is to set up the original mixture with a slight excess of tantalum pentoxide as compared with the stoichiometric quantity, and to use tantalum carbide powder of a definite degree of coarseness [3].

On the basis of what has been said, we carried out investigations confirming the possibility of refining the metal intensively and producing tantalum of high purity. The method of producing tantalum by the means discussed was described earlier [3, 4]. The final operation in this scheme is the sintering of tantalum moldings in a vacuum of $5 \cdot 10^{-3}$ to $5 \cdot 10^{-4}$ mm Hg at a temperature of the order of 2700-2750°C (the brightness temperature in the sintering furnace used was 2450°C), which is 200-240°C below the melting point of the moldings. The greatest purification depends primarily on the duration of holding at the maximum sintering temperature.

Table 2 shows data on the refining of the metal as a function of the duration of sintering at 2700-2750°C. Considering that tantalum absorbs nitrogen and oxygen at temperatures up to 1800-2000°C, and also bearing in mind experience in the sintering of columbium [5], the usual slow heating program with intermediate holding was not used, the moldings being raised to 1800°C in 10 min, the temperature then being raised at a rate of 100°C per 15 min with two-hour holdings at 2400 and 2700-2750°C. We see from Table 2 that holding for 1 h at 2700-2750°C is already sufficient to reduce iron and silicon to concentrations of <0.003%Si and <0.002%Fe, despite the fact that the original tantalum pentoxide contained 0.4%Si and 0.05%Fe. The titanium content fell from 0.39% in the tantalum pentoxide to 0.008% in the metal.

After sintering for 2 h, no sulfur could be found in the metal, while titanium vanished after 3 h. Carbon and oxygen impurities remained in thousandth parts of a percent, their concentration being practically independent of the duration of sintering. More complete removal of these impurities could be achieved, clearly, by sintering in a higher vacuum.

The porosity of the metal for a 1-h sinter is 23-33%, while for a 4-8-h sinter it falls to 5 or 6%; the porosity is to a large extent open, the open component being 22.6 and 24.8%, respectively, for two moldings with total

TABLE 2. Refining of Carbothermal Tantalum as a Result of Sintering in Vacuo at Temperature 2700-2750°C

| Duration of sintering, h | Total porosity after sintering, % | Content, wt.% | | | | | | | | Content after forging and annealing at 2400°C, wt.% | |
|---|---|---|---|---|---|---|---|---|---|---|---|
| | | C | O | H | Ti | Fe | Si | S | C | O |
| 1 | 22,9 | 0,010 | 0,005 | — | 0,008 | Not observed | Not observed | 0,002 | — | — |
| 1 | 33,1 | 0,007 | 0,005 | — | — | The same | The same | — | — | — |
| 2 | 15,7 | 0,008 | 0,001 | $4,6 \cdot 10^{-3}$ | 0,006 | » » | » » | Not observed | 0,006 | 0,006 |
| 3 | 10,2 | 0,007 | — | — | Not observed | » » | » » | The same | — | — |
| 4 | 6,3 | 0,005 | 0,001 | — | The same | » » | » » | » » | — | — |
| 5 | — | 0,005 | 0,002 | $1,7 \cdot 10^{-4}$ | » » | » » | » » | » » | — | — |
| 8 | 4,8 | 0,007 | — | — | » » | » » | » » | » » | 0,005 | 0,0015 |
| 8 | 4,8 | — | — | — | » » | » » | » » | » » | — | — |
| 12 | 6,6 | 0,008 | — | — | » » | » » | » » | » » | 0,004 | 0,007 |
| 16 | 9,1 | 0,005 | — | — | » » | » » | » » | » » | 0,007 | 0,013 |

Note. The tantalum pentoxide from which the tantalum was reduced contained 0.4%Si, 0.05%Fe, 0.39%Ti, 0.005%S. The cross section of the original extruded moldings was 10 x 10 mm. The sintering took place in vacuo ($5 \cdot 10^{-3}$ to $5 \cdot 10^{-4}$ mm Hg). The analytical sensitivity was 0.005% for Ti, 0.002% for Fe, 0.003% for Si, and 0.002% for S.

TABLE 3. Purification of Tantalum from Other Elements

| Element | Content, wt.% | | |
|---|---|---|---|
| | In the tantalum pentoxide | In the tantalum carbide | In the metal |
| Ti | 1,07 | 0,67 | 0,07 |
| Mn | 0,10 | 0,003 | Not observed* |
| Fe | 0,25 | 0,05 | » » |
| Sn | >1 | — | » » |
| Si | 0,16 | 0,05 | » » |
| Al | 0,40 | 0,10 | » » |

* Limits of analytical sensitivity given in Table 4.

porosities of 23.5 and 25.8%. The results of the experiments make it possible to limit the duration of sintering for 10 x 10 mm tantalum moldings at 2700-2750°C to 2-3 h. The pure plastic metal sintered in these conditions, after forging to a 50-60%-thickness reduction and brief annealing (second sintering) at 2450°C, easily lends itself to cold pressure treatment for producing strip, foils, etc.

Since tantalum-bearing raw material usually contains manganese, iron, tin, titanium, silicon, and sometimes aluminum as well, we investigated the possibility of purifying tantalum from these elements all at once. To this end, tantalum pentoxide was dissolved in hydrofluoric acid, and the impurities in question were introduced into the resultant solution in the form of solutions of $MnSO_4$, $FeCl_3$, $Al(NO_3)_3$, $SnCl_2$, $H_2TiF_6$, and $H_2SiF_6$. Then ammonia water was used to precipitate tantalum hydroxide from the solution so obtained, and this was converted into the pentoxide by drying and baking at 900°C in air for 6 h. From the artificially contaminated tantalum pentoxide, we obtained the carbide and then the metal (sintering 2 h at 2700-2750°C), the purity of which may be judged from the data of Table 3.

Only titanium was observed in the sintered metal (0.07%), and the tantalum may be further purified from this by longer sintering at 2700-2750°C.

In order to examine the behavior of other impurities, the presence of which could prove undesirable when using tantalum in various fields of technology, phosphorus (in the form of $H_3PO_4$ solution), copper (in the form of $Cu(NO_3)_2$, and a radioisotope of zinc (in the form of $ZnCl_2$) were introduced into a solution of tantalum pentachloride in hydrochloric acid. Hydrolysis was effected by dilution of the solution and boiling with added sulfuric acid. The tantalum hydroxide was baked to the pentoxide as in the preceding case. The impurity contents in the pentoxide and the metal derived from it are shown in Table 4. In the tantalum carbide there remained 0.02%S, 0.83%P, $10^{-4}$%Zn, and $<10^{-3}$%Cu.

To a hydrofluoric acid solution of tantalum contaminated with tin and lead, we also added hydrochloric acid solutions of antimony, bismuth, and cadmium, afterwards precipitating tantalum hydroxide by ammonia water and obtaining the pentoxide and the metal. These impurities could not be found either in the tantalum carbide or the sintered metal (see Table 4).

Generalized data on the quality of the tantalum obtained in the present investigation are shown in Table 4. For comparison, the same table presents characteristics of the quality of two batches of electron beam meltedingots of tantalum obtained by different means, and also of metallic tantalum powder. This powder, produced in industrial

TABLE 4. Quality of Tantalum Obtainable by the Carbothermal Method with Subsequent Vacuum Sintering (Molding Section 10 × 10 mm)

| Element | Sensitivity of analysis, % | Amt. introduced into the tantalum pentoxide, % | Amt. contained in compact sintered metal, % | Amt. contained in electron beam melted ingots [1] | | Amt. contained in powder of carbothermal metal, % [1] |
|---|---|---|---|---|---|---|
| | | | | batch 1 | batch 2 | |
| Ta+(Nb)* | — | — | 99,98—99,99 | — | — | — |
| Ti | $5 \cdot 10^{-3}$ | 0,39 | Not observed | $< 1 \cdot 10^{-3}$ | — | 0,015 |
| Fe | $2 \cdot 10^{-3}$ | 0,25 | The same | $< 1 \cdot 10^{-3}$ | $8 \cdot 10^{-4}$ | 0,01 |
| Si | $3 \cdot 10^{-3}$ | 0,62 | » » | $2{,}8 \cdot 10^{-3}$ | — | $5 \cdot 10^{-3}$ |
| Mn | $10^{-3}$ | 0,10 | » » | — | — | $2 \cdot 10^{-3}$ |
| Al | $10^{-2}$ | 0,40 | » » | $< 5 \cdot 10^{-3}$ | — | $2 \cdot 10^{-3}$ |
| Sn | $10^{-4}$ | > 1 | » » | — | — | $2 \cdot 10^{-3}$ |
| Cu | $10^{-3}$ | 0,09 | » » | $< 5 \cdot 10^{-3}$ | $3 \cdot 10^{-3}$ | $4 \cdot 10^{-3}$ |
| Zn | $3 \cdot 10^{-6}$ | 0,07 | » » | — | — | $2 \cdot 10^{-3}$ |
| As | $10^{-3}$ | — | » » | — | — | — |
| Cr | $10^{-3}$ | — | » » | — | — | $3 \cdot 10^{-3}$ |
| Mg | $10^{-3}$ | — | » » | — | — | $2 \cdot 10^{-3}$ |
| Ca | $10^{-3}$ | — | » » | — | — | — |
| Pb | $10^{-4}$ | 0,05 | » » | — | — | $2 \cdot 10^{-3}$ |
| Sb | $10^{-4}$ | > 0,1 | » » | — | — | — |
| Bi | $10^{-4}$ | > 0,1 | » » | — | — | — |
| Cd | $10^{-4}$ | 0,03 | » » | — | — | — |
| S | $2 \cdot 10^{-3}$ | 0,8 | » » | — | — | — |
| P | $2 \cdot 10^{-3}$ | 3 | » » | — | — | — |
| H | — | — | $4{,}6 \cdot 10^{-5}$ | $< 1 \cdot 10^{-4}$ | $1{,}4 \cdot 10^{-4}$ | 0,01 |
| O | — | — | $(1—5) \cdot 10^{-3}$ | $< 6 \cdot 10^{-4}$ | $1{,}6 \cdot 10^{-3}$ | |
| C | — | — | $(3—8) \cdot 10^{-3}$ | $2 \cdot 10^{-3}$ | $3 \cdot 10^{-3}$ | |
| N | — | — | $(6—11) \cdot 10^{-3}$ | $1 \cdot 10^{-3}$ | $1 \cdot 10^{-3}$ | |
| B | — | — | — | — | — | $1 \cdot 10^{-4}$ |
| Mo | — | — | — | $< 2{,}5 \cdot 10^{-3}$ | — | $2 \cdot 10^{-3}$ |
| Ni | — | — | — | $< 1 \cdot 10^{-3}$ | $3 \cdot 10^{-4}$ | $2 \cdot 10^{-3}$ |
| V | — | — | — | — | — | $2 \cdot 10^{-3}$ |
| W | — | — | — | — | — | 0,01 |
| Zr | — | — | — | — | — | 0,01 |

*Calculated from the difference between 100% and the total amount of impurities determined. The tantalum loses hardly any columbian impurity during sintering, the amount of columbium in the metal being governed by the amount in the original tantalum pentoxide.

quantities in the United States, is obtained by carbothermal reduction in vacuum induction furnaces at a temperature of approximately 2000°C from a mixture of tantalum carbide and tantalum pentoxide, with subsequent hydrogenation of the porous metal formed, crushing to the required size of powder, and dehydrogenation in vacuo [1]. Naturally, sintering at a temperature of 2700-2750°C enables us to obtain purer metal than does reduction at 2000°C, since in the first case metallic impurities are absent and the oxygen and carbon content is small. As a result the tantalum content (with traces of columbium) is 99.98-99.99%, i.e., metal of high purity is obtained. In order to produce this purity of tantalum, it is not obligatory to use highly pure tantalum pentoxide as raw material, since it follows from Table 4 that in the processes of carbide formation, reduction, and sintering intensive purification of the metal takes place. Certainly, this does not mean that we can obtain as pure tantalum from severely contaminated tantalum pentoxide (containing, for example, all the impurities of Table 4 in the quantities listed simultaneously) as from a more pure variety of tantalum pentoxide under the same technological conditions. It is more appropriate to use tantalum pentoxide of increased purity, since this avoids contaminating the vacuum furnaces with large quantities of evaporating impurities and disrupting the normal flow of the carbide formation, reduction, and sintering processes by the formation of low melting phases, and also offers the possibility of shortening the refining period.

From the results of the present investigation, and from published data, we may conclude that the carbothermal method of reducing tantalum, with subsequent sintering of the directly reduced metal, or with intermediate hydrogenation, crushing, dehydrogenation, and extrusion of moldings, constitutes one of the most efficient means of producing high-purity tantalum, both in the form of compact metal suitable for the preparation of plate, foil, and other articles by pressure treatment, and also in the form of powder (of "dehydrogenated" metal).

## LITERATURE CITED

1. C.L. Hampel, Rare Metals Handbook, London, Chapman Hall Ltd (1961).
2. A. N. Nesmeyanov, Vapor Pressure of Chemical Elements [in Russian], Moscow, Izd. AN SSSR (1961).
3. O. P. Kolchin, N. V. Sumarokova, and I. K. Berlin, Collection of the Scientific Transactions of Giredmet [in Russian], 1 (1959), p. 712.
4. O. P. Kolchin and N. P. Chuveleva, Tsvetnye metally, No. 2, 60 (1959).
5. O. P. Kolchin and N. P. Chuveleva, Tsvetnye metally, No. 12, 65 (1957).

# THERMODYNAMIC CALCULATION OF THE REACTION BETWEEN SODIUM AND WATER FOR A SODIUM–WATER TYPE STEAM HEATER

N. N. Ivanovskii and F. A. Kozlov

Translated from Atomnaya Énergiya, Vol. 17, No. 5,
pp. 406-408, November, 1964
Original article submitted November 20, 1963

In using large sodium–water steam generators, it is a good idea to use a single wall to transmit the heat, since the economics of the steam generator become worse if a double heat generating wall is used, the design becomes more complicated, and, as is shown by experiment, there is a greater probability of its breakdown. However, in a steam generator with a single wall, we again have the danger that water will get into the sodium as a result of leakage. In view of this, a determination of the equilibrium concentrations of chemical reaction products is in order.

From the data published in [1-3], the reaction between sodium and water may be written as

$$Na + H_2O \rightleftarrows NaOH + \frac{1}{2} H_2, \quad (1)$$

$$2Na + NaOH \rightleftarrows Na_2O + NaH, \quad (2)$$

$$NaH \rightleftarrows Na + \frac{1}{2} H_2. \quad (3)$$

The thermodynamic calculation proposed is simply a matter of determining the equilibrium constants of the reactions, and then finding the equibrium concentrations [4]. The calculation is made on the assumption that the amount of water that has got into the system, and the rate of which it gets into the sodium are such that there is no large increase in temperature even at the place where the leak occurs.

The equilibrium constants of the reactions were calculated on the basis of published data (Table 1). The results of the thermodynamic calculation are given in Table 2. The change in the isobaric potential of the reactions as a function of temperature is shown in the figure.

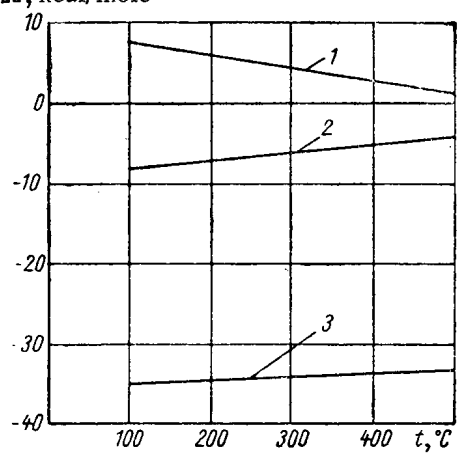


Fig. 1. Change in isobatic potential as a function of temperature of the reactions: 1) $NaH \rightleftarrows Na + {}^{1}{}_{2}H_2$; 2) $2Na + NaOH \rightleftarrows Na_2O + NaH$; 3) $Na + H_2O \rightleftarrows NaOH + {}^{1}/_{2}H_2$.

TABLE 1. Initial Thermodynamic Data

| Material | $\Delta H^{\circ}_{298}$ | $\Delta Z^{\circ}_{298}$ | $C_p = a + bT$ | | Temperature |
|---|---|---|---|---|---|
| | | | $a \times 10^3$ | $b \times 10^6$ | |
| Na (liquid) | 0 | 0 | 8,958 | —4,58 | [2] |
| $H_2O$ (liquid) | —68,32 | —56,69 | 17,996 | 0 | [8] |
| NaOH (crystalline) | —102,3 | —90,6 | 12,23 | 8 | [8] |
| $H_2$ (gas) | 0 | 0 | 6,95 | —0,2 | [8] |
| $Na_2O$ (crystalline) | —99,4 | —90 | 15,7 | 5,4 | [8] |
| NaH (crystalline) | —13,49 | —9 | 8,6 | 0 | [9] |

TABLE 2. Results of the Thermodynamic Calculation

| Reaction | $\Delta H^\circ_{298}$ | $\Delta Z^\circ_{298}$ | $C_p = a + bT$ | | $\Delta H^\circ$ | $I, \times 10^2$ | $\Delta Z^\circ_T$ at temperature, °C | | | | | | $K_{aT}$ at temperature, °C | | | | | |
|---|---|---|---|---|---|---|---|---|---|---|---|---|---|---|---|---|---|---|
| | | | $a \times 10^3$ | $b \times 10^6$ | | | 200 | 300 | 400 | 500 | 200 | 300 | 400 | 500 | 200 | 300 | 400 | 500 |
| $Na + H_2O \rightleftarrows NaOH + \frac{1}{2}H_2$ | —34 | —33,91 | —11,25 | 12,48 | —31,23 | —7,05 | —33,3 | —33,18 | —32,5 | —32,18 | $8,9 \cdot 10^{15}$ | $1,26 \cdot 10^{13}$ | $7,95 \cdot 10^{10}$ | $7,05 \cdot 10^{9}$ | | | | |
| $2Na + NaOH \rightleftarrows Na_2O + NaH$ | —10,59 | —8,4 | —5,85 | 6,56 | —9,14 | —2,96 | —6,98 | —6,12 | —4,89 | —4,3 | $1,7 \cdot 10^{3}$ | $2,14 \cdot 10^{2}$ | 38 | 16,6 | | | | |
| $NaH \rightleftarrows Na + \frac{1}{2}H_2$ | 13,49 | 9 | 3,83 | —4,68 | 12,56 | 0,906 | 6,27 | 4,67 | +2,91 | 1,41 | $1,26 \cdot 10^{-3}$ | $1,66 \cdot 10^{-2}$ | 0,113 | 0,4 | | | | |

The following notation was used in finding the equilibrium concentrations of the products of the chemical reaction between sodium and water.

From Reaction (1). The equilibrium constant is large over the whole range of temperature. As a result, the reaction goes practically to completion. If n moles of water are introduced, we obtain as a result of the reaction

$$n_{NaOH} = A \text{ moles}, \quad n_{H_2} = \frac{1}{2} A \text{ moles}.$$

From Reaction (2). The initial and final reaction products may occur in the equilibrium state. We designate the amount of sodium oxide as

$$n_{Na_2O} = x \text{ moles}.$$

Then, the amount of sodium hydride formed in the reaction is equal to

$$n_{NaH} = x \text{ moles},$$

and the amount of alkali is

$$n_{NaOH} = (A - x) \text{ moles}.$$

From Reaction (3). The hydrogen will be in the gas phase in the equilibrium state. We designate the amount of hydrogen by

$$n_{H_2} = y \text{ moles}.$$

Then, for reaction (1), ($^1/_2$ A − y) moles of hydrogen will occur in a state of combination with sodium. According to reaction (3), each H molecule reacts with two Na molecules, so that

$$n_{NaH} = (x + A - 2y) \text{ moles}.$$

As a result, we have the Eqs. (2) and (3) with the two unknowns x and y. However, use of Eq. (3) is made difficult by the fact that it describes a heterogeneous reaction, occurring under conditions of mutual solubility between the two components (sodium hydride and sodium). To simplify and increase the accuracy of the calculation, we use the data for the dissociation pressure of sodium hydride as a function of temperature and concentration obtained in [5]. According to these data, the amount of gaseous hydrogen is

$$y = \frac{K_{dis} V}{RT}, \qquad (4)$$

where $P_{dis}$ is the dissociation pressure, V the volume of the gas cavity, R the universal gas constant, and T the absolute temperature. Hence,

$$n_{NaH} = (x + A - 2n_{H_2}) \text{ moles}.$$

Accordingly, the calculation is based on the reaction (2) with the single unknown x. Assuming that the reaction is taking place in an ideal solution, we express the equilibrium constant in terms of the mole fractions of the

component

$$K_a = K_N = \frac{N_{Na_2O} N_{NaH}}{N_{NaOH} N_{Na}^2}. \quad (5)$$

The mole fraction of the components is

$$N_i = \frac{n_i}{\sum n_i}, \quad (6)$$

where $\Sigma n_i$ is the total number of moles present in the solution. In a sodium–water steam generator, the water loop is always under a greater pressure then the sodium loop. Accordingly, if a leak occurs in the steam generator, the water goes into the sodium. In this case under actual conditions, the amount of sodium will be much greater than the amount of the other components, i.e., it may be assumed that $\Sigma n_i \approx n_{Na}$.

Determining the mole fractions of the corresponding components from Eq. (6), and substituting in Eq. (5), we obtain

$$K_a = \frac{x(x + A - 2n_{H_2})}{(A - x) n_{Na}}. \quad (7)$$

If, in solving this equation, we use an expansion in Taylor series, limiting the expansion to the first term, we obtain

$$x \approx \frac{AK_a n_{Na}}{A + K_a n_{Na} - 2n_{H_2}}. \quad (8)$$

Neglecting the rest of the terms in the series makes an error of less than 0.01% in the solution. Taking in Eq (8) $n_{Na} >> A$, $n_{Na} >> n_{H_2}$, and $K_2 > 1$ (as given by Table 2), we obtain

$$x \approx A. \quad (9)$$

Thus, the equilibrium concentrations of the initial and final products of reactions (1)-(3) are of the following form under steam generator condition

$$n_{Na_2O} \approx A, \quad n_{NaH} \approx 2(A - n_{H_2}),$$
$$n_{H_2} = \frac{P_{dis} V}{RT}, \quad n_{NaOH} \approx 0.$$

In this paper, numerical calculation is made for reaction (2) only, since experimental data are used for reactions (1) and (3). In view of this, the accuracy of the proposed calculation is determined by the accuracy of calculation from reaction (2). The assumptions made in the solutions were: 1) the reaction occurs in an ideal solution, and 2) the initial characteristics of the components ($Na_2O$, NaH, NaOH) are those for the crystalline state, while they are present in the reaction in the dissolved state. These assumptions do not increase the error in the calculation, since, from Eq. (8), $x \neq A$ only for $K_2 \ll 1$. However, the assumptions cannot produce an error this large.

The calculation made shows that the principal products of the reaction between water and sodium in a state of thermodynamic equilibrium are sodium oxide, sodium hydride, and hydrogen in the gas voids. The amount of alkali is not large. Evidently, the fact that no signs of corrosion were observed in the experiments on corrosion of stainless steel and sodium containing up to 6% alkali [6] may be accounted for by decomposition of NaOH in the presence of sodium. This gives indirect confirmation that the present calculation is correct.

Consider what effect the equilibrium products formed have on the operation of a loop with a steam generator, and possible methods of removing these products from the coolant. The behavior of the sodium oxide in the loop and ways of removing it from the coolant by means of cooling traps have been better studied[10]in the case of sodium hydride. The solubility curve of sodium hydride [7] shows that it may be removed from the coolant by means of a cooling trap. It is also possible to decompose the sodium hydride at elevated temperature, and remove the hydrogen by vacuuming. It is fairly difficult to tell anything about the behavior of gaseous hydrogen in the loop. It may be concluded from the data of preliminary experiments that the rate of reaction (3) is less than that of (1). In this case, the gaseous hydrogen liberated in reaction (1) will get out into the gas voids of the loop in the form of bubbles, and build up there.

## LITERATURE CITED


1. Liquid Metal Coolants, translation edited by A. E. Sheindlin, Moscow, IL (1958), pp. 11,12,95.
2. M. Sittig, Sodium, Production, Properties, Application [Russian translation], Moscow, IL (1962).
3. A. F. Alabyshev et al., Sodium and Potassium [in Russian], Leningrad, Goskhimizdat (1959), pp. 24,39.
4. M. Kh. Karapet'yants, Chemical Thermodynamics [in Russian], Moscow-Leningrad, Goskhimizdat (1949).
5. M. Banus, J. McSharry, and E. Sullivan, J. Amer. Chem. Soc., No. 5, 2007 (1955).
6. A. Amorosi and J. Gevick, Paper No. 2427 presented by the U.S.A. at the Second International Conference on the Peaceful Uses of Atomic Energy.
7. D. Williams, J. Phys. Chem., 61, 379 (1957).
8. Short Handbook of Physicochemical Quantities [in Russian], edited by K. P. Mishchenko, Moscow, Goskhimizdat (1957).
9. M. Kh. Karapet'yants and M. L. Karapet'yants, Tables of Some Thermodynamic Properties of Various Substances [in Russian], transactions of the D. I. Mendeleev, MKHTI (1961).
10. P. L. Kirillov et al., Atomnaya énergiya, 8, 30 (1960).

# THE CRITICAL HEAT FLUXES IN TUBES CARRYING MONOISOPROPYLDIPHENYL, HEATED BELOW THE SATURATION TEMPERATURE

(UDC 621.039.517)

F. F. Boganov

Translated from Atomnaya Énergiya, Vol. 17, No. 5,
pp. 408-410, November, 964
Original article submitted December 6, 1963

So far, no great success has been achieved in attempts at obtaining values of the critical heat fluxes by an analytic method for any heat transfer medium with different amounts of underheating and different rates of motion over a heated surface of any shape. Accordingly, at the present time, experiment provides the only reliable means of determining the values of the critical heat fluxes for a given set of conditions. In view of this, a great deal of experimental work has been devoted to the occurrence of crisis on heating surfaces. The majority of this work deals with the case in which the heating surface is cooled by water [1-4]. In some other cases, a study has been made of the occurrence of the phenomenon in the removal of heat from a heating surface by various organic coolants in large volume, and when moving in tubes [5-7]. The question of the critical loadings on a heating surface bathed by an organic coolant (monoisopropyldiphenyl) has so far been treated only in [8], and there it was simply the relation between the critical loadings in the tube and the underheating over a relatively small range of this parameter for two coolant velocities, that had been formed.

In the present paper, a study has been made of the critical heat fluxes on the inner surface of a vertical tube 15 mm in diameter and 200 mm long, with monoisopropyldiphenyl moving in it at different coolant velocities and with different amounts of underheating below the saturation temperature. The data obtained have made it possible to find the effect of underheating on the critical heat loading, and the relation between the critical loading and the coolant velocity over quite a wide range of values of the parameters.

In investigating the effect of different factors on the values of the critical heat flux, we started with the semi-empirical idea that the critical flux is made up of two components. The first component is constant for any given coolant at a given pressure. Numerically, it is equal to the critical loading for the coolant in a large volume at a fixed pressure. The effect of pressure may be taken account of by the factor $p^k$ in the constant component of Eq. (1). The second component takes account of the increase in the value of $q_{cr}$ involved in the occurrence of and increase in underheating of the coolant and the rate of motion of the underheated coolant. This component is taken care of by the power multipliers $W^n t^m$, together with some free coefficient.[1]

The experiments were made on an experimental setup consisting of a single-tube closed loop with forced motion of the liquid. The experimental part consisted of a vertical segment of the tube, 200 mm long (1Kh18N9T steel, 15 mm in diameter, wall thickness 2.5 mm), heated by a current at low voltage from a step-down transformer.

Measurements were made of the temperature of the coolant before entering and after leaving the experimental section, the temperature of the liquid ahead of the measuring diaphragm, the pressure, the liquid flow, and the amount of electrical energy required to heat the experimental section.

The total error in determining the critical flux was 10%, and the error in determining the liquid flow was not more than 3-4%.

The critical heat fluxes were reached in all the experiments by gradually increasing the electrical loading on the working part of the tube. In the process, readings were taken of all the measuring instruments after each increase in the electrical loading.

[1] The physical constants are taken from [9, 10].

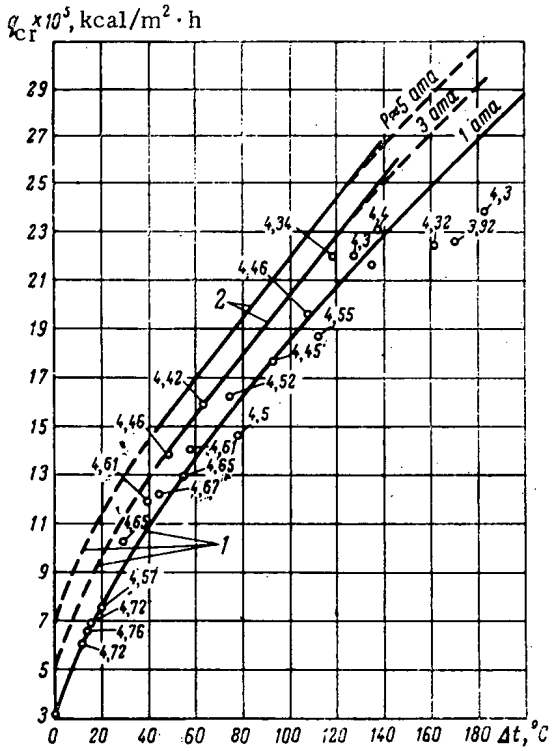


Fig. 1. Critical heat flux as a function of the underheating of the liquid below the saturation temperature (the numbers on the points give the velocities).
1) Equation (1); 2) data of [8].

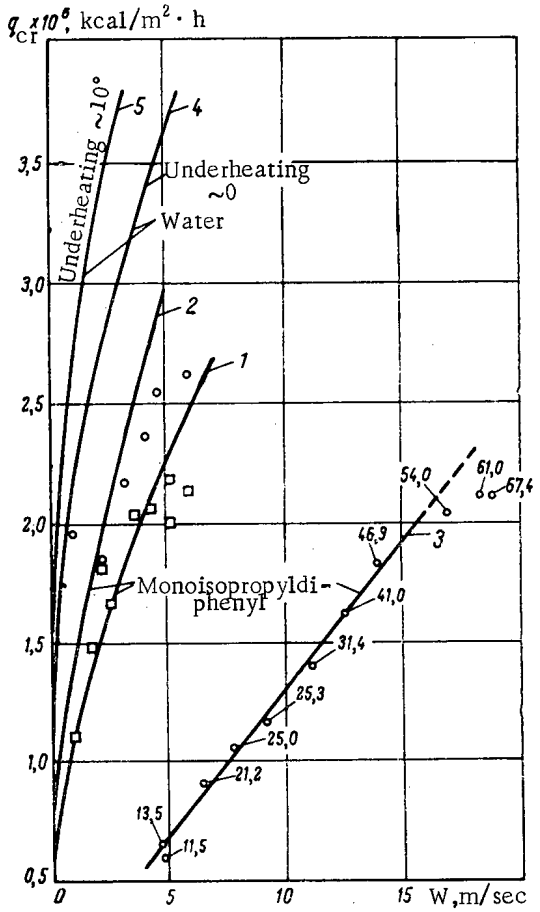


Fig. 2. Critical heat flux as a function of liquid velocity at the heating surface (the numbers on the points give the underheating of the liquid below the saturation temperature).

In the majority of the experiments, the critical loadings were determined from the reddening of the wall of the experimental tube. It should be noted that the tubes did not fail when the wall became red, since the coolant in the tube was at a relatively low pressure ($P \approx 1$-$3$ atm$_{abs}$). Because of this, it was always possible to take the electrical loading off of the experimental part of the tube before it became white hot.

To check the reproducibility of the measurements, the full electrical loading was again put on, and then gradually reduced with an autotransformer, with readings being taken of the instruments at the instant the crisis was removed (the reddening disappeared). In some experiments, the critical loading was taken off by increasing the coolant velocity in the tube.

The primary experimental data were worked up in the form of the simple function

$$q_{cr} = f(W,\ \Delta t)_p,$$

where $q_{cr}$ is the critical heat flux in kcal/m$^2$ · h, W the linear velocity of the coolant stream in the experimental section in m/sec, and $\Delta t$ the amount of underheating of the liquid below the saturation temperature in °C.

Figure 1 gives a curve of the critical heat fluxes as a function of the underheating of the coolant, moving in a tube 15 mm in diameter and 200 mm long at a velocity of 2-4.5 m/sec, with an excess pressure of 200-300 kg/m$^2$. It may be seen from the figure that this is a power law curve, which is satisfactorily described by the empirical relation:

$$q_{cr} = 1{,}6\ (W^{0,6}\Delta t^{0,8}) \cdot 10^4 + 3 \cdot 10^5 \cdot (P)^{0,6}\ \text{kcal/m}^2 \cdot \text{h}. \qquad (1)$$

(The curve in the graph is plotted from this relation.)

At small underheatings (~30°C), the experimental points lie directly on the curve. At moderate underheatings ($\Delta t$ = 40-145°C), there is a certain amount of spread of the points about the curve 1, which, however, does not exceed ±10%, and it is only at large underheating ($\Delta t \sim 150$°C), that any substantial difference between the points and the curve is observed. At large values of the underheating, we see a tendency toward reducing the effect that change in the underheating has on the critical heat flux.

The same figure gives curves approximating the data of [8], which were obtained for the same linear coolant velocity in a tube 10 mm in diameter and 100 mm long at pressures of 3 and 5 $atm_{abs}$.

Comparing these data with ours shows that in the range of underheating covered by the authors of [8], these data, including the effect of pressure, are in satisfactory agreement with out data, and are described by Eq. (1).

The effect of pressure is taken care of by the factor $P^{0.6}$, which includes the increase in the value of $q_{cr}$ resulting from the decrease in volume steam content in the layer at the wall (reduction in diameter of the bubble that breaks loose).

Figure 2 shows the critical heat flux as a function of the linear coolant velocity in the tube at constant underheating below the saturation temperature. Curve 1 is plotted from the experimental data obtained at an underheating of 120° C, and curve 2 at an underheating of 175°C. Both of the approximating curves are plotted from the empirical relation (1). It may be seen from the figure that the curves give a satisfactory description of the experimental data in both cases. Further, data are given obtained in experiments on the effect of velocity on the critical loading for variable underheating (curve 3). A good description of these data is also given by the curve plotted from Eq. (1). The curves 4 and 5 are plotted from the results of [3].

Thus, this relation may be used to make an approximate determination of the critical heat flux in tube with monoisopropyldiphenyl moving in them over the range covered of coolant velocities and underheatings below the saturation temperature in the range of pressures 1-5 $atm_{abs}$.

## LITERATURE CITED.


1. Yu. P. Shlykov et al., Atomnaya énergiya, 8, 144 (1960).
2. M. E. Miropol'skii, Atomnaya énergiya, 11, 515 (1961).
3. A. P. Ornatskii, Transactions of the Heat Power Institute, Academy of Sciences of the UkrSSR [in Russian], No. 2 (1950).
4. G. N. Kruzhilin, Izv. AN SSSR Otd. tekhn. nauk, No. 7 (1948); No. 5 (1949).
5. C. Trilling et al., Paper No. 1779 presented by the U.S.A. at the Second International Conference on the Peaceful Uses of Atomic Energy (Geneva, 1958).
6. A. V. Chechetkin, High-Temperature Heat Transfer Media [in Russian], Moscow, Gosénergoizat (1957).
7. Cichelli and Bonilla, Inst. Chem. Engng., No. 6 (1945).
8. A. S. Sterman, Teploénergetika, No. 2, 85 (1964).
9. N. B. Vargaftik et al., Bulletin of the Universities Chemistry [in Russian], No. 3 (1963).
10. M. P. Vukalovich et al., Teploénergetika, No. 4, 70 (1962).

# ERRORS IN THE CALIBRATION OF γ DOSIMETERS WITH A COLLIMATED BEAM

(UDC 539.16.08)

É. F. Garapov, Yu. N. Gryaznov, and G. A. Dorofeev

Translated from Atomnaya Énergiya, Vol. 17, No. 5,
pp. 410-412, November, 1964
Original article submitted December 4, 1963

The calibration of γ dosimeters, which is based on the use of standard γ sources, is carried out not only with unshielded sources but also with collimated beams of γ radiation [1]. However, when unshielded sources are used, it is impossible to realize the conditions under which the standard sources are certified which leads to errors in the calibration. In addition, distortions of the point-source field are possible because of radiation scattered from materials surrounding the source. The use of a collimated beam makes it possible to reproduce easily the geometry used for standard source certification, to reduce the effect of scattering to a minimum, and to assure radiation protection for operating personnel. However, with changes in the angle of divergence of the collimated beam, the readings of instruments being calibrated can vary significantly because of the scattered radiation contribution [2].

This letter deals with a study of the changes in radiation spectrum as a function of the angle of divergence of the collimated beam and of the distance between source and detector whose purpose was to establish a method for the reduction of the contribution from scattered radiation. A $Co^{60}$ source 2 x 2 mm in dimensions was used as a source of primary radiation. The measurements were carried out on a calibration setup with a collimation unit which was taken as typical for standardization work (Fig. 1a).

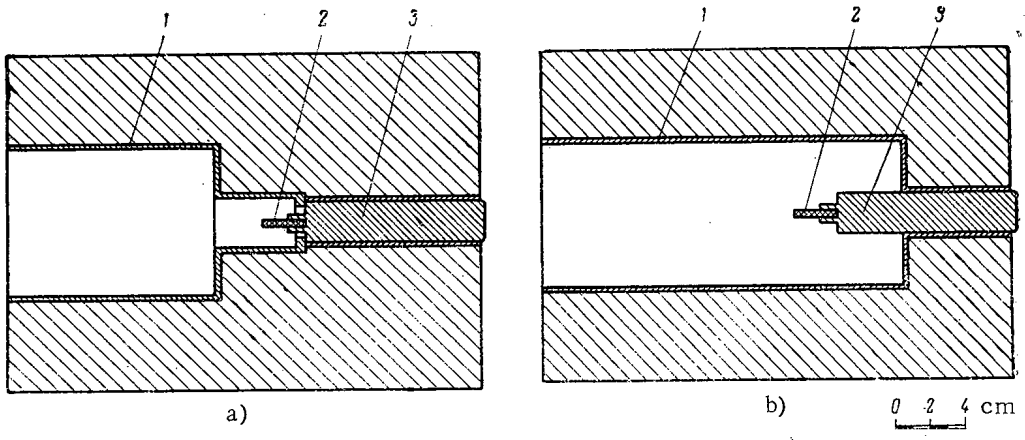


Fig. 1. Diagrams of a typical collimation unit (a) and a unit with a cavity (b): 1) channel for the insertion of exchangeable collimators; 2) standard $Co^{60}$ source; 3) source holder.

A NaI(Tl) crystal with dimensions 40 x 40 mm and an FÉU-13 photomultiplier served as γ-ray detector. The detector was located at distances of 100, 200, 300, and 400 cm from the source. At each distance, spectra were taken for collimating channel diameters of 8, 14, 30, 40, and 60 mm.

The instrumental radiation spectra taken at a distance of 200 cm from the source are shown in Fig. 2. For the various collimating channel diameters, the photopeaks coincide (in area and shape) since they correspond to primary

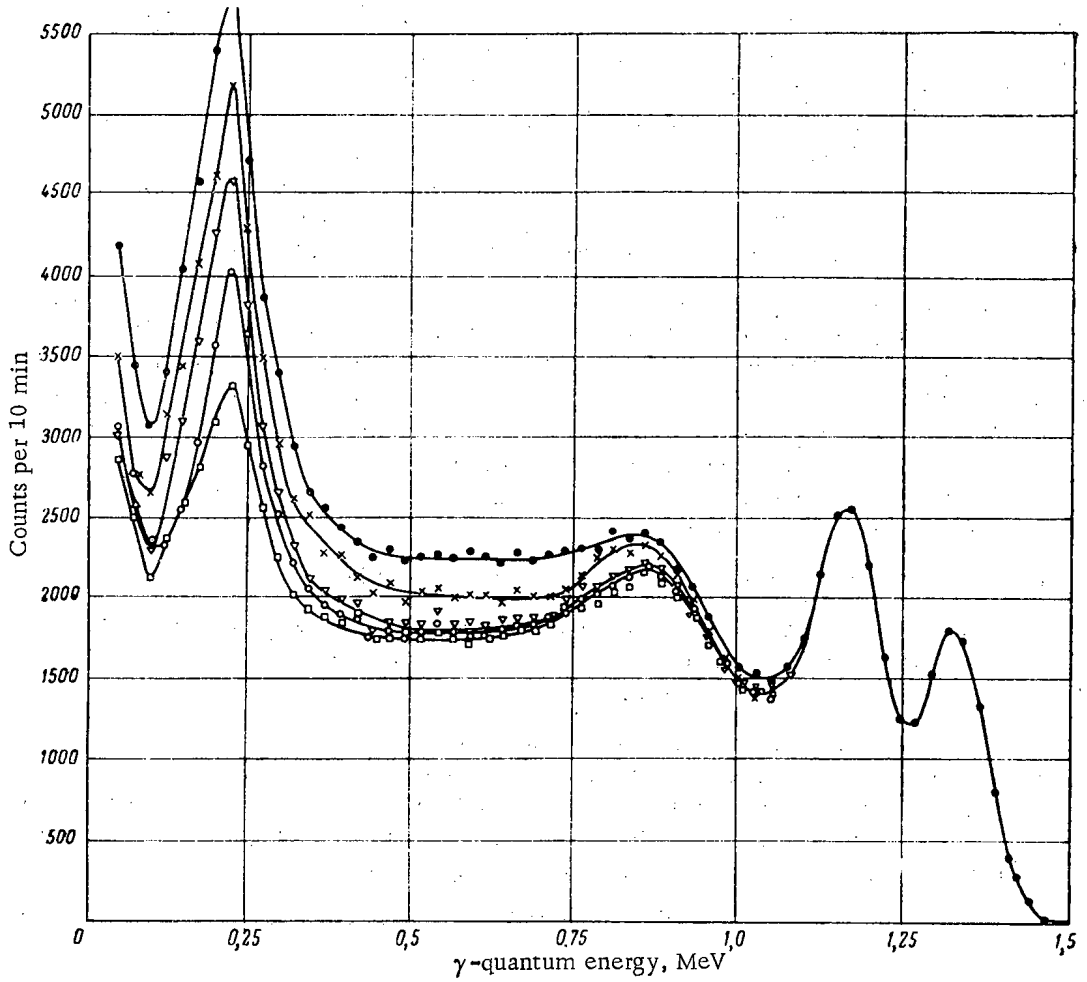


Fig. 2. Instrumental spectra of $Co^{60}$ γ radiation taken in a collimated beam at 200 cm from the source for various collimating channel diameters: □ – 8 mm; ○ – 14 mm; ▽ – 40 mm; × – 40 mm; ◎ – 60 mm.

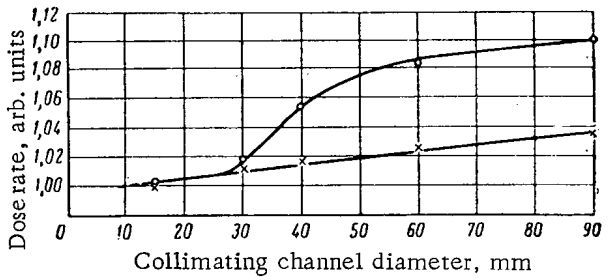


Fig. 3. Dose rate dependence on collimating channel diameter: ○ – typical collimation unit; × – collimation unit with cavity. The data are normalized to the dose rate for 15 mm collimator diameter.

γ quanta with energies of 1.17 and 1.33 MeV. The soft portion of the spectra (up to an energy of 1.05 MeV) increases with increasing collimating channel diameter. A like picture was observed also at other distances from the source. With a variation in collimating channel diameter from 8 to 60 mm, the integral count for all spectra increased by approximately 25%. However, the inverse-square law was satisfied for all diameters with an accuracy of ±2%. Therefore, the main portion of the scattered radiation was produced in the collimation unit close to the source. In order to narrow down the location of the production of scattered radiation, the effect of specific parts of the collimation unit on instrumental radiation spectra was investigated.

A comparison of the spectra that were obtained showed that the scattered radiation was produced in the lead shielding of the collimation unit in the immediate vicinity of the γ-ray source and that it escaped through the shoulder formed by the cavity in which the source was located and the collimating channel if the diameter of the

latter was larger than the 30-mm diameter of the cavity of a typical collimation unit. The contribution of scattered radiation was sharply reduced if the shoulder was removed, i.e., if the cavity was made larger or equal to the diameter of the collimating channel. Such a collimating unit is shown in Fig. 1b. The dependence on collimating channel diameter of the readings from an RP-1 dosimeter with an ionization chamber 2000 $cm^3$ in volume in shown in Fig. 3. In calibrating with a typical collimation unit, the readings of the instrument increased for collimating channel diameters greater than 30 mm because of escape of scattered radiation through the shoulder. The collimating unit suggested by the authors removed this shortcoming, and the increase in readings because of the contribution from scattered radiation did not exceed 4% for a 5-90 mm variation in collimating channel diameters.

Presently, existing operating directions and instructions for calibration and standardization of $\gamma$ dosimeters are set up with consideration of the fact that the readings of dosimeters vary significantly with changes in collimating channel diameter, the variations falling outside the limits of accuracy. In order to assure uniqueness in the reproducibility of dose rate, it has been recommended up to now that one use the typical collimation unit referred to above only with a 30-mm collimating-channel diameter. In calibrating instruments of higher accuracy, it has been recommended that one carry out additional measurements for three or four collimating channel diameters with subsequent linear extrapolation of the results obtained. As follows from Fig. 3, this extrapolation can lead to a systematic error which is different for different instruments.

The results obtained in this work make the following conclusions possible.

1. The main portion of the scattered radiation which is present in a collimated beam is produced in the shielding material in the immediate vicinity of the source, and it escapes through the shoulder formed by a cavity whose diameter is less than that of the collimating channel.

2. The use of a cavity with dimensions equal to, or greater than, the diameter of the collimating channel considerably reduces the scattered radiation contribution, making it possible to use collimating channels with diameters greater than 30 mm without significantly changing the $\gamma$-ray intensity in the beam. The existence of a strict linear dependence of dose rate in the beam on collimator diameter makes possible the highly accurate transfer of the roentgen from a standard to secondary standards and to measuring instrument.

The results of this work were arrived at in the course of developing operating instructions for the calibration of dosimetric instruments.

## LITERATURE CITED

1. M. F. Yudin, Methods and Equipment for the Calibration of Dosimetric Instruments [in Russian], Moscow, Standartgiz (1962).
2. Z. P. Balon et al., Izmerit. tekhnika, No. 12, 47 (1959).

# INTERACTION OF NEUTRONS AND NUCLEI IN THE 1 eV-100 keV RANGE

L. B. Pikel'ner

Translated from Atomnaya Énergiya, Vol. 17, No. 5,
pp. 413-414, November, 1964

A conference on interactions of neutrons and nuclei in the energy range from 1 eV to 100 keV was held in June, 1964 at the Joint Institute for Nuclear Research (Dubna). One hundred and fifty-odd delegates from member nations of the Joint Institute took part in the deliberations. Forty papers were submitted on the properties of nuclear levels, on total neutron cross sections, radiative capture of neutrons, fission of nuclei, $\gamma$-ray spectra in the capture of resonance neutrons, polarized resonance neutrons, and experimental techniques.

A review report by Ya. A. Smorodinskii (Joint Institute) was devoted to the statistics of nuclear levels, developed within the framework of Dyson theory.

In a review paper submitted by I. Ya. Barit, G. M. Vagradov, V. A. Sergeev, and A. V. Stepanov, "Three-quasiparticle excitations and intermediate structure of the energy dependence of nuclear reactions," a model of the formation of the compound nucleus in the presence of excitation of a small number of nucleons in the nucleus was discussed. The cross section in this case was of a resonance character, but with great widths of the order of several ten kiloelectron volts. In the case of heavy nuclides of high-level density, such three-quasiparticle states may be transitional to the excitation of a large number of nucleons in the nucleus. This paper took up some of the experimental findings illustrating the theory under discussion.

A theoretical paper by M. A. Kasymzhanov and B. N. Zakhar'ev (Dubna Joint Institute) discussed the capture of slow p-neutrons by nuclei. It was shown that the treatment of the interaction between bound nucleons in a nucleus and a bombarding particle leads to increased penetrability through the centrifugal barrier.

The problem of how to maximize the probable value of the strength function $\bar{\Gamma}_n^0/D$ from experimentally derived data, taking into account the laws of distribution of reduced neutron widths and level spacings, was dealt with in a paper by G. V. Muradyan and Yu. V. Adamchuk (Institute of Atomic Energy).

An ingenious method for distinguishing between s-wave and p-wave resonances was advanced by G. V. Muradyan (IAE). The measurements were carried out with a self-indicating method, using a transmission specimen moving either in the direction of the neutron source or in the opposite direction. The transmission of the moving specimen was independent of the direction of motion in the case of a symmetrical p-wave resonance, and differs in the case of an s-wave resonance because of interference effects in neutron scattering.

The rates of excitation of levels in the nuclides $K^{40}$, $V^{52}$, and $Co^{60}$ in thermal neutron capture and in the (d,p) reaction were compared in a paper by W. Rudolph, H. Gersch, and K. Alexander (Central Nuclear Research Institute, German Democratic Republic). High-intensity lines appearing in the (n,$\gamma$) reaction are manifested weakly in the (d,p) reaction in some cases.

S. I. Sukhoruchkin (Institute of Theoretical and Experimental Physics) reviewed several topics associated with the energy structure of nuclei. He centered attention on the relationship linking the effect of coincidence of neutron levels in light nuclides and the correlation of the binding energies of those nuclides. A statistical analysis of one-particle energy states of nuclei revealed the presence of a distinct parameter related to the electron rest mass.

A paper presented by Yu. V. Adamchuk, S. S. Moskalev, and G. V. Muradyan (IAE) was devoted to experimental research on strength functions of nuclides in the range of atomic numbers $A \sim 100$. Neutron transmission was measured for zirconium and strontium isotopes. The results yielded values of the strength functions which were higher than those reported by other authors, and which showed improved agreement with predictions based on the optical model.

The results of measurements of the total neutron cross sections of erbium and rhenium isotopes, obtained with a mechanical chopper at the Institute of Physics of the Academy of Sciences of the UkrSSR, were presented in a report submitted by V. I. Vertebnyi, M. F. Vlasov, M. V. Pasechnik, and associates.

Total cross sections of iron, nickel, and calcium nuclides over a broad range of neutron energies (from 0.03 to 70 keV) were investigated in a paper by E. Ya. Doil'nitsyn, M. V. Panarin, and A. I. Stupak (Physics and Engineering Institute).

Polarized neutrons were the subject of a review paper by Yu. V. Taran, and of an experimental research paper by P. Draghicescu, V. I. Lushchikov, V. G. Nikolenko, Yu. V. Taran, and F. L. Shapiro (Dubna Joint Institute). This paper reported the production of a beam of neutrons polarized by passing them through a polarized proton target. This method enabled the investigators to obtain a beam of polarized neutrons of energies up to several ten kiloelectron volts at reasonably high intensity. Polarization was about 20% in the resonance region, as recorded in the first measurements.

A paper by Yu. A. Kazanskii and A. V. Malyshev (Physics and Engineering Institute) took up the contribution of direct radiative neutron capture to the thermal cross section. On the basis of analysis of experimental data referable to a large number of nuclides, the authors drew the inference that this process does take place and plays an important role in nuclides having a low-thermal neutron-capture cross section.

A paper by A. V. Malyshev and S. M. Zakharova (Physics and Engineering Institute) was devoted to calculations of average radiative widths.

The results of an investigation of neutron resonances in rubidium isotopes are found in a paper presented by E. I. Sharapov, L. B. Pikel'ner, N. Iliescu, Kim Hui Sang, and H. Sirazet (Dubna Joint Institute for Nuclear Research). An analysis of the data obtained and earlier data revealed that the dependence of the radiative width on the atomic number of the nuclides in the region of neutron magic number 50 has a minimum, and not a maximum as hitherto supposed. A similar pattern is also possible for other closed neutron shells.

Attention was given to the relationship between scattering length and radiative neutron capture cross section in a paper by Yu. I. Fenin and F. L. Shapiro (Joint Institute), and this relationship was exploited in order to find the radiative widths of the nuclides $Sc^{45}$ and $Cl^{35}$ in an experimental paper by S. A. Romanov and F. L. Shapiro.

The audience manifested keen interest in a survey paper by Yu. P. Popov and Yu. I. Fenin (Joint Institute) devoted to the interaction of p-wave neutrons and nuclei, and to an analysis of averaged cross sections. The possibilities of securing information of the nucleus from averaged capture, scattering, and total cross sections, as well as evaluating the present state of theory and experiment relating the strength functions of nuclides, were discussed. Experimental data on averaged total cross sections for various heavy nuclides in the energy range up to 10 keV may be found in a report by M. N. Nikolaev and U. M. Makhanov (Physics and Engineering Institute). Averaged radiative capture cross sections were studied with a neutron slowing-down time spectrometer (Lebedev Institute of Physics); the results of this research appeared in papers by S. P. Kapchigashev, Yu. P. Popov, and V. A. Konks and Yu. I. Fenin.

Such topics as symmetry in fission, ternary fission, the average characteristics of the capture to fission ratio, as well as other topics involving the interaction of resonance neutrons and fissionable nuclei, were discussed in "Fission of nuclei by low-energy neutrons," a survey paper by N. S. Rabotnov and G. N. Smirenkin (Physics and Engineering Institute). The basic experiments in this area which are of interest for comparison with theoretical prediction are noted in the paper.

Experimental studies of neutron resonances in $U^{235}$ were discussed in a paper by Wang Hsih-Ti, Wang Yeung-Chang, E. Dermendzhiev, and Yu. V. Ryabov (Joint Institute). As a result of a wide variety of measurements (transmission, self-indication, radiative capture, fission) carried out, the parameters of several levels were obtained to a high order of precision. The average radiative width obtained was (40 ±3) MeV. A paper by K. G. Ignat'ev and I. V. Kirpichnikov (Institute of Theoretical and Experimental Physics) was devoted to a study of the parameters of levels in another fissionable nuclide, $Pu^{239}$.

The study of $\gamma$-ray spectra in neutron capture at resonances was reported in papers by F. N. Belyaev and K. G. Ignat'ev (Institute of Theoretical and Experimental Physics) on work using a pair spectrometer and a set of six small NaI crystals (palladium, cadmium, xenon, tungsten resonances were studied), and by V. S. Al'nikov, D. L. Broder, M. V. Panarin, and L. P. Kham'yanov (Physics and Engineering Institute), reporting measurements of the low-energy portion of the $\gamma$-ray spectrum in samarium and indium resonances.

Papers discussing method at the conference dealt principally with neutron time-of-flight spectrometers. These included reports by E. Ya. Doil'nitsyn (Physics and Engineering Institute), J. Skryvanek, F. Bocvar, V. Plasil (Nuclear Research Institute, CzSR), S. Dobrescu, H. Crist, M. Constantinescu, V. Mateiciuk, T. Stadnikova (Institute of Atomic Physics, Rumanian Peoples Republic), V. F. Gerasimov, V. S. Zenkevich, and V. V. Safronov (Institute of Atomic Energy).

Intense interest was stimulated by a paper of Wang Hsih-Ti and Yu. V. Ryabov (Joint Institute) on a liquid scintillation detector for recording fission events, and a paper by D. L. Broder, M. V. Panarin, A. N. Utyuzhnikov, and L. P. Kham'yanov (Physics and Engineering Institute) on a scintillation $\gamma$-ray spectrometer for total absorption on anticoincidences.

# SYMPOSIUM ON CONTROL ROD PHYSICS AND CONTROL ROD MATERIALS

I. R.

Translated from Atomnaya Énergiya, Vol. 17, No. 5,
pp. 414-415, November, 1964

An IAEA symposium on physics of reactor control rods and control rod materials was held in Vienna in November, 1963. One hundred and ten representatives from 19 countries and three international organizations participated in the deliberations. K. V. Orlov (Institute of Metallurgy of the Academy of Sciences of the USSR) represented the USSR at the gathering. A total of nine plenary sessions were held, at which 34 reports were delivered.

The Soviet delegation presented five papers. Yu. V. Petrov and T. I. Sumbaeva noted in their report, "Control rod weight and importance of delayed neutrons in the VVR-M reactor," a 25 ± 3% increase in the effective fraction of delayed neutrons in small reactor cores over the natural fraction. A report by N. N. Ponomarev-Stepnoi and V. I. Nosov, "Theoretical and experimental research on the efficiency of a system of neutron-absorbing rods in a reflected reactor" [see Atomnaya énergiya, 17, 103 (1964)], contains a comparison of the experimentally derived and theoretically predicted values of the effectiveness of single and banked boron-containing rods; moreover, they offered a method for calculations in an arbitrary arrangement of rods in the radial reflector of a thermal reactor. A study of the physical characteristics of Nimonic type alloys containing dispersed rare-earth oxides is presented in "Disperse-phase absorbing materials for thermal reactor controls" [see Atomnaya énergiya, 17, 107 (1964)], by N. N. Ponomarev-Stepnoi, V. I. Nosova, K. I. Portnoi and E. G. Savel'ev. The high absorbing power, satisfactory radiation stability, and excellent mechanical strength of two-phase materials of this type under operating conditions in emphasized. "Patterns of change is absorbing materials in response to changes in the absorber concentration," a paper by K. I. Portnoi, points out the existence of an absorbing power peak in certain concentrations of selected absorber materials. In addition, a paper entitled "Determination of control rod worth in critical assemblies of the VVR reactor" by V. N. Semenov, G. L. Lunin, et al., offers experimental data on the high effectiveness of cadmium-clad trapping rods.

Problems concerning the choice of control rod materials are reflected in a paper "Possible use of cadmium and indium tantalates as material for control rods in high-temperture reactors," by E. Preisler, F. Hausner, and G. Petzow (West Germany). Materials of this type combine excellent absorbing power with satisfactory heat conduction and stability at temperatures upward of 700°C. Compatibility of cadmium and indium tantalates with silver, copper, and nickel at operating temperatures was established. The metallography of dysprosium, erbium, gadolinium, and samarium alloys formed with various nonferrous and rare metals was the subject of a paper by M. Copeland and H. Kato (USA), "Alloys enriched with rare-earth metals." Experience in the use of stainless steel cruciform control rods containing boron carbide is reflected in "Design, fabrication, and performance of boron carbide control rods" by H. Brammer and J. Jacobson (USA).

Some of the papers presented discussed the design, fabrication, and operating experience of control rods. An interesting control system design, the "hydraulic sphere," is found in a paper by S. Wims and associates (USA). The use of an array of tubes with intervening spheres or cylinders of neutron-absorbing material assures a smooth reactivity variation and a uniform neutron flux distribution, thereby allowing a roughly 40% increase in reactor power. A paper by P. Dosch, H. Kraus, and H. Uhrit (West Germany), "The design and experimental evaluation of an electromagnetic scramming system," contains a description of a scram rod actuated by a pulsed electromagnetic generator which provides for rapid acceleration of the control rod drive.

The operational problems affecting control rods found reflection in several of the papers submitted. A paper by P. Blum et al. (France) entitled "Control rods in a high-flux pool-type reactor" discussed the causes for nonuniformity of neutron flux, and suggested a method for minimizing this irregularity. The results of a measurement of cadmium plate burnup are presented in a paper by P. Harvey (Great Britain), "Determination of the service life of the PLUTO reactor shim rod system."

An appreciable number of theoretical papers concerned the design of control rods for thermal reactors. A comparison of theoretical and experimental reactivity data are given in a paper by T. Skardamar (Sweden), "Use of heterogeneous and homogeneous methods in determining the effect of control rods in heavy-water lattices." In the author's view, the observed discrepancies are due to insufficient exactness of the two-group theory and to the effect of the rods of the neutron spectrum. This problem was also discussed in a paper by B. Michaelson (Great Britain), "Study of the ZENITH reactor control rods," where the causes of possible discrepancies at high reactivities are singled out.

Some of the reports dealt with neutron flux flattening. L. Dollet and J. Dirien (France), in a paper entitled "Reactivity control by absorbing elements in dissolved form in the moderator of a power reactor," took note of the possibility of introducing cadmium, lithium, and gadolinium slufates for this purpose, as well as boric acid. In another paper, L. Dollet et al. discussed the introduction of $He^3$ to a system of tubes passing through the reactor core ("Use of gas under a different pressure to monitor reactivity in power reactors").

In conclusion, we should mention a review paper by W. Loewenstein (USA), "Fast reactor control: available methods and future outlook," in which a comparison was made between approximate calculations and experimental data on hand.

The symposium was indubitably of great value, since it allowed an opportunity for the discussion and generalization of the experience amassed in operational experience in the world's major scientific laboratories, and expedited the formulation of the basic trends in the development of reactor control rod work. The IAEA intends to publish the symposium proceedings in order to familiarize the broadest possible number of interested scientists with the work in this field.

# A SYMPOSIUM ON ASSAY OF HUMAN BODY BURDEN

Yu. V. Sivintsev

Translated from Atomnaya Énergiya, Vol. 17, No. 5,
pp. 415-417, November, 1964

IAEA, in conjunction with the International Labor Organization and the World Health Organization, organized a symposium on the evaluation of the content of radioactive substances in the human organism, held in Heidelberg (West Germany) in May, 1964. Over a hundred specialists were present from 31 countries West Berlin, and 6 international organizations (including the International Radiation Safety Commission). Sixty-nine papers containing results of new scientific research on the radiometry of internal exposure in humans were submitted. Almost two thirds of these communications were presented in the name of scientists of three nations: Great Britain (17 papers), USA (15 papers), and West Germany (10 papers); the research group at Lund University (Sweden) submitted 6 papers, and French scientists submitted five.

B. Rajewski (West Germany) made a detailed survey of the history of methods for determining radioactive substances present in the human organism. It is highly intriguing that as far back as the thirties, an organization had been set up in Germany for the physical diagnosis of radium poisoning. Its tasks included $Ra^{226}$ determinations in human excretions and exhalations; but radiometry of the living organism became possible only 20 years later, following the development of scintillation counters. During those years, semiconductor detectors underwent a breathtaking development, and their use in $\gamma$ spectrometers has been a tremendous aid in measuring the tissue burden of the human organism and the quantity of radioactive substances present in various media, particularly in foodstuffs, at a specific sample activity down to as low as $10^{-13}$ Ci/g, where spectrograms with resolution on the order of 40 keV can be obtained. Two spectrometers of this type are described in a paper by V. Maynord and S. Hill (Great Britain), and also cited the results of a study of pollution of the atmosphere with trace quantities of $Po^{210}$ and $Pu^{239}$.

S. Black (USA) reported on the successful application of a method for collecting teeth which had fallen out or been extracted in hospitals, and measuring their $Ra^{226}$ content, in a program calling for the in-vivo monitoring of 35,000 persons consuming river water which was contaminated with uranium process wastes. Concrete information was extracted for improving the system of radon content measurement in exhaled air at low levels of specific radium activity in the organism. Calibration of the apparatus was checked by comparing the results of measurements of individuals and analyses of bone tissue removed in surgical operations and autopsies.

W. Jacobi (West Germany) described a variety of instrument using two filters and a chamber for storing radon and thoron daughters in use in West Germany for the measurement of concentrations of radon and thoron daughters in exhaled air.

The use of the conventional method with an ionization chamber enabled researchers to secure valuable information in measuring thoron concentration in the air exhaled by patients injected in an earlier (pre-war) period with a thorium compound (known as thorotrast) for diagnostic purposes (this drug functioned as a contrast agent in x-ray examinations). On the basis of investigations of 45 patients, R. Grielmaier, H. Muth, and E. Oberhausen (West Germany) found an average of 7% of the thoron formed in the organism to be expelled in the exhaled air, even though 20% of the thoron had been separated from the sites where it was deposited. Of this amount of thoron, only about 9% decays in the blood and about 4% in the lungs.

Particularly close attention was given, at the symposium, to techniques in the radiometry and radiochemistry of bodily excretions. In addition to tutorial review papers outlining the experience accumulated in Great Britain (C. Jackson), USA (G. Hartlye), France (J. Remy), India (P. Kamat, I. Bat, S. Rudran, and M. Iyengar), and Rumania (G. Furnic and N. Racovianu), several papers were devoted to techniques for determining $Pu^{239}$ concentration in the human organism on the basis of an analysis of excretions. The most important data were those reported by W. Langham (USA) as a result of experiments with 16 patients injected intraveneously with small amounts of plutonium citrate. The findings were that approximately 0.002% of the injected material is taken up in the intestines, and that

0.002% is absorbed through unlesioned skin within an hour of contact. It was found that urinary secretion can be described by the relation $D = 435\ Ut^{-0.76}$, where D is the $Pu^{239}$ burden in the organism, U the daily urinary excretion, and t the time elapsed since the plutonium gained access to the organism (in days).

The use of electronic computers to interpret quantitative data on analyses of excretions is discussed in a paper by W. Snyder (USA) on measurements of $Pu^{239}$ body burden. Radiochemical techniques for plutonium determination in samples of excretions and human bodily tissues were compared in a comprehensive paper submitted by J. Nielson and T. Baisley (USA). A comparison of radiometric techniques for detecting this $\alpha$ emitter (ionization chambers, semiconductor detectors, proportional counters and scintillation counters, and nuclear emulsions) and the spectrometry of the $\alpha$ emitter (semiconductor detectors, nuclear emulsions, and liquid scintillation counters) was performed. Important recommendations were made for the most rational sampling of excretions in persons suspected of possible plutonium exposure, in a paper by C. Beach and J. Dolphin (Great Britain).

An analysis of the results of measurements of the radioactive body burden in several patients after accidental $Pu^{239}$ contamination of portions of their skin and of their lungs is found in communications by L. Jeanma ire (France) and J. Dolphin (Great Britain).

Improvements in techniques of plutonium measurement, especially at very low activity levels, are described in papers by F. Sandles and E. Morgan and A. Holmes (Great Britain). In the first of these, the reader may find a proposal for the electrolytic deposition of $Pu^{239}$ from a solution, which would make it possible to obtain a source with virtually no self-absorption, and a method involving the use of a semiconductor device capable of discriminating $\alpha$ particles of energy below 4.2 MeV. As a result, these authors attained very high sensivitity ($\sim$0.1 pCi for a daily urine specimen). The towering defect in the radiochemical excretion sampling techniques (namely, the laborious procedures) was eliminated in the $\gamma$-ray spectrometric method of analyzing biological specimens. The use of computers opens up the way for shortening the measuring time down to 10 min in this instance, and eliminating pretreatment of the specimens. Moreover, with this method clinicians will be able to carry out measurements of several $\gamma$ emitters simultaneously in the same specimen. The Holmes paper offers calculations of the range of sensitivity for this method over a specimen measurement time of 1.10, 100, and 1000 min (on samples ranging from 400 to 2000 $cm^3$ in volume), and detection of $\gamma$ rays of energies from 0.134 to 1.33 MeV. Sources of possible error (particularly in converting to the content of soluble and sparingly soluble compounds of radioactive elements in the lungs) were analyzed by R. Thomas (USA).

Some interesting data on the most dangerous emitters, $Ra^{226}$, $Sr^{90}$, and $Th^{228}$ in chronically affected human organisms (up to 16 years) were communicated by J. Rundo (Great Britain). He reported biological half-lives of $Th^{228}$ for two subjects (6 and 7 years), $Ra^{226}$ (23 years), and $Sr^{90}$ (9 and 6 years). In contrast to these data, M. Fujita (Japan) found in the course of an investigation of $Sr^{85}$ removal may be described suitably as the sum of three exponential terms with biological half-lives of 1.8, 8, and 600 days. The figure of 100 days is recommended for approximate estimates. This paper thereby provided evidence on the existence of some discrepancies in the behavior of a radioactive element, depending on whether it gains access to the human body in chronic exposure or as a single event. Such data were available previously only for experimental animals. $Ra^{226}$ burden figures and tables of $Ra^{226}$ content in excretion samples as a function of contact time and as a function of the rest time elapsed following the end of introduction of the emitter to the human body are very convenient aids to practical work, and may be found in a paper by V. M. Malykhin and V. P. Shamov (USSR).

The specific aspects of the radiometry of bodily excretions a program for monitoring personnel working with uranium were taken up in papers by C. Jackson (Great Britain) and J. Eakens and E. Morgan (Great Britain). Methods for measuring tritium in personnel at the Savannah River plant and in several British firms using tritiated compounds were presented in communications by H. Johns and F. Butler (USA) and B. Lambert (Great Britain).

Another group of papers on the determination of human body burden offered material based on the use of whole-body spectrometers. The biological inconstancy of the organism's physiological functions which, as remarked upon in a paper by E. Poaching (Great Britain), introduces a large uncertainty into the results of analyses of excretions, must be recognized as counting among the foremost reasons for the preferred use of this technique in the first place. A typical example was cited in a report by K. Sill and G. Anderson (USA) devoted to a comparison of whole-body counting methods and analysis of bodily excretions. In radioactive measurements taken on personnel at the national reactor testing station of the USAEC, the whole-body method detected 24 isotopes which had gained access to the organisms of several persons on duty, whereas radiometry of the excretions uncovered only 7 of these cases.

An even more striking discrepancy was noted in contaminations by insoluble compounds taken up into the human organism in the form of radioactive aerosol particulates. The major drawback in the whole-body spectrometers is their high cost and the impossibility of moving them to the site where most of the personnel being monitored are stationed. Because of this, the design of inexpensive and mobile spectrometers of this type is being given a high priority. We note in particular a facility weighing less than 280 kg and installed in a small truck, described in the abovementioned paper by Sill and Anderson, and also a spectrometer weighting about 2 tons and truck-mounted, described in a paper by J. Mittinen (Finland). This last facility was used for $Cs^{137}$ body burden measurements in southern Finland and northern Sweden (covered by a paper submitted by K. Liden and J. Naversten, Sweden) in connection with the anomalously high $Cs^{137}$ level detected in that region (460 pCi on the average for a group of 80 persons in Sweden as against 18 pCi for a group of 11 persons in Helsinki). This last result, communicated by E. Hasanen and J. Mittinen (Finland), is in practically complete accord with the data reported by C. Melandri (Italy, W. Allet and G. Brownell (USA), and by E. Hucke and E. Oberhausen (West Germany). These last-mentioned authors advanced an intriguing hypothesis on the possible dependence of the half-removal time of $Cs^{137}$ on the age of the patients. The data they cited, obtained through radioactivity measurements carried out on 15,000 healthy subjects, confirm this conclusion. In recent communications (J. Naversten and K. Liden, Sweden; R. Hesp, Great Britain; L. Jeanmaire, France; R. Jordan et al., USA), cases of accidental contaminations of human organism by large amounts of $Cs^{137}$ were analyzed. Attempts to speed up the clearance of this emitter from the tissues by medicinal administration of chlorothiazide met with no success (J. Harrison and McNeil, Canada). The possibility of introducing further improvements into the whole-body counter method in the particular case of $Cs^{137}$ measurements was discussed in a report by J. Rundo (Great Britain).

The use of whole-body counters in cases of radium and thorium contamination was analyzed in a paper by the American specialist C. Miller, and the results of a survey of 500 patients who had been working with radium fluorescing plants and dyes over a protracted period are detailed in a report by J. Vennart et al. (Great Britain). Some of the papers were devoted to the application of this technique on research on the use of thorotrast (F. Schales, West Germany; A. Kauhle, West Germany; E. Oberhausen et al., West Germany; P. Keppe, West Berlin).

Some highly promising work on the detection of pure $\beta$ emitters by their bremsstrahlung emission and $Pu^{239}$ from the characteristic radiation penetrating to outside the human organism was reported by G. Bengstson and K. Liden (Sweden), P. Venger and C. Soucasse (France). Despite the first not quite successful results obtained in using this method (reported on by P. Pellerin et al., France; and N. Wald et al., USA), it still holds out great promise.

The whole-body counter has also found new applications in uranium processing plants. Experience on in-plant operation of whole-body counters at the USAEC Y-12 plant was reported on by L. Scott and K. West, and an accident involving inhalation of enriched uranium dust was probed by this method at the Aldermaston nuclear weapons development center (V. Saxby et al., Great Britain).

A curious $Pu^{239}$ emission detector for whole-body spectrometry (a bank of multifilament proportional counters) was proposed in a paper by R. Ehret et al. (West Germany). A similar method found application at the Saclay research center (A. Lanslart and J. Morucci, France). In these investigations, a correct simulation of human lungs acquires special importance, since the bulk of radioactive aerosols inhaled in air settle down in the lungs, as a general rule. An improved phantom of the thoracic cage satisfying most specifications is described in a paper by R. Speight, C. Peabody, and D. Ramsden (Great Britain). Problems of technique in the analysis of $\gamma$-emitter spectra were taken up in papers by K. McNeil and V. Mohinder (Canada) and J. Naversten (Sweden).

The results of investigations of patients by means of whole-body counters were utilized in the 10 papers to secure valuable data on the biological effects of internal exposure and critical tolerance levels and concentrations of radioactive contaminants.

The proceedings of the symposium will be published by IAEA in 1964.

# A POLISH WHOLE-BODY COUNTER

Yu. V. Sivintsev

Translated from Atomnaya Énergiya, Vol. 17, No. 5,
pp. 417-419, November, 1964

The Institute for Nuclear Research (Warsaw) has published a report [Pszona, B. Adamska, and K. Zarnowiecki, Whole-body counter for internal contamination control, Warsaw, Institute of Nuclear Research, report No. 467/XIX, 1963] on the development, calibration, and first try-outs of a new whole-body counter. As is generally known, apparatus of this type is gaining increasing favor in the largest nuclear centers, within the past period, for monitoring internal exposure of personnel to radioactive substances, and in estimating the internal exposure dose. In view of the short time available for a single measurement, whole-body spectrometers are indispensable for performing on-the-spot measurements on persons involved in nuclear accidents.

This Polish whole-body spectrometer consists of a shielding cave made of 12-cm thick steel and lead, two scintillation counters, and a pulse-height analyzer. The patient is seated in an inclined chair (Fig. 1) during the measurements, in a geometry close to the standard Miller chair. The differences from the standard Miller chair are that in this arrangement the detectors are brought to 35 cm of the patient being monitored in order to improve their effectiveness (instead of the 42-cm distance in the case of the Miller chair). In addition, in order to reduce shielding size, the angle of tilt of the chair is increased (from 45 to 56°). With the patient in this position with respect to the radiation detectors, the counting rate of the uniformly distributed counters (e.g., for potassium or cesium) will be independent of the individual features of the patient.

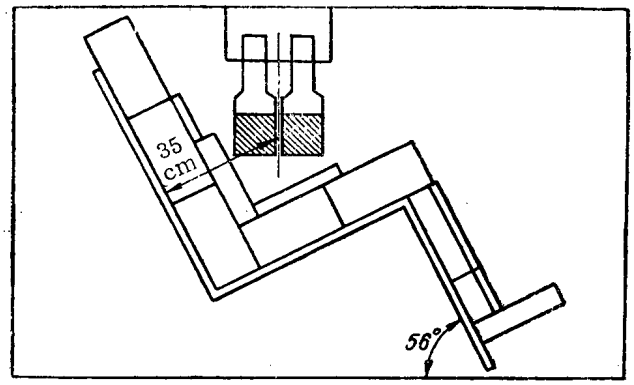


Fig. 1. Polish whole-body counter geometry.

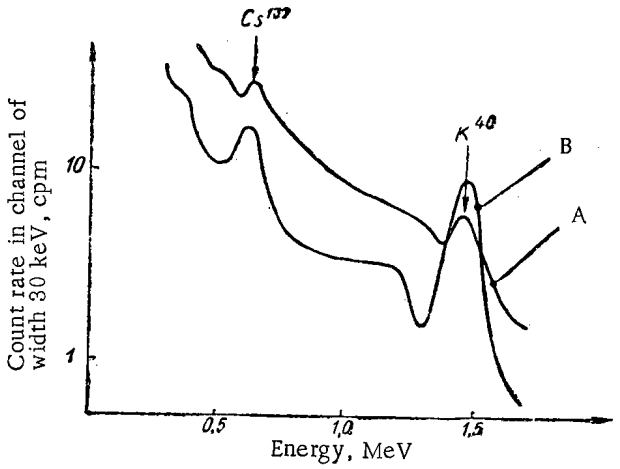


Fig. 2. Background emission spectrum (curve A) and emission spectrum of human having no profession contact with radioactive materials (curve B).

Two NaI(Tl) crystals 76.2×76.2 mm in size, in combination with M112 FQS35 (Zeiss) photomultipliers, were used as the radiation detectors, with the aim of attaining higher sensitivity because of the low tolerable dosages of radioactive isotopes in the human body (as a rule, below 1 $\mu$Ci), and the relatively simple identification of the emitters. The pulses from the counters arrive at the imput of an AI-100 110-channel pulse-height analyzer. The stabilizing circuit used for the sensors makes sure that the counting rate will remain steady as the voltage ranges from 1450 to 1700 V. The energy resolution is 13%, as measured by the photopeak obtained in recording 661 keV $Cs^{137}$ $\gamma$.

The sensors are so arranged under the shielding as to reduce the background counting rate by an average of 29 times in the range from 0.05 to 2.0 MeV (33 times in the low energy range below 0.8 MeV and 9 times in the 0.8-1.6 MeV range). Photopeaks of $Cs^{137}$ and $K^{40}$ $\gamma$ recorded in the shielding cave appear on the background spectrum (Fig. 2, curve A), and

TABLE 1. Sensitivity of the Polish Whole-Body Counter

| Nuclide | Energy, MeV | Sensitivity, pCi |
|---|---|---|
| $Au^{198}$ | 0,41 | 3 |
| $Ir^{132}$ | 0,47 | 6 |
| $Cs^{137}$ | 0,66 | 3 |
| $Mn^{56}$ | 0,88 | 4 |
| $Fe^{59}$ | 1,1 | 8 |
| $Zn^{65}$ | 1,12 | 9 |
| $Co^{60}$ | 1,17 | 4 |
| $Ra^{226}$* | 1,76 | 20 |
| $Na^{24}$ | 2,75 | 8 |

*30% $Ra^{226}$ in equilibrium with decay daughters.

TABLE 2. Natural Radioactivity of Persons Having No Professional Contact with Radioactive Materials

| Subject | Body burden | | $Cs^{137}$ specific activity, in pCi/g K |
|---|---|---|---|
| | $Cs^{137}$, pCi | potassium, g | |
| A | 13 | 151 | 86,5 |
| B | 4,7 | 116 | 40,5 |
| C | — | 135 | — |
| D | 9,3 | 124 | 75 |
| E | 9,3 | 139 | 67 |

seem to be due to contaminants in the structural materials of the shielding and in the glass of the photomultiplier tubes.

A volunteer subject drank down an aqueous solution of $K_2CO_3$ containing 1 $\mu$Ci of the short-lived isotope $K^{42}$ (half-life 12.5 h, photon energy 1.51 MeV). Whole-body measurements established that in the course of 5 h, $K^{42}$ attains an equilibrium state with the potassium present in human muscle tissue. During that time span, 42 liters of aqueous $K_2^{42}CO_3$ with a total activity of 1 $\mu$Ci was introduced into a polyvinyl chloride phantom simulating a human body. A comparison of the measured emission spectrum of the human subject and the phantom showed that the phantom reproduces the scattering and absorbing properties of a human body with a fair amount of accuracy. The area ratios under the photopeak and Compton intervals of the spectrum of patient and phantom were found to be quite similar (0.542 and 0.547, respectively). This led to the conclusion that further calibration could be handled safely using the phantom alone. Experiments conducted revealed the correction factor for the difference in the geometries of the measurements to be 1.35 (with respect to the area ratio of the $K^{42}$ $\gamma$ photopeaks of volunteer patient and phantom). The remaining calibrations were carried out using isotopes $Au^{198}$, $Mn^{56}$, $Na^{24}$, and $K^{42}$ and thereby making it possible to encompass the energy range from 0.4 to 2.75 MeV. The absolute activities of the preparations used were measured on a $4\pi$ counter or on a $\beta$-$\gamma$-coincidence facility ($Au^{198}$, $Na^{24}$). The experimentally derived recording efficiency for $\gamma$ photons of different energies varied in almost linear fashion, from 0.17% at 0.4 MeV ($Au^{198}$) to 0.007% at 2.75 MeV ($Na^{24}$). The sensitivity of the facility as computed in this fashion may be found in Table 1. The values reported are the minimum detectable activity (at 50% error) over a measuring time of 50 min.

Measurements of the radioactivity in persons having no professional contact with radioactive materials, and in personnel working in nuclear laboratories, were carried out on this facility. An example of the spectrogram of a person having no professional contact with radioactive materials is seen in Fig. 2 (curve B). The photopeaks on this spectrogram belong to $K^{40}$, the naturally occurring radioactive isotope of potassium incorporated in muscle tissue, and to $Cs^{137}$, a nuclear weapons test fallout product detected in human organisms since 1955. Measurements of a group of five subjects are given in Table 2.

The design of a new original whole-body spectrometer is evidence of the maturity of nuclear science and engineering in Poland.

# NEW DEVICE UNPACKS IRRADIATED TARGETS

B. G. Chistov

Translated from Atomnaya Énergiya, Vol. 17, No. 5,
pp. 419-420, November, 1964

Radioactive isotopes of certain chemical elements are produced by irradiating the original material with pile neutrons. Special containers of a variety of types, depending on the reactor design, are used in the exposures. The raw material is enclosed in some cases in aluminum cans placed inside the container, these cans consisting of tube segments of varied heights closed at both ends.

The irradiated targets are unpackaged by remote control in specially designed shielded caves. This involves no great difficulty and may be handled by a rotating disk cutter. Opening the cans does involve certain difficulties, however, since the expensive irradiated material may be spilt, and consequently lost, in the process, or process equipment may become contaminated. We have developed and tested under production conditions a device for opening these cans in which any possibility of the target material spilling during the process is minimized. The "can opener" may be stationary or removable and is handled by an operator working a master-slave or through-wall manipulator depending on the type of shielded box in which the process is conducted.

When the clip 1 is dislodged, the cans are set up in vertical position in the cradle of the carriage 2, which moves in the keyways of the body 3. The carriage with cans is pushed into the body of the "can opener" in such a way that the faces of the top lids of the cans contact (on half their perimeter) the tempered gib 4 of the runner 5. The clip 1 is dropped back to the working position and brought to rest by the catch 6. Next, a membrane pneumatic actuator 7 is supplied with compressed air through the lines, and the body of the can is clamped between the the tempered gibs 9 and 10 mounted on the upper faces of the body and clip, the force being transmitted via the

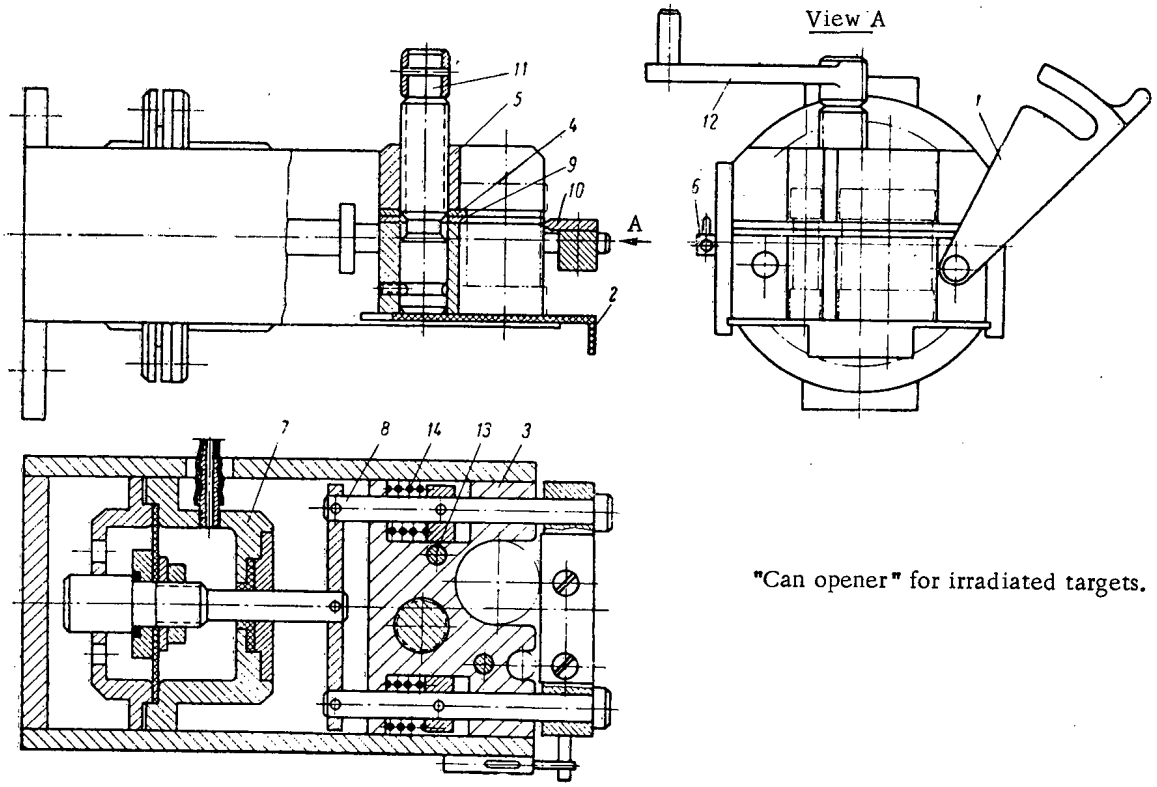


"Can opener" for irradiated targets.

connecting rod 8. In order to set up a high specific pressure in the clamping process and avert slipping, the gibs 9 and 10 are sharpened. By rotating the screw 11 via the lever 12, the runner 5 is raised high along the guide pins 13, while the lids are simulataneously removed from the cans. When the compressed air is let out of the pneumatic actuator, springs 14 disengage the clip 1 from the body of the cans and the latter are thrown free of the facility. Since cans used in target irradiation differ in diameter and height, two cradles of different diameter are provided in the body and runner, and special carriage attachments are available for handling cans of lesser height.

NEWS ITEM

Translated from Atomnaya Énergiya, Vol. 17, No. 5,
p. 420, November, 1964

Chairman A. M. Petros'yants of the USSR State Committee on the Uses of Atomic Energy and W. Penney, Chairman of the United Kingdom Atomic Energy Authority, exchanged letters of agreement on a program of cooperation during 1964-1966, in accord with the agreement on collaboration in the peaceful uses of atomic energy dating back to May 19, 1961. This exchange took place on September 7, 1964, at Geneva, during the Third International Conference on the peaceful uses of atomic energy.

According to this program, Soviet scientists will visit Britain to familiarize themselves with research on plasma physics and controlled thermonuclear fusion (March, 1965), fast reactors (September, 1965), accelerators and nuclear physics (October, 1965). British scientists will in turn visit the USSR to become better acquainted with research there on isotopes (1964), fast reactors (May, 1965), and radiation safety (spring of 1966).

The State Committee on the Uses of Atomic Energy and the UKAEC will continue the mutual exchange of declassified reports and other literature on the peaceful uses of atomic energy. In addition, plans call for exchange visits of two scientists in 1965 on terms up to six months.

# BIBLIOGRAPHY

V. Shevchenko

Translated from Atomnaya Énergiya, Vol. 17, No. 5,
pp. 421-422, November, 1964

1963 Brussels Symposium, aqueous reprocessing chemistry for irradiated fuels; Paris, OECD, 1963.

A symposium on the chemistry of aqueous reprocessing of spent fuel was held in Brussels (Belgium) from April 23 to 26, 1963, under the auspices of the European Atomic Energy Agency and the European Chemical Company. Over 150 specialists from 15 countries and three international bodies participated in the symposium.

Twenty-six papers and communications were submitted. Along with papers on aqueous processes, principally on dissolution, extraction, and ion exchange, there were three papers on nonaqueous techniques and one paper on the present and future role of fuel reprocessing in the costs picture of the fuel cycle.

R. Rometsch (Eurochemic) reported, in the paper "Review of research at Eurochemic," on conditions for dissolving various forms of fuel (applicable to the radiochemical plant now being built at Mol, Belgium) and cladding materials in a tubular unit. NaOH is used to dissolve aluminum cladding, and $H_2SO_4$ is used to dissolve magnesium, magnox, and stainless steel cladding.

"Zirconium dissolution in the NaF–citric acid system," a paper by G. Van Kanehem (Eurochemic) showed that zirconium complexes with fluorine and citric acid ions form when zirconium and zircaloy cladding is dissolved in that mixture.

G. Karlson (Sweden) reported on a new technique for decladding zirconium and zircaloy fuel elements with uranium dioxide meat, in a paper entitled "Dissolution of uranium dioxide fuel elements clad with zircaloy-2." The essence of this "thermox" method consists in first oxidation of the zircaloy at 825° C in a mixture of oxygen and water vapor using nitrogen as catalyst. The dioxide is thereby transformed to the mixed (uranous-uranic] oxide and dissolves readily in nitric acid, while the fuel-element jacket is dumped in solid form in a disposal ground. Improvement of the familiar zirces process (gas-phase chlorination) and zirflex process is reported.

P. Regnaud (France) sees promise in the anodic dissolution of several types of fuel elements and particular $UO_2$ elements jacketed in zircaloy and stainless steel, as well as uranium-aluminum alloys and uranium-molybdenum alloys, in $HNO_3$.

V. Bahr (West Germany), in a paper entitled "Problems in the dissolution of fuel elements containing large amounts of molybdenum," followed the example of Rometsch and Regnaud in devoting a good deal of attention to the problem of dissolving uranium-molybdenum base alloy fuel elements. Research on the dissolution of U–Pu–Mo base fuel elements, and on the type of fuel used in the Rhapsodie reactor (a $UO_2$–$PuO_2$ mixture) and the ceramic $UO_2$–$ThO_2$ mixture, was reported in these papers.

The symposium centered its attention on the chemistry and technology of solvent extraction processes. T. Hughes (Great Britain) reported on an extraction process for reprocessing spent fuel which has been adopted for the new Windscale plant, in his paper "Windscale studies of the TBP–kerosene system and purification problems"; this process is based on the use of TBP solution in kerosene. The now existing two-extractant scheme of solvent extraction cycles at Windscale is published in the report; butex at the beginning of the process and a 20% TBP solution in kerosene at the end with two types of apparatus in use; towers for the butex and mixer-settlers for the TBP.

Research work on ethers as extraction solvents is not slackening, in view of the industrial applications of butex, as is evidenced by the papers submitted by J. Fletcher (Great Britain) "Ethers as extractants" and W. Ochsenfeld (West Germany) "Dibutyl ether solvent extraction." C. Jouannot (France) delivered a report "Marcoule research on a tributyl phosphate extraction flowsheet for fuel reprocessing." The process flowsheet, data on decontamination factors by cycles, and the design of an operationally safe mixer-settler type extractor may be found there.

A solvent extraction arrangement for fuel reprocessing at the radiochemical plant under construction at Mol is discussed in a paper by E. Detillo (Eurochemic), "Tributyl phosphate solvent extraction scheme of Eurochemic."

Considerable attention was centered on the stability of extractants, with particular emphasis on diluents, and on their purification following radiation, thermal, and chemical decomposition. These topics were tackled in a paper by R. Blanco et al. (USA), "Survey of recent developments in TBP liquid extraction." The same topics came under scrutiny in a paper by T. Hughes (Great Britain). T. Siddoll (USA) presented a paper entitled "Organophosphorous compounds (other than TBP) for reprocessing spent fuel and isolating by-products." In this paper, as well as in the one by R. Blanco et al., organosphosphorous compounds of greater radiation stability of the type di-2-amyl-2-butyl phosphonate (DABP) in n-dodecane and dibutylphenyl phosphonate (DBPP) in an aromatic diluent, which were pilot-plant tested, as well as several bidentate organoshosphorous extractants suitable for solvent extraction of rare earths and actinides, were discussed.

Applications of amines in the extraction reporcessing of irradiated materials were the topic of papers by L. Berger et al. (USA), "Amine systems in liquid extraction," M. Ziferero (Italy) "Amine process flowsheet," G. Rolandi (Eurochemic) "Eurochemic flowsheet for ultimate purification of plutonium by trilaurylamine extraction," E. Lopez-Menchero (Eurochemic), "Quaternary ammonium systems." We see from the reports that research on amine extraction in plutonium technology is making headway in almost all countries. In the USA, this technology is based on the use of a 0.3 M solution of alamine-336 (a mixture of aliphatic amines of composition $C_8 \cdot C_{12}$ in the aromatic diluent Solvesso-100). Back extraction of the plutonium is accomplished either by acetic acid or by the reagent di-tert-butylhydroquinone dissolved in an organic phase and exhibiting reducing properties with respect to plutonium. In France and Eurochemic, the solvent extractant used is a 0.3 M solution of trilaurylamine in Solvesso-100. In France, back extraction is carried out with sulfuric acid solutions, but with oxalic acid at Eurochemic. The use of amines in plutonium refining is rivaled by the development of schemes for using amines at the head of the process for recovery of irradiated material. The reprocessing technology for irradiated fuel based on U—Al alloy underlies the design of a new plant in Italy (Saluggia, in the Turin area). Some drawbacks of tertiary amines, such as the limited solubility of their salts in aliphatic diluents and difficulty in back extraction, may be eliminated by resorting to quaternary ammonium bases. The extractant Vantoc—CL, the formula of which is $C_6H_5—CH_2—N(CH_3)_2C_{12}H_{23}HCl$, is now recommended in a Eurochemic paper. Tertiary amines are likewise recommended for use in the isolation technology of americium, curium, californium, and other elements in concentrated solutions of either HCl or LiCl. The radiation stability of the tertiary amines is higher than that of the more commonly used solvent TBP.

Techniques for recovering uranium in nitrate media in order to utilize the uranium (IV) subsequently to reduce plutonium in uranium and plutonium extraction and separation processes are undergoing investigation in Britain and Italy, and at Eurochemic. R. De Leone (Italy), in his paper "Catalytic reduction of uranium in nitric acid solutions," discussed the effect of various process factors on uranium recovery. The best results were obtained when gaseous hydrogen and formic acid were employed with a platinum catalyst carried on aluminum pellets. H. McKaye and R. Streaton (Great Britain) took note of the difficulties encountered in a process for extractive separation of uranium and plutonium, using tetravalent uranium as reductant, in their paper "Uranium (IV) nitrate as a reducing agent in uranium and plutonium separation." B. Edwall (Eurochemic) reported on research on new methods for preparing solutions of uranium (IV) containing only nitric acid and a stabilizer, in his paper "Experience in the use of uranium (IV) nitrate."

Two papers appeared on ion exchange processes. S. Arland (Sweden) expressed a hopeful outlook for the use of zirconium phosphates and silica gel in a report "Uses of inorganic ion exchange resins for reprocessing irradiated fuel." R. Billiaud et al. (Belgium) reported on a purification flowsheet for irradiated fuel based on plutonium and uranium dioxides, in a paper "Investigation of final purification of plutonium for subsequent fuel element fabrication." The purification was carried out in ion exchange columns loaded with Permutit SK. After two cycles, the purification factor was $10^5$ in the case of uranium. High-purity oxide powders (10.7 g/cm$^3$ in density after calcination at 1300° C) were obtained in the precipitation of plutonium peroxide, oxalate, and hydroxide only in the hydroxide precipitate.

M. D'honte (Eurochemic) presented a review paper: "Aqueous methods in reprocessing irradiated fuel." J. Smets (Belgium) presented "Latest progress in volatility reprocessing of fuel." P. Foguerat (France) reported on the processing of spent fuel by volatilization of fluorides. H. Vogg (West Germany) presented "Reprocessing of fast reactor fuel elements. F. Kaller (USA) submitted an extensive report, "Present and future role of fuel reprocessing in fuel cycle costs," in which he took up ways of reducing fuel cycle costs.

# Soviet Journals Available in Cover-to-Cover Translation

| ABBREVIATION | RUSSIAN TITLE | | TITLE OF TRANSLATION | PUBLISHER | TRANSLATION Vol. | Issue | BEGAN Year |
|---|---|---|---|---|---|---|---|
| AÉ | Atomnaya énergiya | | Soviet Journal of Atomic Energy | Consultants Bureau | 1 | 1 | 1956 |
| Akust. zh. | Akusticheskii zhurnal | | Soviet Physics – Acoustics | American Institute of Physics | 1 | 1 | 1955 |
| | Astronomicheskii zhurnal | | Soviet Astronomy – AJ | American Institute of Physics | 34 | 1 | 1957 |
| Astr(on). zh(urn). | Avtomaticheskaya svarka | | Automatic Welding | Br. Welding Research Assn. (London) | 12 | 1 | 1959 |
| Avto(mat). svarka | Avtomatika i Telemekhanika | | Automation and Remote Control | Instrument Society of America | 27 | 1 | 1956 |
| | Biofizika | | Biophysics | National Institutes of Health** | 6 | 1 | 1961 |
| | Biokhimiya | | Biochemistry | Consultants Bureau | 21 | 1 | 1956 |
| Byull. éksp(erim). biol. (i med.) | Byulleten' éksperimental'noi biologii i meditsiny | | Bulletin of Experimental Biology and Medicine | Consultants Bureau | 41 | 1 | 1959 |
| DAN (SSSR) Dokl(ady) AN SSSR | Doklady Akademii Nauk SSSR (The translation of this journal is published in sections) | Life Sciences | Doklady Biological Sciences Sections (includes: Anatomy, biochemistry, biophysics, cytology, ecology, embryology, endocrinology, evolutionary morphology, genetics, histology, hydrobiology, microbiology, morphology, parasitology, physiology, zoology) | National Science Foundation* | 112 | 1 | 1957 |
| | | Life Sciences | Doklady Botanical Sciences Sections (includes: Botany, phytopathology, plant anatomy, plant ecology, plant embryology, plant physiology, plant morphology) | National Science Foundation* | 112 | 1 | 1957 |
| | | Chemical Sciences | Proceedings of the Academy of Sciences of the USSR, Section: Chemical Technology | Consultants Bureau | 106 | 1 | 1956 |
| | | Chemical Sciences | Proceedings of the Academy of Sciences of the USSR, Section: Chemistry | Consultants Bureau | 106 | 1 | 1956 |
| | | Chemical Sciences | Proceedings of the Academy of Sciences of the USSR, Section: Physical Chemistry | Consultants Bureau | 112 | 1 | 1957 |
| | | Earth Sciences | Doklady Earth Sciences Sections (includes: Geochemistry, geology, geophysics, hydrogeology, lithology, mineralogy, oceanology, paleontology, permafrost, petrography) | American Geological Institute | 124 | 1 | 1959 |
| | | Earth Sciences | Proceedings of the Academy of Sciences of the USSR, Section: Geochemistry | Consultants Bureau | 106-123 | 1 6 | 1956-1958 |
| | | Earth Sciences | Proceedings of the Academy of Sciences of the USSR, Section: Geology | Consultants Bureau | 112-123 | 1 6 | 1957-1958 |
| | | Mathematics | Soviet Mathematics – Doklady | American Mathematical Society | 130 | 1 | 1960 |
| | | Physics | Soviet Physics – Doklady (includes: Aerodynamics, astronomy, crystallography, cybernetics and control theory, electrical engineering, energetics, fluid mechanics, heat engineering, hydraulics, mathematical physics, mechanics, physics, technical physics, theory of elasticity sections) | American Institute of Physics | 106 | 1 | 1956 |
| | Elektrosvyaz' | | Telecommunications | Am. Inst. of Electrical Engineers | | 1 | 1957 |
| Entom(ol). oboz(r). | Entomologicheskoe obozrenie | | Entomological Review | National Science Foundation** | 37 | 1 | 1958 |
| FMM | Fizika metallov i metallovedenie | | Physics of Metals and Metallography | Acta Metallurgica | 5 | 1 | 1957 |
| FTT, Fiz. tv(erd). tela | Fizika tverdogo tela | | Soviet Physics – Solid State | American Institute of Physics | 1 | 1 | 1959 |
| Fiziol. Zh(urn). SSSR | Fiziologicheskii zhurnal imeni I.M. Sechenov | | Sechenov Physiological Journal USSR | National Institutes of Health** | 47 | 1 | 1961 |
| Fiziol(ogiya) rast. | Fiziologiya rastenii | | Plant Physiology | National Science Foundation* | 4 | 1 | 1957 |
| | Geodeziya i aerofotosyemka | | Geodesy and Aerophotography | American Geophysical Union | | | 1962 |
| | Geokhimiya | | Geochemistry | The Geochemical Society | 1 | 1 | 1956 |
| Geol. nefti i gaza | Geologiya nefti i gaza | | Petroleum Geology | Petroleum Geology | 2 | 1 | 1958 |
| | Geomagnetizm i aeronomiya | | Geomagnetism and Aeronomy | American Geophysical Union | 1 | 1 | 1961 |
| | Iskusstvennye sputniki zemli | | Artificial Earth Satellites | Consultants Bureau | 1 | 1 | 1958 |
| Izmerit. tekhn(ika) | Izmeritel'naya tekhnika | | Measurement Techniques | Instrument Society of America | 7 | 1 | 1958 |

| | | | | | | |
|---|---|---|---|---|---|---|
| Izv. AN SSSR O(td). Kh(im). N(auk) | Izvestiya Akademii Nauk SSSR: Otdelenie khimicheskikh nauk | Bulletin of the Academy of Sciences of the USSR: Division of Chemical Science | Consultants Bureau | 16 | 1 | 1952 |
| Izv. AN SSSR O(td). T(ekhn). N(auk): Metall). i top. | (see Met. i top) | | | | | |
| Izv. AN SSSR Ser. fiz(ich). | Izvestiya Akademii Nauk SSSR: Seriya fizicheskaya | Bulletin of the Academy of Sciences of the USSR: Physical Series | Columbia Technical Translations | 18 | 3 | 1954 |
| Izv. AN SSSR Ser. geofiz. | Izvestiya Akademii Nauk SSSR: Seriya geofizicheskaya | Bulletin of the Academy of Sciences of the USSR: Geophysics Series | American Geophysical Union | 7 | 1 | 1957 |
| Izv. AN SSSR Ser. geol. | Izvestiya Akademii Nauk SSSR: Seriya geologicheskaya | Bulletin of the Academy of Sciences of the USSR: Geologic Series | American Geological Institute | 23 | 1 | 1958 |
| Iz. Vyssh. Uch. Zav., Tekh. Teks. Prom. | Izvestiya Vysshikh Uchebnykh Zavedenii Tekhnologiya Tekstil'noi Promyshlennosti | Technology of the Textile Industry, USSR | The Textile Institute (Manchester) | 4 | 1 | 1960 |
| Kauch. i rez. | Kauchuk i rezina | Soviet Rubber Technology | Palmerton Publishing Company, Inc. | 18 | 3 | 1959 |
| | Kinetika i kataliz | Kinetics and Catalysis | Consultants Bureau | 1 | 1 | 1960 |
| | Koks i khimiya | Coke and Chemistry, USSR | Coal Tar Research Assn. (Leeds, England) | | 8 | 1959 |
| Kolloidn. zh(urn). | Kolloidnyi zhurnal | Colloid Journal | Consultants Bureau | 14 | 1 | 1952 |
| | Kristallografiya | Soviet Physics – Crystallography | American Institute of Physics | 2 | 1 | 1957 |
| Metallov. i term. | Metallovedenie i termicheskaya obrabotka metallov | Metals Science and Heat Treatment of Metals | | 6 | 1 | 1958 |
| | Metallurg | Metallurgist | Acta Metallurgica | | 1 | 1957 |
| Met. i top.(gorn.) | Metallurgiya i toplivo (gornoye delo) | Russian Metallurgy and Fuels (mining) | Scientific Information Consultants, Ltd. | | 1 | 1960 |
| Mikrobiol. | Mikrobiologiya | Microbiology | National Science Foundation* | 26 | 1 | 1957 |
| | Ogneupory | Refractories | Acta Metallurgica | 25 | 1 | 1960 |
| OS, Opt. i spektr. | Optika i spektroskopiya | Optics and Spectroscopy | American Institute of Physics | 6 | 1 | 1959 |
| Paleontol. Zh(urn) | Paleontologicheskii Zhurnal | Journal of Paleontology | American Geological Institute | | 1 | 1962 |
| | Pochvovedenie | Soviet Soil Science | National Science Foundation** | 53 | 1 | 1958 |
| | Poroshkovaya Metallurgiya | Soviet Powder Metallury and Metal Ceramics | Consultants Bureau | 2 | 1 | 1962 |
| | Priborostroenie | Instrument Construction | Taylor and Francis, Ltd. (London) | 4 | 1 | 1959 |
| Pribory i tekhn. éks(perimenta) | Pribory i tekhnika éksperimenta | Instruments and Experimental Techniques | Instrument Society of America | 3 | 1 | 1958 |
| Prikl. matem. i mekh(an). | Prikladnaya matematika i mekhanika | Applied Mathematics and Mechanics | Am. Society of Mechanical Engineers | 22 | 1 | 1958 |
| PTE | (see Pribory i tekhn. éks.) | | | | | |
| | Problemy Severa | Problems of the North | National Research Council of Canada | | 1 | 1958 |
| | Radiokhimiya | Radiochemistry | Consultants Bureau | 4 | 1 | 1962 |
| Radiotekh. | Radioteknika | Radio Engineering | Am. Institute of Electrical Engineers | 16 | 1 | 1961 |
| Radiotekhn. i élektron(ika) | Radiotekhnika i électronika | Radio Engineering and Electronic Physics | Am. Institute of Electrical Engineers | 6 | 1 | 1961 |
| | Stal' | Stal (in English) | Iron and Steel Institute | 19 | 1 | 1959 |
| | Stanki i instrument | Machines and Tooling | Production Engineering Research Assoc. | 30 | 1 | 1959 |
| Stek. i keram. | Steklo i keramika | Glass and Ceramics | Consultants Bureau | 13 | 1 | 1956 |
| Svaroch. proiz-vo | Svarochnoe proizvodstvo | Welding Production | Br. Welding Research Assn. (London) | 5 | 4 | 1959 |
| Teor. veroyat. i prim. | Teoriya veroyatnostei i ee primenenie | Theory of Probability and Its Application | Soc. for Industrial and Applied Math. | 1 | 1 | 1956 |
| Tsvet. metally | Tsvetnye metally | The Soviet Journal of Nonferrous Metals | Primary Sources | 33 | 1 | 1960 |
| UFN | Uspekhi fizicheskikh nauk | Soviet Physics – Uspekhi (partial translation) | American Institute of Physics | 66 | 1 | 1958 |
| UKh, Usp. khimi | Uspekhi khimii | Russian Chemical Reviews | Chemical Society (London) | 29 | 1 | 1960 |
| UMN | Uspekhi matematicheskaya nauk | Russian Mathematical Surveys | Cleaver-Hume Press, Ltd. (London) | 15 | 1 | 1960 |
| Vest. mashinostroeniya | Vestnik mashinostroeniya | Russian Engineering Journal | Production Engineering Research Assoc. | 39 | 4 | 1959 |
| Vop. onk(ol). | Voprosy onkologii | Problems of Oncology | National Institutes of Health** | 7 | 1 | 1961 |
| Zav(odsk). lab(oratoriya) | Zavodskaya laboratoriya | Industrial Laboratory | Instrument Society of America | 24 | 1 | 1958 |
| ZhAKh, Zh. anal(it). Khim(ii) | Zhurnal analiticheskoi khimii | Journal of Analytical Chemistry | Consultants Bureau | 7 | 1 | 1952 |
| ZhETF<br>Zh. éksperim. i teor. fiz. | Zhurnal eksperimental'noi i teoreticheskoi fiziki | Soviet Physics – JETP | American Institute of Physics | 28 | 1 | 1955 |
| ZhFKh<br>Zh. fiz. khimii | Zhurnal fizicheskoi khimii | Russian Journal of Physical Chemistry | Chemical Society (London) | 33 | 7 | 1959 |
| ZhNKh<br>Zh. neorg(an). khim. | Zhurnal neorganicheskoi khimii | Journal of Inorganic Chemistry | Chemical Society (London) | 4 | 1 | 1959 |
| ZhOKh<br>Zh. obshch. khim. | Zhurnal obshchei khimii | Journal of General Chemistry USSR | Consultants Bureau | 19 | 1 | 1949 |
| ZhPKh<br>Zh. prikl. khim. | Zhurnal prikladnoi khimii | Journal of Applied Chemistry USSR | Consultants Bureau | 23 | 1 | 1950 |
| ZhSKh<br>Zh. strukt(urnoi) khim. | Zhurnal strukturnoi khimii | Journal of Structural Chemistry | Consultants Bureau | 1 | 1 | 1960 |
| ZhTF | Zhurnal tekhnicheskoi fiziki | Soviet Physics – Technical Physics | American Institute of Physics | 26 | 1 | 1956 |
| Zh. tekhn. fiz. | Zhurnal vychislitel'noi matematika i matematicheskoi fiziki | U.S.S.R. Computational Mathematics and Mathematical Physics | Pergamon Press, Inc. | 1 | 1 | 1962 |
| Zh. vyssh. nervn. deyat. (im. Pavlova) | Zhurnal vysshei nervnoi deyatel'nosti (im I. P. Pavlova) | Pavlov Journal of Higher Nervous Activity | National Institutes of Health** | 11 | 1 | 1961 |

*Sponsoring organization. Translation published by Consultants Bureau.
**Sponsoring organization. Translation published by Scripta Technica.

CC 2



Declassified and Approved For Release 2013/03/14 : CIA-RDP10-02196R000600120001-5

# SIGNIFICANCE OF ABBREVIATIONS MOST FREQUENTLY ENCOUNTERED IN SOVIET PERIODICALS

| | |
|---|---|
| FIAN | Phys. Inst. Acad. Sci. USSR. |
| GDI | Water Power Inst. |
| GITI | State Sci.-Tech. Press |
| GITTL | State Tech. and Theor. Lit. Press |
| GONTI | State United Sci.-Tech. Press |
| Gosenergoizdat | State Power Press |
| Goskhimizdat | State Chem. Press |
| GOST | All-Union State Standard |
| GTTI | State Tech. and Theor. Lit. Press |
| IL | Foreign Lit. Press |
| ISN (Izd. Sov. Nauk) | Soviet Science Press |
| Izd. AN SSSR | Acad. Sci. USSR Press |
| Izd. MGU | Moscow State Univ. Press |
| LEIIZhT | Leningrad Power Inst. of Railroad Engineering |
| LET | Leningrad Elec. Engr. School |
| LETI | Leningrad Electrotechnical Inst. |
| LETIIZhT | Leningrad Electrical Engineering Research Inst. of Railroad Engr. |
| Mashgiz | State Sci.-Tech. Press for Machine Construction Lit. |
| MEP | Ministry of Electrical Industry |
| MES | Ministry of Electrical Power Plants |
| MESEP | Ministry of Electrical Power Plants and the Electrical Industry |
| MGU | Moscow State Univ. |
| MKhTI | Moscow Inst. Chem. Tech. |
| MOPI | Moscow Regional Pedagogical Inst. |
| MSP | Ministry of Industrial Construction |
| NI ZVUKSZAPIOI | Scientific Research Inst. of Sound Recording |
| NIKFI | Sci. Inst. of Modern Motion Picture Photography |
| ONTI | United Sci.-Tech. Press |
| OTI | Division of Technical Information |
| OTN | Div. Tech. Sci. |
| Stroiizdat | Construction Press |
| TOE | Association of Power Engineers |
| TsKTI | Central Research Inst. for Boilers and Turbines |
| TsNIEL | Central Scientific Research Elec. Engr. Lab. |
| TsNIEL-MES | Central Scientific Research Elec. Engr. Lab.-Ministry of Electric Power Plants |
| TsVTI | Central Office of Economic Information |
| UF | Ural Branch |
| VIESKh | All-Union Inst. of Rural Elec. Power Stations |
| VNIIM | All-Union Scientific Research Inst. of Metrology |
| VNIIZhDT | All-Union Scientific Research Inst. of Railroad Engineering |
| VTI | All-Union Thermotech. Inst. |
| VZEI | All-Union Power Correspondence Inst. |

Note: Abbreviations not on this list and not explained in the translation have been transliterated, no further information about their significance being available to us. —Publisher.

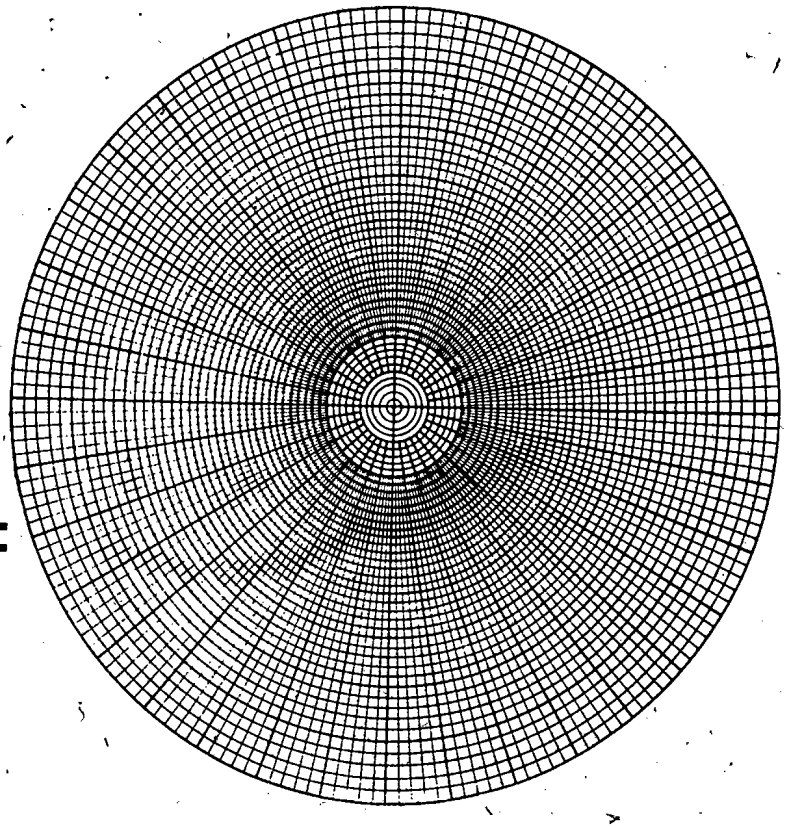

# HANDBOOK OF X-RAY STRUCTURE ANALYSIS OF POLYCRYSTALLINE MATERIALS

**by Lev Iosifovich Mirkin** Translated from Russian

In this exceptional volume, the calculated and experimentally determined constants and data essential to the production and interpretation of x-ray patterns of polycrystalline materials have been collected from the world literature (463 references), and are presented in a single volume in tabular, graphic, and nomographic form.

Dr. Mirkin, of the Moscow University Institute of Mechanics, with the collaboration of researchers at the Moscow Steel Institute, the Institute of Crystallography, Institute of Physical Chemistry, Hard Alloys Research Institute, and many other internationally known Soviet research organizations, has combed Russian and non-Russian sources for essential information in conveniently presented form, and has organized this material with beautiful logic in the sequence in which the analysis is usually performed.

Selection of radiation and method of recording are simplified by the data in Chapters 1 and 2 (including description and parameters of Soviet instruments, which will be of great assistance to all who follow the Russian literature on Crystallography); patterns are indexed with the assistance of the graphs and tables in Chapter 3. The measured intensities are compared with the values found from the tables in Chapter 4.

The second half of the work provides data to assist in the solution of the particular problem at hand (determination of stresses, phase analysis, etc.).

The type of material normally found in textbooks has been excluded, and deductions of formulas and descriptions of methods held to a minimum, but concise explanations for the use of the tables and nomograms are provided. A number of the tables are published here for the first time; others have been expanded especially for the English edition.

**752 pages** **$35.00**

Contents on request

(c/b) CONSULTANTS BUREAU 227 W. 17th St., New York, N.Y. 10011